وزارة التعليم العالي و البحث العلمي
جامعة بابل/ كلية العلوم
قسم الفيزياء

تاثير الكوبالت/المغنيسيوم على الخصائص الفيزيائية لاغشية كبريتيد الكاديوم المحضرة بتقنية الرش الكيميائي

أطروحة مقدمة إلى
مجلس كلية العلوم في جامعة بابل وهي جزء من متطلبات
نيل درجة دكتوراه فلسفة في العلوم/ الفيزياء

من قبل

معمر حسن عيدان عبود

(بكالوريوس علوم فيزياء /٢٠١٦)
(ماجستير علوم فيزياء /٢٠١٩)

إشراف

الاستاذ الدكتور
رحيم كعيد كاظم حسين

الاستاذ المساعد الدكتور
محمد احمد محمد حسون

١٤٤٥هـ

٢٠٢٤م

Ministry of Higher Education and Scientific Research
University of Babylon
College of Science
Department of Physics

Mg/Co effect on the physical properties of CdS thin films prepared by chemical spray pyrolysis technique

A Thesis

Submitted to the Council of College of Science, University of Babylon in Partial Fulfillment of the Requirements of the Degree of Doctorate of Philosophy in Science / Physics.

By

Moamer Hassan Idan Abod

(B.Sc. in Physics /2016)

(M.Sc. in Physics/2019)

Supervised by

Prof. Dr.
Rahem Gaayid Khadum Hussain

Asst. Prof . Dr.
Mohammed Ahmed Mohammed

2024A.D.

1445A.H.

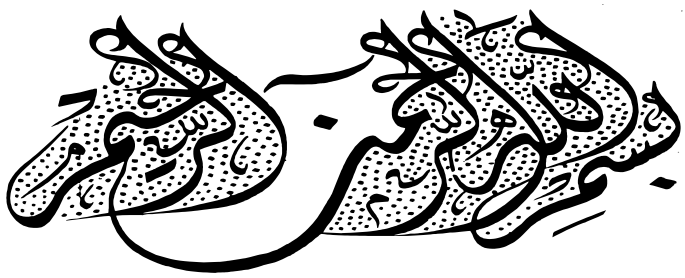

شَهِدَ اللَّهُ أَنَّهُ لَا إِلَهَ إِلَّا هُوَ وَالْمَلَائِكَةُ

وَأُولُوا الْعِلْمِ قَائِمًا بِالْقِسْطِ لَا إِلَهَ إِلَّا هُوَ

الْعَزِيزُ الْحَكِيمُ

صدق الله العظيم

سورة آل عمران

(الآية 18)

Dedication

If the gift is even part of the fulfillment

The gift

To the teacher of mankind and the source of science Prophet (Muhammad peace be upon him)

To whom the cup is drawn empty to hold me down a drop of love

To whom have you hoped to give us a moment of happiness

To those who harvest thorns from Derby to guide me through the flag

To the great heart

My dear father

To those who knelt tender in front of her feet and gave us of her soul and age love and determination and push for a beautiful future

To the precious that we see hope only from her eyes

Dear mother

To those who are closer to me than my soul

To those who share my mother's bosom, and with whom I draw my strength and determination

My brothers and sister

To those who planted optimism in our path and provided us with facilities, ideas and information

My professors are proud

To those who have forgotten me in my studies and shared my thoughts " and memories

My colleagues applied for graduate studies

Give the fruit of my humble efforts

MOAMAR

Acknowledgments

In the name of Allah (the Almighty), the most gracious and the most merciful. I praise Allah (the Almighty), the lord of earth and heaven for completing my thesis.

I would like to extend my thanks and gratitude to my supervisor, Prof. Dr.Raheem G.Kadhim and Mohammed Ahmed Mohammed for having suggested this topic for me and for he distinguished efforts, sound advice and directions that have helped in smoothing out every difficulty encountered during my work. I wish him to have the highest scientific rank and success in his work.

Many thanks to the Deanery of the College of Science in Babylon University and the Department of Physics for offering me the opportunity to complete my study.

I am very grateful to Assist. Prof. Dr.Hikmat Adnan Jawad for their help throughout the research work.

I would like to extend my sincere thanks, appreciation and respect to Prof. Dr. Naheda B.Hassan for providing me with support, help and advice throughout the period of study. I wish her to be the highest and highest scientific and health and wellness.

Finally, I would like to thank my father , my mother and all the members of my family for their help and encouragement and everyone who helped me during the preparation of this thesis.

MOAMAR

الخلاصة :

حضر المركب النانوي كبريتيد الكادميوم بطريقة التفاعل الكيميائي من املاح الكبريت والكادميوم وبعد تحضير المركب كبريتيد الكادميوم تم اضافة املاح الكوبالت والمغنيسيوم وحضرت جميع الاغشية بسمك 100 نانومتر باستخدام تقنية الرش الكيميائي .

تم دراسة الخصائص التركيبية المتضمنة قياس حيود الاشعة السينية حيث بينت النتائج ان جميع الاغشية المحضرة ذات تركيب متعدد التبلور والمركب كبريتيد الكادميوم ذات تركيب من النوع المكعب وان اضافة املاح الكوبالت والمغنيسيوم الى المركب كبريتيد الكادميوم ادى الى نقصان في قيم عرض المنحني لمنتصف ذروة العظمى وزيادة في معدل الحجم الحبيبي.

من خلال نتائج حيود الاشعة السينية تم حساب كل من كثافة الانخلاعات والمطاوعة الاجهادية وعدد بلورات لوحدة المساحة وبينت الحسابات ان اضافة املاح الكوبالت والمغنيسيوم الى المركب كبريتيد الكادميوم ادى الى نقصان في قيم كثافة الانخلاعات وعدد البلورات والمطاوعة الاجهادية.

تم دراسة الخصائص المورولوفجية المتضمنه قياس AFM SEM TEM حيث بينت النتائج ان جميع الاغشية محضرة متجانسة وخالية من العيوب والتشققات وان اضافة املاح الكوبالت والمغنيسيوم ادى الى زيادة في الحجم الحبيبي وخشونة سطوح الاغشية المحضرة وهذا نتائج تتوافق مع نتائج قياس حيود الاشعة السينية.

تم دراسة الخصائص البصرية حيث تم قياس الامتصاصية والنفاذية وحساب الانعكاسية والثوابت البصرية المتضمنة معامل الامتصاص ومعامل الخمود وثابت العزل وفجوة الطاقة البصرية . حيث بينت النتائج ان معامل الامتصاص لجميع الاغشية المحضرة من النوع المباشر وان اضاقة املاح الكوبالت والمغنيسيوم ادى الى زيادة في قيم الامتصاصية ونقصان في النفاذية والانعكاسية ونقصان في قيم فجوة طاقة البصرية .

تم دراسة وقياس الخصائص الكهربائية حيث تم قياس التوصيلية الكهربائية المستمرة و تاثير هول وتيار-فولتية وسعة-جهد .حيث بينت نتائج قياس توصيلية الكهربائية ان اضافة املاح الكوبالت والمغنيسيوم ادئ الى زيادة في قيم التوصيلية الكهربائية. حيث بينت النتائج ان اعلى قيمة لتوصيلية الكهربائية هي لغشاء المحضر CdS:Mg .

وتم حساب طاقة التنشيط حيث وجد المركب كبريتيد الكادميوم له طاقة تنشيط واحدة بينما اضافة املاح الكوبالت والمغنيسيوم ادى الى وجود طاقتين تنشيط .

بينت نتائج قياس السعة الجهد ان جميع الاغشية المحضرة ذات مفرق من النوع الحاد وتم حساب جهد البناء الداخلي وبينت النتائج وان اضافة املاح الكوبالت والمغنيسيوم ادى الى زيادة في قيم جهد البناء الداخلي .

تم دراسة وقياس تيار فولتية في حالتين الاضاءة والظلام لجميع الاغشية المحضرة وبينت النتائج ان اضافة املاح الكوبالت والمغنيسيوم ادى الى زيادة في قيم التيار الضوئي عند تسليط اضاءه بشدات مختلفة .

تم دراسة وحساب معلمات الكاشف الضوئي المتضمنه الاستجابة الطيفية والكفاءة الكمية والكشفية النوعية لجميع الكواشف المحضرة وبينت النتائج ان اضافة املاح الكوبالت والمغنيسيوم ادى الى تحسن في الكفاءة الكمية والاستجابة الطيقية والكشفية حيث وجد ان اعلى كفاءة كانت عند اضافة املاح الكوبالت فقط الى المركب كبريتيد الكادميوم حيث وصلت الكفاءة 87.876% .

تم دراسة وقياس تحسسية الغازات كبريتيد الهيدروجين والايثانول لجميع الاغشية المحضرة حيث تم حساب التحسسية وزمن الاستجابة وزمن الاسترجاع وبينت النتائج ان اضافة املاح الكوبالت والمغنيسيوم ادى الى نقصان في قيم تحسسية الاغشية المحضرة . وبينت النتائج ان افضل تحسسية لغشاء المحضر هو كبريتيد الكادميوم لغاز كبريتيد الهيدروجين حيث وصلت تحسسية 53%.

تم دراسة وفحص اختبار نشاط فعالية الاغشية المحضرة ضد نوعين مختلفين من انتي البكتيريا هما bacteria Staphylococcus و bacteria Escherichia coil وبينت النتائج ان الاغشية لها فعالية عالية في تثبيط وقتل البكتريا وهذا يعد دراسة متداخلة بين علوم الفيزياء وعلوم البايولوجي.

Abstract :

The cadmium sulfide compund was prepared by chemical reaction from Thiourea and cadmium acetate. After preparing the cadmium sulfide compound, cobalt acetate and magnesium acetate were added, and all films with a thickness of 100 nm were prepared using the chemical spray Pyrolysis technique.

The structural properties were studied, including X-ray diffraction measurement, and the results showed that all the prepared thin films had a polycrystalline structure, and the cadmium sulfide compound had a cubic type structure, and that adding cobalt acetate and magnesium acetate to the cadmium sulfide compound led to a decrease in the values of the full width half maximum and an increase in the rate of crystaillite size.
Through the results of X-ray diffraction, the density of dislocations, the micro-strain, and the number of crystals per unit area were calculated. The calculations showed that adding cobalt acetate and magnesium acetate to the cadmium sulfide compound led to a decrease in the values of the density of dislocations, the number of crystals, and themicro-strain.

The morphological properties were studied including AFM SEM TEM measurement, and the results showed that all the prepared thin films were homogeneous and free of defects and cracks, and that the addition of cobalt acetate and magnesium acetate led to an increase in the grain size and surface roughness of the prepared thin films, and these results are consistent with the results of X-ray diffraction measurement.

Optical properties were studied, where absorbance and transmittance were measured, reflectivity was calculated, and optical constants including absorption coefficient, extinction coefficient, dielectric constant, and optical energy gap were calculated. The results showed that the absorption coefficient for all prepared films was of the

direct type, and that the addition of cobalt acetate and magnesium acetate led to an increase in the absorption values, a decrease in transmittance and reflectivity, and a decrease in the optical energy gap values.

The electrical properties were studied and measured, where the continuous electrical conductivity, Hall effect, current-voltage, and voltage-amplitude were measured. The results of electrical conductivity measurement showed that the addition of cobalt acetate and magnesium acetate led to an increase in electrical conductivity values. The results showed that the highest value of electrical conductivity is for the CdS:Mg thin film.

The activation energy was calculated, and the cadmium sulfide compound was found to have one activation energy, while the addition of cobalt acetate and magnesium acetate salts to two activation energies.

The results of the capacitance-voltage measurement showed that all the prepared thin films had a sharp junction. The internal building voltage was calculated and the results showed that the addition of cobalt acetate and magnesium acetate led to an increase in the internal building voltage values.

voltage-current was studied and measured in both light and dark conditions for all the prepared thin films, and the results showed that the addition of cobalt acetate and magnesium acetate led to an increase in the values of the optical current when illuminating it with different intensities.

The photodetector parameters, including the spectral response, quantitative efficiency, and specific detection efficiency, were studied and calculated for all the prepared reagents. The results showed that the addition of cobalt acetate and magnesium acetate led to an improvement

in the quantitative efficiency, optical response, and detection. It was found that the highest efficiency was when adding only the cobalt acetate to the cadmium sulfide compound, where the efficiency was reached. 87.876%.

The sensitivity to the gases hydrogen sulfide and ethanol was studied and measured for all the prepared thin films. The sensitivity, response time, and recovery time were calculated. The results showed that the addition of cobalt acetate and magnesium acetate led to a decrease in the sensitivity values of the prepared thin films. The results showed that the best sensitivity of the prepared thin film cadmium sulfide to hydrogen sulfide gas, where the sensitivity reached 53%.

The activity of the prepared membranes was studied and examined against two different types of bacteria: Staphylococcus bacteria and Escherichia coil bacteria. The results showed that the membranes have high effectiveness in inhibiting and killing bacteria. This is an interdisciplinary study between the physical sciences and the biological sciences.

Supervisors Certification

We certify that this thesis titled **(Mg/Co effect on the physical properties of CdS thin films prepared by chemical spray pyrolysis technique)** was prepared by **(Moamer Hassan Idan Abod)** under our supervision at the Department of Physics, College of Science, University of Babylon, as a partial fulfillment of the requirements of P h.D.

Signature**:**

Supervisor**: Dr. Rahem Gaayid Khadum Hussain**

Title: **Prof.**

Address: **Department of Physics, College of Science , University of Babylon**

Date**: / / 2024**

Signature:

Supervisor**: Dr. Mohammed Ahmed Mohammed**

Title: **Assistant prof.**

Address: **Department of physics, College of Agiculture ,University of AL-Qadisiyah**

Date: **/ / 2024**

Certification of the Head of the Department

In view of the available recommendation, I forward this thesis for debate by the examination committee.

Signature:

Name : **Dr. Samira A. Mahdi**

Title: **Assistant Prof.**

Address: **Head of Department of Physics-**

College of Science –University of Babylon.

Date: **/ / 2024**

Committee Certification

We certify that we have read the thesis entitled "***Mg/Co effect on the physical properties of CdS thin films prepared by chemical spray pyrolysis tecnique***" for the student (**Moamer Hassan Idan Abod**) as a committee examining the student in its contents and according to our opinion, it is accepted as a thesis for Degree of Doctor of Philosophy in Physics.

Signature
Name: Dr. Nahida Bukheet Hasan
Title: Professor
Address: College of Science / University of Babylon
Data : / /2024
(Chairman)

Signature
Name: Dr. Raad M. S. Al-Haddad
Title: Professor
Address: College of Science / University of Baghdad
Data: / /2024
(Member)

Signature
Name: Dr. Hikmat Adnan Banimuslem
Title: Professor
Address: College of Science/University of Babylon
Data: / /2024
(Member)

Signature
Name: Dr. Hussein Hakim Abed
Title: Asst. Professor
Address: College of Science/University of Babylon
Data: / /2024
(Member)

Signature
Name: Dr. Mohsin K. Al-Khaykanee
Title: Asst. Professor
Address: College of Science/ University of Babylon
Data: / /2024
(Member)

Signature
Name: Dr. Rahem Gaayid Khadum Hussain
Title: Professor
Address: College of Science / University of Babylon
Data: / /2024
(Member and Supervisor)

Signature
Name: Dr. Mohammed Ahmed Mohammed
Title: Asst. Professor
Address: College of Agiculture / University of AL-Qadisiyah
Data: / /2024
(Member and Supervisor)

Approved by the University of Babylon a committee on graduate studies
Signature
Name: Dr. Mohammed Hadi Shinen Alshammeri
Title: Professor
Address: Dean of College of Science/ University of Babylon
Data: / /2024

List of Contents

Title	*Page*
Examination Committee Certification	
Dedication	
Acknowledgments	
Contents	***I***
List of Symbols and Abbreviations	***V***
List of Figures	***VII***
List of Tables	***XII***
Abstract	***XIV***

Paragraph No.	*Subjects*	*Page No.*
	Chapter One **Introduction and Review**	
1.1	Introduction	1
1.2	Preparation Method of Thin Films	2
1.3	The Spray Pyrolysis Technique	3
1.3.1	The Main Features of Spray Pyrolysis Technique	4
1.3.2	Particular Considerations of the Chemically Sprayed Thin Films	4
1.4	Properties of Cadmium Sulfide (CdS)	5
1.5	Cobalt (Co) and Magnesium (Mg) materials	8
1.6	Applications of Cadmium Sulfide (CdS)	9
1.7	Nanomaterials for Antibacterial Applications	10
1.8	Physical and Chemical Properties of Gas Hydrogen Sulfide	10
1.9	Ethanol Gas	11
1.10	Literature Review	12
1.11	Aim of the work	19
	Chapter Two Theoretical Part	
2.1	Introduction	21

2.2	Structural Properties and Surface Morphology	21
2.2.1	Fourier Transform Infrared (FTIR)	21
2.2.2	X-Ray Diffraction (XRD) Spectroscopy:	23
2.2.3	Atomic Force Microscopy (AFM):	28
2.2.4	Scaning Electron Microscopy (SEM):	29
2.3	Optical Properties	30
2.3.1	Absorptance (A)	30
2.3.2	Transmittance (T)	31
2.3.3	Reflectance (R)	31
2.3.4	Absorption Coefficient (α)	31
2.3.5	Extinction Coefficient (k_o)	32
2.3.6	Refractive Index (n)	33
2.3.7	Dielectric Constant	33
2.3.8	The Fundamental Absorption Edge	34
2.3.9	Electronics Transition	35
2.4	Electrical Properties:	37
2.4.1	D.C Conductivity	37
2.4.2	Hall Effect	40
2.5	Heterojunction (HJ)	42
2.6	Electrical Properties of Heterojunctions	43
2.6.1	Capacitance -Voltage Characteristics	43
2.6.2	Dark Current–Voltage Characteristics	44
2.6.3	Current Voltage Characteristics Under Illumination	45
2.7	Photodetector Characteristics	45
2.7.1	Responsivity	46
2.7.2	Quantum Efficiency	46
2.7.3	Detectivity and Specific Detectivity	46
2.8	Gas Sensor Characteristics	47
2.8.1	The Sensitivity	47
2.8.2	Response Time	48
2.8.3	Recovery Time	48
2.9	The Classification of Bacteria	49
2.10	Staphylococcus aureus	50
	Chapter Three Experimental Part	
3.1	Introduction	52
3.2	The Materials Used in This Work	52
3.3	work diagram	53
3.4	Sample Preparation	54

3.4.1	Preparation CdS ,CO and Mg:	54
3.4.2	Substrate Clwaning	56
3.4.3	Thin Films Deposition	56
3.5	Chemical Spray Pyrolysis System	56
3.5.1	Spray nozzle	57
3.5.2	Hot plate	57
3.5.3	Air pump	57
3.5.4	Electronic Temporary	57
3.5.5	Temperature Controller	58
3.6	Thin Films Examinations and Measurements	58
3.6.1	Thickness Measurement	59
3.6.1.1	The Optical Method	59
3.6.2	Structural Properties	60
3.6.2.1	FT-IR measurement	60
3.6.2.2	X-ray diffraction (XRD)	61
3.6.2.3	Atomic Force Microscopy (AFM)	62
3.6.2.4	Scanning Electron Microscopy(SEM)	63
3.6.3	Optical Measurements	64
3.6.4	Preparation of Masks and Electrodes Deposition	65
3.6.5	Electrical Properties	66
3.6.5.1	Hall Effect Measurements	66
3.6.5.2	D.C Electrical Conductivity Measurements	67
3.6.5.3	Capacitance-Voltage Measurements for the Heterojunction	68
3.6.5.4	Current-Voltage Measurements for the Heterojunction	68
3.6.6	Detector Characteristic Measurement	69
3.6.7	Sensing System	70
	Chapter Four Results and Discussion	
4.1	Introduction	72
4.2	purity Tests	72
4.3	Structural Properties	73
4.3.1	FTIR Test	73
4.3.2	X-ray diffraction analysis (x-ray)	77
4.4	Morphology Properties	86
4.4.1	The atomic force microscope (AFM)	86
4.4.2	Scanning Electron Microscope (SEM)	90
4.4.3	Energy Dispersive X-Ray Spectroscopy (EDX)	93
4.4.4	Transmission Electron Microscopy (TEM)	95

4.5	Optical Properties	98
4.5.1	Absorbance (A)	98
4.5.2	Ttransmittance(T)	101
4.5.3	Reflectivity (R)	103
4.5.4	Absorption coefficient (α)	105
4.5.5	Optical Energy Gap (Eg)	107
4.5.6	Refractive Index (n)	109
4.5.7	Extinction Coefficient (K)	111
4.5.8	Dielectric Constant	113
4.5.8.1	Real Dielectric Constant (εreal)	113
4.5.8.2	imaginary dielectric constant	115
4.6	Electric Properties	117
4.6.1	Current-Voltage measurent (I-V)	117
4.6.2	D.C Conductivity	120
4.6.3	Hall effect	127
4.6.4	Capacitance-Voltage Measurement(C-V)	129
4.7	Photodector Resultss	134
4.7.1	current-voltage Characteristics under Drak and illumination	134
4.8	Photo Detoctor	138
4.8.1	Responsivity	138
4.8.2	Specific Detectivity	143
4.8.3	Efficiency	147
4.8.4	Life time	150
4.9	Gas Senser	154
4.9.1	Sensitivity and Response and Recovery Time	154
4.10	Anti bectri Measurments	163
	Chapter Five Conclusions	
5.1	Conclusions	166
5.2	Suggestions for Future Work	167
	References	168

List of Symbols & Abbreviations

Symbol	***Meaning***
Cd	Cadmium Acetate
S	Thiourea
Mg	Magnesium Acetate
Co	Cobalt Acetate
CdS	Cadmium Sulfide
Mw	Molecular Weight
Mv	Viscosity average Molecular Weight
FTIR	Fourier Transform Infrared
XRD	X-Ray Diffraction Spectroscopy
δ	Dislocation Density
N	Crystalline Number
ε	Lattice Micro-Strain
β	Peak Full-Width Half Maximum
θ	Braggs Angle of the Peaks
AFM	Atomic Force Microscopy
SEM	Scaning Electron Microscopy
EDX	Energy Dispersive X-Ray Spectroscopy
TEM	Transmission Electron Microscopy
A	Absorptance
T	Transmittance
R	Reflectance
α	Absorption Coefficient
K	Extinction Coefficient
n	Refractive Index
Eg	Energy Gap
ρ	Resistivity
R_H	Hall Coefficient
n_H	Carrier Concentration
C-V	Capacitance -Voltage
I-V	Current–Voltage
R_λ	Responsivity
η	Quantum Efficiency
D	Detectivity
H_2S	Hydrogen Sulfide Gas
M.P	Melting Point
G.S	Grain Size
λ	Wavelength

c	Velocity of Light
$\boldsymbol{\varepsilon}$	Dielectric Coefficient
ε_r	Real Dielectric Coefficient
ε_i	Imaginary Dielectric Coefficient
E_{ph}	Energy of Phonon
λ_C	Cut off Wavelength
FAP	Fundamental Absorption Process
$E_{ph.}$	Energy of Phonon
n_p	Density of Holes
q	Charge of Electron
E_a	Activation Energy
k_B	Boltzmann Constant
$\sigma_{d.c}$	D.C Conductivity
h	Planck Constant
μ_H	Mobility of Hall
t	Thickness
V	The Voltage
V_H	Hall Voltage
n_H	carrier density
n-type	Type of carriers in the material (electrons)
n_e	Electron Density
I	The Current
ℓ	Space Between the Electrode
E	Electric Field
S	Cross Section Area
B	Magnetic Field
R	Resistance
FWHM	The full width half maximum
δ	The Dislocations Density
(hkl)	Miller Indices
t	Life Time
Tres.	Response Time
Trec.	Recovery Time
S%	The Sensitivity Gas

List of Figures

Figure No.	***Description***	***Page***
1.1	Formation Stages of a Thin Film.	5
1.2	Cadmium Sulfide Sample.	6
1.3	Representative diagram for the Crystal Structure of Cadmium Sulfide CdS unit cell, (a) Wurtzite,(hcp), (b) Zinc Blend,(ccp) and (c) Rock Salt (ccp) phases.	7
1.4	Chemical Formula of Ethanol	12
2.1	Show the FTIR System	22
2.2	X-ray- Diffractometer	24
2.3	Diffraction of X-ray by Planes of Atoms.	25
2.4	Scheme of AFM device	29
2.5	The variation of Absorption Edge With Absorption Regions .	35
2.6	The transition Types	37
2.7	Schematic Diagram of Hall Effect	41
2.8	Atypical Response Curve of a Conductmetric Gas Sensor	49
3.1	Work Digram	53
3.2	Chemical Spray Pyrolysis System.	58
3.3	Show the Lambda (LIMF-10).	60
3.4	System FTIR	61
3.5	X-ray Diffraction System	62
3.6	Photograph Illustrates the AFM	63
3.7	SEM System.	64
3.8	UV-IR 1800 Spectrophotometer System	65
3.9	Masks pattern, which used in (a) Sensing Measurement (b) Hall Effect (c) Conductivity Measurement. D.C	66
310	Photograph Illustrates the Hall Effect	67
3.11	Photograph Illustrates the D.C Electrical Conductivity	67
3.12	Show the System Multi-Frequency LRC Meter.	68
3.13	Show the Image of the Electrometer Keithly Device.	69
3.14	Show the Detector Measurement Device	70
3.15	Diagram of Electrical Circuit of Gas Sensing Measurements	71
4.1a	Shows the Measurement of FTIR for the Prepared Thin Film CdS	75
4.1b	Shows the Measurement of FTIR for the Prepared Thin Film CdS:Co.	75

4.1c	Shows the Measurement of FTIR for the Prepared Thin Film CdS:Mg.	76
4.1d	Shows the Measurement of FTIR for the Prepared Thin Film CdS:Co:Mg.	76
4.2	Shows the Measurement of X-ray Diffraction for all Prepared Thin Films.	80
4.3a	Shows AFM Images of the Thin Film CdS	88
4.3b	Shows AFM Images of the Thin Film CdS:Co.	88
4-3c	Shows AFM Images of the Thin Film CdS:Mg.	89
4.3d	Shows AFM Images of the Thin Film CdS:Co:Mg.	89
4.4a	Shows an Image of the SEM Examination of the Thin Film CdS.	91
4.4b	Shows an Image of the SEM Examination of the Thin Film CdS:Co.	91
4.4c	Shows an Image of the SEM Examination of the Thin Film CdS:Mg.	92
4.4d	Shows an Image of the SEM Examination of the Thin Film CdS:Co:Mg.	92
4.5a	Shows EDX of the Prepared Thin Film CdS.	93
4.5b	Shows EDX of the Prepared Thin Film CdS:Co.	94
4.5c	Shows EDX of the Prepared Thin Film CdS:Mg.	94
4.5d	Shows EDX of the Prepared Thin Film CdS:Co:Mg.	95
4.6a	Shows the TEM Examination of the Thin Film CdS.	96
4.6b	Shows the TEM Examination of the Thin Film CdS:Co.	96
4.6c	Shows the TEM Examination of the Thin Film CdS:Mg.	97
4.6d	Shows the TEM Examination of the Thin Film CdS:Co:Mg.	97
4.7	Shows the Absorption Spectrum of all Prepared Thin Films as a Function of Wavelength.	100
4.8	Shows the Transmittance Spectrum of all Prepared Thin Films as a Function of Wavelength.	102
4.9	Shows the Reflectivity Spectrum of all Prepared Thin Films as a Function of Wavelength.	104
4.10	Shows the Absorption Coefficient Spectrum of all Prepared Thin Films as a Function of Wavelength.	107
4.11	Show the Direct Energy Gap of all Thin Films	108
4.12	Shows the Refractive Index Spectrum of all Prepared Thin Films as a Function of Wavelength.	110
4.13	Shows the Extinction Coefficient Spectrum of all Prepared Thin Films as a Function of Wavelength.	112
4.14	Shows the Real Dielectric Constant Spectrum of all Prepared Thin Films as a Function of Wavelength.	114

4.15	Shows the Imaginary dielectric Constant Spectrum of all Prepared Thin Films as a Function of Wavelength	116
4.16a	Measuring Current-Voltage of the Thin Film CdS	118
4.16b	Measuring Current-Voltage of the Thin Film CdS:Co	119
4.16c	Measuring Current-Voltage of the Thin Film CdS:Mg	119
4.16d	Measuring current-voltage of the thin film CdS:Co:Mg	120
4.17a	Shows the Electrical Conductivity as a Function of Temperature for the Prepared Thin Film CdS	123
4.17b	Shows the Electrical Conductivity as a Function of Temperature for the Prepared Thin Film CdS:Co	123
4.17c	Shows the electrical conductivity as a function of temperature for the prepared thin film CdS:Mg.	124
4.17d	Shows the electrical conductivity as a function of temperature for the prepared thin film CdS:Co:Mg.	124
4.18a	The Relationship Between Inδ and 1000/T for the CdS.	125
4.18b	The Relationship Between Inδ and 1000/T for the CdS:Co.	125
4.18c	The Relationship Between Inδ and 1000/T for the CdS:Mg.	126
4.18d	The Relationship Between Inδ and 1000/T for the CdS:Mg:Co	126
4.19a	Shows the Capacitance-Voltage Measurementp of the Thin Film CdS	130
4.19b	Shows the Capacitance-Voltage Measurementp of the Thin Film CdS:Co.	131
4.19c	Shows the Capacitance-Voltage Measurementp of the Thin Film CdS:Mg.	131
4.19d	Shows the Capacitance-Voltage Measurementp of the Thin Film CdS:Co:Mg.	132
4.20a	Shows the Relationship of the Inverse Square of the Capacitance with the Reverse Bias Voltage of the Thin Film CdS.	132
4.20b	Shows the Relationship of the Inverse Square of the Capacitance with the Reverse Bias Voltage of the Thin Film CdS:Co.	133
4.20c	Shows the Relationship of the Inverse Square of the Capacitance with the Reverse Bias Voltage of the Thin Film CdS:Mg.	133
4-20d	Shows the Relationship of the Inverse Square of the Capacitance with the Reverse Bias Voltage of the Thin Film CdS:Co:Mg.	134

4.21a	Shows a Current-Voltage Measurement of the CdS/Si	136
4.21b	Shows a Current-Voltage Measurement of the CdS:Co/Si	137
4.21c	Shows a Current-Voltage Measurement of the CdS:Mg/Si	137
4.21d	Shows a Current-Voltage Measurement of the CdS:Mg/Si	138
4.22a	Shows the Spectral Response as a Function of the Wavelength of the Prepared Detector CdS/Si	141
4.22b	Shows the Spectral Response as a Function of the Wavelength of the Prepared Detector CdS:Co/Si	142
4.22c	Shows the Spectral Response as a Function of the Wavelength of the Prepared Detector CdS:Mg/Si	142
4.22d	Shows the Spectral Response as a Function of the Wavelength of the Prepared Detector CdS:Co:Mg/Si	143
4.23a	Shows the Qualitative Detection as a Function of the Wavelength of the Prepared Detector CdS/Si	145
4.23b	Shows the Qualitative Detection as a Function of the Wavelength of the Prepared Detector CdS:Co/Si	145
4.23c	Shows the Qualitative Detection as a Function of the Wavelength of the Prepared Detector CdS:Mg/Si	146
4.23d	Shows the Qualitative Detection as a Function of the Wavelength of the Prepared Detector CdS:Co:Mg/Si	146
4.24a	Shows the Efficiency as a Function of the Wavelength of the Prepared Detector CdS/Si	148
4.24b	Shows the Efficiency as a Function of the Wavelength of the Prepared Detector CdS:Co/Si	149
4.24c	Shows the Efficiency as a Function of the Wavelength of the Prepared Detector CdS:Mg/Si	149
4.24d	Shows the Efficiency as a Function of the Wavelength of the Prepared Detector CdS:Co:Mg/Si	150
4.25a	Shows the Measurement of the Lifetime of the Charge Carriers of the Record Detector CdS/Si	152
4.25b	Shows the Measurement of the Lifetime of the Charge Carriers of the Record Detector CdS/Si	152
4.25c	Shows the Measurement of the Lifetime of the Charge Carriers of the Record Detector CdS/Si	153
4.25d	Shows the Measurement of the Lifetime of the Charge Carriers of the Record Detector CdS/Si	153
4.26a	Shows the Change in Resistance with the Response Time of Hydrogen Sulfide Gas to the Prepared Thin Film CdS	158
4.26b	Shows the Change in Resistance with the Response Time of Hydrogen Sulfide Gas to the Prepared Thin Film CdS:Co	158

4.26c	Shows the Change in Resistance with the Response Time of Hydrogen Sulfide Gas to the Prepared Thin Film CdS:Mg	159
4.26d	Shows the Change in Resistance with the Response Time of Hydrogen Sulfide Gas to the Prepared Thin Film CdS:Co:Mg	159
4.27a	Shows the Change in Resistance with the Response Time of Eathnoal Gas to the Prepared Thin Film CdS	160
4.27b	Shows the Change in Resistance with the Response Time of Eathnoal Gas to the Prepared Thin Film CdS:Co	160
4.27c	Shows the Change in Resistance with the Response Time of Eathnoal Gas to the Prepared Thin Film CdS:Mg	161
4.27d	Shows the Change in Resistance with the Response Time of Eathnoal Gas to the Prepared Thin Film CdS:Co:Mg	161
4.28a	Shows the Change in the Response and Recovery Time for all Thin Films by use H_2S Gas	162
4.28b	Shows the Change in the Response and Recovery Time for all Thin Films by use Eathanol Gas	162
4.29a	Show the Activity of the Films Against Bacteria Escherichia	164
4.29b	Show the Activity of the Films Against Bacteria Staphylococcus	165

List of tables

Table No.	***Description***	***Page***
1.1	Chemical and Physical properties of Cadmium Sulfied	6
3.1	Chemical Components used in the Present Study	52
3.2	Show Mixing Ratios for Preparing Thin Films	55
4.1	The Experimental and Therretical Values of Melting Point	73
4.2	Shows the Absorbance Packe of the all Thin Films	74
4.3a	Show the Result of X-ray of Thin Film CdS	82
4.3b	Show the Result of X-ray of Thin Film CdS:Co	83
4.3c	Show the Result of X-ray of Thin Film CdS:Mg	84
4.3d	Show the Result of X-ray of Thin Film CdS:Co:Mg	85
4.4	Shows the Values of the Grain Size, Mean Square Root, and Surface Roughness of the Prepared Thin Films	87
4.5	Shows the Grain Size Values for all Prepared Thin Films	90
4.6	Shows the Absorbance Values all Prepared Thin Films	100
4.7	Shows the Transmittance Values for all Prepared Thin Films	103
4.8	Shows the Reflectivity Values for all Prepared Thin Films	105
4.9	Shows the Absorption Coefficient Values for all Thin Films	107
4.10	The Direct Energy Gap Values of all Thin Films	109
4.11	Shows the Refractive Index Values for all Thin Films	110
4.12	Shows the Extinction Coefficient Values for all Thin Films	112
4.13	Shows the Real Dielectric Constant Values for all Thin Films	114

4.14	Shows the Imaginary Dielectric Constant Values for all Thin Films	116
4.15	Shows the Conductivity Values from a Current-Voltage Measurement	120
4.16	Shows the Activation Energy Values for all Prepared Thin Films	127
4.17	Shows the Results Obtained from the Hall Effect Measurement of the Perpared all Thin Films	128
4.18	Show the Internal Building Voltage of all Thin Films	130
4.19	Shows the Spectral Response Values for all the Prepared Reagents	141
4.20	Shows the Qualitative Detection Values for all the Prepared Reagents	144
4.21	Shows the Efficiency Values for all the Prepared Reagents	148
4.22	Shows the Values of the Life Time of Carriers for the Prepared Reagents	151
4.23	Shows the Sensitivity Values, Response and Recovery Time for all Prepared Thin Films	157
4.24	Shows the Values of the Diameters of the Inhibited Areas for all the Films Prepared Against Bacteria	164

CHAPTER ONE

INTRODUCTION AND REVIEW

CHAPTER TWO

THEORETICAL PART

CHAPTER THREE

EXPERIMENTAL PART

CHAPTER FOUR

RESULT AND DISCUSSION

Chapter Five

CONCLUSION AND SUGGESTIONS

REFERENCES

1.1 Introduction

The thin-film coating is a sheet of substance extending from a nanometer segment to micrometers in thickness. Since their characteristics of the film rely on the number of interrelated criteria and also on the process used to produce thin-film, they have very fascinating characteristics that are distinct from those of the bulk content they create[1,2].

Thin film is used for many broad applications, including its usage to shield such products from degradation, deterioration, and tear, transmitting or reflection in a certain region of wavelength, as well as in filters, color isolation, fire resistance, high-temperature superconductors, silicon sensors, anti-fog, and memory sensors. This ensures thin-film that has a broad variety of uses in both the civil and military sectors, the major uses gained from the development of thin films are electronic semiconductor and optical coatings [3, 4].

Semiconductor sensors, wireless communications, phones, rectifiers, integrated circuits, transistors, solar cells, photoconductors, light crystal display, magneto-optical memory, audio, and video device, light emitting diodes, portable disks, electro-optical coating, batteries, multilayer capacitors, flat-panel monitor, smart monitors, computer processors, a microelectromechanical system (MEMS), magneto-optical disks, lithography, and multi-functional new coatings, as well as other evolving cutting techniques, are the thin-film content divisions that have already been utilized in the process[5, 6].

Nanostructures material is a modern material type, with a large variety of non-linear optics, with unique characteristics in specific sectors [7]. In areas such as electrical, magnetic, optical, and mechanical systems, nanomaterials have a

technological application[8]. In recent years they have drawn tremendous attention and provide fascinating prospects in many structural applications [9].

The Nanoparticles matter is an interesting substance that can be performed by modifying its scale or structure, both optically and electronically. Semiconductors such as (CdSe, CdS, ZnS, ZnSe) with a scale of a few nanometers exhibit large excitation of all wavelengths, strong brightness, clear and symmetrical emissions, and excellent photostability. The semiconductor can also be utilized as biological fluorescent labels and as photodetectors photovoltaic devices [10].

1.2 Preparation Methods of Thin Films

The vast varieties of thin-film materials are the deposition processing and the manufacturing techniques, spectroscopic properties, and optical characterization probes that are used to produce the devices. Those techniques can be classified into two methods:

1) Physical methods

2) Chemical methods

The physical solution requires deposition techniques, which rely on the evaporation or ejection of the material from the source; i.e., sputtering or evaporation, although the methods of chemical focus on the physical properties, the main features of these tools and the thin-film technique are the relation between structure and property[6]. Because of its ease and simplicity, chemical precipitation approach is the most suitable process. While other approaches also require sophisticated equipment/instruments, considerable time periods, and extreme environmental conditions (temperature, pH, strain, etc.), Normally the chemical precipitation process requires basic laboratory instruments, ambient

factors, and a full hour trial .The formation of a separable solid material (component) from a solution requires chemical precipitation, either by transforming the substance into an insoluble state or by varying the solvent composition to decrease the solubility of the substance therein. This method is most widely used in both aqueous and non-aqueous media during the liquid phase[11].

1.3 The Spray Pyrolysis Technique

Spray pyrolysis was first used commercially more than half a century ago in 1947 as in U.S. patents registered for (H. A. McMaster and W. O. Lytle) to deposited conductive oxide films on heated glass substrates [12,13]. In the spray pyrolysis method, the starting material is required to be in solution form which when sprayed onto the preheated substrate, results in the formation of a thin film on the substrate. When the droplets of spray solution reach the hot substrate, and due to the pyrolytic decomposition character of the solution, they will be well adhered [14]. It considers as the easy and cheapest method for the preparation, thin film that used to prepare the films from materials which can dissolve and convert it to the solution -that spray by pyrolysis system, then the solution deposits on a substrate which heated by a significant temperature in which the reaction occurs in it to form a uniform film without prior. In this method the rate of pyrolysis and the thickness of the film can control by the spraying time [14].

The characteristic of the prepared films is the strongest sticking of the materials on the substrate and it is suitable for preparing films of conductor, semiconductor, and insulator [13]. H_2O is the most common convenient oxidizing agent, but it is usually helpful to dilute the solution by adding ethanol or propanol. N_2 ,O_2 , Ar , or air are generally used as carrier gases. The control parameters are

the substrate temperature, solution composition, the gas and solution flow rates, the deposition time and the nozzle to substrate distance [14].

1.3.1 The Main Features of Spray Pyrolysis Technique

Although the quality of the pyrolytic spraying thin film is less than the quality of other films that are prepared by most of the other ways, the spray pyrolysis technique has several features such as [15]:

i. It is an inexpensive process
ii. Low technological complexity.
iii. Possibility of large area fabrication.
iv. Producing a sufficiently high deposition rate.
v. Ease of processibility.
vi. There is no need for high purity materials.
vii. Thin films prepared by this method are adhesive.

1.3.2 Particular Considerations of the Chemically Sprayed Thin Films

A chemical reaction takes place when the falling drops reach the hot substrate, thus the prerequisite material will follow the above stages to form a thin film. Since there are many drops reaching the hot substrate, everyone will crystallize separately, and spotty film will form as shown in Fig. (1.1) [16].

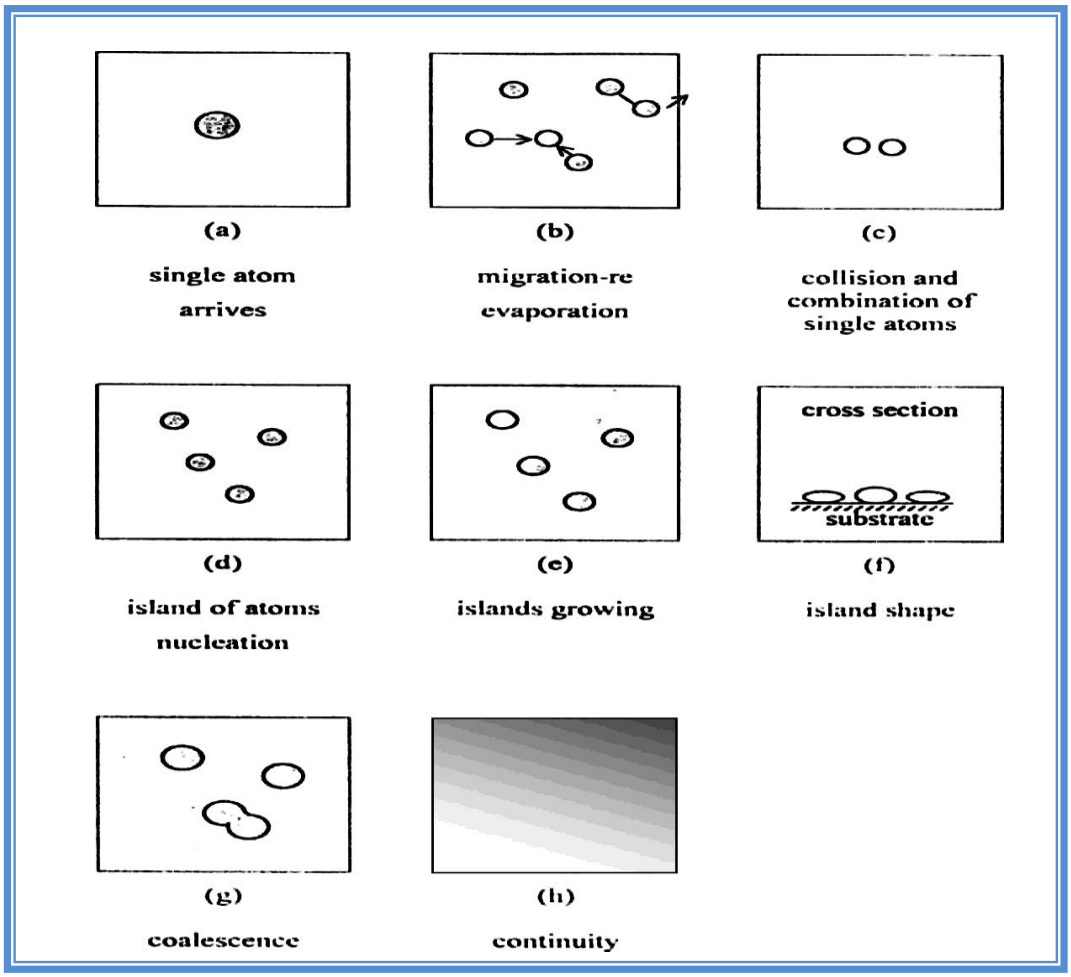

Fig.(1.1): Formation Stages of a Thin Film[16].

1.4 Properties of Cadmium Sulfide (CdS)

Cadmium sulfide is a semiconductor compound, it is a compound semiconductor II-VI with a yellow-orange color Fig. (1.2), three forms of crystal structures can be obtained, including wurtzite, zinc blend, and rock-salt phase with high pressure Fig. (1.3).

Wurtzite is among these most stable and simple to synthesize the three phases. In both bulk and nanocrystalline CdS was found Wurtzite phase, while cubic and rock-salt phases are found only in nanocrystalline Cadmium Sulfide[17, 18], the properties of CdS are summarized in Table (1.1) [19].

Fig.(1.2) : Cadmium Sulfide.

Table (1.1) : Chemical and physical properties of cadmium sulfide CdS [20].

Chemical Formula	CdS
Molecular Weight	144.477
Crystal structure	Cubic and Hexagonal structures
Lattice Constant	For Zincblende(**cubic**) 5.8320 Å Wurtzite(**hexagonal**) a=4.160; c=6.756
Energy gap	2.42 eV
Point of Melting	1750°C at 100 bar
Color	Yellow to orange
Density and phase	4.82 g/cm^3 solid
Semiconductor type	n-type semiconductor
group	II-VI
Conductivity type	n-type

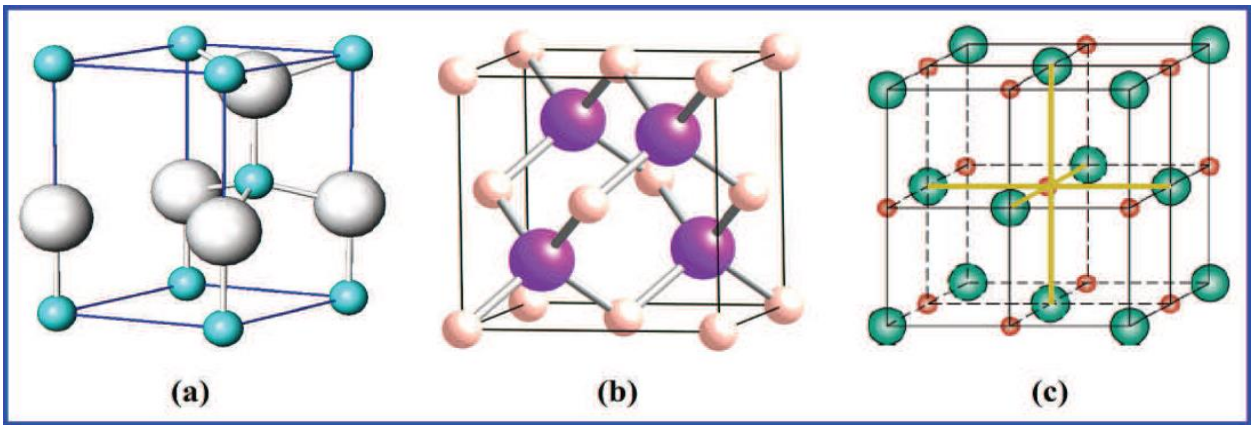

Fig.(1.3) : Representative diagram for the crystal structure of cadmium sulfide CdS unit cell, (a) Wurtzite,(hcp), (b) Zinc blend,(ccp) and (c) Rock salt (ccp) phases[21].

Bulk Cadmium sulfide has an energy bandgap of 2.42eV at 300 K with maximum absorption of 515 nm [21, 22], so that the crystal absorbs the blue zone of the spectrum [23], Its photoconductivity is high [24], It is also a dual semiconductor compound of great interest at the moment. This is because of this material's high potential uses as sensitive photodetectors, heterojunction diodes, solar cells, and semiconductor devices. The most significant explanation for utilizing CdS is the availability of this material as a chemical solution, direct bandgap, strong absorption coefficient, and its simplicity of having good quality as a thin film [25]. The chalcogenide families are being used as a window substrate for the Cd solar cells, they are also useful as buffer materials for solar cells and continue to be subjects to intense study due to their possible applications in high-efficiency CdS thin film nanostructures solar devices belonging to this family [26].

Cadmium Sulfide has appeared as a significant material owed to its uses in optical filter sand multilayer light-emitting diodes, photoelectron, thin-film field-effect transistors also that CdS is an n-type material and may appear in cubic and hexagonal structure [27]. And it usually has a sulfur deficiency, with a high

electron affinity in the sulfur vacancies. This makes CdS easy to obtain electrons, which makes the material n-type in nature. CdS produced electron-hole pairs are well separated by strongly localized electrodes [27].

1.5 Magnesium (Mg) and Cobalt (Co) Metals

Magnesium is an exceptionally lightweight metal. With a density of 1.74g/cm^3, magnesium is 1.6 and 4.5 times less dense than aluminum and steel, respectively[27,28]. The fracture toughness of magnesium is greater than ceramic biomaterials such as hydroxyapatite, while the elastic modulus and compressive yield strength of magnesium are closer to those of natural bone than is the case for other commonly used metallic implants. Moreover, magnesium is essential to human metabolism and is naturally found in bone tissue. It is the fourth most abundant cation in the human body, with an estimated 1mol of magnesium stored in the body of a normal 70kg adult, with approximately half of the total physiological magnesium stored in bone tissue [28].

Cobalt is a chemical element with the symbol Co and atomic number 27. Like nickel, cobalt is found in the Earth's crust only in a chemically combined form, save for small deposits found in alloys of natural meteoric iron [29]. The free element, produced by reductive smelting, is a hard, lustrous, silver-gray metal. Cobalt-based blue pigments (cobalt blue) have been used since ancient times for jewelry and paints, and to impart a distinctive blue tint to glass, but the color was later thought to be due to the known metal bismuth [30]. Miners had long used the name kobold ore (German for goblin ore) for some of the blue-pigment-producing minerals; they were so named because they were poor in known metals, and gave poisonous arsenic-containing fumes when smelted. In 1735, such ores were found

to be reducible to a new metal (the first discovered since ancient times), and this was ultimately named for the kobold [31].

1.6 Applications of Cadmium Sulfide (CdS)

CdS nanomaterials can be used in various life sectors due to their high stability, excellent electrical, chemical, and structural properties, affordability, ease of processing, and handling. CdS will demonstrate new optical and electrical properties, magnetic properties, and chemical and structural properties due to the quantity effects and surface effects that could be used in many significant technical applications. The arrangement of atoms across the surface is the major component of CdS semiconductor electrodes apart from the size/volume ratio [32]. Photo-conductive cells, light sensors, laser parts, optical waveguides, and non-linear hybrid optics, as well as CdS nanostructures thin film, are one of the most common materials used in electro-optic products [31].

CdS Nanostructures thin films are used to manufacture photocells that are sensitive to visible light and exhibit ratios of photoconductivity (resistance in dark / resistance in light) up to 10,000 for visible light. The CdS are also used as automated on / off switches on street lamps and are often seen in cameras and light meters. Also in heat-seeking rockets, the CdS were often used to detect targets [19] The most widely studied nanocrystalline semiconductor, due to its ideal bandage, as a photoanode in photoelectrochemical cells, long service life, substantial optical properties, high stability, ease of manufacture and various product applications [12]. Within the visual range of the electromagnetic spectrum, Cadmium Sulfide with a clear bandgap of 2.42 eV is regarded as an outstanding material for different optoelectronic applications. These are nonlinear optical instruments, LEDs, and solar cells that are used in applications [32,33].

1.7 Nanomaterials for Antibacterial Applications

Products manufactured at the micro- or nanoscale typically play distinctive roles, which have attracted considerable attention in recent years to their antibacterial properties. The bacterium killing process includes physical or chemical damage to organisms that exist on or within their surface and somewhat share antibiotic-like antibacterial mechanisms [31].

For several antibacterial formulations, the bacterial membrane is a major goal. Regular antibiotics can digest the membrane chemically, or prevent new cell walls from forming. In particular, direct contact between bacteria and nanomaterials can also damage the bacterial cell membrane due to the unique physicochemical characteristics of nanomaterials, such as surface topology, size, geometry, surface charging, and hydrophobicity. The antibacterial role of this synthetic surface lies in the physical damage to the bacterial cell membrane, irrespective of the nature of the germ (gram-negative or gram-positive) [32]. This technique is therefore successful for a broad range of applications with a reduced probability of triggering resistance. Sheet-like graphene oxide (GO), for example, has been shown to interact perpendicularly with the bacterial surface, splitting the lipid bilayer around the edges of the sheet. Individual nanoparticles with sharp edges can also achieve physical breakup of the bacterial cell membrane [33].

When compared with the micrometer bacteria, the interaction with the nanoparticles and even penetration of them into bacteria can also lead to severe damage to the cell wall [33].

1.8 Physical and Chemical Properties of Gas Hydrogen Sulfide

Hydrogen sulfide (H_2S) is the chemical compound with the chemical formula H_2S. It is a colorless, flammable, extremely hazardous gas with a “rotten

egg" smell. It occurs naturally in crude petroleum and natural gas, and can be produced by the breakdown of organic matter and human/ animal wastes. It is heavier than air and can collect in low-lying and enclosed, poorly ventilated areas such as basements, manholes and sewer lines.

Hydrogen sulfide is a gas included in the list of toxic and reactive highly hazardous chemicals from the Occupational Safety and Health Administration (OSHA) [34]. A concentration of 100 ppm of H_2S is considered immediately dangerous to life and health (IDLH). Since H_2S occurs in crude Petroleum, natural gas, and hot springs, the main activities in which occupational exposure is likely are petroleum and natural gas drilling, refining, and coke ovens. Additionally, since hydrogen sulfide is formed during the decay of organic matter, wastewater treatment plants, landfills, and tanneries are also important emitting sources [35]. Finally, the Kraft process employed in many paper mills, which involves using sodium hydroxide and sodium sulfide results in the emission of H_2S.

Besides the odor nuisance, often resulting from hydrogen sulfide emissions, human toxicology data is available, compiled from acute poisoning case reports and occupational exposures. Reported health effects in humans following exposure to hydrogen sulfide include death and respiratory, ocular,
Neurological, cardiovascular, metabolic, and reproductive effects. The lowest-observed-adverse-effect level (LOAEL) is as low as 2.8 mg/m3 (1.87 ppm) in asthmatic individuals for respiratory and Neurological effects [35].

1.9 Ethanol Gas

Ethanol, also called ethyl alcohol, pure alcohol, grain alcohol, or drinking alcohol, is a volatile, flammable, colorless liquid. It is a psychoactive drug, best known as the type of alcohol found in alcoholic beverages and in modern

thermometers. Ethanol is one of the oldest recreational drugs known to man. In common usage, it is often referred to simply as alcohol. Ethanol is abbreviated as EtOH (Methanol organic chemistry), using the common organic chemistry notation of representing the ethyl group (C_2H_5) with Ethanol [35] Fig. (1.4), shows a chemical formula of ethanol.

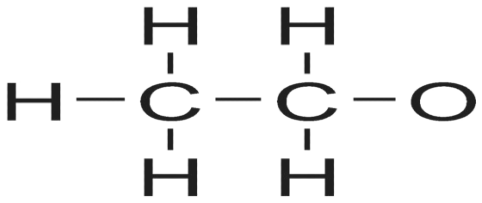

Fig (1.4) : Chemical formula of ethanol .

The direct oxidation of ethanol to acetic acid using chromic acid is given below.

$$C_2H_5OH + 2[O] \rightarrow CH_3COOH + H_2O$$

1.10 Literature Review

1- Pal, *et al.* In 2011[36] CdS nanowires nanorods, nanoflakes like nanostructures of different order diameters, lengths and morphologies changes by assisting of the surfactant Poly Ethylene Glycol with high uniformity and high yield by hydrothermal method. the XRD pattern show all the diffraction peaks corresponding to the hexagonal wurtzite phase of CdS. No impurity peaks were detected, indicating high purity product. In addition, the intense and sharp diffraction peaks (0 0 2) and (1 0 0), suggest that the obtained product is well crystallized. The absorption peak position in the UV–vis spectrum was found at 465 nm due to optically allowed transition of CdS between the electronic state in

the conduction band and hole state in the valence band. The band gap of CdS nanorods are higher than that of bulk CdS (515 nm), indicating a quantum size effect.

2- Abdullah M.A. Al-Hussam and Salah Abdul-Jabbar Jassim in 2012 investigationSynthesis, structure, and optical properties of CdS thin films nanoparticles prepared by chemical bath technique. CdS nanocrystalline thin films were deposited onto glass substrates by chemical bath deposition (CBD). The films deposited at 80 C for 6 h with two different concentrations of thiourea. The deposition parameters were optimized. The obtained films were characterized for structural and optical properties, X-ray diffraction patterns revealed that the films were nanocrystalline in nature with cubic structures. A blue shift in the band gap was observed in the UV–visible absorption spectra indicating the formation of nano particles of sizes between 3.826 and 8 nm[37].

3- Jing, *et al*. In 2013 [38] CdS nanoparticles have been prepared by solvothermal method. All the diffraction peaks can be assigned to cubic, and the mean crystalline size is ~ 10nm. Antibacterial activities of the CdS nanomaterials were evaluated by microcalorimetric method and the antibacterial activity of CdS nanoparticles against *Escherichia coli* was investigated. Suggested that the CdS nanoparticles may be applied as good antimicrobial at room temperature. Thus, the obtained CdS nanoparticles can be used as not only excellent photocatalyst for potential application in control of environmental organic pollutants but also as good antibacterial agents.

4- Li, *et al*. show in 2014[39] Preparation CdS/TiO_2 nanocomposites by combining chemical bath deposition (CBD) and microwave-assisted hydrothermal synthesis (MAHS) at 160 C for different microwave irradiation times. the XRD pattern of CdS/TiO_2 display CdS hexagonal phase. Average crystallite sizes of CdS/TiO_2 is increase with increase microwave irradiation time. the absorbance intensity of the CdS/TiO_2 nanocomposites in the visible light region reduced with increasing microwave exposure because of the size quantization effect. The CdS/TiO_2 nanocomposites showed better absorption of visible light the CdS/TiO_2 nanocomposites because the band-gap energy of CdS/TiO2 nanocomposites is different from those of CdS and TiO_2, resulting in an excellent synergistic effect between them.

5- Kumar, et al. In 2014 [40]. In this research, CdS nanoparticles (pure and 1 percent Cu doped) antibiotic sensitivity testing was performed against Staphylococcus aureus, Salmonella typhimurium, Pseudomonas aeruginosa, E. Klebsiella, and Coli pneumonia. The nanoparticles antimicrobial activity was measured using a well-diffusion test. And the activity was determined by inhibition zone measurement. Cu doped CdS nanoparticles were more effective with MIC range (0.078-0.52) mg. Compared with CdS nanoparticles of 0.15-0.83 mg / mL range.

6- Rajeshkumar, *et al.* they did a study in 2014 [41]. The study reveals that CdS nanoparticles have strong antimicrobial activity against various microorganisms. Where it is verified that CdS nanoparticles have a strong antibacterial ability and thus have a large potential in the preparation of biomedical applications crystalline nature of nanoparticles, The SEM images show that the synthesized CdS NPs are predominantly spherical with aggregates the morphology and size of the CdS nanoparticles were observed to be (50 – 180) nm. From XRD diffractometer show

the peaks at 2h values of 26.3 ºθ and integrated intensity values of (111) cubic CdS phase the average particle size of the cadmium sulfide nanocrystals was found to be 12 nm.

7- Conducted a study by Ayodhya, *et al*. in 2015[42]. Cadmium sulfide nanoparticles (CdS NPs) were successfully prepared using a sonochemical method by employing Schiff-base as a complexing agent. XRD patterns show that the synthesized CdS NPs have cubic structures. The XRD pattern analysis show CdS NPs belong to the face-center cubic phase with the zinc blende structure. The average particle sizes were in the range of (5–15) nm based on (111) crystal plane. The absorption peak of CdS NPs can be easily found in the visible region. The wavelength for pure CdS NPs was about 590 nm, corresponding to a band gap of 2.10 eV. A blue shift was observed for the uncapped and SB capped CdS NPS. It may be due to the size quantization effect; the grain size decrease leads to the energy gap wider. The prepared samples were test for their antibacterial activity against bacteria. The results showed that the SB capped CdS NPs are biologically active.

8- Abd-Elkader, *et al*. In 2015 [43] The thin CdS nanocrystalline films were It was prepared using a chemical bath deposition(CBD) Process at varying thicknesses (50,80 and100) nm. CdS Nanostructures thin films have the amazing antibacterial ability in dark and light and can be used as medical antimicrobial agents. The bandgap energy of prepared CdS Nanostructures thin films were observed to be 2.4eV, based on the optical measurements in the range of 300–2500 nm.

9- Jana, *et al.* [44] In this study, simple wet chemical synthesis method was employed to t In 2016 une the morphology of the CdS/ZnO nanocomposites by

changing the ratio of CdS to ZnO., XRD patterns show a cubic zinc blend structure and ZnO phase. The SEM image of CdS reveals that CdS nano seed of average size ~ 94 nm is the starting condition of the composite and the bare ZnO. Theantibacterial activity was tested against Escherichia coli, Staphylococcus aureus and Klebsiella pneumoniae in Muller Hinton agar plates by the well diffusion method, and results showed significant antibacterial activity in CdS/ZnO composite with the heights ZnO content in the samples (1:3 ratio).

10- Nisha, *et al In 2017 [45]*. for a short reaction time (an hour), CdS nanostructures were successfully designed using a simple solvothermal process at a low temperature (120 C), pure CdS sample displayed a rock - like structure with a rough surface and lot of striations (uneven surfaces). The XRD patterns of the uncapped CdS indexed to the cubic phase of CdS with lattice constants of a =5.820 Å, but, after presence piperazine significantly has been influenced the structure of CdS, transforming it to hexagonal phase. the observed absorption edges are blue shifted with respect to the bulk CdS.

11- Narasimman, et al. In 2017 [46]. The films Zr-doped CdS display excellent antibacterial activity against K. Pneumonia (gram−ve) bacteria which make them useful for applications in pharmaceutical devices, the antibacterial studies confirmed that the inhibition zone increased from 18 mm to 31mm with Zr doping.

12- Al Balushi, *et al. In 2018* [47]. CdS microspheres were synthesized through a hydrothermal method. The CdS microspheres were applied in the photocatalytic degradation of pharmaceutical compounds under visible light irradiation. The microspheres of about 0.5μm size were observed to have lower band gap energy of about 2.26 eV. XPS analysis confirmed the formation of impurity-free CdS

microspheres. XRD analysis results refer to the hexagonal CdS phase, the average grain size of the CdS was (39-26) nm. The band gaps of CdS decreased with an increase in the sulfur content from 2.27 eV to 2.25 eV. Sample showed no reduction in photodegradation efficiencies of pharmaceutical indicating high stability of synthesized sample.

13- Wang, *et al* in 2019 [48]. The CdS is made by hydrothermal synthesis, the CdS crystal size has been estimated at 9.2 nm from the XRD patterns of 3.0 % CdS and the CdS absorption edge is ~530 nm. And it was calculated that the bandgap of CdS from Kubelka-Munk was 2.41eV, also confirmed the visible light-driven Ag/CdS photocatalyst may be suitable for use in environmental applications.

14- Fatma Ibraheem and *et, al,* in 2020 study Tuning Paramagnetic effect of Co doped CdS diluted magnetic semiconductor quantum dots. Diluted magnetic semiconductor quantum dots (DMS-QDs) are known for their outstanding optical and magnetic properties. II–VI DMS-QDs, in particular, are interesting for spintronics, nonvolatile memory, and magneto-optical devices. Therefore, studying the optical and magnetic properties of different II-VI semiconductors doped with transition metal atoms is of great importance. Tuning II-VI QDs optical properties can be mastered by changing the QDs particle size and/or structure. However tuning the magnetic properties of DMS-QDs is still within trial and error verification, although it is crucial in targeting different applications in spintronics. We hereby demonstrate, the ability to tune the paramagnetic effect of homogeneous Co-doped CdS QDs following a co-precipitation synthesis route with different co_2+ concentrations. The structural, optical and magnetic properties have been comprehensively studied. The dopant cobalt atoms concentration and chemical-configuration were precisely tracked by X-ray photoemission

spectroscopy. Excitingly, the different Coconcentrations of (2, 5 and 10%) significantly improve the magnetic properties of the CdS QDs, which exhibit a paramagnetic concentration dependent effect. With 10% of Co atoms, we were able to achieve molar susceptibility, that is, the same value to that of pure CoS. Thus we could obtain the highest possible paramagnetic effect in the CdS semiconducting matrix exhibiting 2.76 eV band gap, i.e. in the visible range. This efficacious result encourages the use of the present method in preparing DMS-QDs materials targeting various spintronics applications[49].

15- ZHAO, *et al*. In 2020[50]. In this analysis, the nanoparticles of the CdS are generated using a single stage hydrothermal process and the hydrothermal temperature regulated (150,180,210 °C) is generated inside the nanoparticles of the CdS for 12 hours respectively. The peaks of XRD diffraction of the sample of 150 ° C correspond to hexagonal CdS and showed a pure hexagonal phase of the CdS obtained at 150 ° C. The 180 and 210 samples comprise both cubic and hexagonal phases. The nanoparticles in CdS are converted into a cubic hexagonal phase and the cubic phase content is steadily increasing, the sample crystallinity is increased as well, the reaction temperature to 210 raises the particle size range to (20-60) nm.

16- Zgura, *et al*. In 2020 [51]. In this research, ZnO – CdS composite powders synthesized by a simple process of chemical precipitation were characterized thoroughly. The biological characteristics of ZnO, CdS, and CdS composites such as their antioxidant ability, antibacterial activity, and cytotoxicity have been evaluated. The composites collected have had medium antioxidant effects, ***Escherichia coli*** biocidal activity, and no toxicity (less than 0.05 mg / mL in concentrations for low CdS composites) for human fibroblast cells.

17- Parisa Khani and *et, al* in 2021 study Improved chemical deposition of cobalt-doped CdS nanostructured thin films via nucleation-doping strategy: Surface and optical properties. In the majority of the chemical deposition techniques used for doping thin films, dopant cations are usually added to the reaction simultaneously with the host cations, or even after the formation of the host matrix. This approach reduces the dopant efficiency and reproducibility of dopant-related properties. In the present work, the nucleation-doping strategy usually used for colloidal nanocrystals is extended into the chemical bath deposition technique to prepare cobaltdoped CdS nanostructured thin films. The Co:CdS thin films showed %2.5 doping yield with a root-mean-square roughness below 22 nm and absorption edge below 510 nm. The PL emission spectra of the films revealed two distinct peaks at 490 and 530 nm, attributed to the recombination processes through excitonic states and impurity levels, respectively. Almost all the experimental variables were optimized to reach a partially single-emission peak at 530 nm, which can prove the successful incorporation of Co ions into CdS nanostructures[52].

1.11 Aim of the work

The principle aim of this research is to synthesis of cadmium sulfide modified cobalt acetate and maganisium acetate thin film utilizing spray deposition technique for the photo detection sensing and anti bacterial application. During the work, many objectires have been achieved:

1- To study the structural properties of prepared samples including SEM, AFM, TEM, FTIR, EDX and XRD.

2- To study the optical properties of the thin films using UV-Visible absorption spectrophotometer to inrestigate the optical parameters for the samples under investigation.

3- To study the electrical properties including I-V curve, DC conductivity, hall effect and C-V characteristics.

4- To apply the prepared sample as photodetectors, gas sensor and as active media for anti bacteria.

2.1 Introduction

This chapter includes a general description of the theoretical part of this study, physical concepts, scientific clarifications, relationships, and laws used to interpret the study results.

2.2 Structural Properties and Surface Morphology

The structural properties represented by X-ray diffraction, FTR and morphological measurements were studied including AFM ,SEM, EDX and TEM.

2.2.1 Fourier Transform Infrared (FTIR)

When molecules are irradiated with IR, the IR with the same wavelength resulting from the frequency of the vibration or other modes of the molecular bonds will be absorbed, and an absorption peak will appear at this wavelength or wave number. If we consider that the characteristic bonds of molecules are wavelength absorber, each absorber can absorb a characteristic wavelength to show an absorbance peak at the corresponding wavelength when an IR wave passes through the sample. Therefore, IR spectroscopy can be used to

1. Identify a known component present in an unknown sample.
2. Study the formation of new chemical bonds or substitutions.
3. Perform quantitative analysis for a component of interest.

In a classic dispersive IR spectrometer, an IR spectrum is measured byscanning the sample with a continuous wavelength range of IR. The setup of Fourier transform infrared (FTIR) spectrometer does not record the spectral intensity directly as a function of wavelength, but an interferogram (interfered waves) is taken instead. In an interferometer, a beam of light is split into two beams, beam 1 and 2 in Fig. (2.1) by a beam splitter [53,54].

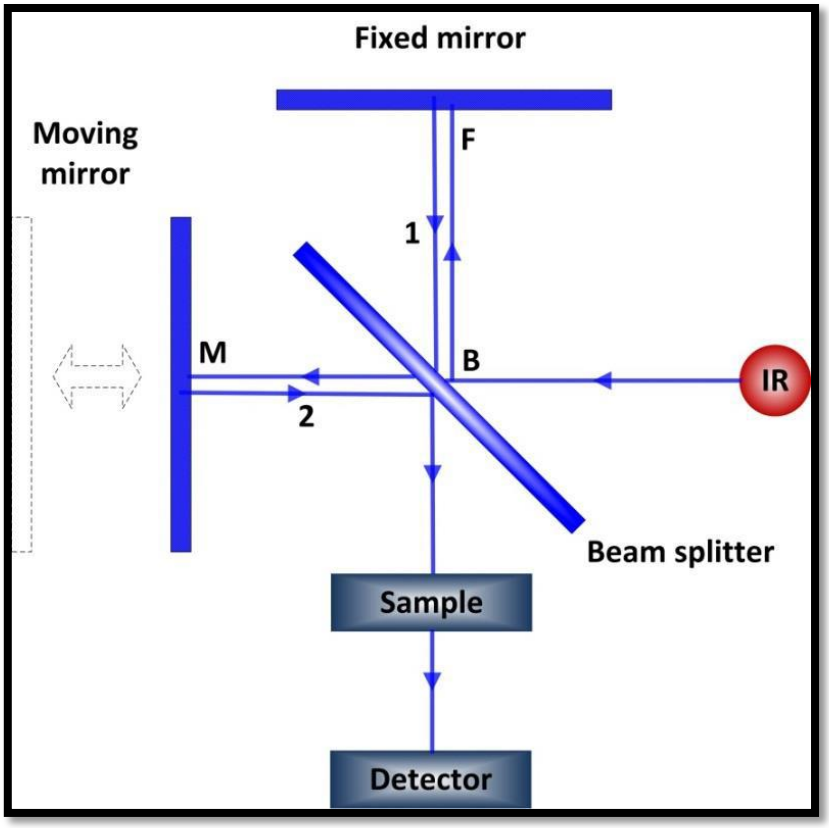

Fig.(2.1) : Show the FTIR system.

Where : Interferometer: IR, infrared radiation source; B, beam splitter; F, fixed mirror; M, moving mirror[55]

The beam splitter is designed to transmit half of the radiation and reflect the other half. Beam 1 travels a distance of 2FB, while beam 2 travels a distance of 2MB. Due to the movement of the moving mirror, the distance FB is different from the distance MB. This difference is called the optical path difference. Phase shift will occur depending on the optical path difference resulting in an interference pattern, or interferogram. The interference pattern varies with the displacement of the moving mirror resulting in constructive and destructive interface. This makes FTIR more powerful and faster than the conventional IR spectrometer because more energy will reach the sample than

that possible with a dispersive spectrometer. As a result, the signal to noise ratio can be increased [55].

2.2.2 X-Ray Diffraction (XRD) Spectroscopy:

X-ray diffraction is an important and flexible method for assessing and analyzing the crystal structure of nanomaterials. XRD approach analyses the average crystallographic structure in samples and assigns the necessary information on crystallite size, structural imperfections resulting from stress/strain, crystallographic defects (dislocations and defects) by precisely examining the diffraction line shape [56].

XRD is an effective tool used to classify and quantify the structural features of crystalline phases found in materials. XRD provides unprecedented precision in atomic distance measurement and is the technique of choice to determine strain conditions in thin films. XRD is contactless and non-destructive, making it suitable for in situ studies. The standard powder XRD system contains four primary components, such as X-ray source, specimen point, optical receipt and X-ray detector as shown in Fig. (2.2). The source and detector with their related optics lie at the middle of the diameter of the focusing circle and the sample stage. The angle between the plane of the specimen and X-ray source is θ, known as Bragg's angle and the angle between the projection of X-ray and the detector is 2θ [57].

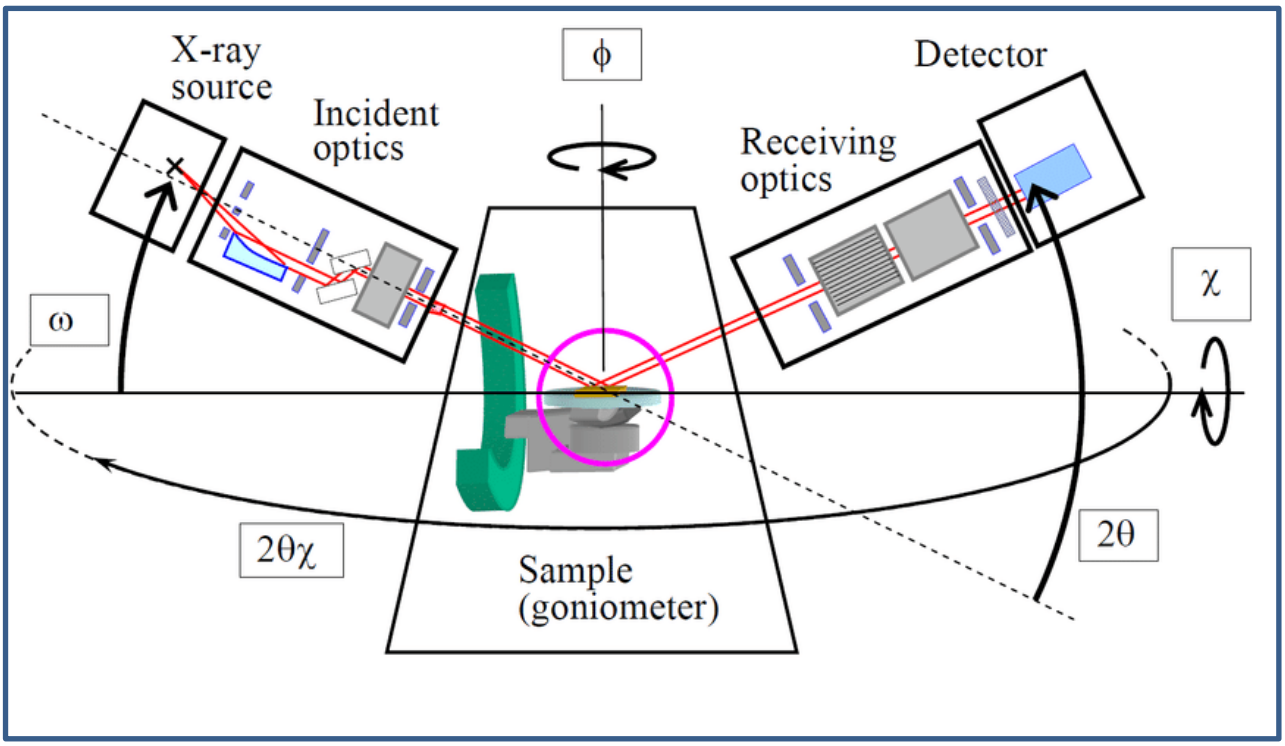

Fig.(2.2) : X-ray- Diffractometer [57].

X-rays are a type of electromagnetic radiation with high energies and short wavelengths according to the order of solid atomic spacing. When a pulse of x-rays affects a rigid object, part of this pulse can be distributed in all directions by the electrons connected to either atom or ion in the course of the beam [58]. For the XRD analysis, the sample holder holds thin powder samples, and the powder is intended to consist of randomly focused crystallites. If a beam of X-rays appears on the sample, X-rays are distributed around each atom in the sample. If the distributed beams are in phase, they constructively interact and optimize energy at this particular angle. Fig. (2.3) Shows the basic characteristics of the Bragg law x-ray diffractometer in which diffraction angle 2θ is the angle between the incident and diffracted x-rays when lattice planes are divided by a distance d in a clear crystal, the law of

Bragg applies to the wavelength (λ) of the reflected rays, the distance between the atomic planes (d_{hkl}), and the diffraction angle (θ) as follows:

$$n\lambda = 2d_{h\,k\,l}\ sin\ \theta \qquad (2.1)$$

As the Figure shows (2-2) [57].

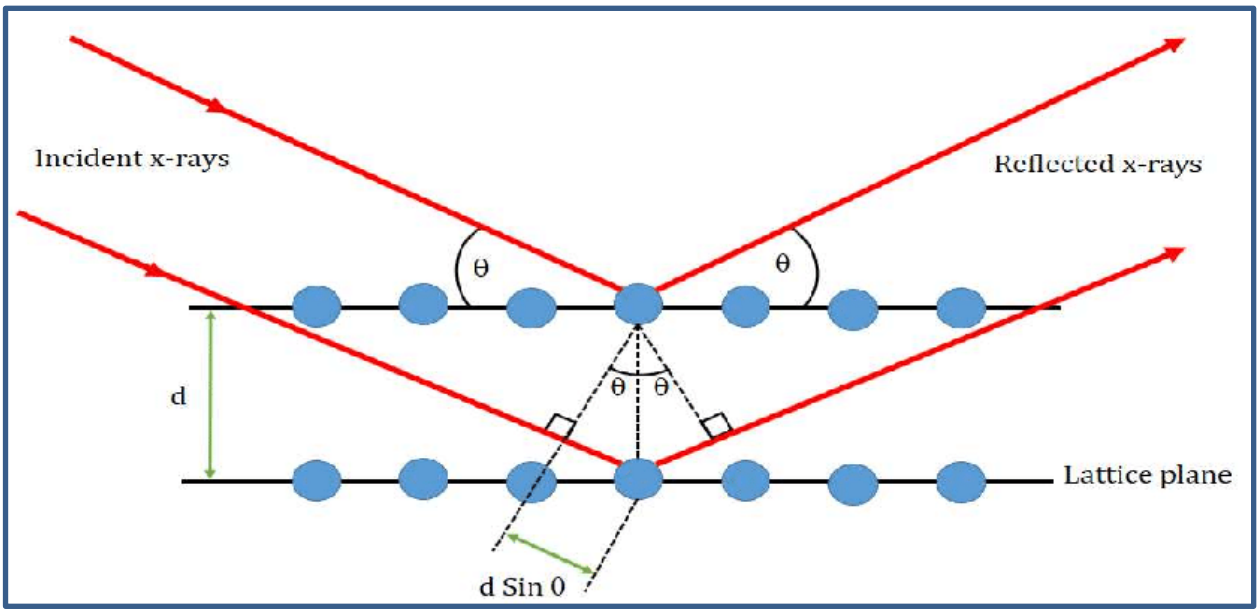

Fig.(2.3) : Diffraction of X-ray by planes of atoms [57].

Where (h k l) are Miller indices, (θ) is the scattering angle, and (λ) the wavelength of the incident X-ray radiation. The distance between two opposite and parallel atomic planes (i.e., the interplanar spacing $d_{h\,k\,l}$) is a function of the Miller indices (h, k, and l) as well as the lattice parameter(s). The Bragg Law, Eq. (2.1), is known as Bragg's law; when n equal 1. If Bragg's law is not satisfied, then the interference will be nonconstructive to yield a very low-intensity diffracted beam[59]. For example, for crystal structures that have cubic symmetry [60].

$$d_{hkl} = \frac{a}{\sqrt{h^2+k^2+l^2}} \qquad (2.2)$$

a: is the grid parameter (cell unit length).For crystal structures that have hexagonal symmetry, the interplanar spacing (d_{hkl}) can be calculated as[61].

$$\frac{1}{d_{hkl}^2} = \frac{4}{3}\left(\frac{h^2+hk+k^2}{a^2}\right) + \frac{l^2}{c^2} \qquad (2.3)$$

In the tetragonal scheme, the spacing equation naturally includes a and c, since these are usually not identical [60]

$$\frac{1}{d_{hkl}^2} = \frac{h^2+k^2}{a^2} + \frac{l^2}{c^2} \qquad (2.4)$$

And for orthorhombic[61]

$$\frac{1}{d_{hkl}^2} = \frac{h^2}{a^2} + \frac{k^2}{b^2} + \frac{l^2}{c^2} \qquad (2.5)$$

Where, Parameters a, b and c give the lengths of the crystallographic unit cell, and h, k, and l give of Miller indices.

The grain size(G.S or D) of a polycrystalline metal or alloy has pronounced effects on all of its properties, the most known is the rise of strength and stiffness following a reduction in grain size. This dependency on grain size properties measures grain size is important for the control of most metal forming operations. The word 'particle scale' is commonly used when the scale of the individual crystals is less than 10^{-5} cm (1000A) [61]. The crystallite size was measured using the Debye-Scherrer equation [57] which is given by:

$$D = \frac{k\lambda}{\beta cos\theta} \qquad (2.6)$$

Where (D) is the crystallite size, (β) is the full width at half maximum of a diffraction line located at an angle (θ) while (λ) is the X-ray diffraction wavelength of Cu Kα radiation (0.1514 nm and ķ are a Scherrer constant (0.94)), which depends on the peak width, the crystallite size distribution, and the crystallite shape.

The other structural property of the dislocation density (δ) is defined as the number of lines dislocation which cut the unit area in the crystal and can be determined using the formula below [62]:

$$\delta = \frac{1}{D^2} \qquad (2.7)$$

The crystalline number (N) was estimated with the formula [63]:

$$N = \frac{t}{D^3} \qquad (2.8)$$

Which, t is the thickness of the film. The lattice micro-strain (ε) is the percentage of deformation of the material during the growth of the film or arises from expansion or compression and can be calculated from the following relation [63]:

$$\varepsilon = \frac{\beta cos\theta}{4} \qquad (2.9)$$

Where (β) is the peak full-width half maximum, and (θ) is Braggs angle of the peaks.

2.2.3 Atomic Force Microscopy (AFM):

The atomic force microscope (AFM) also known as scanning force microscope – SFM) is a very high-resolution type of scanning probe microscopy, with demonstrated resolution of the order of a nanometer. An atomic force microscope is capable of imaging features as small in diameter as a carbon atom (0.25 nm) and as large as the cross section of a human hair (80 μm), what gives enormous possibilities for investigating samples surface topography and morphology [63,64].

The direct precursor to the AFM was the scanning tunneling microscope (STM), developed by Gerd Binnig and Heinrich Rohrer in the early 1980s. This achievement earned them the Nobel Prize in Physics in 1986. But the STM has one major disadvantage: it was possible to use it only with conducting specimens.

The first AFM delineated lateral features as small as 300Å. However, the considerable development in the AFM method application began after introduction of microcantilevers, new modified nano tips and new optical beam deflection methods in order to measure the tip movement and twist [65,66].

The beam–bounce method is now widely used as a result of the excellent work by Alexander and colleagues [67]. The new tips (the top of the tip can be built of the order of tens to hundreds atoms) and micro cantilevers, are usually made from silicon or silicon nitride [68]. The Scheme of AFM device is shown in Fig. (2.4).

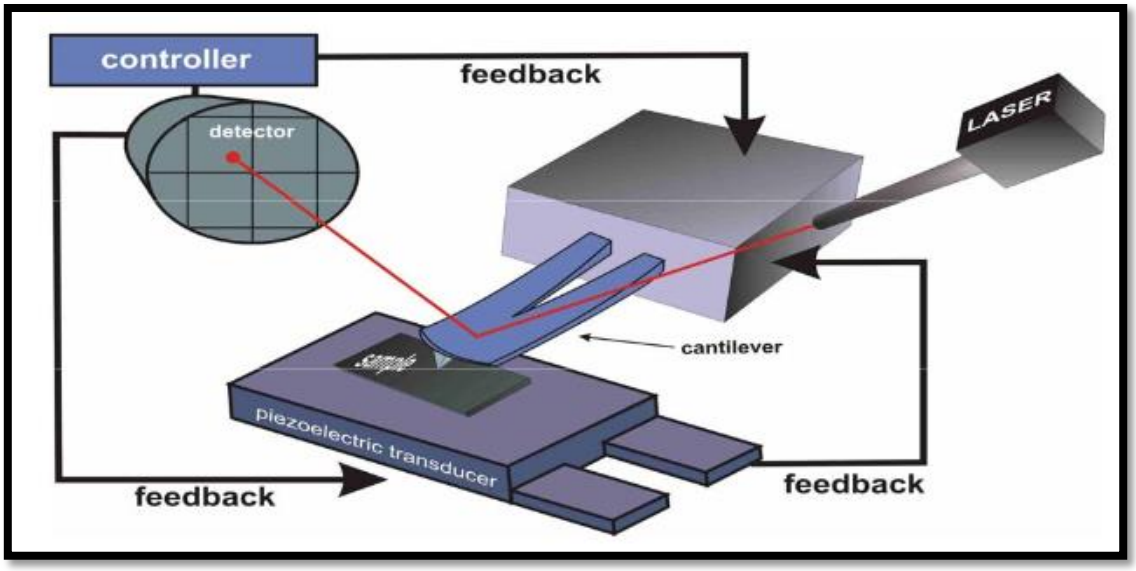

Fig.(2.4) : Scheme of AFM device [67].

2.2.4 Scaning Electron Microscopy (SEM):

Scanning electron microscope with energy dispersive X-ray spectroscopy (SEM/EDX) is the best known and most widely-used of the surface analytical techniques. High resolution images of surface topography, with excellent depth of field, are produced using a highly-focused, scanning (primary) electron beam. The primary electrons enter a surface with an energy of 0.5 – 30 kV and generate many low energy secondary electrons. The intensity of these secondary electrons is largely governed by the surface topography of the sample [68]. An image of the sample surface can thus be constructed by measuring secondary electron intensity as a function of the position of the scanning primary electron beam. High spatial resolution is possible because the primary electron beam can be focused to a very small spot (<10 nm). High sensitivity to topographic features on the outermost surface (< 5 nm) is achieved when using a primary electron beam with an energy of < 1 Kv [69].

In addition to low energy secondary electrons, back scattered electrons and X-rays are generated by primary electron bombardment. The intensity of backscattered electrons can be correlated to the atomic number of the element within the sampling volume. Hence, some qualitative elemental information can be obtained. The analysis of characteristic X-rays (EDX or EDS analysis) emitted from the sample gives more quantitative elemental information. Such X-ray analysis can be confined to analytical volumes as small as 1 cubic micron. SEM, accompanied by X-ray analysis, is considered a relatively rapid, inexpensive, and basically non-destructive approach to surface analysis. It is often used to survey surface analytical problems before proceeding to techniques that are more surface-sensitive and specialized [70, 71].

2.3 Optical Properties

The study of the optical properties of a material is interesting for many reasons. Firstly, the use of materials in optical applications such as interference filters, optical fibers, and a reflective coating requires accurate knowledge of their optical constants over a wide range of wavelengths. Secondly, the optical properties of all materials may be related to their atomic structure, electronic band structure and electrical properties [72,73].

2.3.1 Absorptance (A)

Absorption can be defined as the ratio between absorbed light intensity (I_A) by material and the incident intensity of light (I_o) [74].

$$A = \frac{I_A}{I_o} \qquad (2.10)$$

2.3.2 Transmittance (T)

Transmittance is given by the ratio of the intensity of the transmitting rays (I_T) through the film to the intensity of the incident rays (I_o) on it as follows [75]:

$$T = \frac{I_T}{I_o} \qquad (2.11)$$

We can also find a transmittance as a function of wavelength through the exponential relationship for both absorbance and transmittance which [76]:

$$A = \log\left(\frac{1}{T}\right) \qquad (2.12)$$

2.3.3 Reflectance (R)

Reflectance can be obtained from absorption and transmission spectrum in accordance to the law of conservation of energy by the relation [77]:

$$R + T + A = 1 \qquad (2.13)$$

2.3.4 Absorption Coefficient (α)

Absorption coefficientα can be defined as the relative rate of decrease in light intensity (I) along it is propagation path. According to Beer Lambert low [78]:

$$I - I_o \exp(\alpha t) \qquad (2.14)$$

Where

I: is the intensity of light in (W/cm^2)

t: is the thickness of thin film in (cm).

α can be given by [76]:

$$\alpha = \frac{2.303 \, . A}{t} \qquad (2.15)$$

In semiconductors, the absorption coefficient is a strong function of the wavelength or photon energy. Photon energy is given by [78]:

$$E = h\upsilon \qquad (2.16)$$

Where:

υ: frequency in (Hz.)

h: Plank constant (6.625×10^{-34} J.s).

2.3.5 Extinction Coefficient (k_o)

It represents the imaginary part of complex refractive index (n*) [79]:

$$n^* = n - ik_o \qquad (2.17)$$

Where :

n : the real part of refractive index , equal (c/v).

c : velocity of light in space

v : velocity of light in thin film

n*: complex refractive index which depends on the material type, crystal structure (grain size), crystal defects, stress in the crystal and extinction coefficient (k_o), is given by following equation [79]:

$$k_o = \frac{\alpha\,\lambda}{4\,\pi} \qquad (2.18)$$

Where:

λ : is the wavelength of incident photon rays.

α : absorption coefficient .

2.3.6 Refractive Index (n)

The refractive index can be defined as a ratio between velocity of light in vacuum (c), to its velocity inside the material. The value of refractive index (n) was calculated by using equation depending on the reflectance and extinction coefficient (k_o) as in the following equation [80] :

$$R = \frac{(n-1)^2 + k_o^2}{(n+1)^2 + k_o^2} \qquad (2.19)$$

The refractive index can be expressed through the following equation [80]:

$$n = \left[\left(\frac{1+R}{1-R}\right)^2 - (k_o^2 + 1)\right]^{\frac{1}{2}} + \frac{1+R}{1-R} \qquad (2.20)$$

2.3.7 Dielectric Constant

When a light incident on the atoms in the material, a reaction between incident radiation and the charges of the material will happen. This will lead to a polarization of the charges of the material [75]:

$$\varepsilon = \varepsilon_1 - i\varepsilon_2 \qquad (2.21)$$

Where:

ε_1 : is the real part of the complex dielectric constant,

ε_2 : is the imaginary part of it. For the calculation of the dielectric constant in its two parts, one can use the following expressions [75]:

$$\varepsilon_1 = n_o^2 - k_o^2 \qquad (2.22)$$

$$\varepsilon_2 = 2\, n_o\, k_o \qquad (2.23)$$

2.3.8 The Fundamental Absorption Edge

The fundamental absorption refers to band-to-band or to excitation transitions (i.e. the excitation of an electron from the valence band to the conduction band), it manifests itself by a rapid rise in absorption, which can be used to determine the energy gap of the semiconductor. Absorption regions can be classified into three regions [81].

a) High Absorption Region

This region is shown in Figure (2-5). In part (A), the magnitude of absorption coefficient (α) is larger or equal to (10^4 cm^{-1}). From this region the magnitude of forbidden optical energy gap ($E_g^{opt.}$) can be introduced.

b) Exponential Region

This region is shown as in Figure (2.4). In part (B) the value of absorption coefficient (α) is equal to (1 cm^{-1}<α< 10^4 cm^{-1}). It refers to the transition between the extended levels from the (V.B) to the local levels in the (C.B) and from local levels in (V.B) to extend the levels in (C.B) .

c) Low Absorption Region

The absorption coefficient (α) in this region is very small. It is about (α< 1 cm^{-1}). The transition happens in this region because of density of state in mobility gap resulted from faults structural, as in Fig. (2.4), the part (C).

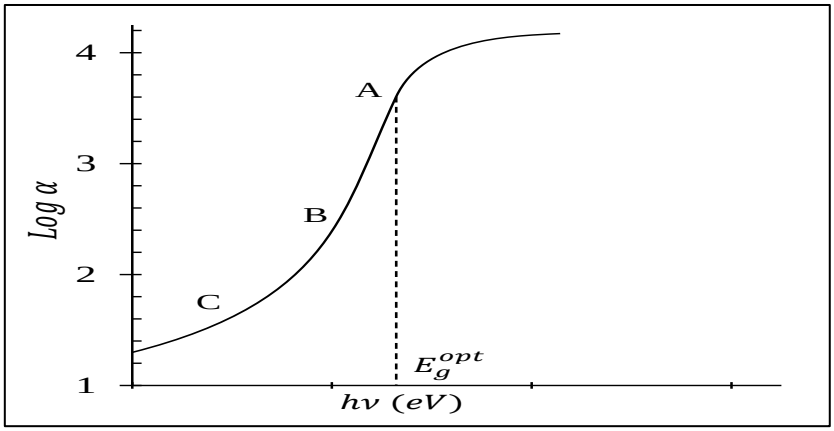

Fig. (2.5) : The variation of absorption edge with absorption regions [81].

2.3.9 Electronics Transition

The absorption of radiation, which leads to electronic transition between the valence and conduction bands, is split into direct and indirect transition as shown in Fig. (2.5) [82].

The direct transition happens in semiconductors when the bottom of (C.B) is exactly over the top of (V.B). This means that they have the same value of wave vector, i.e. ($\Delta K=0$) in this state the absorption appears when ($h\upsilon=E_g^{opt.}$). This transition type is required for the Law's of conservation of energy and momentum. These direct transitions have two types [81]:

a) Direct Allowed Transitions

The transition happens from the top points in the (V.B) and the bottom point in the (C.B), as shown in Figure (2-6.a).

b) Direct Forbidden Transitions

This transition happens from near top points of (V.B) and the bottom points of (C.B) [80], as shown in Figure (2-6.b).

The absorption coefficient for this transition type is given as relation:

$$(\alpha\, h\upsilon) = B\,(\, h\upsilon - E_g^{opt.})^r \qquad (2.24)$$

Where:

$E_g^{opt.}$: energy gap between direct transition.

B: constant depended on type of material.

r: exponeat constant, its value depended on type of transition:

r =1/2 for the allowed direct transition.

r =3/2 for the forbidden direct transition.

For the indirect transition in this case the bottom of (C.B) is not over the top of (V.B), in curve (E-K). The electron transits from (V.B) to (C.B) is not perpendicularly where the value of the wave vector of electron before and after the transition is not equal ($\Delta K \neq 0$). This transition type happens with helpful of particle called "Phonon", for conservation of the energy and momentum law. There are two types of indirect transitions, they are [83]:

c) Allowed Indirect Transitions

These transitions happen between the top of (V.B) and the bottom of (C.B) which is found in the difference region of (K-space) as in Figure (2-6.c).

d) Forbidden Indirect Transitions

These transitions happen between the nearest points on the top of (V.B) and near points in the bottom of (C.B) [83], as shown in Figure (2-6.d). The absorption coefficient for transition with a photon absorption is given by:

$$\alpha\, h\upsilon = B\,(\, h\upsilon - E_g^{opt.} \pm E_{ph.})^r \qquad (2.25)$$

Where:

$E_{ph.}$: energy of the phonon, is (-) when phonon absorption, and (+) when photon emission.

r = 2 for the allowed indirect transition.

r = 3 for the forbidden indirect transition.

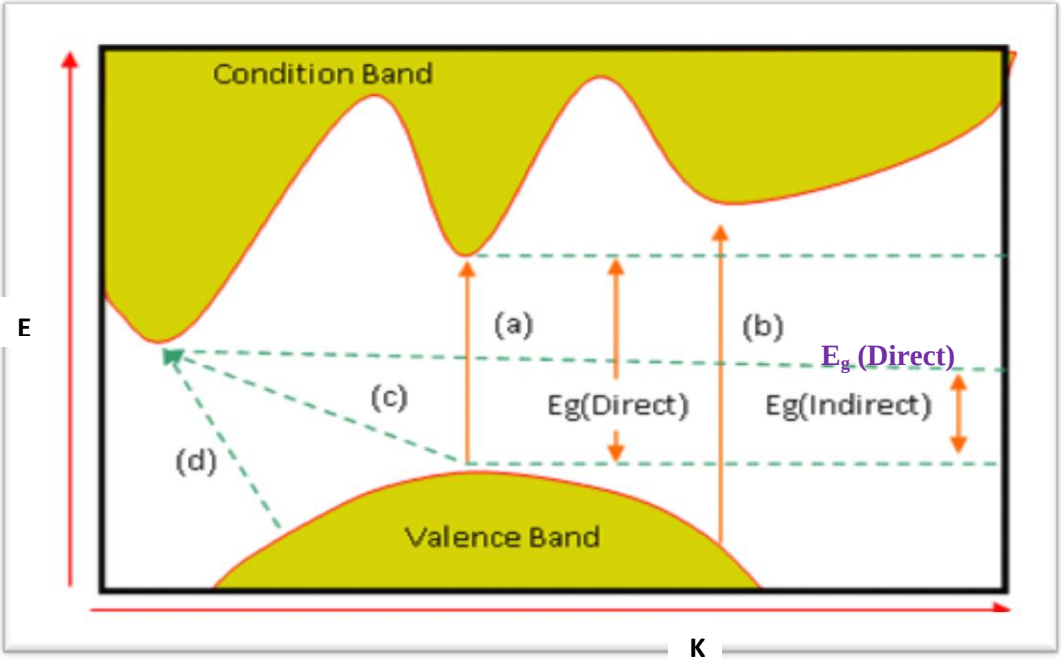

Fig.(2.6) : The transition types [83].

(a) Allowed direct transition. **(c) Allowed indirect transition.**

(b) Forbidden direct transition. **(d) Forbidden indirect transition.**

2.4 Electrical Properties:

2.4.1 D.C Conductivity

The variation of conductivity with temperature (T) is the main tool in investigation properties of semiconductors. It is very useful to determine the extrinsic range the activation energies of impurity centers and in the intrinsic

range the main energy gap [84]. In case of semiconductors the resistance rapidly decreases with increasing the temperature. The empirical formula connecting the resistance and absolute temperature valid within a limited temperature range is given by:

$$R(T) = R_o \exp -(\beta / T) \qquad (2\text{-}26)$$

where (R_o) is the resistance at (0K) and ('β) is the temperature coefficient , is constant characteristic for each semiconducting material, this formula may be written for conductivity[85]:

$$\sigma = \sigma_o \exp(-E_a / k_B T) \qquad (2\text{-}27)$$

This equation is basically derived to give the change of the electrical conductivity with temperature for most cases of intrinsic semiconductors. The quantity (E_a) of a given semiconductor is called activation energy, T is the absolute temperature, (k_B) is the Boltzmann constant , (σ_o) is the maximum electrical conductivity, when T → very large.

(σ_o) is not constant but it varies with $T^{3/2}$ according to the follows equation [85]:

$$\sigma_o = const(\mu_e + \mu_h) T^{3/2} \qquad (2\text{-}28)$$

where (μ_e) and (μ_p) are electron and hole mobility respectively. That can state ohm's law in terms of the shape independent resistivity (ρ) or conductivity (σ) [86].

$$E = p\ J \qquad (2\text{-}29)$$

E: is the electrical field and J is the current density .A good general picture of the physical behavior of a semiconductor can be obtained as following :Let there is n electrons concentration in the conduction band and (p) holes concentration in the valence band.

The current density (J) is given by the equation [87].

$$J = e(n\mu_e + p\mu_h)\varepsilon \qquad (2\text{-}30)$$

so that

$$\sigma = e(n\mu_e + p\mu_h) \qquad (2\text{-}31)$$

The resistivity (ρ) of the films is calculated by using the following equation [87]:

$$\rho = \frac{RA}{L} \qquad (2\text{-}32)$$

Where (R) is the sample resistance, A is the cross section area of the film and L is the distance between the electrodes. The conductivity of the films was determined from the relation:

$$\sigma_{D.C} = \frac{1}{\rho} \qquad (2\text{-}33)$$

The activation energies could be calculated from the plot of lnσ versus 1000/T according to equation (2-27).

2.4.2 Hall Effect

The Hall effect is one of the rich sources of information about the conduction properties of semiconductors. The mobility and carrier concentration can be obtained from the Hall constant in conjunction with the resistivity [88]. Hall effect measurements have been used extensively in determining majority carrier concentrations and their mobilities in bulk and thin-film materials. Two-dimensional electron gases formed in quantum wells and at heterojunction interfaces have been investigated by this technique. Electric and magnetic fields are essential to observe this effect [85]. The ratio of the voltage created is divided by the current and the magnetic field (I×B) product by the element thickness, is called Hall coefficient (R_H) which is known as a characteristic of the material from which the conductor is made, as its value depends on the type, number and properties of the charge carriers that constitute the current [84]. When a constant current (i) follows along the x-axis from left to right in the presence of a z-directional magnetic field (B); electrons are subjected to the Lorentz force initially, and they drift toward the negative y-axis, resulting an excess surface electrical charge on the side of the sample and causing a transverse voltage; this transverse voltage is known as the Hall voltage (V_H) as shown in Fig. (2.7) [88].

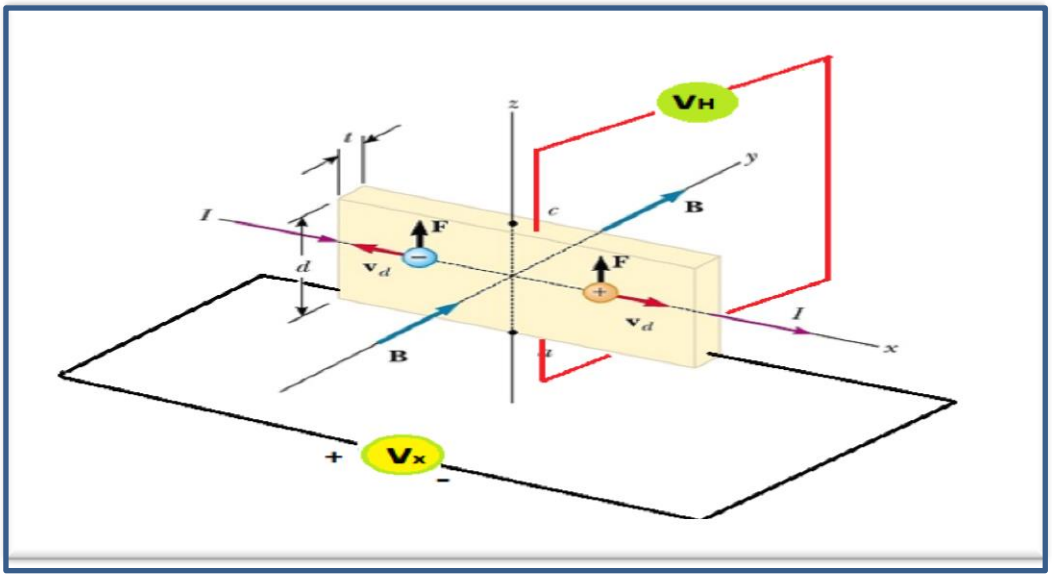

Fig. (2.7) : Schematic diagram of hall effect [84].

The Hall coefficient (R_H) is determined by measuring the Hall voltage that generates the Hall field across the sample of thickness (t), by [88]:

$$R_H = \frac{V_H}{i} \cdot \frac{t}{B} \qquad (2.34)$$

Carrier concentration can be determined by using the relation [88]:

$$n_H = \frac{-1}{qR_H} \quad \text{for electrons} \qquad (2.35)$$

or

$$n_H = \frac{+1}{qR_H} \quad \text{for holes} \qquad (2.36)$$

With the directions of control current and magnetic field illustrated in Figure (2-7) , the charge carriers, which produce the current are deflected to the front edge of the sample, therefore, the current is mainly due to electrons (as in the case of an n-type sample) the front edge becomes negatively charged. In the case of holes conduction (p-type sample) it becomes positively charged [89].

So from the sign of the Hall coefficient (R_H) in the equation (2-34), we can determine the type of semiconductor that we have been using.

From (σ) and (R_H) we may determine the Hall mobility [89].

$$\mu_H = \sigma / R_H \qquad (2.37)$$

or

$$\mu_H = \frac{\sigma}{n_e q} \qquad (2.38)$$

Where (n_e) represents electron density.

2.5 Heterojunction (HJ)

A heterojunction is a junction formed between two different energy gap values semiconductors materials, dielectric constant, electron affinity and work function as well as a difference in lattice constant .If the two semiconductors involved have similar type of conductivity, then the junction is called isotype HJ (p-p) or (n-n), otherwise it is called anisotype HJ (n- p) or (p- n) [90].

Anderson fabricated the first isotype and anisotype HJ in (1960). He also presented a more detailed model for the arrangement of the energy bonds near the interface between the two semiconductors. In 1951, Shockley proposed the abrupt heterojunction to be used as an efficient emitter-base junction in a bipolar transistor. Since then, heterojunctions have been extensively studied, and many important applications have been made, among them light – emitter diode, photodetector, solar cell, and gas sensor [91]. HJ can be classified as abrupt or graded according to the distance during which the transition from one material to the other is completed near the interface. The abrupt HJ are classified in to two types , abrupt anisotype HJ and abrupt isotype HJ, Oldham and Milne's have constructed a model for HJ in which

the effect of junction grading (i.e. continuous variation of energy gap and electron affinity through the transition region) during fabrication has been included [92].

2.6 Electrical Properties of Heterojunctions

The electrical properties which characterize a heterojunction are the current – voltage and the capacitance –voltage characteristics. In fact, these properties which do not only yield information regarding the band structure of a heterojunction (i.e. the type of heterojunction and the built –in junction potential) but also enable one to determine its device usefulness. Since these properties of a heterojunction depend strongly on the method of formation and the condition of preparation [93].

2.6.1 Capacitance -Voltage Characteristics

The measurement of the junction capacitance (C= dQ/dV) as a function of reverse bias is often used as a powerful experimental technique for the analysis of the depletion region potential and the charge distribution in a heterojunction. The expression of the capacitance per unit area under reverse bias voltage can be written as [94].

$$C = \frac{dq}{dV} = \frac{\varepsilon_s A_j}{W} \qquad (2\text{-}39)$$

where ε_s is the semiconductor permittivity of the two semiconductor materials, V applied voltage, W depletion width layer, and A_j is the effective area of the junction. The cross point ($1/C^2=0$) of the ($1/C^2$-V) curve represents the built-in potential of the heterojunction, the charge-carrier density N_d and width of the depletion layer for both devices are calculated by the following equations [94].

$$N_d = \frac{2}{q\varepsilon_s}[dV/d(1/C^2)] \quad (2\text{-}40)$$

where q charge of electron, and it equals (1.6×10^{-19} C).

$$w = \left[\frac{2\varepsilon_s V_{bi}}{qN_d}\right]^{1/2} \quad (2\text{-}41)$$

where V_{bi} built-in potential, is calculated by the following equation:

$$V_{bi} = V_{a+}\ \frac{kT}{q} \quad (2\text{-}42)$$

where V_a is the applied voltage.

2.6.2 Dark Current–Voltage Characteristics

These measurements usually provide a valuable source of information about the junction properties, such as the rectification ratio (R_F), the ratio of the forward current to the reverse current at a certain applied voltage is defined as the rectification factor, tunneling factor (γ), the barrier height, the reverse saturation current density, and the ideality factor (η) [93]. The total dark current of the heterojunctions can be represented as a sum of several components such as generation-recombination current, diffusion current, tunneling current, surface leakage current, and emission current. If generation-recombination and diffusion mechanisms are dominant, then the dark current (I_d) obeys the following formula [95].

$$I_d = I_s[e^{-qV/\eta k_B T} - 1] \quad (2\text{-}43)$$

where I_s is the reverse saturation current and is given as:

$$I_s = A^* T^2 e^{-q\Phi_B/\eta k_B T} \quad (2\text{-}44)$$

where A^* is Richardson constant, V is the applied voltage, Φ_B is barrier height, and T is the temperature in Kelvin. The ideality factor (β) is calculated from the (I-V) characteristics by using the following equation [96].

$$\beta = \frac{q}{k_B T} \frac{V}{ln\frac{I_S}{I}} \qquad (2\text{-}45)$$

The value of the (β) is determined from the slope of the straight line region of the forward bias logarithm of the current as a function of the applied voltage.

2.6.3 Current–Voltage Characteristics Under Illumination

Optoelectronic properties of heterojunctions were studied under illumination , it can be classified into two groups, one which deals with the generation of photocurrent due to the absorption of photons while the other deals with the emission of photons as a result of electronic excitation in heterojunctions. There are two important absorption processes which often have an influence on the photoelectric properties of heterojunctions: the creation of free electrons or holes (i.e. photo-excitation of an impurity or interface state) and of free electron - hole pairs (i.e. electron transition from the valence band into the conduction band). The free carriers generated by these processes at the interface or within a diffusion length from it, in the two semiconductors forming a heterojunction, give rise to photocurrents in the heterojunction [97].

2.7 Photodetector Characteristics

Photodetectors are characterized by certain key parameters. Among them are responsivity, quantum efficiency, signal to noise ratio, noise equivalent power and detectivity. There are important parameters that characterize and specify the detector in detail as included below:

2.7.1 Responsivity (R_λ)

Responsivity is defined as the ratio between the electrical signal output (voltage or current) to the incident radiation power or is defined as the r.m.s. signal voltage to the r.m.s. value of the incident radiation power. The responsivity for monochromatic light of wavelength incident normally is given by [98].

$$R_\lambda = \frac{I_{ph}}{P_{in}} \quad \text{or} \quad R_\lambda = \frac{V}{P_{in}} \qquad (2.46)$$

The responsivity which defines the wavelength range of interest or the responsivity to monochromatic radiation of λ is called spectral response.

2.7.2 *Quantum Efficiency (η)*

The responsivity may also be expressed as a Quantum efficiency (η). When, a detector absorbs a photon, its quantum energy transfers to a single electron with the surface. Therefore, the quantum efficiency (η) of radiation detector is defined as the number of collected electrons/number of incident electrons . It can be expressed [99].

$$\eta = (I_{ph}/e).(h\upsilon/p_{in}) \qquad (2.47)$$

$$\eta = R_\lambda . \ (h\upsilon/e) \qquad (2.48)$$

The quantum efficiency for an ideal detector is unity.

2.7.3 *Detectivity (D) and Specific Detectivity (D*)*

The detectivity (D) is defined as the signal to noise ratio per incident radiation power and it is the reciprocal of the noise equivalent power (NEP), it is defined as [98].

$D=1/NEP=R_\lambda/I_n \quad Watt^{-1}$ (2.49)

Specific Delectivity D*(normalized detectivity), the detector signal to noise ratio when 1Watt of the optical power is incident on the detector with optical area $1cm^2$ and the noise could measured with a band width of 1Hz. It is used because it is normally independent of the size of the detector and the bandwidth of the measurement circuit while D depends on both. The peak value of D* that occurs at wavelength somewhat below λ_0, is zero above λ_0, since the detector generates no signal, and it is defined as[98].

$D^*=D\,(A\,\Delta F)^{1/2} \quad cm.\,Hz^{1/2}/Wat$ (2.50)

Or

$D^*=R_\lambda(A\,\Delta F)^{1/2}/I_n$ (2.51)

2.8 Gas Sensor Characteristics

2.8.1 The Sensitivity

Sensitivity can be defined as response of a gas sensor per unit change in the gas concentration. In the case of resistive gas sensors, it is defined as the relative change in resistance or conductivity of the thin film. It is the ratio of the change in the resistance (approximately to 90 %) of the thin film in air to the change in resistance in particular gas atmosphere. The sensitivity is given by the equation (2-54) for p-type semiconductor with oxidizing gas and equation (2-55) for reducing gas [100]:

$$\text{Sensitivity (S)} = \frac{\Delta R}{R_a} = \left|\frac{R_a - R_g}{R_a}\right| \times 100\% \qquad (2-52)$$

$$\text{Sensitivity (S)} = \frac{\Delta R}{R_g} = \left|\frac{R_g - R_a}{R_g}\right| \times 100\% \qquad (2-53)$$

Where:

R_a is resistance of the film sensor in air presence.

R_g is resistance of the film sensor in a gas presence.

Although it can be calculated from current as in the relation [100]:

$$S = \frac{I_g - I_a}{I_a} \times 100\% \qquad (2-54)$$

I_a is the sample current measured at ambient environment , I_g is that under the test gas. The sensitivity is highly dependent on film thickness, operating temperature, presence of additives and crystallite size.

2.8.2 Response Time

It is the time interval over which the resistance of the sensor material attains a fixed percentage (usually 90 %) of final value when the sensor is exposed to the full scale concentration of the gas. A small value of the response time is highly desirable in application such as detection of flammable or combustible gases to prevent fire [100].

2.8.3 Recovery Time

It is the time interval above which sensor resistance reduced to (10 %) of the saturation rate when the target gas is switched off and the sensor sited in artificial (or reference) air a sensor should have a small recovery time so that it can be ready for the next detection [100].

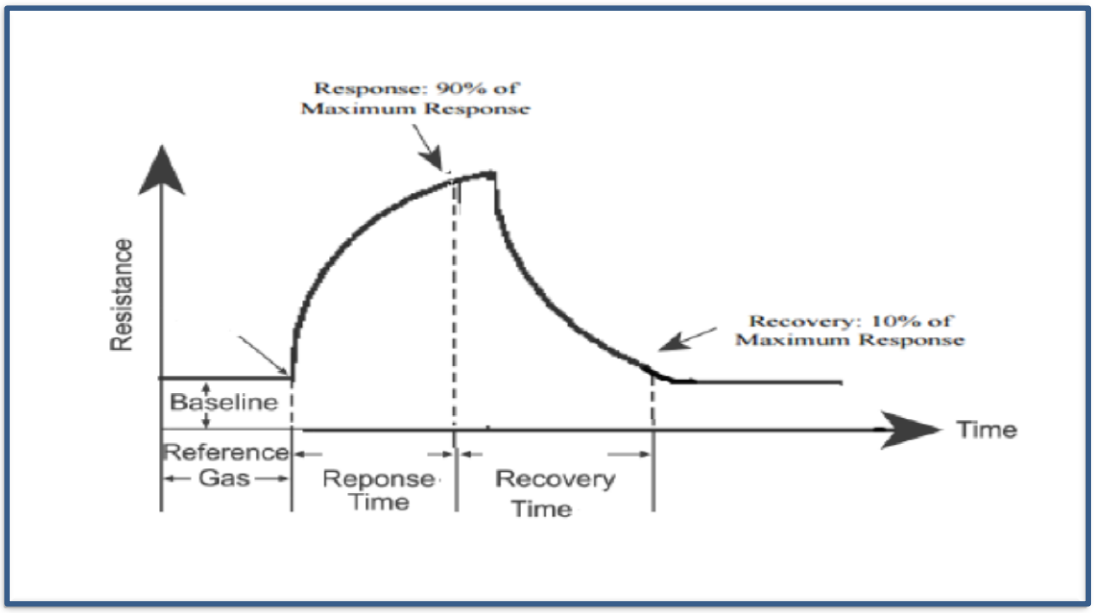

Fig.(2.8) : Atypical response curve of a conductmetric gas sensor [100].

2.9 The Classifications of Bacteria

Bacteria are microscopic living organisms that have only one cell. The word for just one is "bacterium." Millions (if not billions) of different types of bacteria can be found all over the world, including in your body[101,102]. They're on your skin and in your airways and mouth. They're also in your digestive system, reproductive system and urinary tract. Scientists estimate you have 10 times more bacterial cells than human cells in your body. Scientists classify bacteria as gram-positive or gram-negative based on which color they turn under a Gram stain. They stain differently because their cell walls are different[103]. "Positive" and "negative" don't mean "good" or "bad."

A-Gram-Positive Bacteria

look blue to purple under a Gram stain. Examples of gram-positive bacteria include: • Corynebacterium. • Clostridium• Listeria etal.

B-Gram-Negative Bacteria

Bacteria look red to pink under a Gram stain. They cause different types of infections than gram-positive bacteria. They also need different types of antibiotics to treat them. Examples of gram-negative bacteria include• Pseudomonas. • Proteus. • Klebsiella etal.

2.10 Staphylococcus Aureus

is a Gram-positive (purple stain by Gram stain) bacteria that is spheroid shaped and tends to be arranged in clusters that are described as "grape-like"Infections are common both in community-acquired as well as hospital-acquired settings and treatment remains challenging to manage due to the emergence of multi-drug resistant strains such as MRSA (Methicillin-Resistant Staphylococcus aureus) AND found in the environment and is also found in normal human flora, located on the skin and mucous membranes (most often the nasal area) of most healthy individuals *S. aureus* does not normally cause infection on healthy skin; however, if it is allowed to enter the bloodstream or internal tissues, these bacteria may cause a variety of potentially serious infections [103].

In general, penicillin remains the drug of choice if isolates are sensitive (MSSA, or methicillin sensitive S. aureus strains) and vancomycin for MRSA strains [104].

Staphylococcus is the main colonists of the medical devices and allows the biological growth of the growth on which staphylococcus depends on the infections associated with the stability due to increased tolerance of antibiotics and immunological evasion properties. Thus, the only possible

treatment is the surgical replacement of the affected devices, which causes heavy physical, emotional and financial burdens Alternative strategies that are followed up to develop new biological materials, vital coating, vital membranes dispersal, vaccines, and bacteria. However, each one approach represents a problem for various reasons and an effective vital treatment in general that may pass the requirements of food and drug management (FDA) not on the horizon However, given that the infection associated with the pi - film on medical devices represents a general health problem that has not been solved, with more intense basic and laris research around the infection of the medical system through staphylococcus and other pathogens associated with it urgently required [105].

3.1 Introduction

This chapter includes a presentation of the practical steps, starting from the preparation of the cadmium sulfide compound and the addition of cobalt acetate and magnesium acetate to the sample preparation process using the thermal chemical spraying technique, as well as conducting structural, optical and electrical measurements, and employing them in the applications of the photodetector, gas sensor, and antibacterial.

3.2 The Materials Used in This Work

High purity materials were used from various international origins, as indicated in the shown table (3.1).

Table (3.1) : Chemical components used in the present study.

Materials	Molecular Formula	Purity
Cadmium acetate	$(CH_3.COO)_2Cd.2H_2O$	98.5%
Thiourea	$NH_2.CS.NH_2$	99%
Cobalt acetate	$(CH3COO)CO.4H_2O$	97%
Magnesium acetate	$(CH_3COO)_2.4H_2O$	98%
Ethanol	(C_2H_5OH)	99.8%

3.3 work Diagram

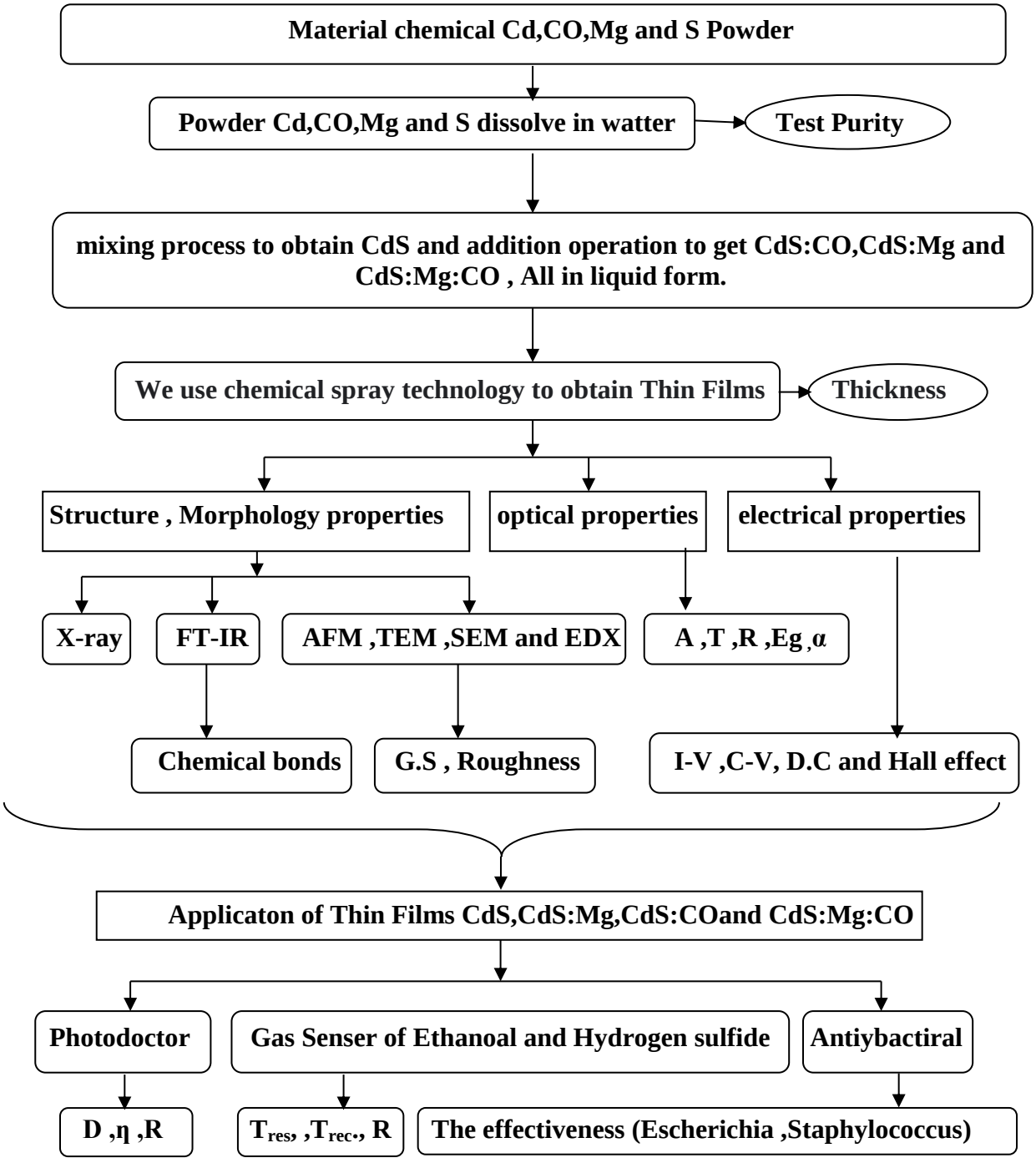

Fig.(3.1) : Work digram

3.4 Sample Preparation

3.4.1 Preparation CdS, CO and Mg:

All salts were dissolved to prepare the films using the equation

$$M = W/Mt * V \qquad (3\text{-}1)$$

Where M/ Molar concentration, Mt/ The weight of salts to be dissolved in water and V/ The volume of water used to dissolve salts

The cadmium sulfide compound was prepared by three steps :

The First process puts (100) ml of distilled water and a percentage of cadmium acetate by weight of (13.326gm) were placed in a glass flask and placed on magnetic stirrer at a temperature of (60C) with the use of a magnetic needle for the dissolution process for a period of time of (30) minutes. We obtained an amount of cadmium acetate liquid of (90) ml.

The Second process puts (100) ml of distilled water and a percentage of Thoreau by weight of (3.806gm) were placed in a glass flask and placed on a centrifuge at a temperature of (60C) with the use of a magnetic needle for the dissolution process for a period of time of (30) minutes. We obtained an amount of thiourea liquid of 88ml.

The third process puts (50) ml of cadmium acetate liquid in a glass beaker with (50) ml of thiourea liquid, and the process of mixing between them is done using a setter at a temperature of (50C) for a period of (20) minutes to obtain the liquid cadmium sulfide compound.The compound cadmium sulfide was prepared according to the chemical equation

$$Cd + S \longrightarrow CdS$$

Cobalt Acetate Preparation

A weight ratio of (14.55)g cobalt acetate was placed with (100) ml of distilled water in a glass beaker and placed on a stirrer at a temperature of (50C), using a magnetic needle for the melting process, and it continued for a period of (35) minutes. We got (85) ml of cobalt acetate liquid.

Magnesium Acetate Preparation

A weight ratio of (10.72g) was placed with (100) ml of distilled water in a glass beaker and placed on a stirrer at a temperature of (50C), using a magnetic needle for the melting process, and it continued for a period of (35) minutes. We got (87) ml of magnesium acetate liquid.

After all the solution were prepared, 70% of cadmium sulfide solution was added to 30% of the mixture of cobalt acetate and magnisium acetate solution.

Table (3.2) : Shows mixing ratios for preparing thin films.

sample	Thin Flim	CdS	Co	Mg
1	CdS	100%	0%	0%
2	CdS:Co	70%	30%	0%
3	CdS:Mg	70%	0%	30%
4	CdS:Co:Mg	70%	15%	15%

3.4.2 Substrate Cleaning

Glass bases and silicon slides were used in the process of deposition of the films, where they are cleaned as follows:

Washing the glass bases and silicone slides in distilled water, then immersing them in high-purity alcohol for (5) minutes, then placing them in distilled water with an ultrasound device for a period of (15) minutes, after which they are left to dry completely and placed in a completely closed container.

3.4.3 Thin Films Deposition

The thermal chemical spraying technique was used for thin film deposition, where it was deposited on each of the glass bases and silicon slides at 350C, and the number of spraying times was 12 times, and between each spraying a period of time of one minute separated, and the spraying time was 3 seconds.

3.5 Chemical Spray Pyrolysis System

It has been using a simple homemade spray pyrolysis system manufactured by the researcher and supervisor in the laboratory of thin films at the University of Babylon / College of Science/ department of physics employed to prepare thin films, the system consists of several parts have been arranged so as to make use of them in the preparation of various the films on various substrates. Fig.(3.2) shows the system in all its parts, and the system consists of the following devices:

3.5.1 Spray Nozzle

It is made up of plastic with of an Copper headd diameter (0 - 0.1) mm contains within it on a piece of iron and other passes through the air and related tube two pieces, one for the transfer of compressed air and the second relates to a small solution container containing 30 ml solution from the material to be deposited. As shown in Fig. (3.2).

3.5.2 Hot Plate

The iron disc (with diameter 16 cm and thickness 0.7 cm to which 2000 W heating coil is fixed) served as a hot plate. A maximum temperature of 700 ± 20 ^{o}C can be achieved with this arrangement. The chromel-alumel thermocouple is used to measure the temperature of the substrates and is fixed at the center of the front side of the iron plate. The temperature of the hot plate is monitored with the help of temperature controller, as showing in Fig. (3.2).

3.5.3 Air Pump

It has been used pneumatic pump compressed air to drive inside the tube connected to the spraying. The air pressure is stable here. The compressed air is the useful pushing particulate material deposited is that we want to spray toward the substrate. The air pump is shown in Fig.(3.2).

3.5.4 Electronic Temporary

Through its control the number of sprinkles and the time of spraying through a pump or stop pump the air. Where we need to pause after each spray solution on the hot substrate to regain substrate temperature. Because after all spraying the substrate will cooled . The electronic temporary is shown in Fig.(3.2).

3.5.5 Temperature Controller

Digital temperature controller (GEMO DT109) was used for the purpose of temperature control that we need where it connects thermocouple and upon arrival at the thermal class required electricity is separated from the heater, and at low temperature are re-electric current for the purpose of re-heating is shown in Fig. (3.2).

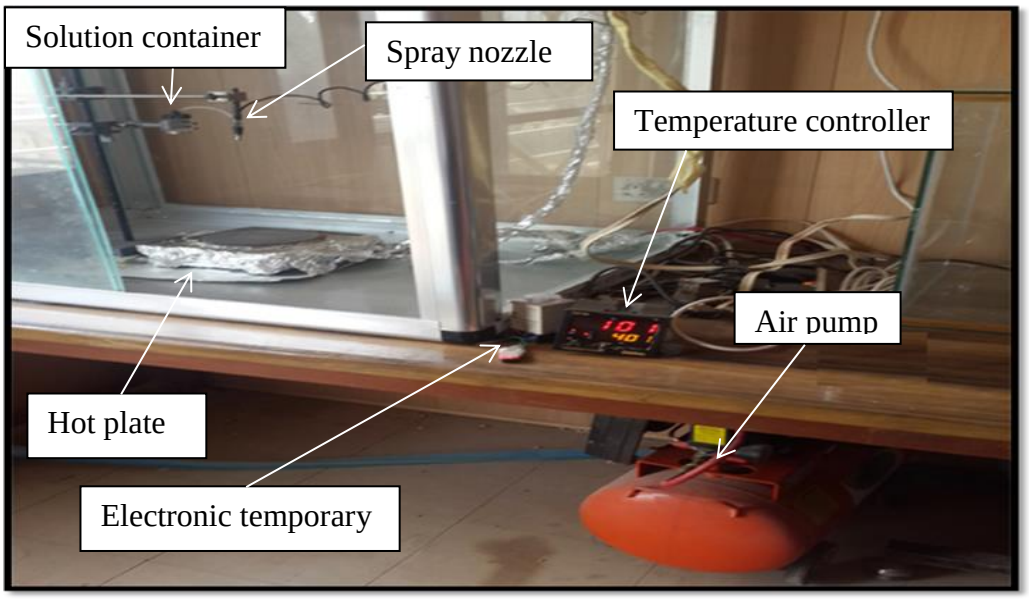

Fig. (3.2): Chemical spray pyrolysis system.

3.6 Thin Films Examinations and Measurements

There are many examinations and measurements that had been done to study the structural, optical, electrical, detector and sensing properties of the thin films. These measurements were done using the following examination devices:

3.6.1 Thickness Measurement

Thickness is one of the most important thin film parameters since it largely determines the properties of the film. The thickness of the films is usually measured by monitoring the rate of the deposition during the coating process. However, there are several methods used for measuring thickness of the film, such as weight, optical, electrical and other methods. In our work the thickness of the thin films was measured by the weight method and optical method.

3.6.1.1 The Optical Method

This method is done by using Lambda (LIMF-10), this measurement system is easy to set up and the software is user friendly. It is suitable for both on-line manufacturing and desktop measuring with the ability to connect to your microscope to reduce the spot size or to dismantle for sole spectroscopic use. We found that the thickness of prepared thin films is (100) nm. Fig.(3.3) show the Optical thin film measurement system uses in my research, this device is present in the laboratory of optics to the university of Babylon / college of science/ department of physics.

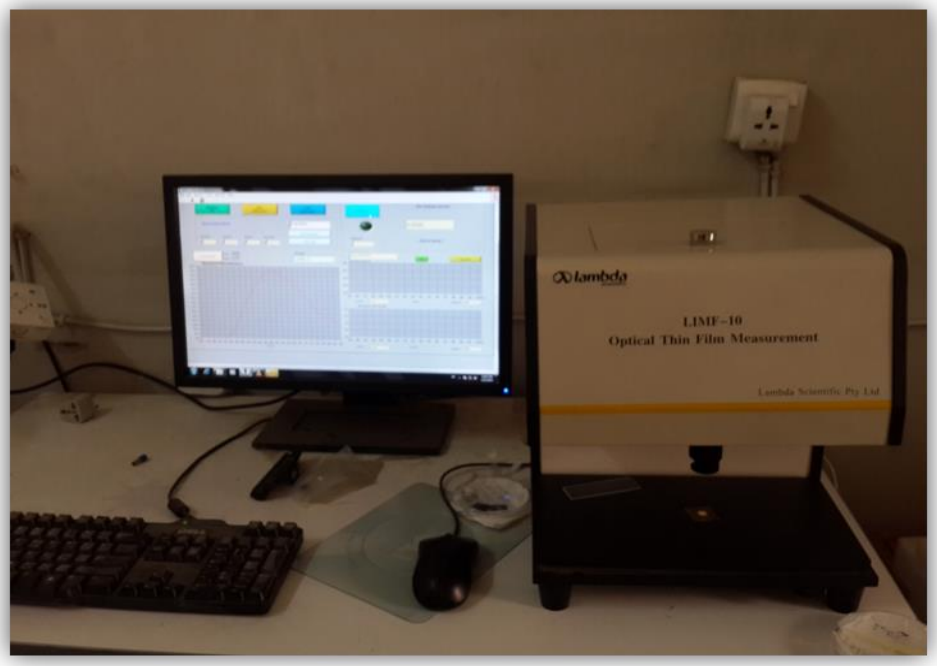

Fig.(3.3) : Show the lambda (LIMF-10).

3.6.2 Structural Properties

3.6.2.1 FT-IR measurement

Use the infrared device Fourier Transform Infrared Spectrophotometer of type FT-IR-8400S supplied by the company Shemadzu as in Fig. (3.4) in the diagnosis of the recorded polymer by knowing the active groups of polymer and the association of some groups in the compound and detect the type of bonds that bind the particles of the material.

Fig.(3.4) : system of the (FTIR).

3.6.2.2 X-ray diffraction (XRD)

X-ray diffraction (XRD) analysis was used to recognize the crystal structure of thin films. When an incident beam of (X-ray) diffracts from a mono wavelength on film surface, this will exhibit peaks on limit angels for each material because of Bragg's reflection on parallel crystalline surface. The X-ray diffraction instrument type (Shimadzu 6000) made in Japan as in Fig.(3-5) , used with the following specifications is used.

Target : Cu

Wavelength : 1.5406 Å

Current : 30 (mA)

Voltage : 40 (kV)

Fig.(3:5) : X-ray diffraction system .

3.6.2.3 Atomic Force Microscopy (AFM)

In order to observe the surface roughness and topography of deposited thin films, Atomic Force Microscope (AFM) micrographs were taken with a Digital Intruments, Inc. BY3000. Typical data have been taken from AFM height images include root mean square (RMS) roughness and grain size. It has three main modes of mapping topography: contact, non-contact, which was used in our morphology investigation and intermittent contact or tapping. The most important part of an AFM is the tip with its nanoscale radius of curvature. The tip is attached to a micron-scale cantilever which reacts to the Van der Waals interaction and other forces between the tip and sample. This device is present in the laboratory of thin films at the University of Babylon / College of Science/ department of physics as shown in Fig. (3.6).

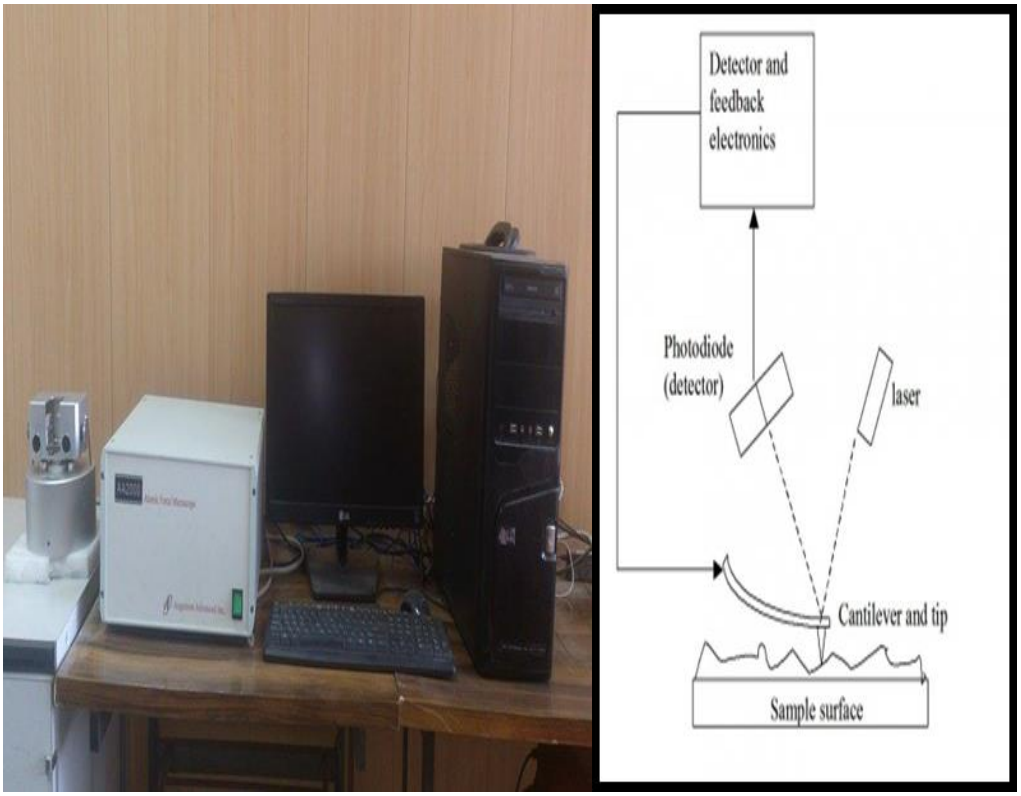

Fig. (3.6) : Set-up and photograph illustrates the AFM.

3.6.2.3 Scanning Electron Microscopy (SEM)

Scanning electron microscopy with energy dispersive X-ray spectroscopy (SEM/EDX) used in this research. The SEM study has been carried out by Inspect550 scanning electron microscope equipped with energy dispersive X-ray (EDAX) the magnification power 250000, the setting in Department of biology Sciences / University of Kufa. As shown in the Fig. (3.7).

Fig.(3.7) : SEM system .

3.6.3 Optical Measurements

A double–beam UV-IR 1800 Spectrophotometer was used to measure the absorption of thin films in the range (180-1100) nm. The background correction was taken for each scan. The transmittance and reflectance data can be used to calculate absorption coefficients of the films at different wavelength which have been used to determine the band gap Eg . This device is present in the laboratory of polymer at physics department / college of science / university of Babylon as show in Fig.(3.8).

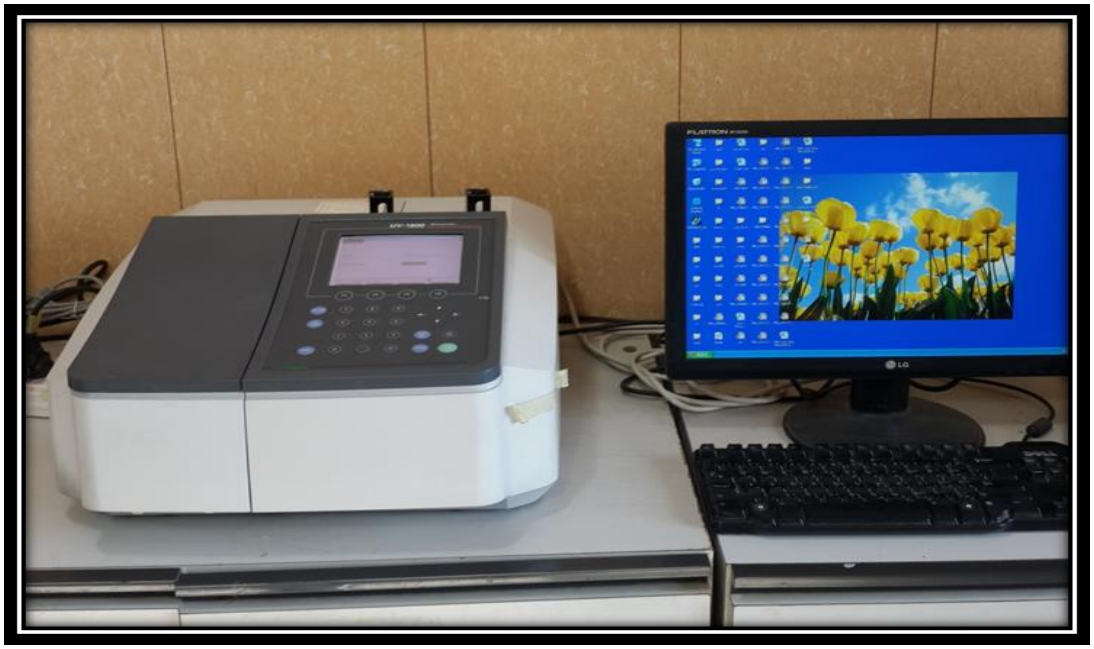

Fig. (3.8) : UV-IR 1800 spectrophotometer system .

3.6.4 Preparation of Masks and Electrodes Deposition

Three kinds of masks have been made for electrical and sensing measurements. All the masks are showed in Fig. (3.9) from aluminum foil sheets in order to get the desired shape of electrodes. These masks have the same dimensions of the substrate and were exactly attached and fixed to cover the substrate after being cleaned. The gold electrodes deposited on the surface of CdS, CdS:Co, CdS:Mg and CdS:Co:Mg films by using sputtering technique of type (CRESSINGTON-108), this instrument is present in the laboratory of thin films at the University of Babylon /College of Science/Department of Physics.

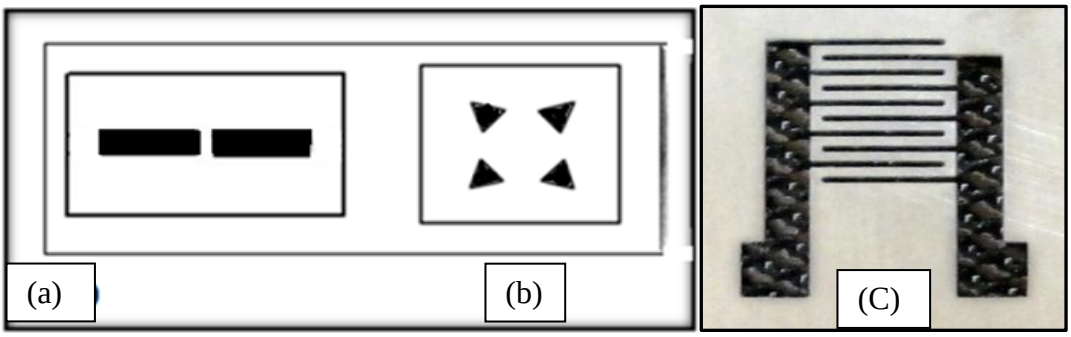

Fig. (3.9) : Masks pattern, which used in (a) sensing measurement D.C (b) Hall effect (c) conductivity measurement.

3.6.5 Electrical Properties

The electrical properties of the films were study by D.C electrical conductivity and Hall effect , current-volte and Capacitance-Voltage measurements.

3.6.5.1 Hall Effect Measurements

The Hall effect was carried out according to the electrical circuit shown in Fig. (3.10), which contains a D.C. power supply with (0 – 40) volt and two digital electrometers (HMS-3000) to measure the current and voltage. This device is present in the laboratory of Polymer at physics department / college of science / university of Babylon.

Fig. (3.10): Photograph illustrates the hall effect.

3.6.5.2 D.C Electrical Conductivity Measurements

The electrical conductivity has been measured as a function of temperature for films in the range (30– 200) ^{o}C by using the electrical circuit. The measurements have been done using sensitive digital electrometer type Keithley and electrical oven as show in Fig.(3.11).

Fig. (3.11) : Photograph the D.C electrical conductivity.

3.6.5.3 Capacitance-Voltage Measurements for the Heterojunction

The capacitance of the heterojunction was measured as a function of the reverse bias voltage in the range (0–1) volt with fixed frequency of 600MHz by using multi-frequency LRC meter. This measurement was used to determine the type of heterojunction (abrupt or graded), built in voltage (V_{bi}), carrier concentration and finally the width of depletion layer.

This device is present in the laboratory of thin films at physics department/ college of science / university of Babylon.

Fig. (3:12) : Show the system multi-frequency LRC meter.

3.6.5.4 Current-Voltage Measurements for the Heterojunction

The current and voltage were measured using a the type 2400 electrometer Keithly device type device attached to a calculator and a halogen lamp with different light intensities, where the light intensity is controlled through the height of the halogen lamp, and the current and voltage are

measured. Note that the apparatus was assembled at the Department of Physics, college of Science , University of Babylon.

Fig. (3:13) : Show the image of the electrometer keithly device

3.6.6 Detector Characteristic Measurement

The spectral response of the manufactured detectors was measured using the type detector test system consisting of a light source and a wavelength uniform that operates within the wavelength range (350-1000) nm and a lens to collect the light coming from the spectral analyzer to fall on the prepared detector and the digital ammeter as well as the radiation power meter falling on the detector for each wavelength.

Fig. (3:14) : Show the detector measurement device.

3.6.7 Sensing System

A schematic cross-sectional view of the gas sensor testing system, test chamber, and photos of the mounted sensor and test chamber are illustrated schematically in Fig. (3.15). The unit consists of a vacuum-tight stainless steel cylindrical test chamber of diameter (26 cm) and of height (10 cm) with the bottom base made removable. The effective volume of the chamber is (5306.6 cm^3); it has an inlet for allowing the test gas to flow in and an air admittance valve to allow atmospheric air after evacuation. Another third port is provided for vacuum gauge connection. A multi-pin feed through at the base of the chamber allows the electrical connections to be established to the heater assembly as well as to the sensor electrodes via spring-loaded pins. The heater assembly consists of a hot plate and a k - type thermocouple inside the chamber to control the operating temperature of the sensor. The thermocouple senses the temperature at the surface of the film exposed to the analyte gas. PC-interfaced digital multimeter of type (UNI-T UT81B), and laptop PC, is used to register the variation of the sensor conductance

(reciprocal of resistance) exposed to predetermined air - gases ratio. The chamber can be evacuated using a rotary pump to a rough vacuum. A gas mixing manifold is incorporated to control the mixing ratios of the test and carrier gases before being injected into the test chamber. This test is carried out in the thin films Laboratory of University of Babylon/ College of Science/ Department of Physics.

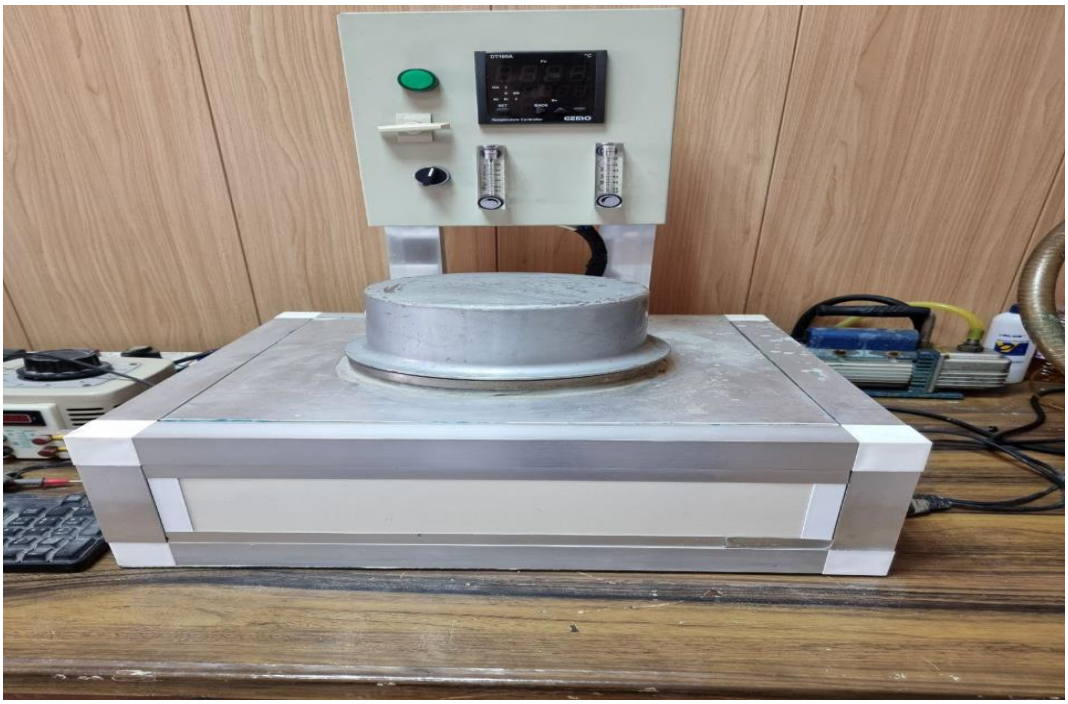

Fig. (3.15) : Diagram of electrical circuit of gas sensing measurements.

4.1 Introduction

This chapter presents and discusses the results of the prepared thin films CdS,CdS:Mg ,CdS:Co and CdS:Mg:Co by using the chemical spray pyrolysis technique obtained by measuring and studying the structural,morphology, optical and electrical properties and employing them in the applications of the photodetector, the gas sensor, as well as in a medical application that links the physics and biology sciences, which is the study of the effectiveness of the films Prepared against two types of bacteria.

4.2 Purity Tests

The purity of the chemical elements, cadmium acetate (Cd), cobalt acetate (Co), thiourea (S), and magnesium acetate (Mg), was calculated by measuring the melting point.

Table (4.1) shows the theoretical and experimental melting point values for all chemicals that were used in the preparation of thin films (CdS, CdS:Co , CdS:Mg , CdS:Co:Mg). The results showed that the obtained purity values are completely identical to their theoretical values .

Table (4.1) : The experimentaland theoretical values of melting point (M.P).

sample	Exp. M.P.(°C)	Theo. M.P(°C)	Range M.P	Purity % ($M.P_{Exp.}/M.P._{Theo.}$)×100%
Cadmium acetate	251.2	255	1.3	98.5
Thiourea	174.4	176	1.5	99
Cobalt acetate	135.9	140	1.3	97
Magnesium acetate	78.4	80	1.4	98

4.3 Structural Properties

4.3.1 Fourier Transform Infrared (FTIR) Test

The chemical bonds of the prepared thin films (CdS, CdS:Co, CdS:Mg, CdS:Co:Mg) were studied and determined by measuring FTIR spectrometer within the wave number range (450-4000) cm^{-1} as shown in Fig. (4.1,a,b,c,d).

Table (4.2) shows the type and location of the chemical bonds for all the prepared thin films that were determined through their vibration sites in the FTIR, where we notice from the results that the addition of cobalt acetate and magnesium acetate to the cadmium sulfide compound led to the emergence of new chemical bonds.This result was also found rouguly in[36,106].

This indicates an interaction between cobalt acetate and magnesium acetate with the compound cadmium sulfide.

In FTIR spectra , the energy used is the vibrational energy and the vibrational strain is of two types stretching and bending. We always use strain stretching in our work because it is within the frequency range (400-4000) cm^{-1}, while strain bending is within the frequency range (400-1600) cm^{-1} [26,33].

Table (4.2) : Shows the absorbance paaks of the all thin films.

sample	Absorption paaks (cm^{-1})	Shaky group
1,2,3,4	530	C-O
1,2,3,4	660	C-N
2,4	1600	C=C
2,4	1700	C=O
3,4	2100	C=N
1,2,3,4	2380	C≡C
1,2,3,4	2400	C≡N
`1,2,3,4	3700	O-H
2, 3,4	3800	N-H

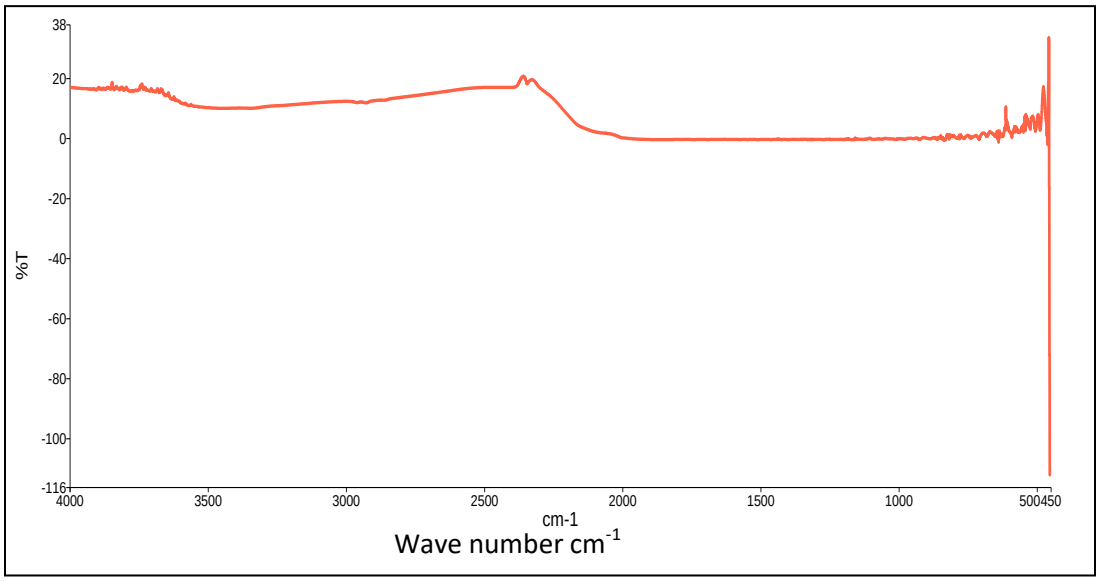

Fig. (4.1)a : Shows the measurement of FTIR for the prepared thin film CdS.

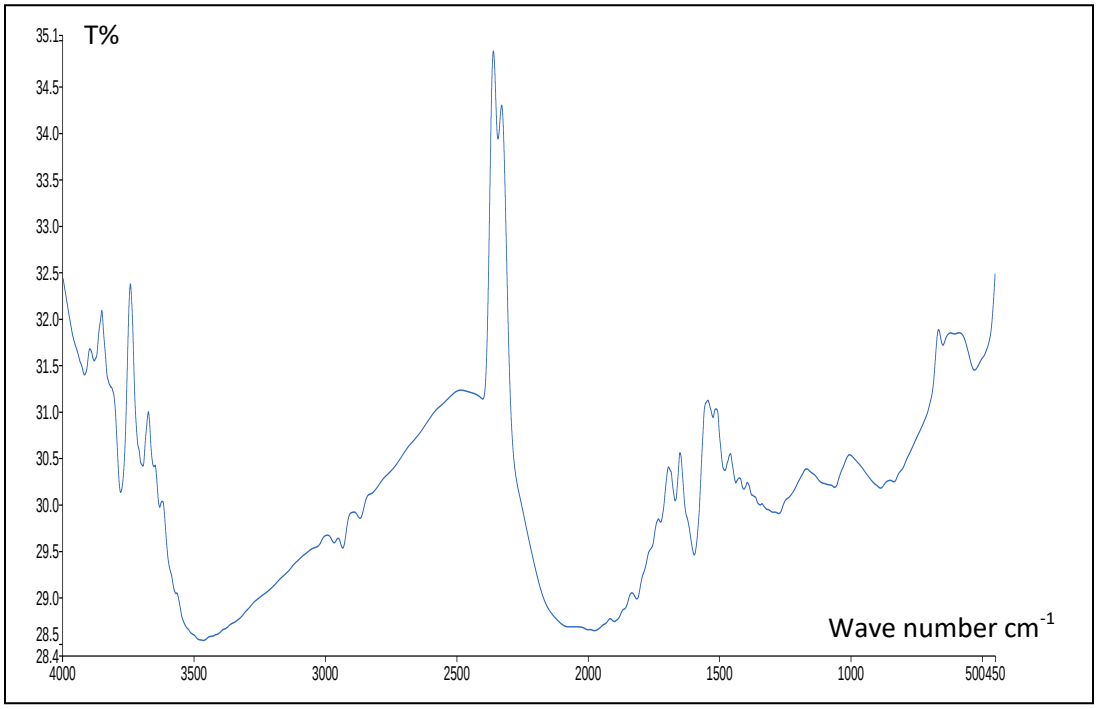

Fig. (4-1)b : Shows the measurement of FTIR for the prepared thin film CdS:Co.

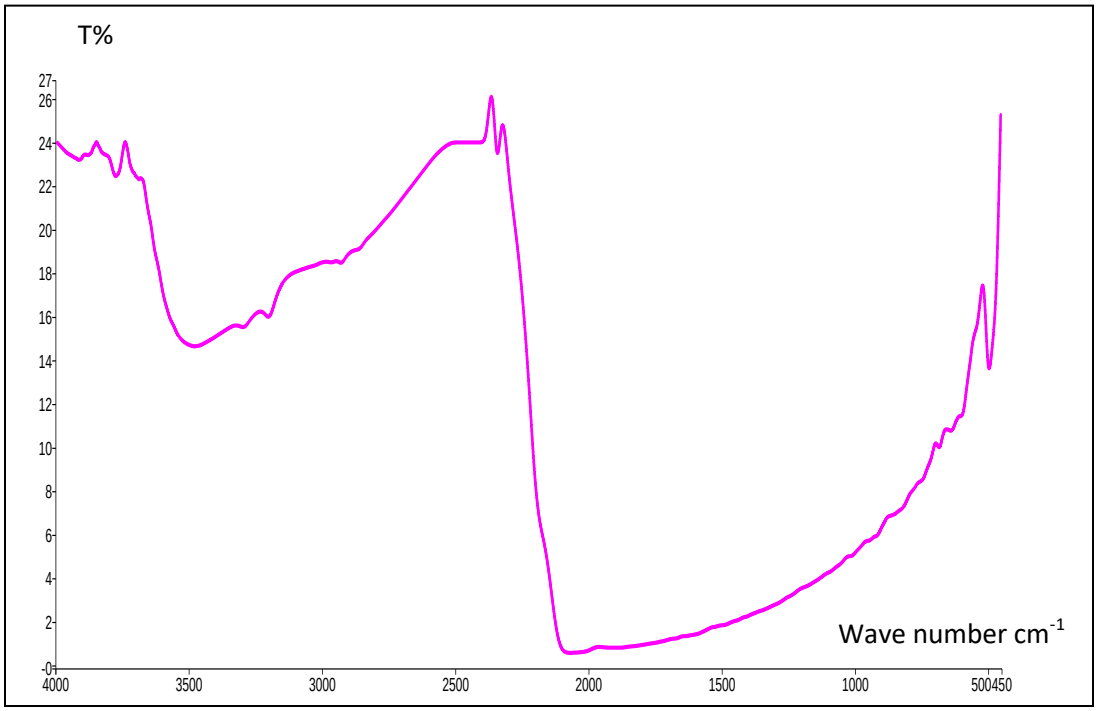

Fig. (4.1)c : Shows the measurement of FTIR for the prepared thin film CdS:Mg.

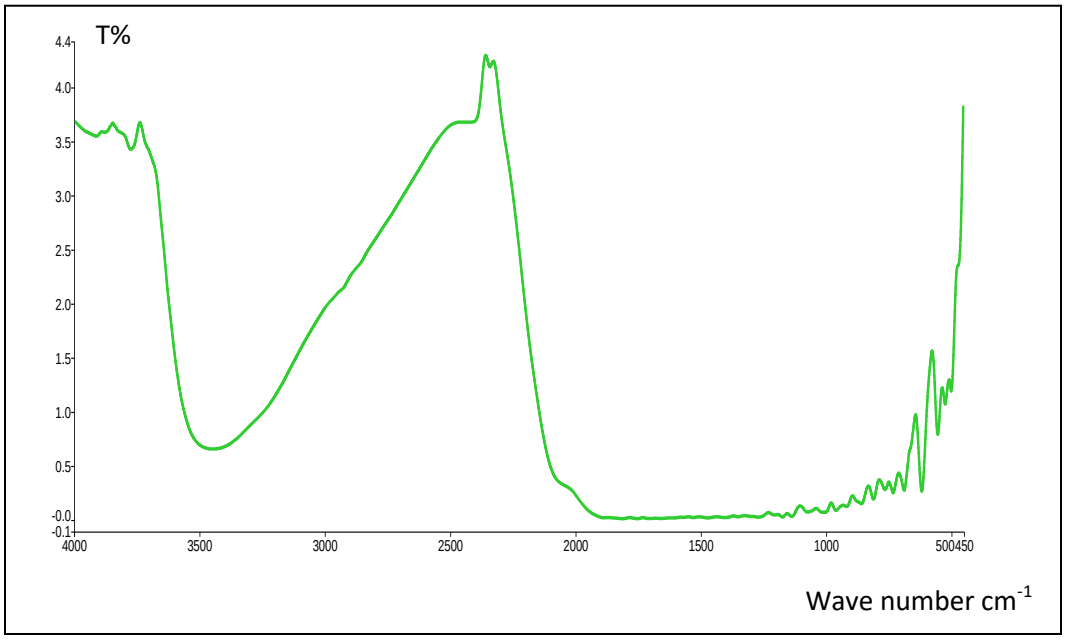

Fig. (4.1)d : shows the measurement of FTIR for the prepared thin film CdS:Co:Mg.

4.3.2 X-ray Diffraction Analysis

In Fig.(4.2) shows the results of X-ray diffraction measurements for the prepared thin films CdS, CdS:Co, CdS:Mg, CdS:Co:Mg .

The results of the diagnosis by X-ray diffraction showed that all the prepared thin films had a polycrystalline structure, and that the prepared thin film cadmium sulfide had a cubic structure and this result was also found rouguly in [35,36,38] .

The interfacial distance(d_{hkl}) between the atomic levels of all thin films prepared from X-ray diffraction points and Bragg angles(2Ɵ) was calculated using Eq. (2.1). Where it was found that the values of the distance between the atomic levels obtained are very close to their theoretical values and this result agree with rouguly agree with[40,107].

Through the values of the distance between the atomic levels and the Miller coefficients, the lattice constants (a,b and c) were calculated for the levels that represent the Miller coefficients for a cadmium sulfide compound with a cubic type structure. Where it was found that the values of the obtained lattice constants are completely identical to their theoretical values and this result agree with rouguly agree with[41,43,108].

The full width half maximum (FWHM) was calculated from the X-ray spectrum for all prepared thin films.Where it was found that the addition of cobalt acetate and magnesium acetate to the cadmium sulfide compound led to a decrease in the full width half maximum values.

The reason is that there is an increase in the average particle size values, because the inverse relationship between the full width half maximum and grain size. This result agree with rouguly agree with [44,109]

The average grain size (G.S) of all prepared thin films was calculated by substituting the values obtained from the results of X-ray diffraction using Debye-Sherrer Eq. (2.6) based on the values of the full width half maximum[57].Where the result showed that the addition of cobalt acetate and magnesium acetate to the cadmium sulfide compound led to an increase in the values of the average grain size . This result was also found rouguly in [46,48,110].

The reason for this is that the addition of cobalt acetate and magnesium acetate led to the cancellation of some granular boundaries when the granules coalesced to form crystals of a larger size, meaning the alignment or coalescence of cobalt acetate or magnesium acetate atoms with the atoms of the cadmium sulfide compound, as well as the elimination of some existing defects after the growth and rearrangement of the crystalline granules and this result was also found rouguly in [46,111].

Through the average grain size values for all prepared thin films, the dislocations density (δ) and the number of crystals per unit area (N) were calculated using Eqs. (2.7) (2.8), respectively[60,61].

Where the result showed that the addition of cobalt acetate and magnesium acetate to the compound cadmium sulfide led to a decrease in the values of each of the density of dislocations and the number of crystals per unit area This result agree with rouguly agree with [48,49,112].

The reason for this is as a result of an increase in the values of the average particle size, which in turn led to a decrease in the values of both the density of dislocations and the number of crystals, because the density of dislocations is inversely proportional to the square of the particle size.While the number of crystals per unit area is inversely proportional to the cube of the particle size. This result was also found rouguly in. [60,61,113].

Through the values of the full width half maximum, the strain elasticity (ε) was calculated for all the prepared thin films using Eq. (29)[61].

The result showed that the addition of cobalt acetate and magnesium acetate to the compound cadmium sulfide led to a decrease in the values of the strain elasticity. This result was also found rouguly in [49,114]

The reason for this is that the addition of cobalt acetate and magnesium acetate led to a decrease in the values of the full width half maximum. This in turn leads to a decrease in the values of the strain elasticity because the strain elasticity is directly proportional to the full width half maximum and this result was also found rouguly in [60,61].

Table (4-3a,b,c and d) shows all the results obtained from measuring X-ray diffraction for all prepared thin films and when compared with the values contained in the card numbered(01-080-0019), (00-001-0783),(96-100-8133) of the american standard of testing materials (ASM), it was found that the results are somewhat identical.

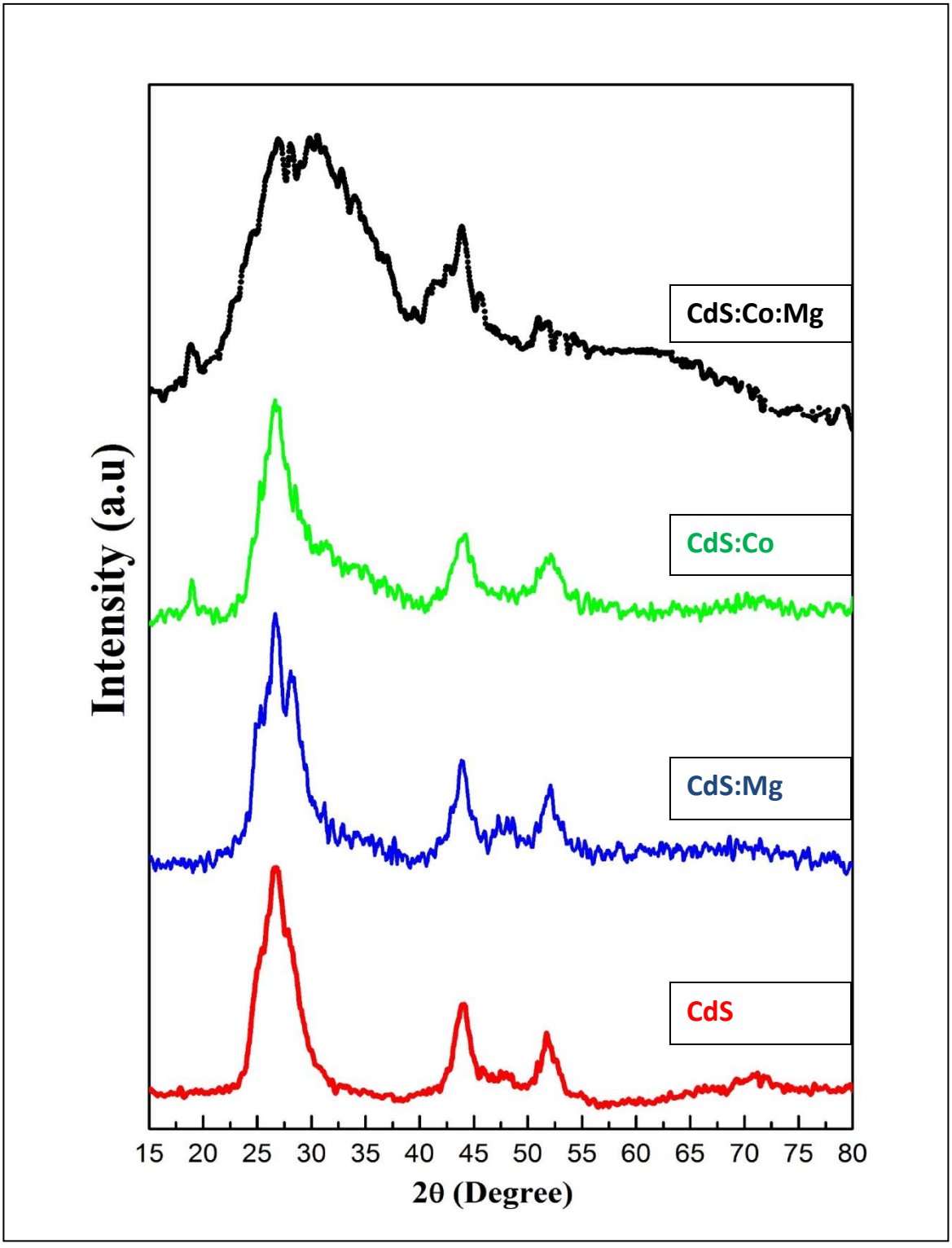

Fig. (4.2): Shows the measurement of X-ray diffraction for all prepared thin films.

Tabel (4.3)a : Show the result of X-ray of CdS thin film.

N0.	Exp. Pos. 2 Theta degree	FWHM degree	Crystallite size Nm	Exp.d-spacing A	(hkl)	Compound	$\delta \times 10^{-3}$	ε	N	Cell Parameter	Crystal System	Reference Code
1	26.547	0.984	8.4	3.354	(111)	CdS	88.896	0.239	1.587	a = b = c =5.811	Cubic	01-080-0019
2	44.040	0.590	14.7	2.054	(220)	CdS	4.627	0.136	0.047			
3	52.163	0.394	22.9	1.752	(311)	CdS	1.906	0.088	0.012			
ave.	-----	0.656	15.333	-------	------	-----	31.809	0.154	0.548	-----	-----	------

Tabel (4.3)b : Show the result of X-ray of CdS:Co thin film.

N0.	Exp. Pos. 2 Theta Degree	FWHM degree	Crystallite sizenm	Exp.d-spacing A	(hkl)	Compound	$\delta \times 10^{-3}$	ε	N	Cell Parameter	Crystal System	Reference Code
1	19.069	0.394	20.9	4.765	(101)	Co	2.289	0.097	0.016	a = b = c =5.811	Cubic	96-100-8133
2	26.547	0.982	8.4	3.354	(111)	CdS	88.896	0.239	1.587			
3	44.040	0.591	14.7	2.054	(220)	CdS	4.627	0.136	0.047			
4	52.163	0.391	22.9	1.752	(311)	CdS	1.906	0.008	0.012			
Ave.	-----	0.589	16.725	-----	-----	-----	24.429	0.140	0.415	-----	-----	-----

Tabel (4.3)c : Show the result of X-ray of CdS:Mg thin film.

N0.	Exp. Pos. 2 Theta degree	FWHM degree	Crystallite size nm	Exp. d-spacing A	(hkl)	Compound	$\delta \times 10^{-3}$	ε	N	Cell Parameter	Crystal System	Reference Code
1	28.238	0.590	14.1	3.140	(101)	Mg	5.029	0.143	0.053	a = b = c =5.811	Cubic	00-001-0783
2	48.104	0.246	36.6	1.890	(103)	Mg	0.746	0.056	0.003			
3	26.547	0.983	8.4	3.354	(111)	CdS	88.896	0.239	1.587			
4	44.040	0.591	14.7	2.054	(220)	CdS	4.627	0.136	0.047			
5	52.163	0.389	22.9	1.752	(311)	CdS	1.906	0.088	0.012			
Ave.	-----	0.559	19.34	-----	-----	----	20.809	0.132	0.340	-----	-----	-----

Tabel (4.3)d : Show the result of X-ray of CdS:Mg:Co thin film.

N0.	Exp. Pos. 2 Theta degree	FWHM degree	Crystallite size nm	Exp.d-spacing A	(hkl)	Compound	$\delta \times 10^{-3}$	ε	N	Cell Parameter	Crystal System	Reference Code
1	28.238	0.592	14.1	3.140	(101)	Mg	5.029	0.143	0.053	a = b = c =5.811	Cubic	01-080-0019
2	48.104	0.244	36.6	1.890	(103)	Mg	0.746	0.056	0.003			
3	26.547	0.985	8.4	3.354	(111)	CdS	88.896	0.239	1.587			
4	44.040	0.596	14.7	2.054	(220)	CdS	4.627	0.136	0.047			
5	52.163	0.396	22.9	1.752	(311)	CdS	1.906	0.008	0.012			
6	19.069	0.390	20.9	4.765	(101)	Co	2.289	0.097	0.016			
Ave.	-----	0.533	19.6	-----	-----	-----	17.248	0.126	0.286	-----	-----	-----

4.4 Morphology Properties

The morphological characteristics of AFM, SEM and TEM were measured and studied, through which the grain size and surface roughness of all prepared films were known.

4.4.1 The Atomic Force Microscope (AFM)

The topography of the surfaces of the prepared thin films were studied and the effect of adding cobalt acetate and magnesium acetate to the cadmium sulfide compound was studied by conducting an atomic force microscope measurement. The device has the ability to photograph and analyze the surfaces of the films and give very accurate statistical values for the values of the particle size and the roughness values of the surfaces of the prepared thin films depending on the values of the square root of the mean roughness[62,63].

Fig. (4.3)a,b,c and d shows the AFM examination images for all the prepared thin films, where we notice through the images that the surfaces of the prepared films are free from cracks or needle holes that can occur to the films during their preparation and have good surface homogeneity. We can notice that the composition of the prepared films has the same composition Polycrystalline, where the granular boundaries can be distinguished clearly, and this is consistent with the results of X-ray diffraction, which showed that all the prepared thin films have a polycrystalline structure and this result agree with [35,36,115,116].

Table (4.4) shows the values of the particle size and roughness of the surfaces of the prepared thin films. It was found that the addition of cobalt acetate and magnesium acetate to the compound cadmium sulfide led to an increase in the values of the particle size.

This result is identical to the results of X-ray diffraction measurement. The reason for the increase in the particle size is that the addition of cobalt acetate and magnesium acetate atoms It coalesced with the atoms of the compound cadmium sulfide to form crystals with a larger granular size, as well as canceling some granular boundaries and this result agree with [43,44].

Through the AFM results, we also note that the addition of cobalt acetate and magnesium acetate to the cadmium sulfide compound led to an increase in the surface roughness values of the prepared films depending on the square root values[65]. The square root which represent the sum of the surface elevations and depressions squared divided by their total number under[66]. The square root this value explains the average surface roughness. The higher the value of the square root, the greater the surface roughness of the prepared films, and vice versa. Due to the change in the surface roughness of the prepared films, they can be used in gas sensor applications and this result agree with[64,115].

Table (4.4) : shows the values of the grain size, mean square root, and surface roughness of the prepared thin films.

Sample	G.S (nm)	Root Mean Square (nm)	Roughness (nm)
CdS	33.407	10.044	7.644
CdS:Co	48.181	10.752	8.585
CdS:Mg	87.721	24.956	17.441
CdS:Co:Mg	67.1355	11.420	9.732

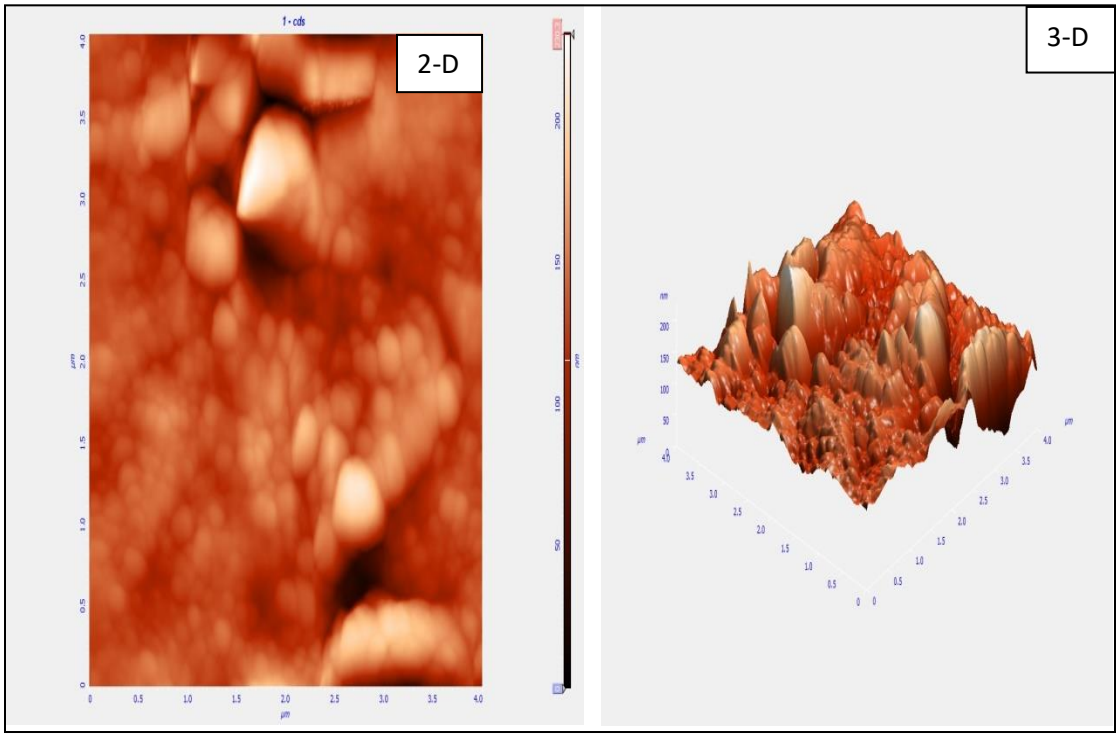

Fig. (4.3)a : Shows AFM images of CdS thin film.

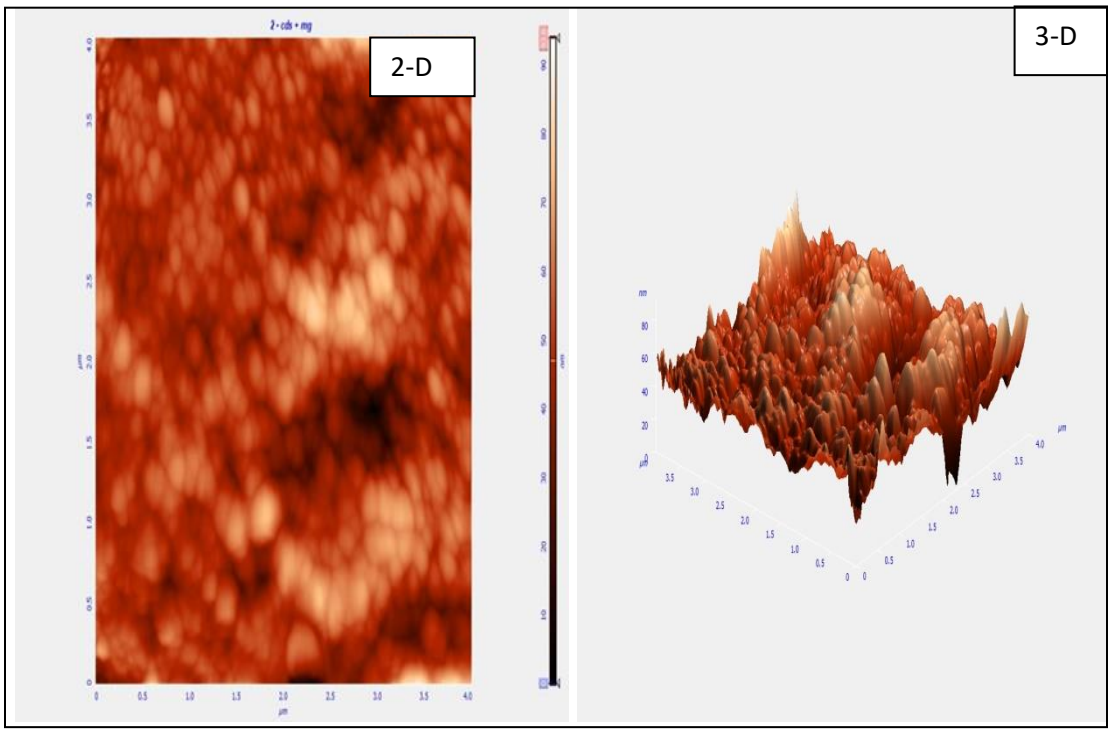

Fig. (4.3)b : Shows AFM images of CdS:Co thin film.

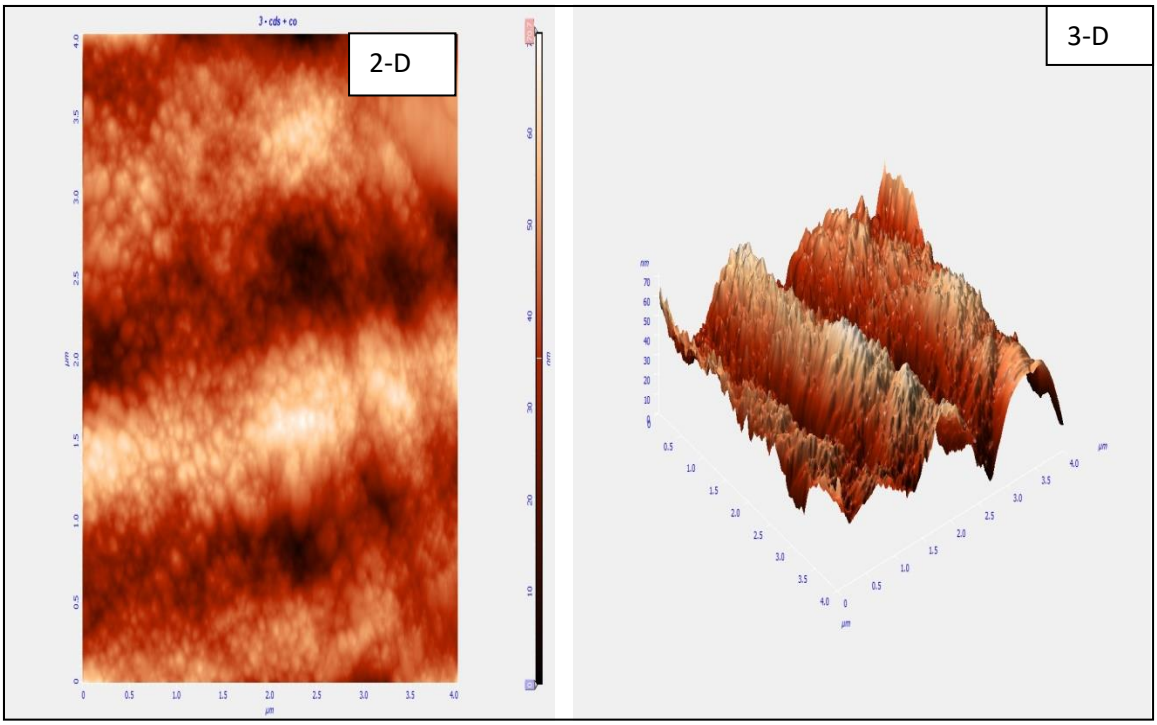

Fig. (4.3)c : Shows AFM images of CdS:Mg thin film.

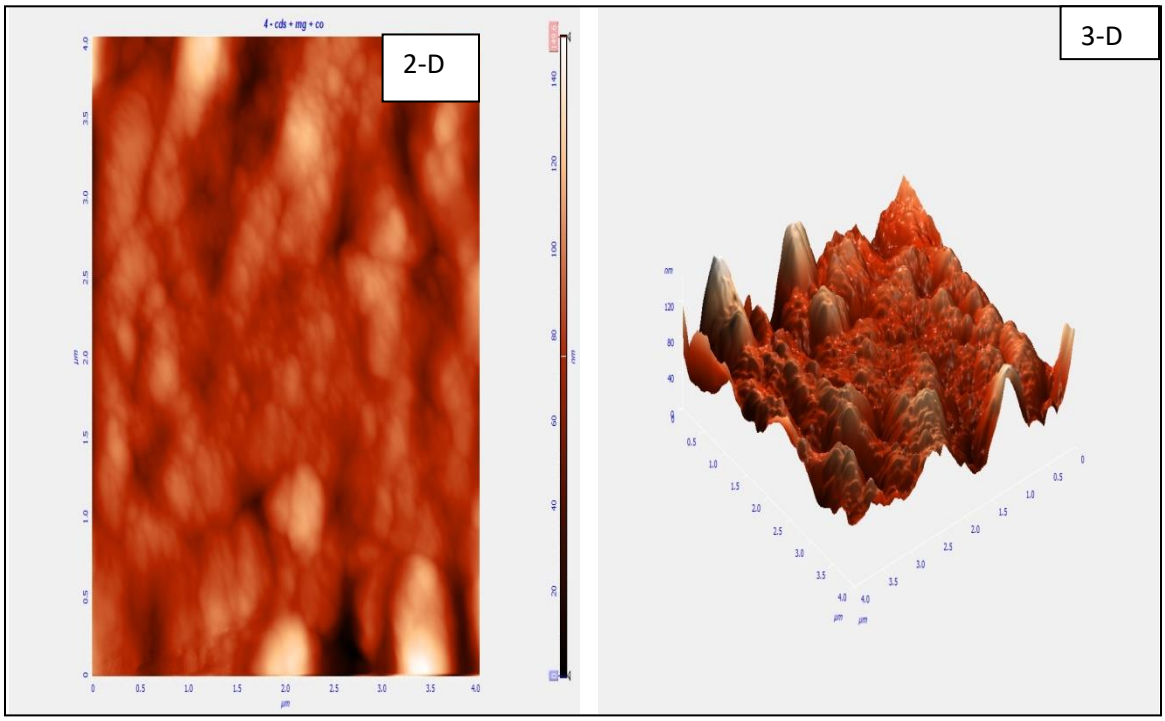

Fig. (4.3)d : Shows AFM images of CdS:Co:Mg thin film.

4.4.2 Scanning Electron Microscope (SEM)

Fig. (4.4) a,b,c and d shows the images of the SEM examination with the ability to analyze 200nm of the prepared thin films.We notice through the images that all the prepared films are homogeneous and free from crystalline defects such as cracks or needle holes that can occur to a membrane during its preparation and this result agree with[40,43].

We also notice through the pictures that the addition of cobalt acetae and magnesium acetate atoms to the cadmium sulfide compound is distributed mostly in a regular or consistent manner in the cadmium sulfide lattice, which makes it have an almost regular crystalline structure, despite the presence of some clusters or small clusters on the surfaces of the prepared films and this result agree with [43,115].

Table (4.5) shows the particle size values obtained from the SEM test for all prepared films.It was found that the addition of cobalt acetate and magnesium acetate to the cadmium sulfide compound led to an increase in the particle size values, and this result is identical to the results of X-ray diffraction and AFM .

Table (4-5): shows the grain size values for all prepared thin films.

sample	D1 or G.S (nm)
CdS	49.78
CdS:Co	113.69
CdS:Mg	86.90
CdS:Co:Mg	71.97

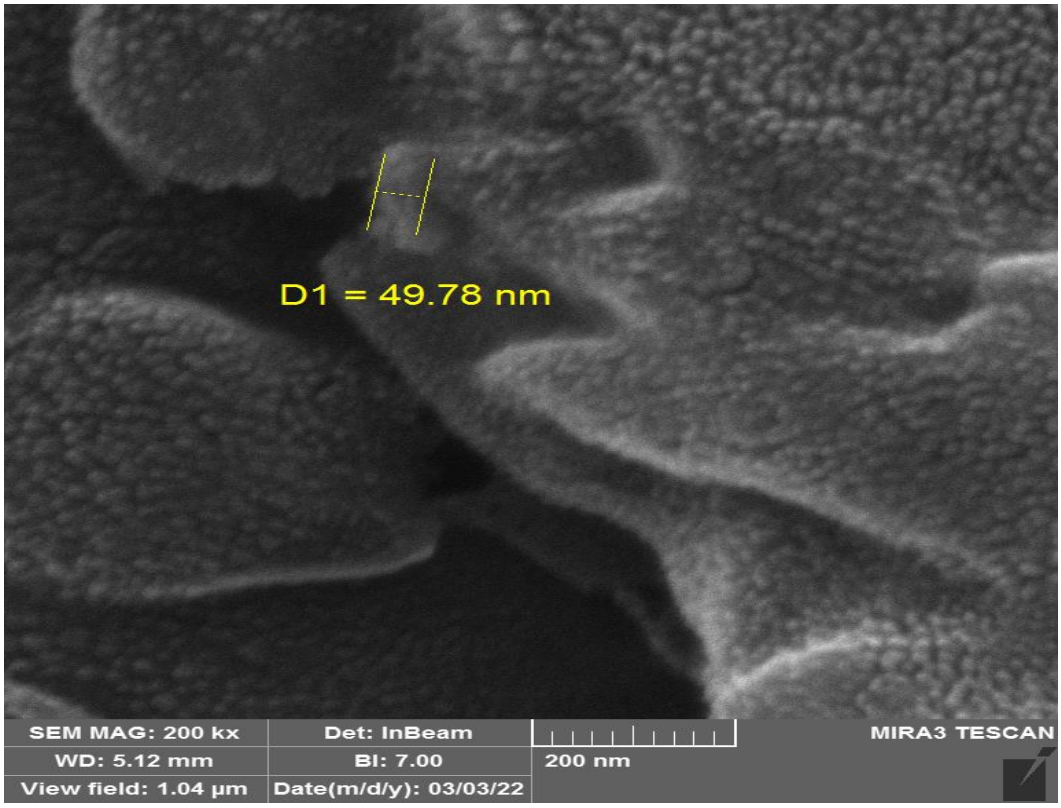

Fig.(4.4)a : Shows an image of the SEM examination of CdS thin film.

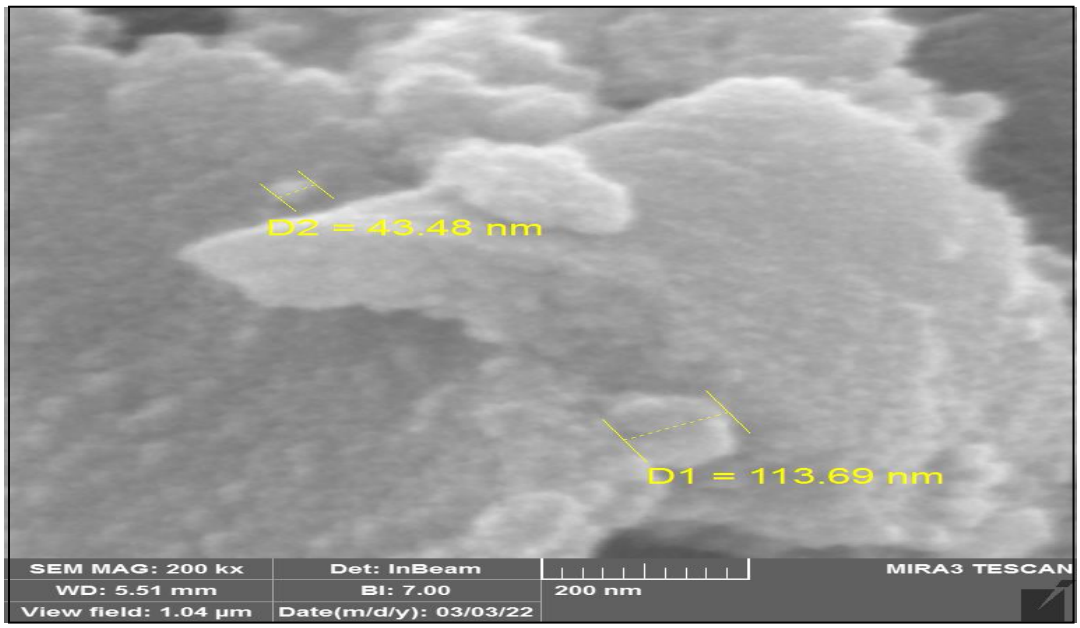

Fig. (4.4)b : Shows an image of the SEM examination of CdS:Co thin film.

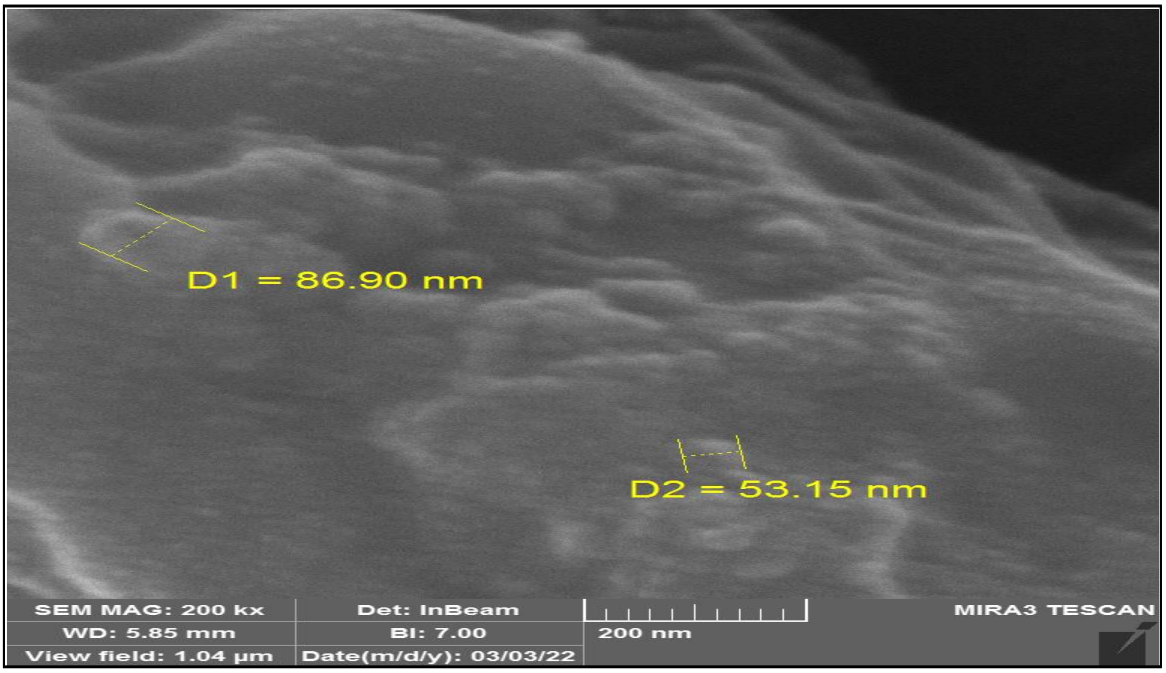

Fig.(4.4)c: Shows an image of the SEM examination of CdS:Mg thin filn.

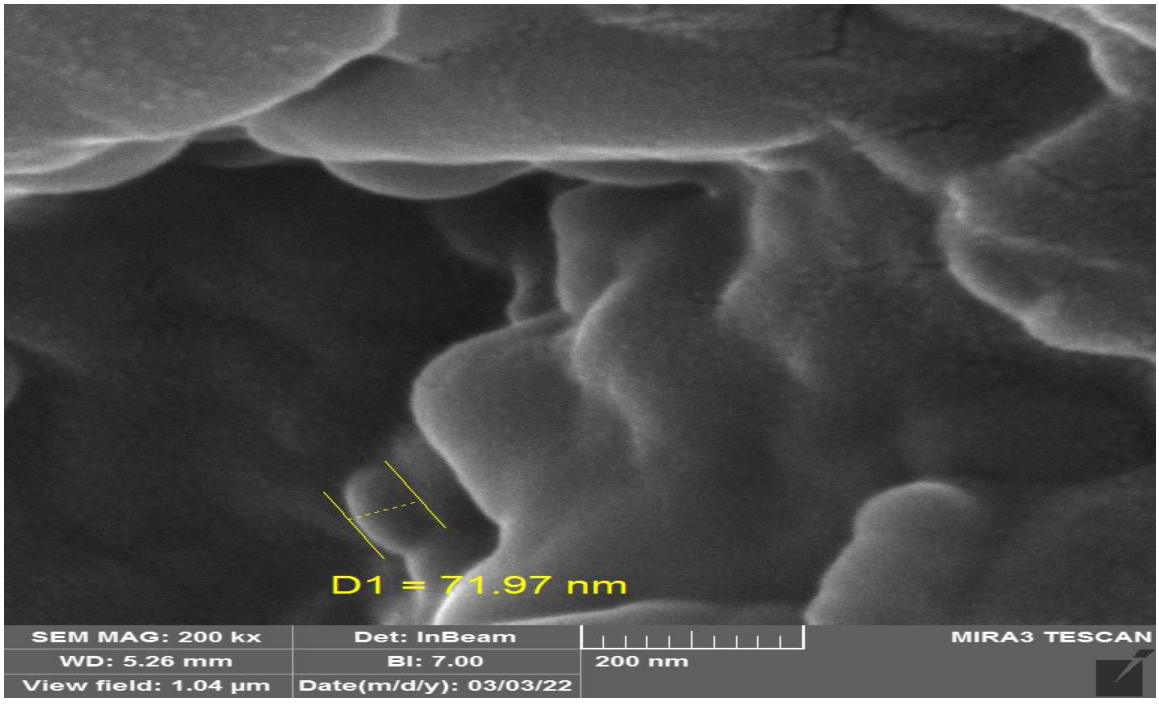

Fig. (4.4)d : Shows an image of the SEM examination of CdS:Co:Mg thin film.

4.4.3 Energy Dispersive X-Ray Spectroscopy (EDX)

Fig. (4.5)a,b,c and d shows the energy dispersive X-ray spectroscopy examination of the energies (0-20Kev) resulting from the SEM examination of the prepared thin films. The results showed an analysis of the chemical elements involved in the preparation of the films, and their chemical composition was confirmed, as the prepared films. Showed cadmium sulfide prepared from cadmium and thiourea only. While the prepared film CdS:Co consisted of cadmiumsulfide and cobalt acetate. while the prepared film CdS:Mg consisted of cadmium sulfide and magnesium acetate. The prepared film CdS:Co:Mg consisted of cadmium sulfide, cobalt acetate and magnesium acetate. This result is expected to be obtained because it depends on the chemicals that were used in preparing the films and this was also found rouguly in[35] .

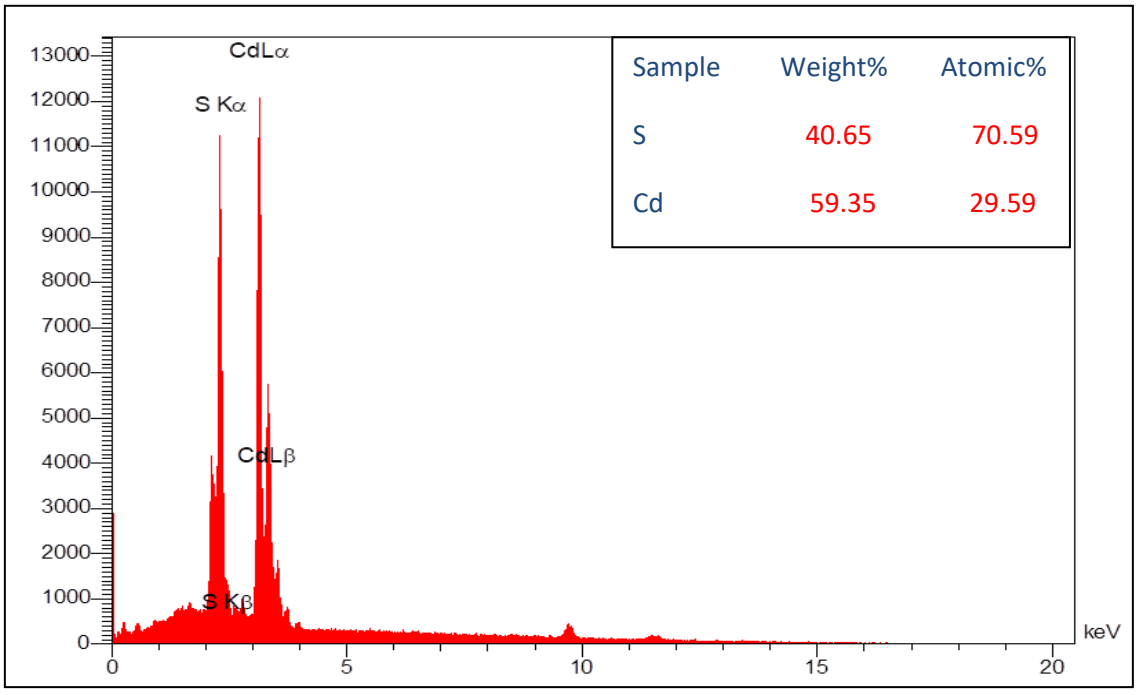

Fig. (4.5)a : Shows EDX of the prepared CdS thin film.

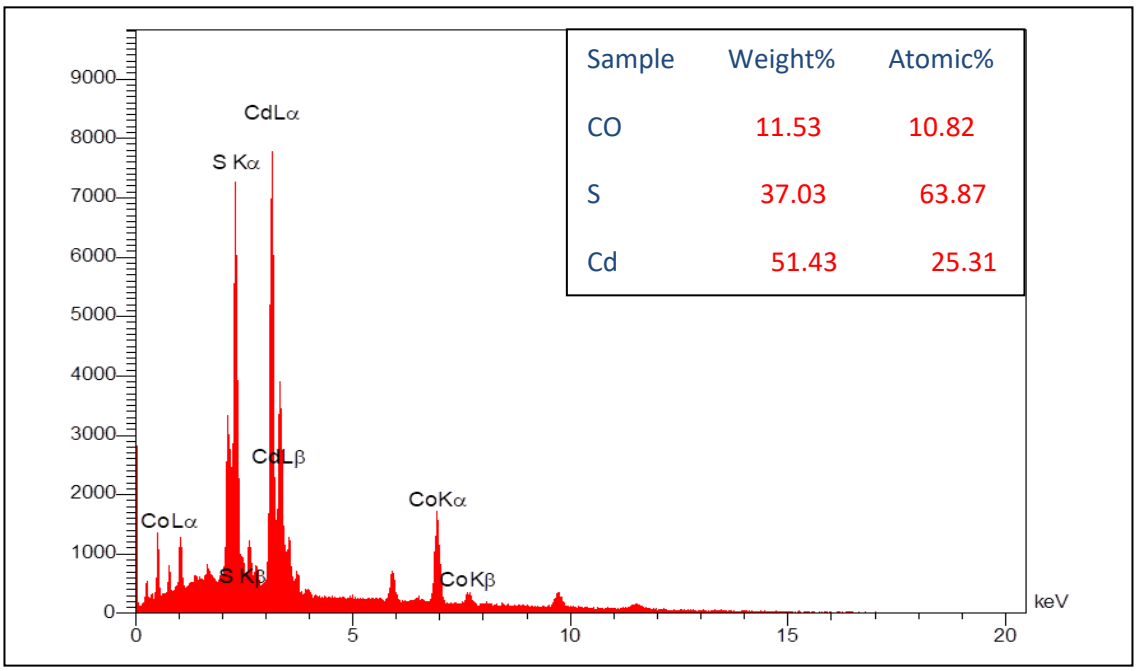

Fig. (4.5)b: Shows EDX of the prepared CdS:Co thin film.

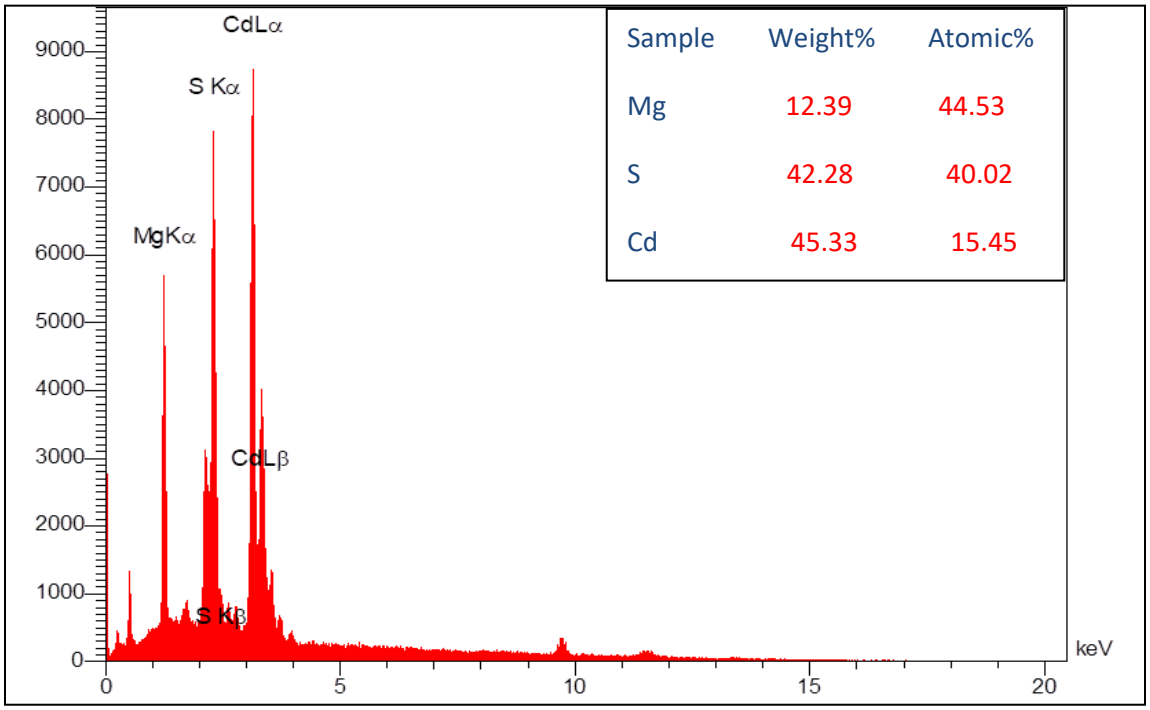

Fig. (4.5)c : Shows EDX of the prepared CdS:Mg thin film.

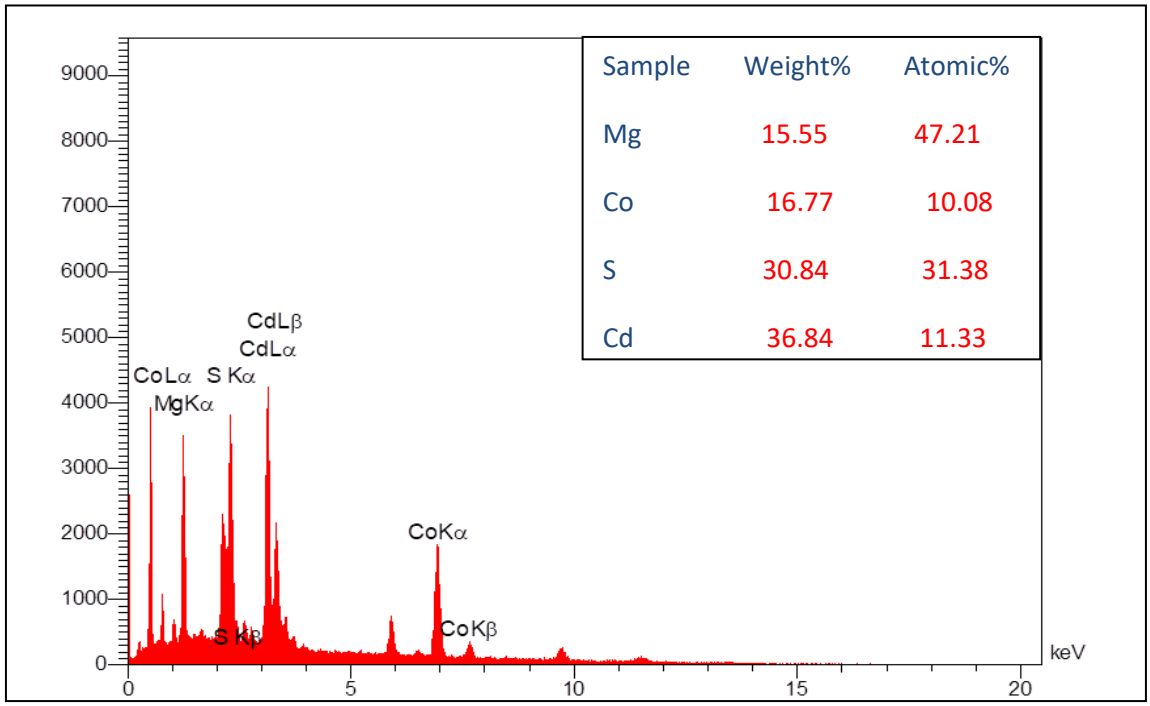

Fig. (4.5)d : Shows EDX pictures of the prepared CdS:Co:Mg thin film.

4.4.4 Transmission Electron Microscopy (TEM)

Fig. (4.6)a,b,c and d shows the images of the TEM examination of the prepared thin films. The images showed that the surfaces of the prepared films have a different color nature, and this is confirmed by the chemical composition of the prepared films. This may be attributed to the cobalt acetate and magnesium acetate atoms that were added to the cadmium sulfide compound and this result agree with[44,116].

The TEM test images showed that the all prepared thin films are homogeneous and have spherical crystalline granules, some of which are superimposed and others are not, and differ in granular size. We note from the granular size scale that the addition of cobalt acetate and magnesium acetate to the cadmium sulfide compound led to an increase in the granular

size. This result is identical to the results of X-ray diffraction, AFM and SEM .

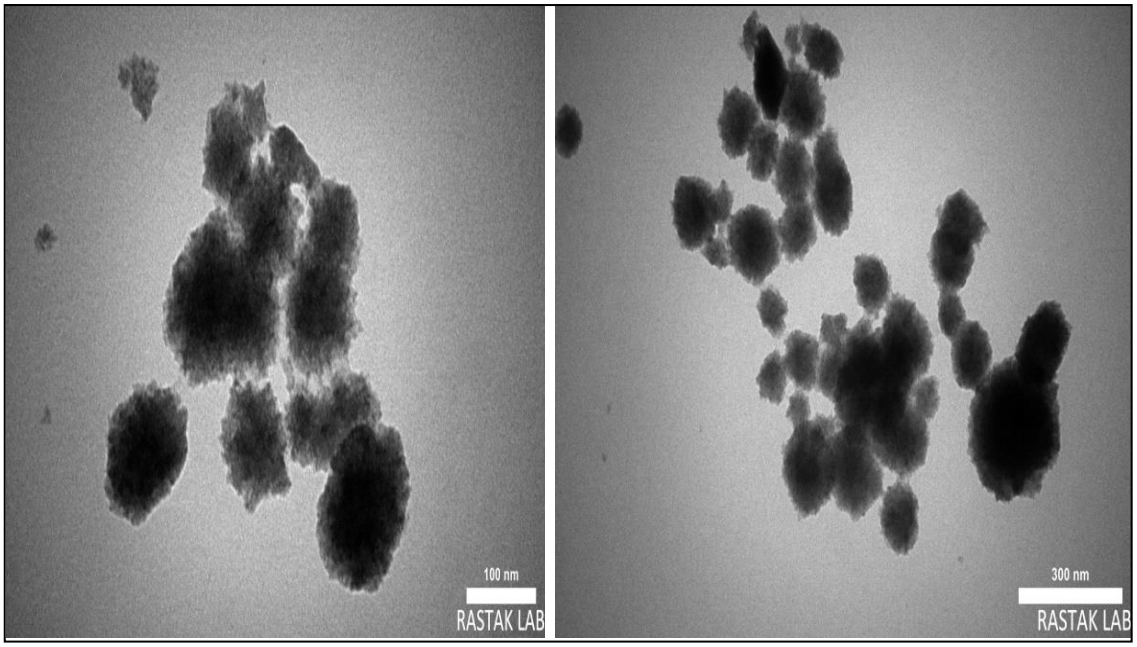

Fig. (4.6)a: Shows the TEM examination of CdS thin film.

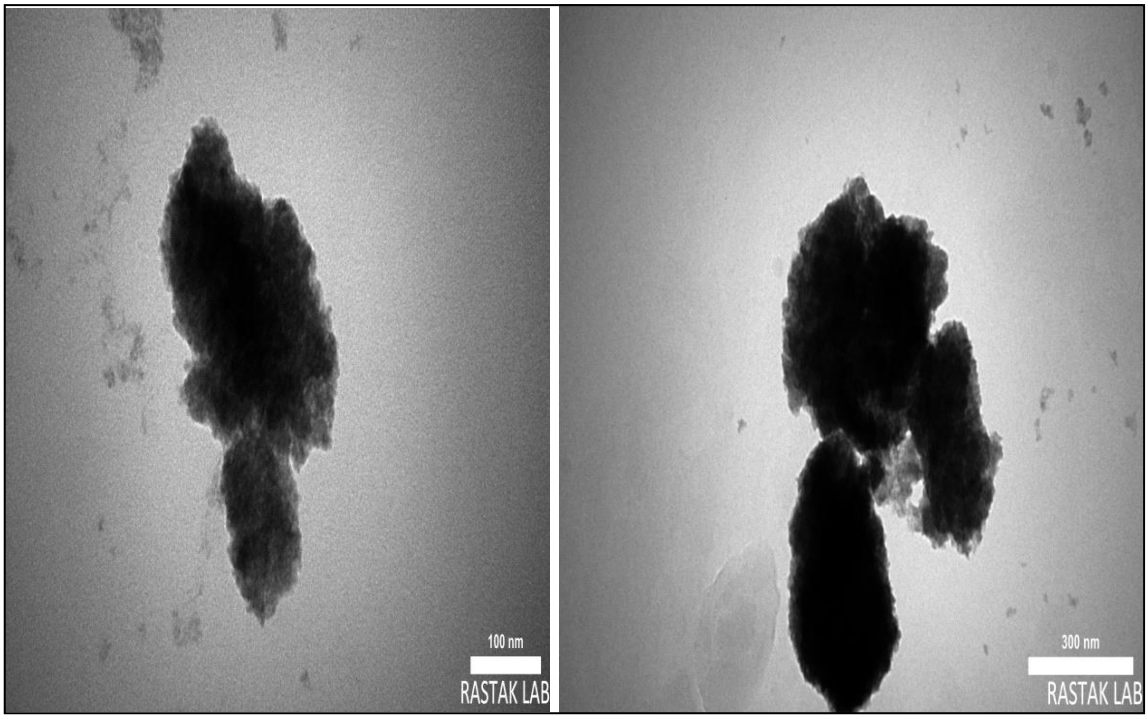

Fig. (4.6)b : Shows the TEM examination of CdS:Co thin film.

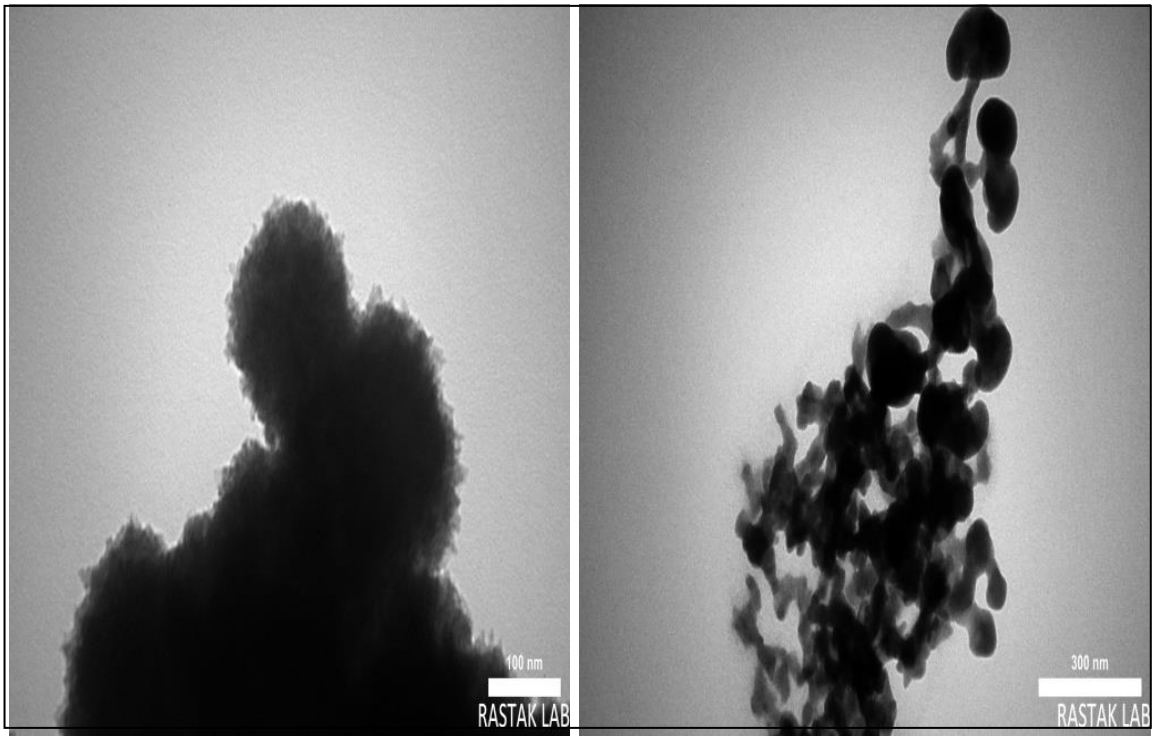

Fig. (4.6)c : Shows the TEM examination of CdS:Mg thin film.

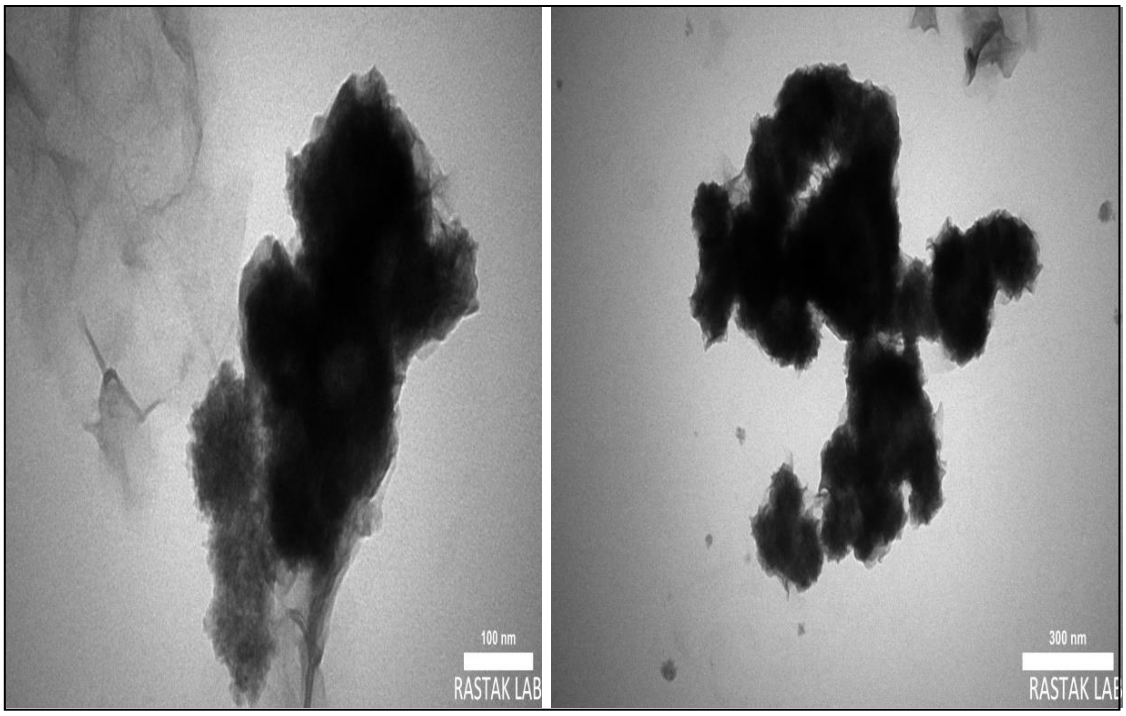

Fig. (4.6)d : Shows the TEM examination of CdS:Co:Mg thin film.

4.5 Optical Properties

The optical properties were measured and studied using a UV – Visible spectro-photometer for all prepared films, through which the absorption or transmittance spectrum is measured and the reflectivity and optical constants are calculated.

4.5.1 Absorbance (A)

The absorbance spectrra of the prepared thin films were measured based on Eq. (2.10)[72]. Fig. (4.7) shows the spectra of the absorbance curve for all the prepared films as a function of wavelength within the range from (400-1100) nm.

The results show through the figure that the prepared thin film CdS has high absorbance in the region of wavelengths less than 555 nm up to 80% of the incident ra and this was also found rouguly in [42,117,118]

This indicates that the prepared films is effective in the visible region range.Then we notice a rapid or sharp decrease in the absorption spectrum at wavelength 555 nm. The decrease in the absorption spectrum continues gradually with increasing wavelength. This means that the prepared thin films has high optical transparency.Therefore, we can consider this film prepared film like to TGO material. The diffraction occurring in the region of wavelengths less than 420 nm indicates the state of dispersion that occurs in the glass that was used in preparing the films and this was also found rouguly in [51,118].

We notice from the figure that the addition of cobalt acetate and magnesium acetate to the cadmium sulfide compound led to a displacement

of the absorption edge towards the long wavelengths region. This in turn leads to an increase in the absorbance of the prepared films. This result agree with [47,51,119].

The results of the absorption spectrum showed that all the prepared thin films exhibit similar optical behavior.That the absorption spectrum decreases with increasing wavelength.

This means physically that the falling photon cannot excite an electron and transfer it from the valence band to the conduction band. Because the energy of the incident photon is less than the value of the energy gap of the semiconductor [119].

Table (4.6) shows the absorbance values of all films prepared at a wavelength of 475 nm. The result showed that the addition of cobalt acetate and magnesium acetate to the cadmium sulfide compound led to an increase in the absorbance values.

Because the addition of cobalt acetate and magnesium acetate led to a change in the particle size shown by the results of X-ray diffraction. This confirms the entry of cobalt acetate and magnesium acetate into the crystal structure of the cadmium sulfide compound, which in turn leads to an increase in the absorbance values. This result agree with rouguly agree with[118,119] .

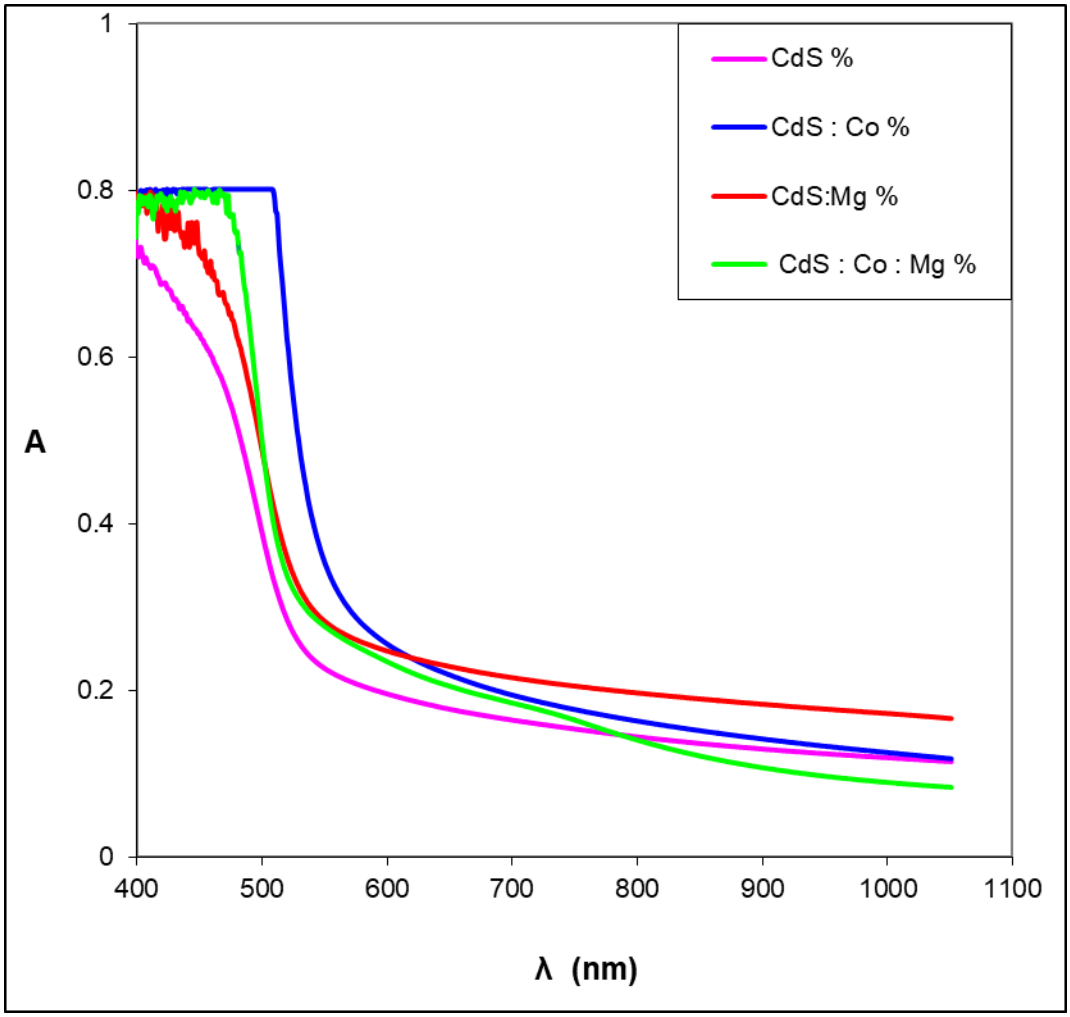

Fig. (4.7) : Shows the absorption spectrum of all prepared thin films as a function of wavelength.

Table (4.6): Shows the absorbance values for all prepared thin films.

sample	A
CdS	0.389
CdS:Co	0.801
CdS:Mg	0.489
CdS:Co:Mg	0.499

4.5.2 Ttransmittance(T)

The transmittance of the prepared thin films was calculated based on Eq. (2.11) . In Fig. (4.8) shows the transmittance spectrum for all the prepared thin films as a function of wavelength within the range from (400-1100) nm.

The results showed through the figure that the transmittance spectrum of all prepared films behaves optically opposite to the absorption spectrum. The prepared thin film cadmium sulfide has a low transmittance at wavelengths less than 430 nm this result agree with rouguly agree with[48,120].

Then we notice a rapid increase in the spectrum of the transmittance curve at wavelength 430 nm. This increase continues gradually at wavelengths greater than 430 nm with the increase in wavelength. This indicates that the prepared film has a high transmittance of about 70% in the visible wavelengths range, and it acts as a permeable layer for these wavelengths and above.

We notice from the figure that the transmittance spectrum behaves similar optically for all the prepared films. The transmittance curve increases with increasing wavelength.

Where he confirms that the rapid or sharp increase in the transmittance spectrum at the cutting edge indicates that the optical energy gap is of the direct type. Through the results of the absorption and transmittance spectrum, these prepared films can be used in the applications of solar cells and photodetectors and this result agree with [42,121].

Table (4.7) shows the transmittance values for all prepared thin films at an average wavelength of 475 nm. The results showed that the addition of cobalt acetate and magnesium acetate to the cadmium sulfide compound led to a decrease in the transmittance values.

This is due to the large attenuation of the incident rays on the prepared films, which works to increase the dispersion of the incident radiation and thus leads to a decrease in the transmittance values.

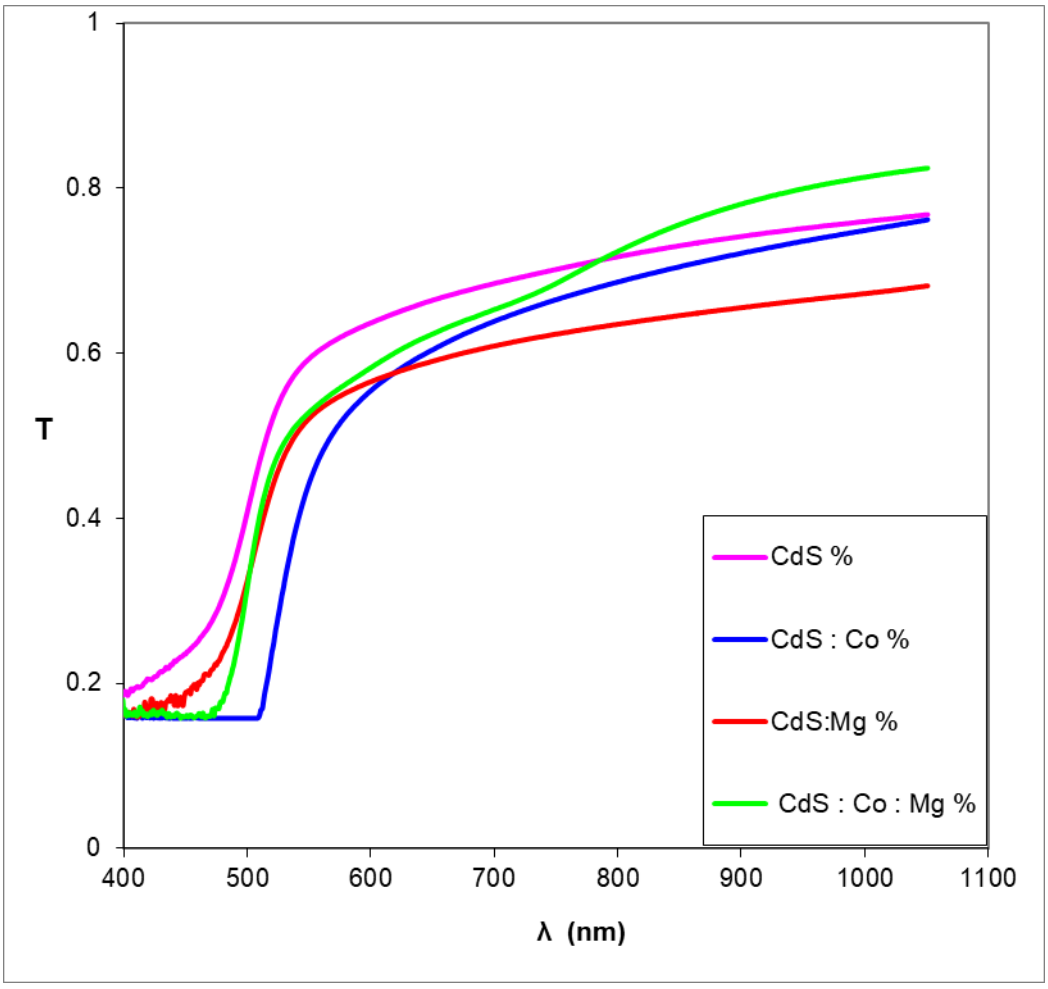

Fig. (4.8) : Shows the transmittance spectrum of all prepared thin films as a function of wavelength.

Table (4.7) : Shows the transmittance values for all prepared thin films.

sample	T
CdS	**0.407**
CdS:Co	**0.157**
CdS:Mg	**0.324**
CdS:Co:Mg	**0.316**

4.5.3 Reflectivity (R)

The reflectivity was calculated from the absorption and transmittance spectrum of the prepared thin films using the energy conservation law based on Eq. (2.13). In Fig. (4.9) shows the reflectance spectrum of all the prepared films as a function of wavelength within the range of (400-1100) nm.

The results showed through the figure that the prepared cadmium sulfide film has low reflectivity at short wavelengths. Then we notice a rapid increase in the reflectivity spectrum at wavelength 480 nm and this was also found rouguly in [34,38,122] .

This meaning that the prepared film has the highest reflectivity values in the visible region. There was a gradual decrease in the reflectivity spectrum at wavelengths higher than 480 nm. This decrease continues in the reflectivity spectrum with increasing wavelength and this was also found rouguly in [47,121].

We notice from the figure that the prepared thin film CdS has greater reflectance values than the prepared films CdS:Co, CdS:Mg, CdS:Co:Mg.

Because the addition of cobalt acetate and magnesium acetate to the cadmium sulfide compound led to a change in the crystal structure and the nature of the surfaces of the prepared films and this was also found rouguly in [121,123].

The addition of cobalt acetate and magnesium acetate led to an increase in the roughness of the surfaces of the prepared film, and this was confirmed by the results of the AFM measurement. The reflectivity decreases as the surface roughness of the prepared thin films increases .

Table (4.8) shows the reflectivity values of all prepared hin films at a wavelength of 475 nm. The results showed that the addition of cobalt acetate and magnesium acetate led to a decrease in the reflectivity values of the prepared films. Because cobalt acetate and magnesium acetate are reflective reducing materials[28,29].

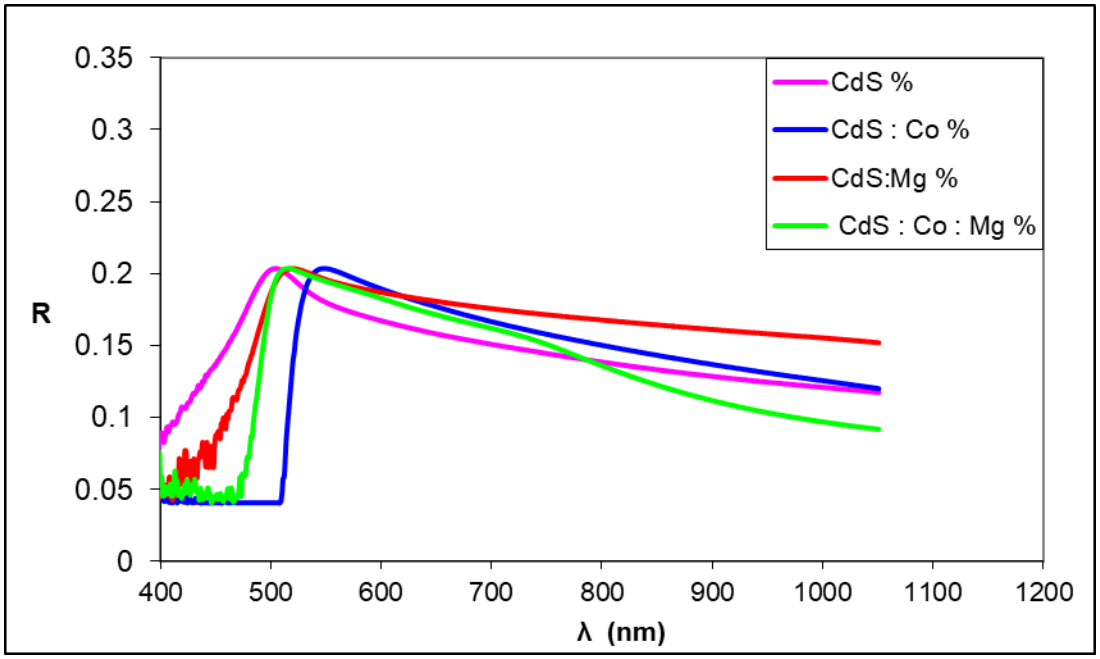

Fig. (4.9) : Shows the reflectivity spectrum of all prepared thin films as a function of wavelength.

Table (4.8) : shows the reflectivity values for all prepared thin films.

sample	R
CdS	**0.202**
CdS:Co	**0.040**
CdS:Mg	**0.186**
CdS:Co:Mg	**0.183**

4.5.4 Absorption coefficient (α)

The absorption coefficient of the prepared thin films was calculated from the absorbance values using Eq. (2.15) . In Fig. (4.10) show the spectrum of the absorption coefficient curve for all prepared thin films as a function of wavelength within the range from (400-1100) nm.

The results showed that the shape of the absorption coefficient spectrum curve for all the prepared films exhibits the same behavior optically and is similar to the shape of the absorption spectrum curve. This is because the relationship is direct between the absorption coefficient and the absorbance according to the Lambert equation and this was also found rouguly in [46,51,124]

We notice from the figure that the prepared thin film cadmium sulfide has lower absorption coefficient values than the prepared films CdS:Co, CdS:Mg and CdS:Co:Mg .

The absorption coefficient changes according to the change of wavelength. It depends on the energy of the incoming photons and the

properties of the semiconductor, which include the type of electronic transitions that occur between the bands and the optical energy gap and this was also found rouguly in [51,124].

The results showed that the prepared thin film cadmium sulfide had the highest value of the absorption coefficient at the 400 nm wavelength region in the visible region and this was also found rouguly in [121] .

Then we notice a decrease in the spectrum of the absorption coefficient at wavelengths greater than 400 nm, and this decrease continues gradually with increasing wavelength.

The results also showed that the values of the absorption coefficient are greater than 10000 cm^{-1}. This indicates the occurrence of electronic transitions of the direct type and this result agree with [51,124].

The table (4.9) shows the values of the absorption coefficient for all films prepared at a wavelength of 475 nm. The results showed that the addition of cobalt acetate and magnesium acetate to the compound cadmium sulfide led to an increase in the values of the absorption coefficient[75]. The reason for this is because the addition of cobalt acetate and magnesium acetate led to the formation of donor levels within the energy gap near From the conduction band. It in turn leads to the absorption of photons of low energies, and then an increase in the absorption coefficient values and this was also found rouguly in [46,121].

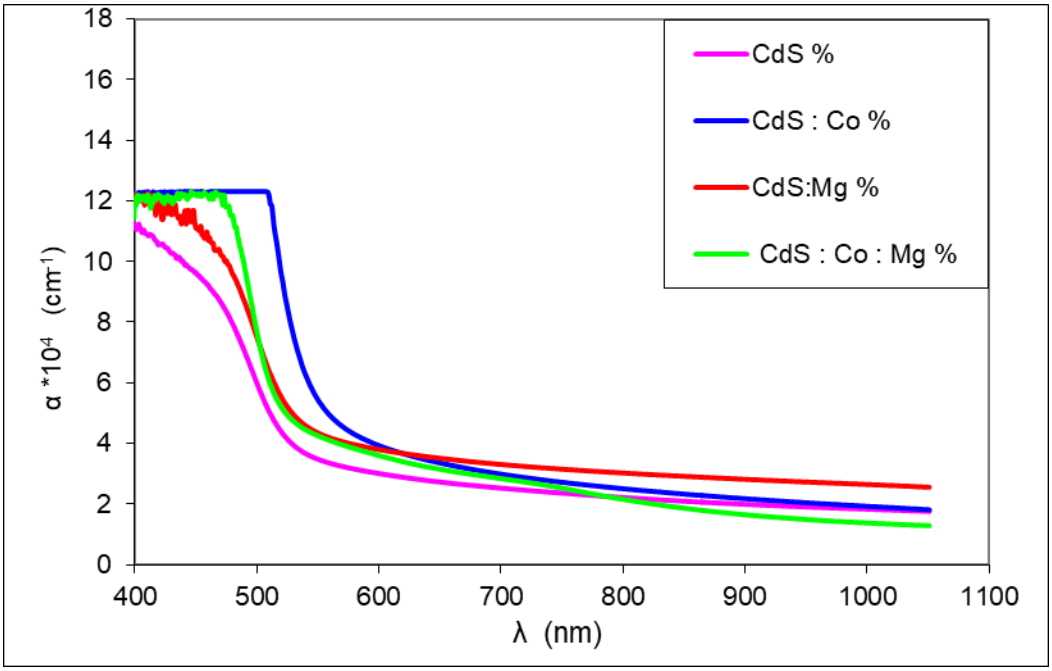

Fig. (4.10) : Shows the absorption coefficient spectrum of all prepared thin films as a function of wavelength.

Table (4.9) : shows the absorption coefficient values for all thin films.

sample	$\alpha \times 10^{-4}$
CdS	5.984
CdS:Co	12.306
CdS:Mg	7.510
CdS:Co:Mg	7.676

4.5.5 Optical Energy Gap (Eg)

In Fig. (4.11) shows the optical energy gap curves for direct transmission for all prepared films. The optical energy gap values for direct electronic transitions were calculated by drawing the linear relationship between $(\alpha h\nu)^2$ and the incident photon energy ($h\nu$) and by extending the

straight line part of the curve to cut the photon energy axis at point $(\alpha h\nu)^2 = 0$ and the Eq. (2.25) is achieved[79,80].

Table (4.10) shows the optical energy gap values for direct electronic transitions for all prepared films. The results showed that the prepared thin film cadmium sulfide (CdS) has an optical energy gap value greater than the optical energy gap values for the prepared films CdS:Co,Cd:Mg and CdS:Co:Mg and this was also found rouguly in [44,51,125] .

Because the addition of cobalt acetate and magnesium acetate to the cadmium sulfide compound led to the formation of donor levels within the optical energy gap, which reduces the width of the optical energy gap[133]. This in turn leads to the absorption of photons with low energies. Then leads to an increase in the absorption coefficient and the occurrence of the direct type of electronic transitions. This is confirmed by the absorption coefficient values that are greater than 10000 cm^{-1} for the prepared films and this was also found rouguly in [51,122,125].

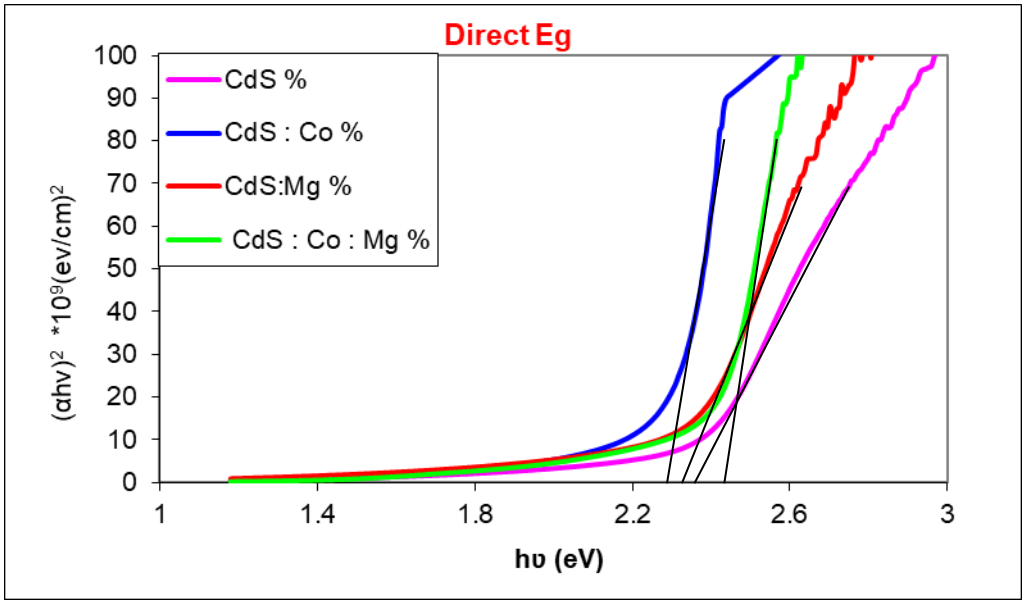

Fig.(4.11) : Show the direct energy gap of all thin films.

Table (3.10) : The direct energy gap values of all thin films.

sample	Eg eV
CdS	2.39
CdS:Co	2.24
CdS:Mg	2.31
CdS:Co:Mg	2.35

4.5.6 Refractive Index (n)

The refractive index of the prepared thin films was calculated by usivg Eq. (2.20) . In Fig. (4.12) shows a spectrum of the refractive index curve for all the prepared thin films as a function of wavelength within the range from (400-1100) nm.

The results showed that the shape of the refractive index spectrum curve for all prepared films is similar to the reflectance spectrum curve.

The prepared thin film cadmium sulfide has the lowest values of the refractive index at the wavelength of 400 nm. Then we notice an increase in the spectrum of the refractive index curve at wavelength 400 nm. But at wavelengths greater than 400 nm, there is a gradual decrease in the spectrum of the refractive index. This decrease continues with the increase in wavelength and this was also found rouguly in [122,123,126].

Table (4.11) shows the refractive index values for all films prepared at an average wavelength of 475 nm. The results showed that the prepared thin film cadmium sulphide had greater refractive index values than the prepared films CdS:Co, CdS:Mg and CdS:Co:Mg.

Because the addition of cobalt acetate and magnesium acetate to the cadmium sulfide compound led to an increase in the absorbance values and a decrease in the transmittance and reflectivity values. This in turn leads to a decrease in the refractive index values because it depends on the reflectivity values and this was also found rouguly in [119,125].

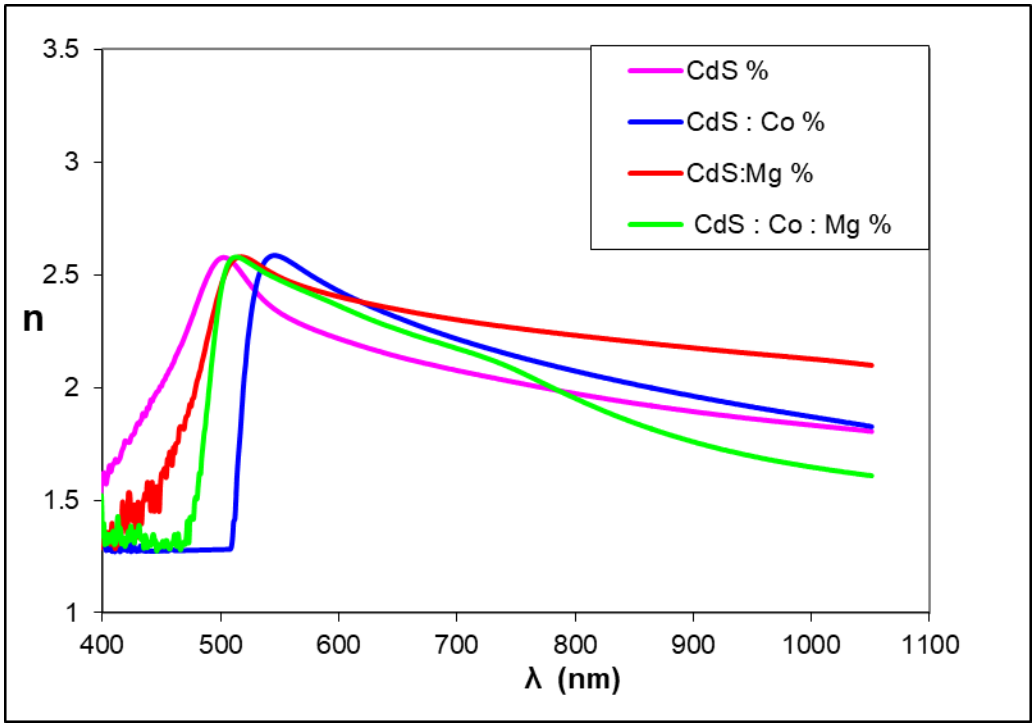

Fig. (4.12) : Shows the refractive index spectrum of all prepared thin films as a function of wavelength.

Table (4.11) : Shows the refractive index values for all thin films.

sample	n
CdS	2.573
CdS:Co	1.280
CdS:Mg	2.445
CdS:Co:Mg	2.421

4.5.7 Extinction Coefficient

The extinction coefficient was calculated for the prepared thin films using Eq. (2.18). In Fig. (4.13) shows the curve of the extinction coefficient spectrum for all the prepared films as a function of wavelength within the range from (400-1100) nm.

The results showed that each of the extinction coefficient spectrum curves of the prepared films exhibited an optical behavior similar to the absorption coefficient spectrum curve and this was also found rouguly in [122,127] .

We note that the prepared cadmium sulfide film has the Larger value of the extinction coefficient at the 400 nm wavelength region. Then we notice a rapid decrease in the spectrum of the extinction coefficient at wavelength 500 nm.

Then a gradual decrease in the spectrum of the extinction coefficient at wavelengths greater than 500 nm. This gradual decrease in the spectrum of the extinction coefficient continues with the increase in wavelength and this was also found rouguly in [36,119].

Table (4.12) shows the values of the extinction coefficient for all the thin films prepared at an average wavelength of 475 nm. The results showed that the prepared thin film cadmium sulfide had lower extinction coefficient values than the values of the films prepared CdS:Co, CdS:Mg and CdS:Co:Mg.

This is because the addition of cobalt acetate and magnesium acetate to the cadmium sulfide compound led to a decrease in the values of the optical energy gap and an increase in the absorbance values[126]. This in turn led to

an increase in the values of the absorption coefficient and the extinction coefficient because the extinction coefficient depends on the values of the absorption coefficient and this is the reason for the increase in the values of the extinction coefficient and this was also found rouguly in [118,127].

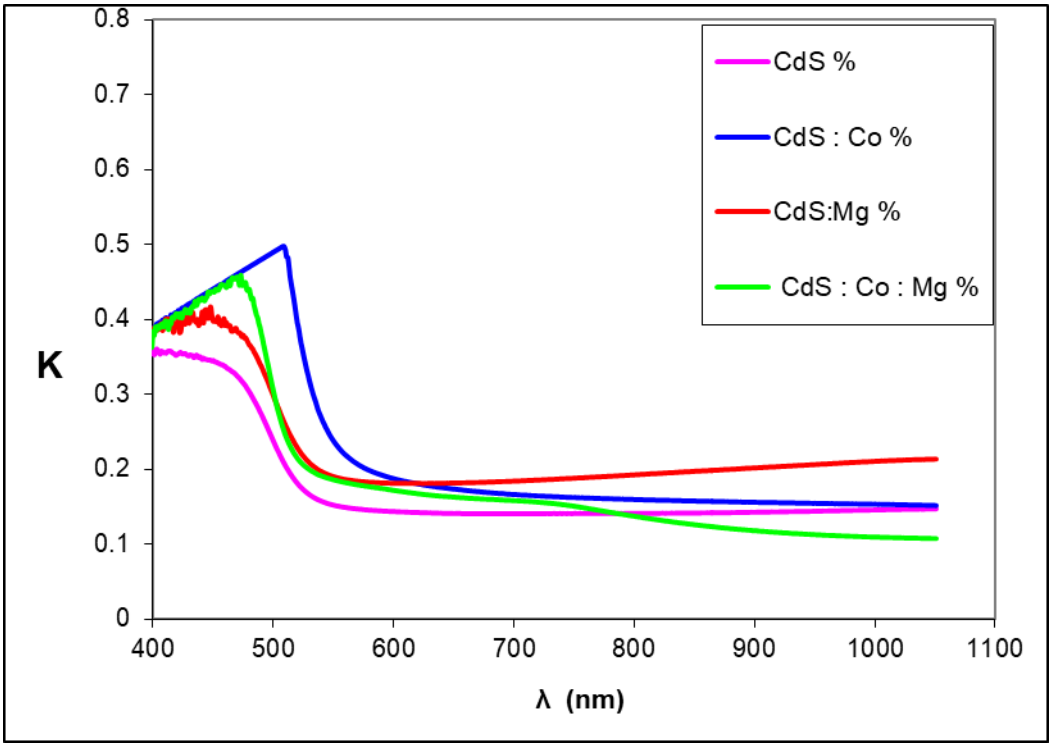

Fig. (4.13) : Shows the extinction coefficient spectrum of all prepared thin films as a function of wavelength.

Table (4.12) : Shows the extinction coefficient values for all thin films.

sample	K
CdS	0.238
CdS:Co	0.489
CdS:Mg	0.298
CdS"Co:Mg	0.305

4.5.8 Dielectric Constant

4.5.8.1 Real Dielectric Constant (ε_{real})

The real dielectric constant of the prepared thin films was calculated using Eq. (2.22) . In Fig. (4.14) shows a spectrum of real dielectric constant curve for all the prepared thin films as a function of wavelength within the range from (400-1100) nm.

The results showed through the figure that the spectrum curve of the real dielectric constant behaves optically similar to the curve of the refractive index spectrum.

The prepared thin film cadmium sulfide has the lowest value at wavelength 400 nm. Then we notice an increase in the spectrum of the real dielectric constant at wavelength 470 nm. But at wavelengths greater than 470 nm, the spectrum of the real dielectric constant begins to gradually decrease, and this decrease continues with increasing wavelength and this was also found rouguly in [119,126,127].

Table (4.13) shows the values of the real dielectric constant for all the films prepared at an average wavelength of 475 nm. The results showed that the prepared thin film cadmium sulfide has a real dielectric constant value greater than the prepared films CdS:Co, CdS:Mg and CdS:Co:Mg.

Because the real dielectric constant depends on the refractive index values more than the extinction coefficient, because the extinction coefficient values are very few compared to the refractive index values. Since the addition of cobalt acetate and magnesium acetate to the compound cadmium sulfide led to a decrease in the refractive index values, and this in

turn leads to a decrease in the values of the real dielectric constant of the prepared films and this was also found rouguly in [36,46,127].

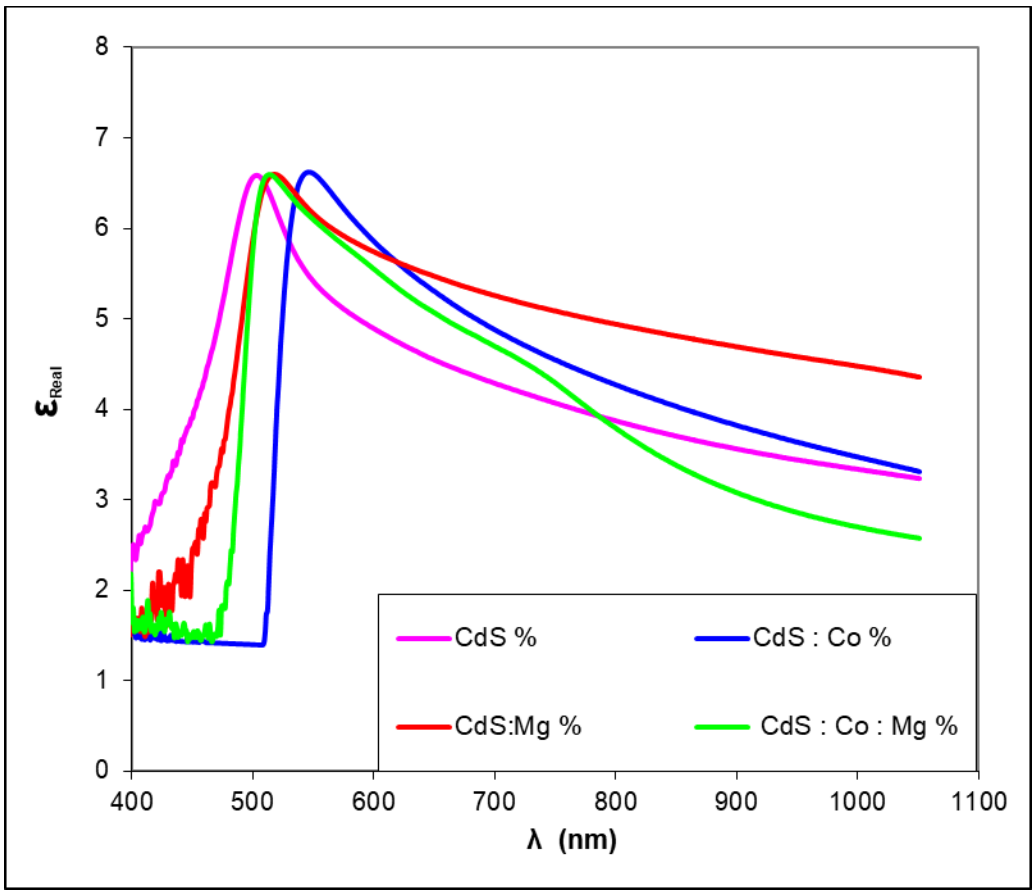

Fig. (4.14) : Shows the real dielectric constant spectrum of all prepared thin films as a function of wavelength.

Table (4.13) : Shows the real dielectric constant values for all thin films.

sample	ε_{real}
CdS	6.565
CdS : Co	1.400
CdS : Mg	5.892
CdS : Mg : Co	5.770

4.5.8.2 imaginary dielectric constant

The imaginary dielectric constant of the prepared thin films was calculated by using Eq. (2.23). In Fig. (4.15) shows a curved spectrum of imaginary dielectric constant for all prepared films as a function of wavelength within the range from (400-1100) nm.

The results showed that the shape of the imaginary dielectric constant curve behaves optically similar to the exciton coefficient spectrum curve.

We notice from the figure that the prepared thin film cadmium sulfide has an imaginary dielectric constant value less than the prepared films CdS:Co, CdS:Mg and CdS:Co:Mg.

It was found that the lowest value of the dielectric constant for all films prepared at short wavelengths is 400 nm. As for certain wavelengths between (480-510) nm. The spectrum of the dielectric constant has the highest value, and at wavelengths greater than that. We notice a gradual decrease in the spectrum of the dielectric constant, and this decrease continues with the increase in wavelength and this was also found rouguly in [35,127,128].

Table (4.14) shows the imaginary dielectric constant values for all thin films prepared at an average wavelength of 475 nm. The results showed that the addition of cobalt acetate and magnesium acetate to the cadmium sulfide compound led to an increase in the dielectric constant values. Because the imaginary dielectric constant depends on the values of the exction coefficient and this was also found rouguly in [35,128].

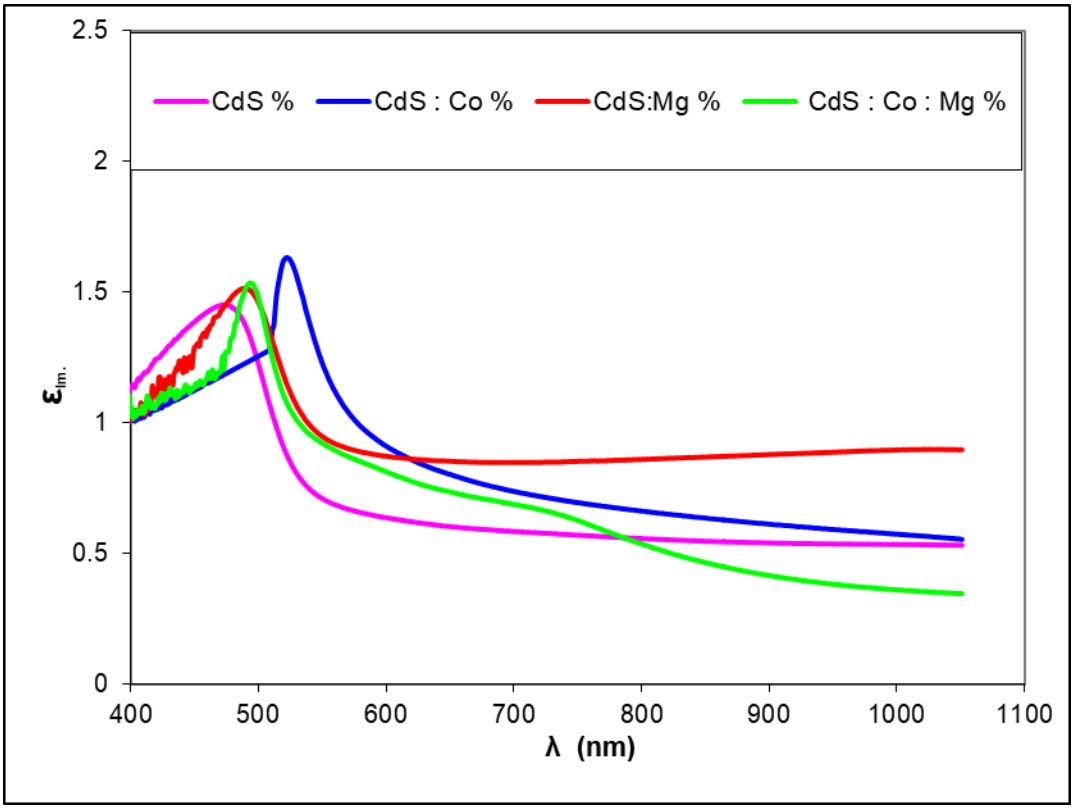

Fig. (4.15) : Shows the imaginary dielectric constant spectrum of all prepared thin films as a function of wavelength.

Table (4.14) : Shows the imaginary dielectric constant values for all thin films.

sample	$\varepsilon_{Im.}$
CdS	1.226
CdS : Co	1.255
CdS : Mg	1.462
CdS : Mg : Co	1.480

4.6 Electric Properties

4.6.1 Current-Voltage measurent (I-V)

The behavior of the prepared thin films CdS, CdS:Co, CdS:Mg and CdS:Co:Mg was studied by measuring the current-voltage. Shows a graphic representation of the current values against the potential difference. Whereas, ohmic conductors are represented by straight lines, while non-ohmic conductors are represented by curves.

The results showed through Fig. (4.16) a,b,c and d that the relationship between the current and the voltage is linear.This indicates that the relationship is ohmic, and this confirms that all the prepared films behave in an ohmic behavior. The constant ratio between the voltage difference and the current is known as the resistance. Where the conductivity was calculated based on the Eq. (2.33) after knowing the resistance values based on the Eq. (2.32) by knowing the values of the reciprocal of the slope and calculating the resistivity for all the prepared films and this was also found rouguly in [35,129,130].

Table (4.15) shows the values of conductivity and resistivity of all prepared thin films obtained by measuring current-voltage.

The results showed that the electrical conductivity of the prepared thin film cadmium sulfide had lower values than the prepared CdS:Co,CdS:Mg and CdS:Co:Mg films.

This means that the addition of cobalt acetate and magnesium acetate to the cadmium sulfide compound led to an increase in the electrical conductivity values of the prepared films. The reason for this is because the

addition of cobalt acetate and magnesium acetate led to an increase in the current values and a decrease in the resistance values, as indicated by current-voltage measurements and this was also found rouguly in [123]

This result applies to Ohm's law because the relationship between current and resistance is inverse. The increase in current leads to an increase in electrical conductivity values and a decrease in resistance values and this was also found rouguly in [85,129].

This result is identical to the results of the Hall effect measurement, which showed that the addition of cobalt acetate and magnesium acetate leads to an increase in the electrical conductivity values of the prepared films as a result of an increase in the concentration values of charge carriers and this was also found rouguly in [129,130].

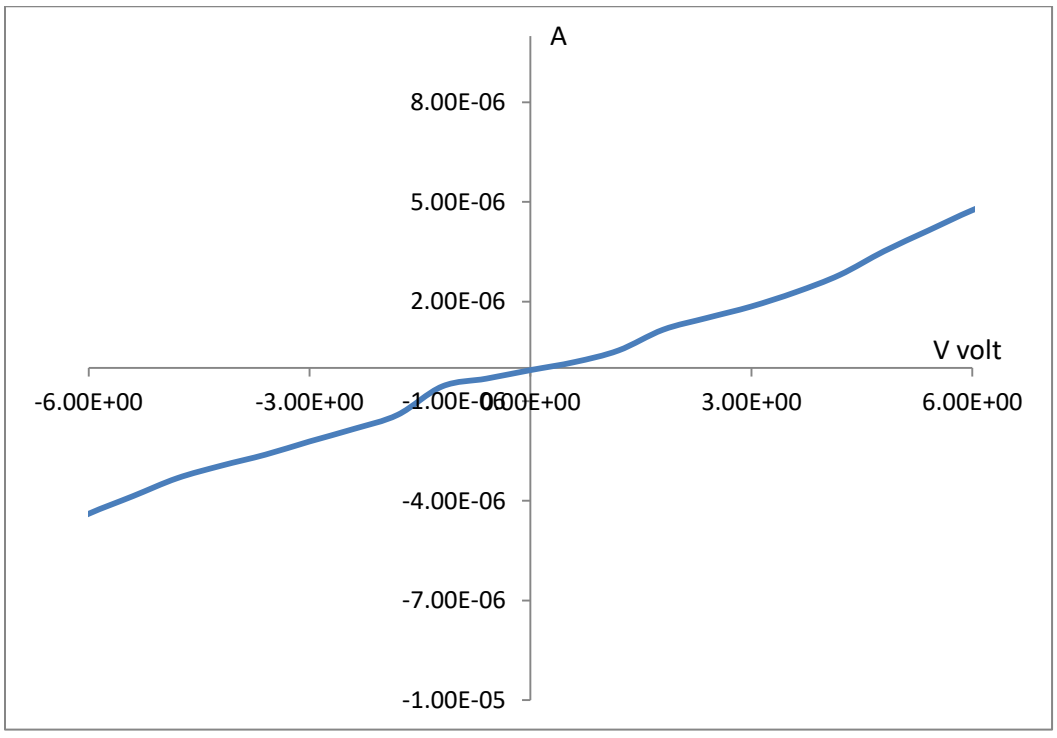

Fig. (4.16)a : Measuring current-voltage of CdS the thin film.

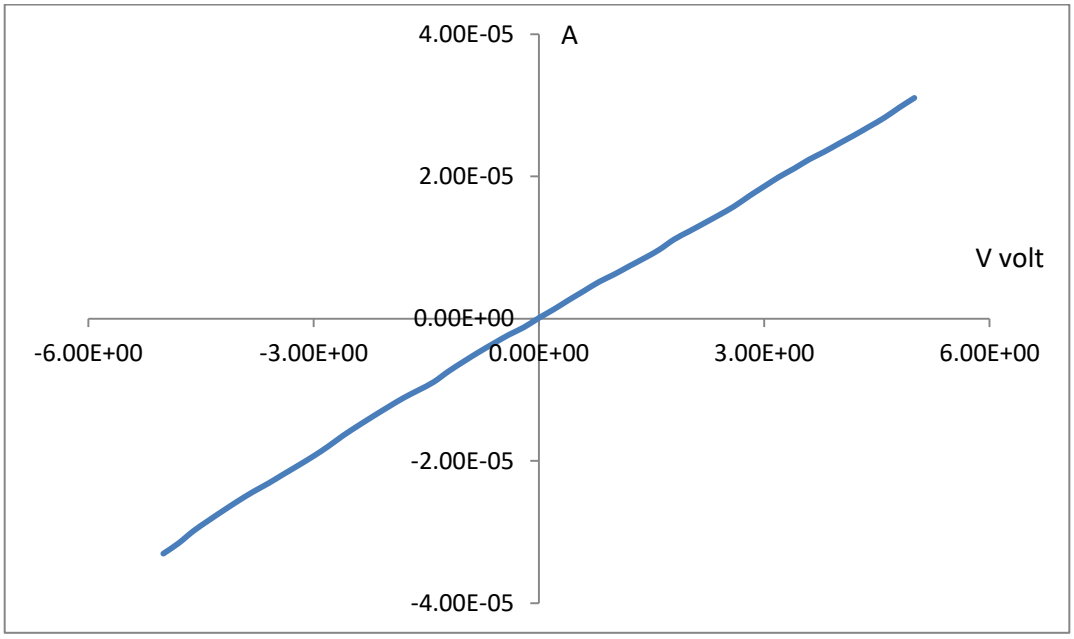

Fig.(4.16)b : Measuring current-voltage of CdS:Co thin film.

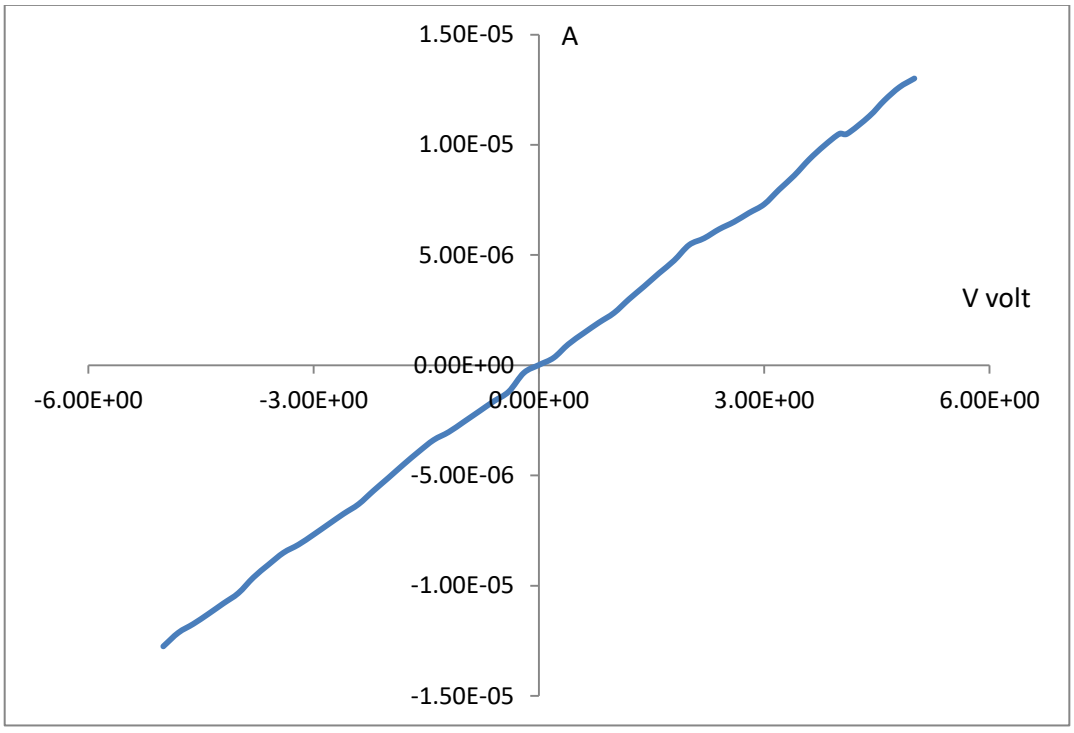

Fig. (4.16)c : Measuring current-voltage of CdS:Mg thin film.

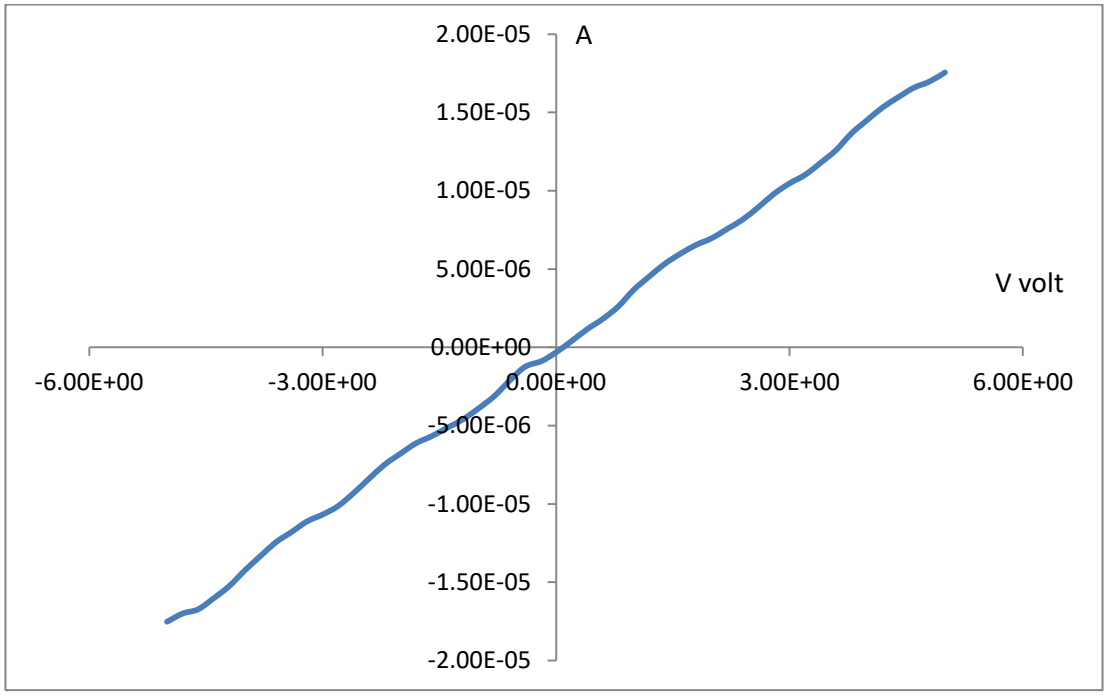

Fig. (4.16)d : Measuring current-voltage of CdS:Mg:Co thin film.

Table (4.15) : Shows the conductivity values from a current-voltage measurement.

Sample	Slope	R=1/Slope	ρ (Ω.cm)	σ $(\Omega.cm)^{-1}$
CdS	6.791×10^{-7}	0.147×10^{7}	58.901	0.016
CdS:Co	6.302×10^{-6}	0.138×10^{6}	6.347	0.157
CdS:Mg	2.548×10^{-6}	0.392×10^{6}	15.699	0.063
CdS:Co:Mg	3.526×10^{-6}	0.283×10^{6}	11.344	0.087

4.6.2 $\sigma_{D.C}$ Conductivity

The continuous electrical conductivity of the prepared thin films was calculated based on Eq. (2.33) by measuring and studying the change of electrical resistance with temperature within the range of (300-500) K.

The electrical conductivity values were known after calculating the resistivity using Eq. (2.32)[85].

Also, by drawing the graphic relationship between (Inσ) on the y- axis and the reciprocal of temperature (1000/T) on the x –axis . The slope values were known, and according to the Stock relation, the activation energy values were calculated based on Eq. (2.27)[83].

Fig. (4.17) a,b,c and d shows the continuous electrical conductivity of all prepared thin films as a function of temperature within the range of (300-500) K. The results showed that the electrical resistance decreases for all prepared thin films with increasing temperature. This confirms that semiconductors have a resistance with a negative thermal coefficient, which in turn leads to an increase in electrical conductivity with an increase in temperature and this was also found rouguly in [35,130,131]

While Fig. (4.18) a,b,c and d shows the change of (Inσ) as a function of the reciprocal of temperature (1000/T). Where we notice that the electrical conductivity increases with the increase in temperature and this is a characteristic of semiconductors. Because the increase in temperature leads to an increase in the number of electron-hole pairs generated and this in turn leads to an increase in the continuous electrical conductivity and this was also found rouguly in [123,130].

Table (4.16) shows the activation energy values for all prepared thin films. The results showed that the prepared thin film cadmium sulfide has only one value for the activation energy. This explains the existence of one mechanism for the transfer of charges within the range of temperatures at

which the activation energy was calculated and this was also found rouguly in [121].

We note that the films prepared CdS:Co, CdS:Mg and CdS:Co:Mg have two values of activation energy. This explains the existence of two types of cargo transport mechanics or electronic transport. The first mechanism occurs at low temperatures at which the first activation energy was calculated. The conduction is gradual in a jumping or tunneling manner between local levels within the energy gap according to Davised and Mose model. The second mechanism occurs at relatively high temperatures, at which the second activation energy was calculated, and the transfer of charges is by thermal irritation and this was also found rouguly in [123,129,131].

The results showed that the addition of cobalt acetate and magnesium acetate to the cadmium sulfide compound led to an increase in the electrical conductivity values and a decrease in the initial activation energy values.

The reason for this is because the addition of cobalt acetate and magnesium acetateled to the formation of secondary levels within the energy gap that accommodate mobile electrons. This leads to a decrease in the values of the energy gap.The transition between levels becomes faster, so the electrical conductivity increases and the activation energy needed by charge carriers to move decreases and this was also found rouguly in [129,130].

We conclude that the relationship is direct between the activation energy and the optical energy gap. While the relationship is inverse between the electrical conductivity and the activation energy, because the increase the

electrical conductivity, the less activation energy is needed for the electrons and this was also found rouguly in [123,130].

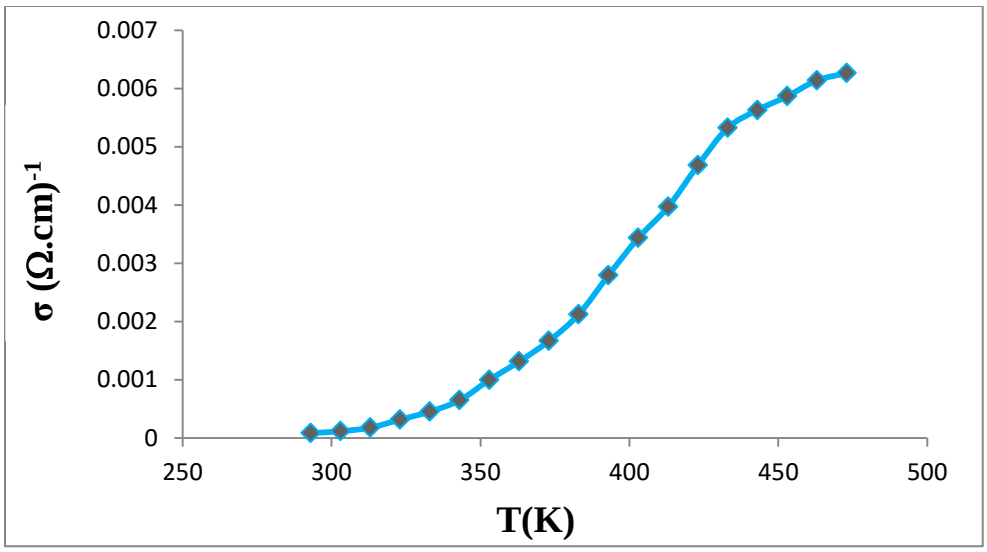

Fig. (4.17)a : Shows the electrical conductivity as a function of temperature for the prepared CdS thin film.

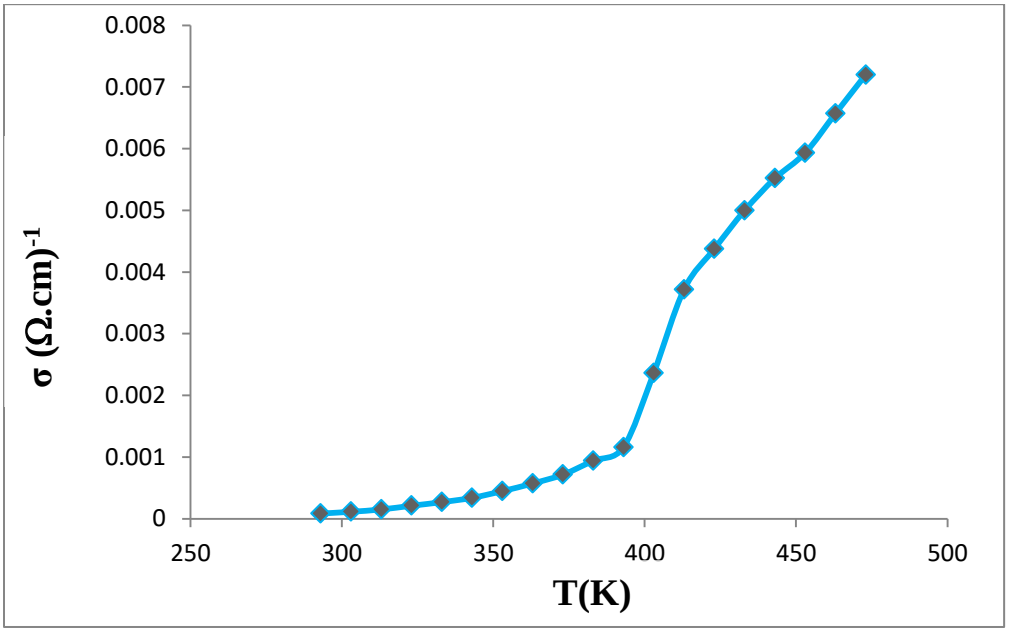

Fig. (4.17)b : Shows the electrical conductivity as a function of temperature for the prepared CdS:Co thin film .

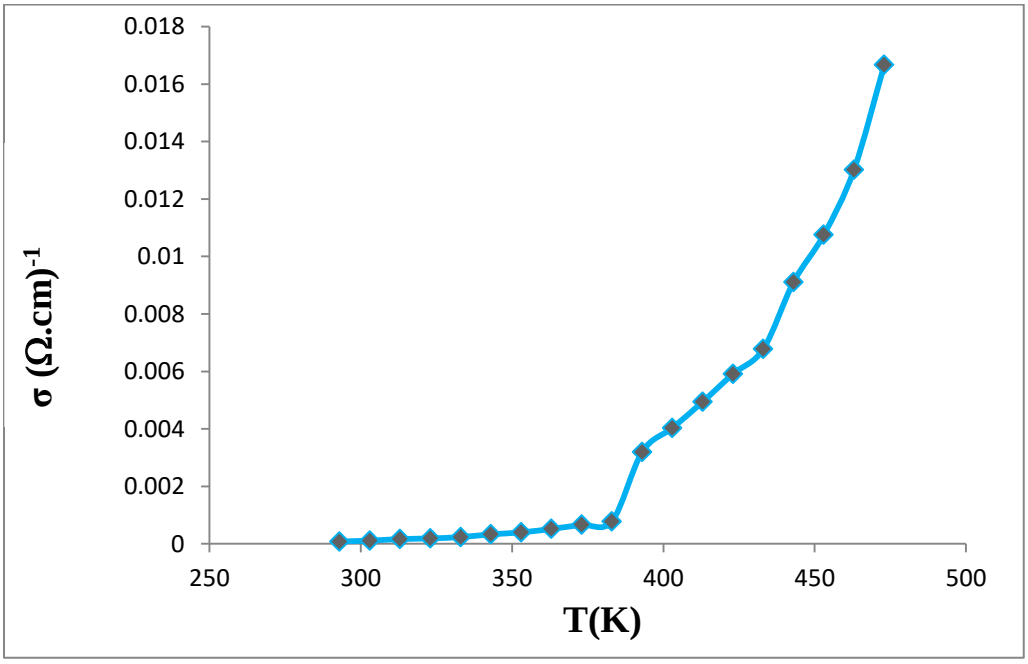

Fig. (4.17)c : Shows the electrical conductivity as a function of temperature for the prepared CdS:Mg thin film.

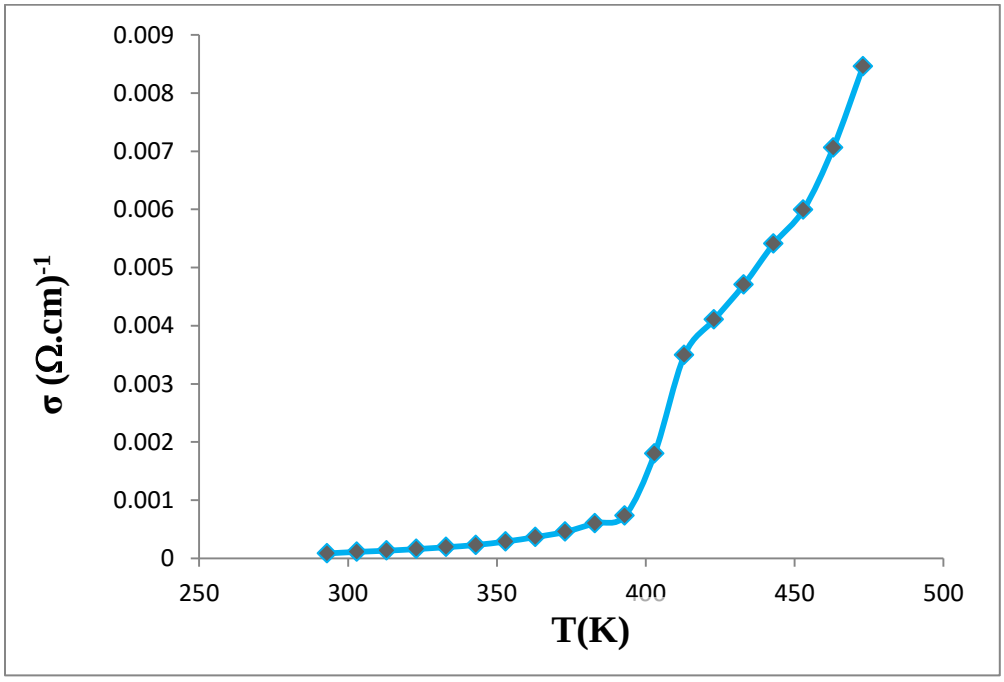

Fig.(4. 17)d : Shows the electrical conductivity as a function of temperature for the prepared CdS:Co:Mg thin film.

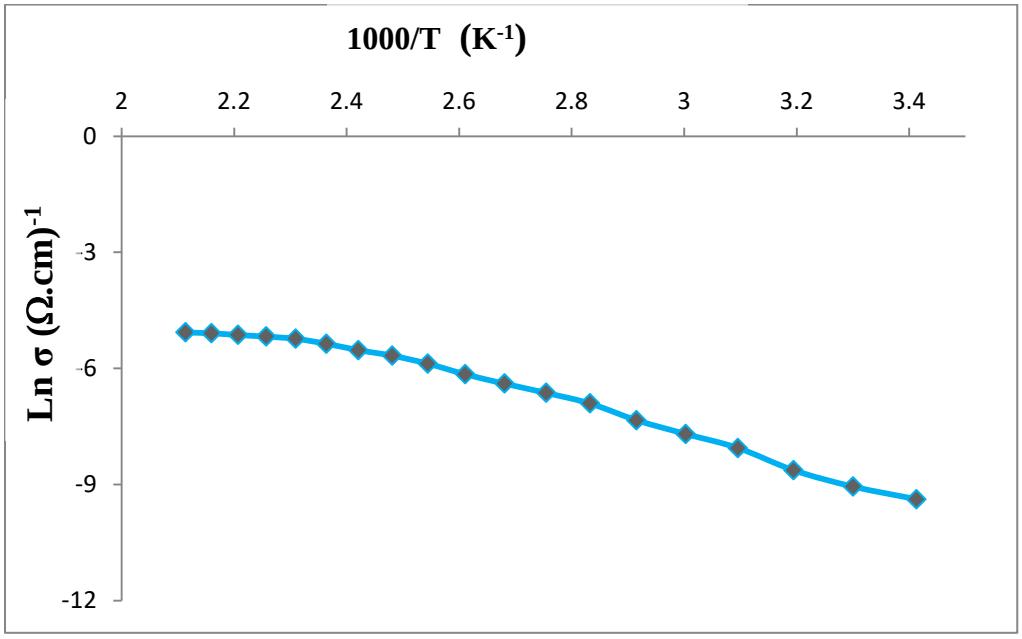

Fig. (4.18)a : The relationship between Inδ and 1000/T for the prepared CdS thin film.

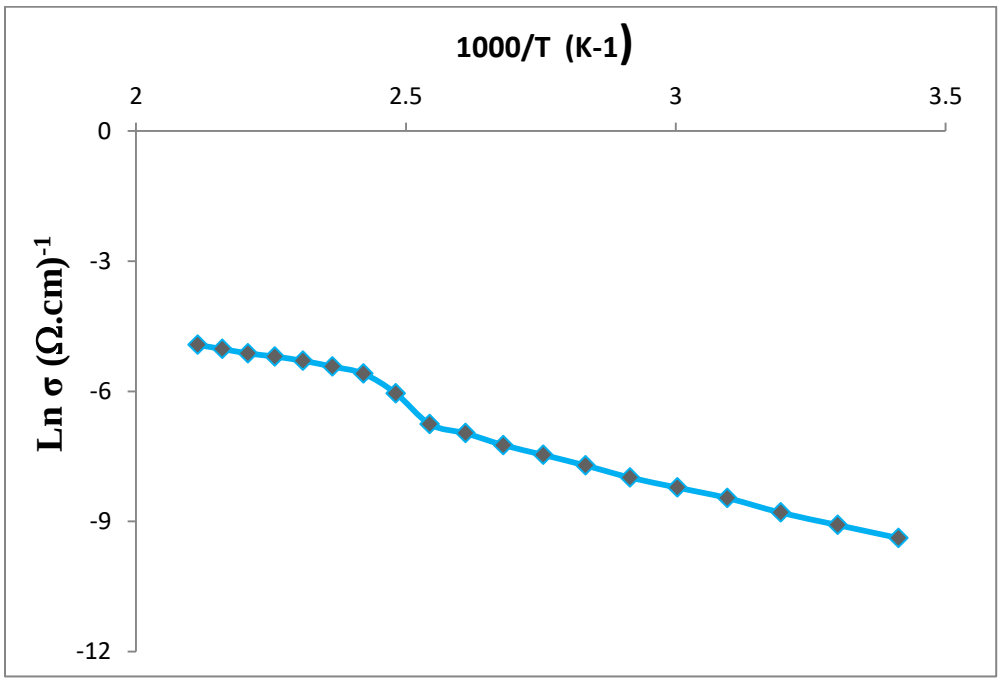

Fig. (4.18)b : The relationship between Inδ and 1000/T for the prepared CdS:Co thin film.

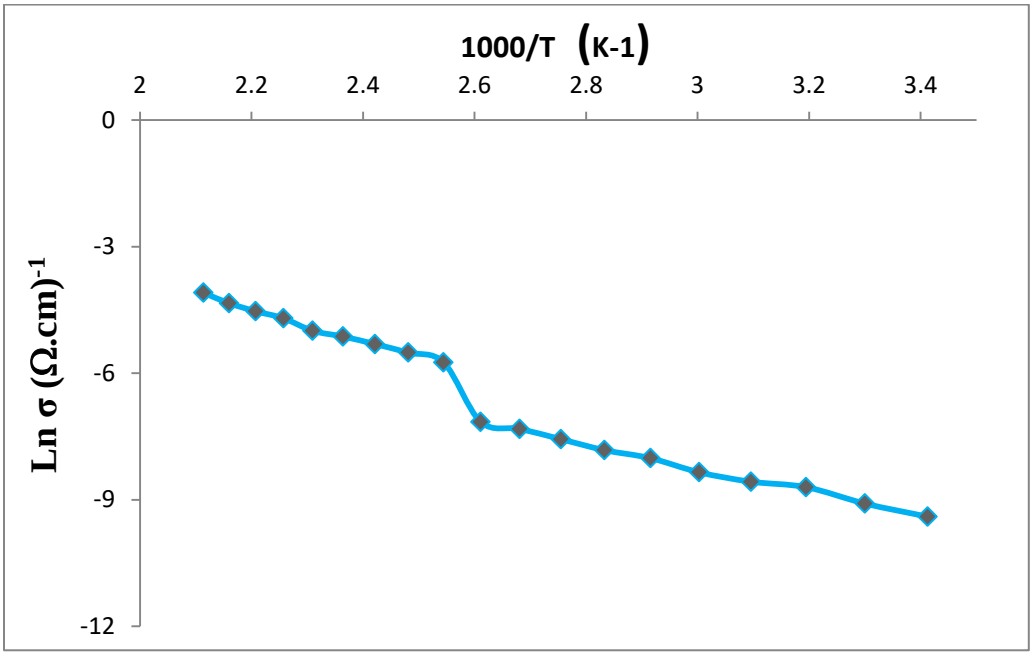

Fig. (4.18)c : The relationship between Inδ and 1000/T for the prepared CdS:Mg thin film.

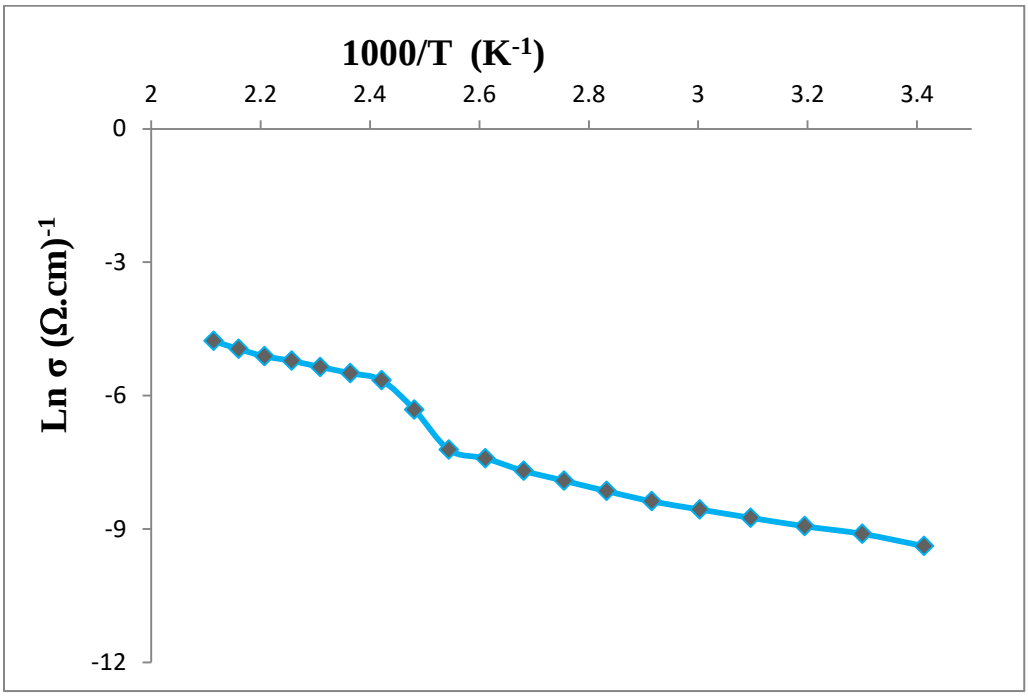

Fig.(4.18)d : The relationship between Inδ and 1000/T for the prepared CdS:Co:Mg thin film.

Table (4.16) : shows the activation energy values for all prepared thin films.

sample	Ea1	Ea2
CdS	0.348	------
CdS:Co	0.315	0.257
CdS:Mg	0.322	0.240
CdS:Co:Mg	0.239	0.210

4.6.3 Hall effect

The hall effect was measured at room temperature for the prepared thin films. We notice when an electric current is passed through the prepared thin films and in the presence of a constant magnetic field of 0.550 Tesla.

From measuring the change in the hall voltage generated at both ends of the films with the change of the main current passing through it. It was possible to know and calculate the hall coefficient based on Eq. (2.34). The density of charge carriers, mobility and conductivity were calculated based on Eqs. (2.35) (2.36) (2.37), respectively[86,87].

Table (4.17) shows the results of the hall measurement of the prepared thin films. Where we notice through the results that the values of the hall coefficient for the prepared thin films have negative values. This indicates that the prepared films are of the negative type. This means that the majority carriers are electrons and the minority carriers are the holes and this was also found rouguly in [131,132].

We note that the addition of cobalt acetate and magnesium acetate to the cadmium sulfide compound led to a decrease in the values of hall

coefficient and resistivity, and an increase in the values of mobility, concentration of charge carriers, and electrical conductivity.

The decrease in the hall coefficient values is due to an increase in the concentration of charge carriers. When the values of the concentration of charge carriers in the prepared films increase. It works to reduce the area between the Fermi level and the conduction band, and this is consistent with the decrease in the activation energy that was calculated in the measurement of continuous electrical conductivity and the decrease in the optical energy gap as shown by the measurements of the optical properties. This in turn leads to an increase in electrical conductivity and mobility because the relationship between them is direct and this was also found rouguly in [123,132].

Table (4.17) : shows the results the Hall effect measurement of the perpared thin films.

Sample	R_H (cm^{-3}/C)	n_H ($1/cm^3$)	ρ (Ω.cm)	μ_H ($cm^2/V.S$)	σ $1/(\Omega.cm)$
CdS	-3.529×10^{8}	-2.205×10^{11}	1.529×10^{6}	1.526×10^{1}	6.539×10-7
CdS:Mg	-2.149×10^{7}	-2.905×10^{11}	1.471×10^{5}	1.461×10^{2}	6.797×10^{-6}
CdS:CO	-3.994×10^{6}	-1.563×10^{12}	4.179×10^{4}	9.558×10^{1}	2.393×10^{-5}
CdS:Co:Mg	-2.505×10^{7}	-2.492×10^{11}	1.606×10^{5}	1.560×10^{2}	6.228×10^{-6}

4.6.4 Capacitance-Voltage Measurement

The capacitance-voltage measurement is an important standard method for obtaining several parameters of the hybrid junction CdS/Si, CdS:Co/Si, CdS:Mg/Si and CdS:Co:Mg/Si . Where it is possible to calculate the internal building voltage and determine the type of junction.

In Fig. (4.19)a,b,c and d shows the capacitance-voltage characteristics of the hybrid junction CdS/Si, CdS:Co/Si, CdS:Mg/Si and CdS:Co:Mg/Si. We notice the change of the junction capacity with the forward and reverse bias voltage at a fixed frequency of 600KHZ. The results showed a decrease in the junction capacitance with the bias voltage as a result of the increase in the width of the depletion region. Because the direct relationship between the depletion region and the internal building voltage and this was also found rouguly in [98,123,133].

The addition of cobalt acetate and magnesium acetate to the cadmium sulfide compound led to a decrease in the junction capacity. This may be attributed to the improvement of the crystalline properties of the prepared films, which led to the reduction of structural defects and an improvement in the electrical properties, as indicated by current-voltage measurements and the Hall effect. Increasing the concentration of charge carriers increases the internal building voltage, and thus increases the width of the depletion region[133].

Where the internal building voltage was calculated from drawing the relationship between the inverted square of the capacitance $1/c^2$ with the reverse bias voltage as in Fig. (4.20) a,b,c and d. We note that the relationship is linear between the voltage and the reciprocal of the square of the capacitance.This indicates that the prepared separator is of the abrut type.

From the intersection of the straight line with the voltage axis $1/c^2 = 0$, then the internal construction effort values are determined as in Table (4-18) and this result agree wiht[132,133].

Table (4.18) : Show the internal building voltage of all thin films.

sample	V_{bi}
CdS	0.24
CdS:Co	1.65
CdS:Mg	0.32
CdS:Co:Mg	1.35

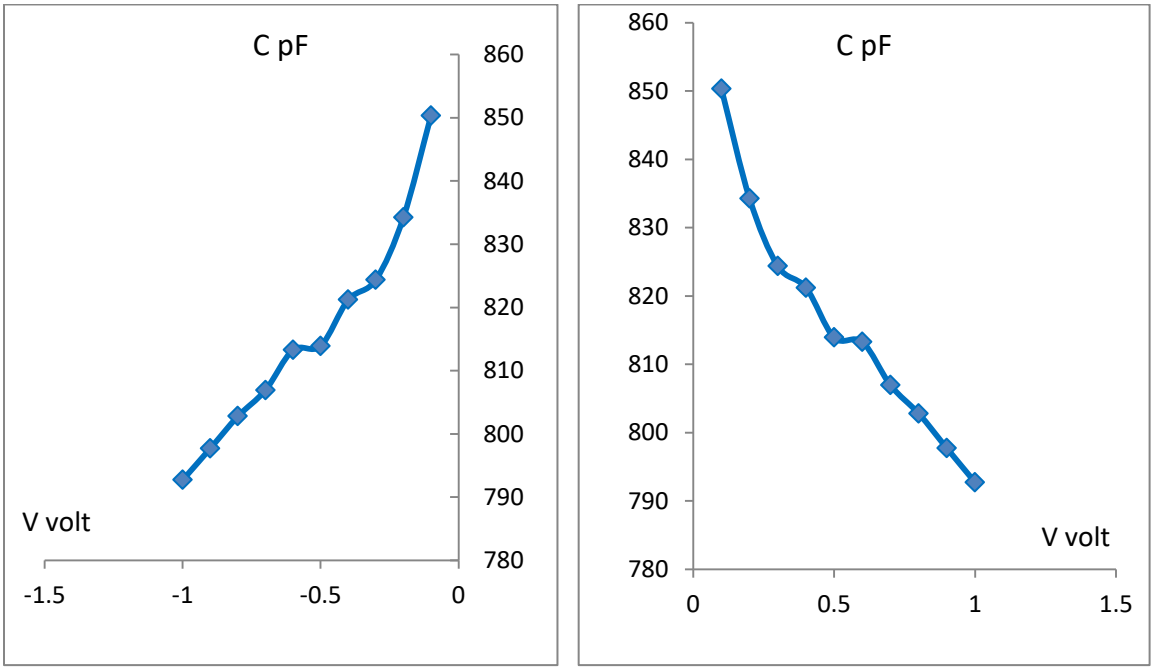

Fig. (4.19)a : Shows the capacitance-voltage measurementp of CdS thin film.

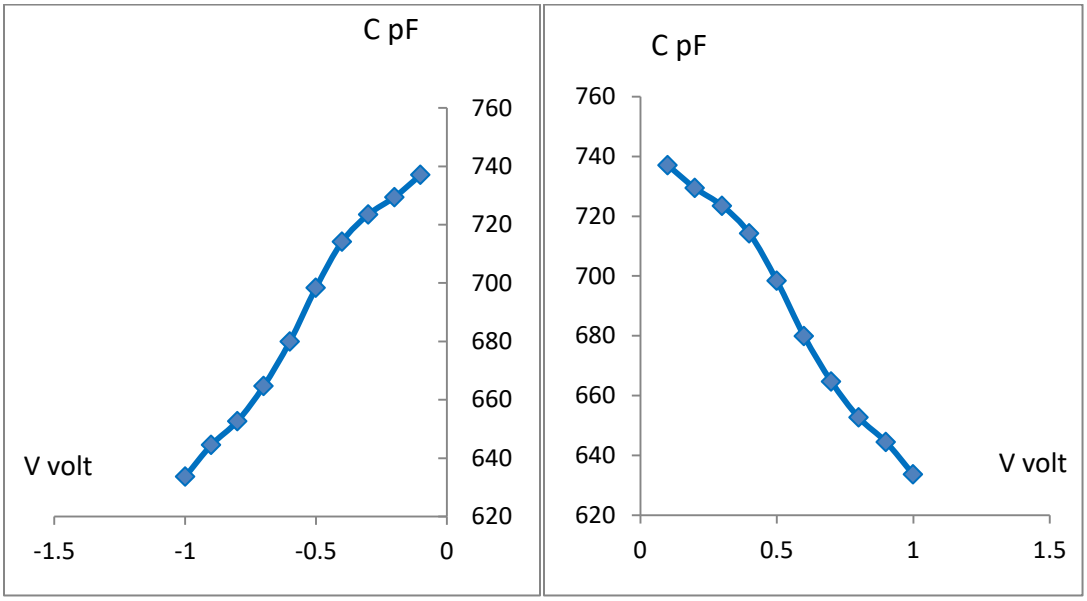

Fig. (4.19)b : Shows the capacitance-voltage measurementp of CdS:Co thin film.

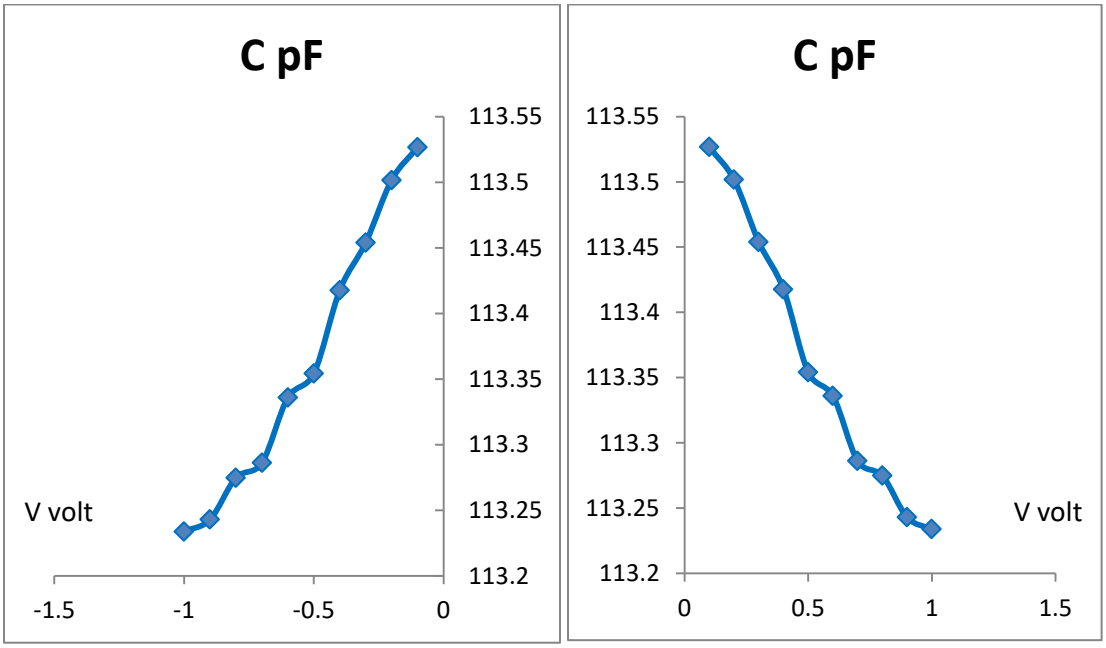

Fig. (4.19)c : Shows the capacitance-voltage measurementp of CdS:Mg thin film.

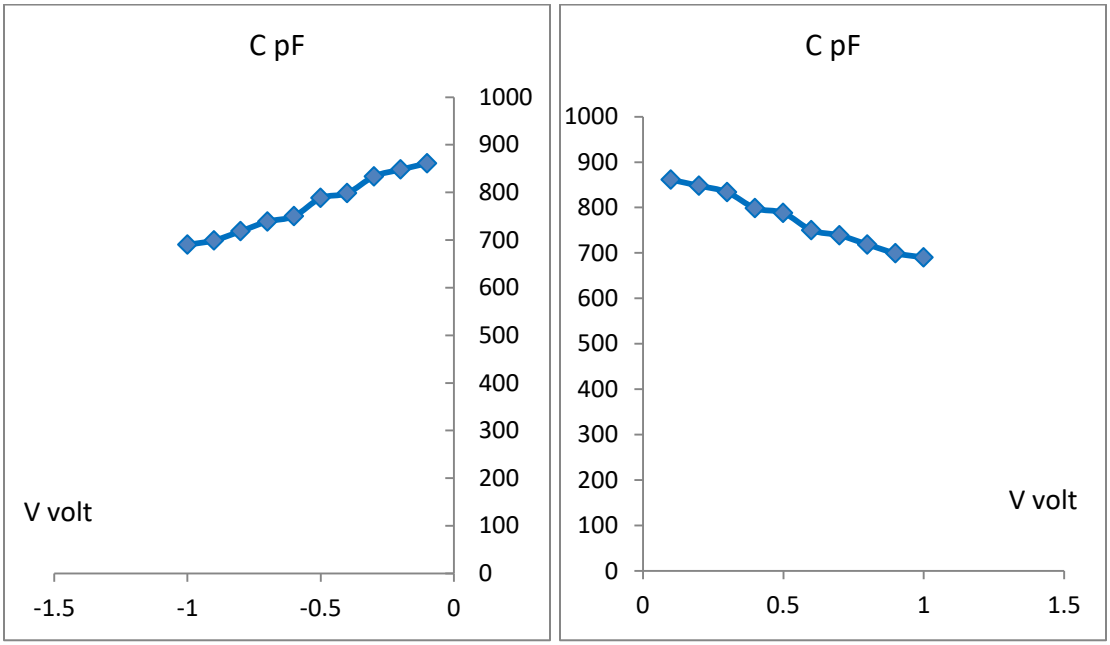

Fig. (4.19)d : Shows the capacitance-voltage measurementp of CdS:Co:Mg thin film.

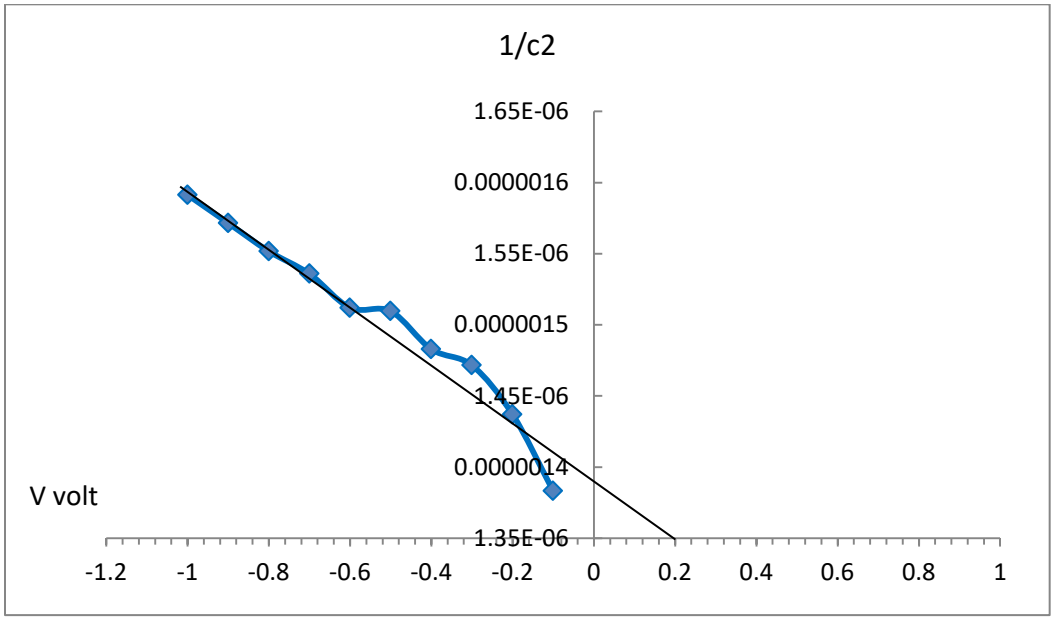

Fig. (4.20)a: Shows the relationship of the inverse square of the capacitance with the reverse bias voltage of CdS thin film.

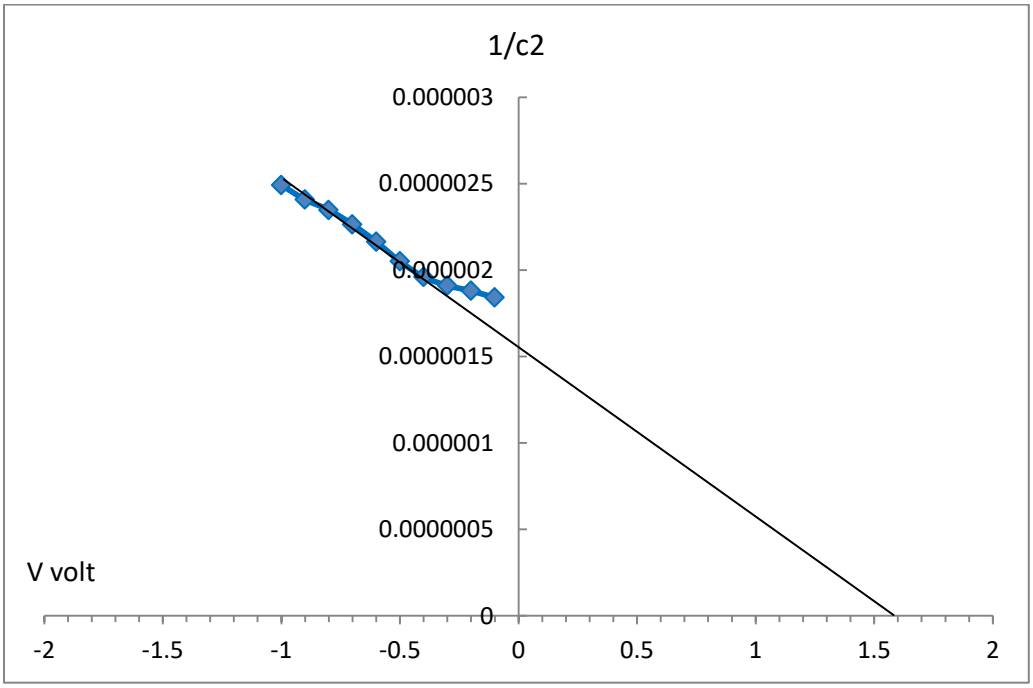

Fig. (4.20)b : Shows the relationship of the inverse square of the capacitance with the reverse bias voltage of CdS:Co thin film.

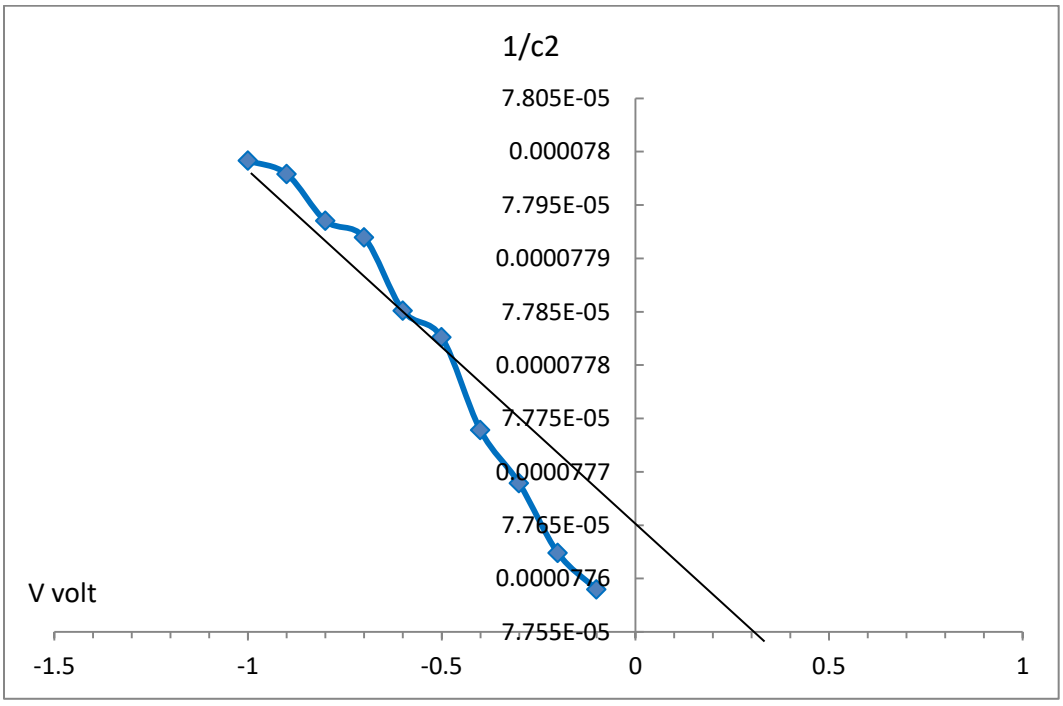

Fig. (4.20)c: Shows the relationship of the inverse square of the capacitance with the reverse bias voltage of CdS:Mg thin film.

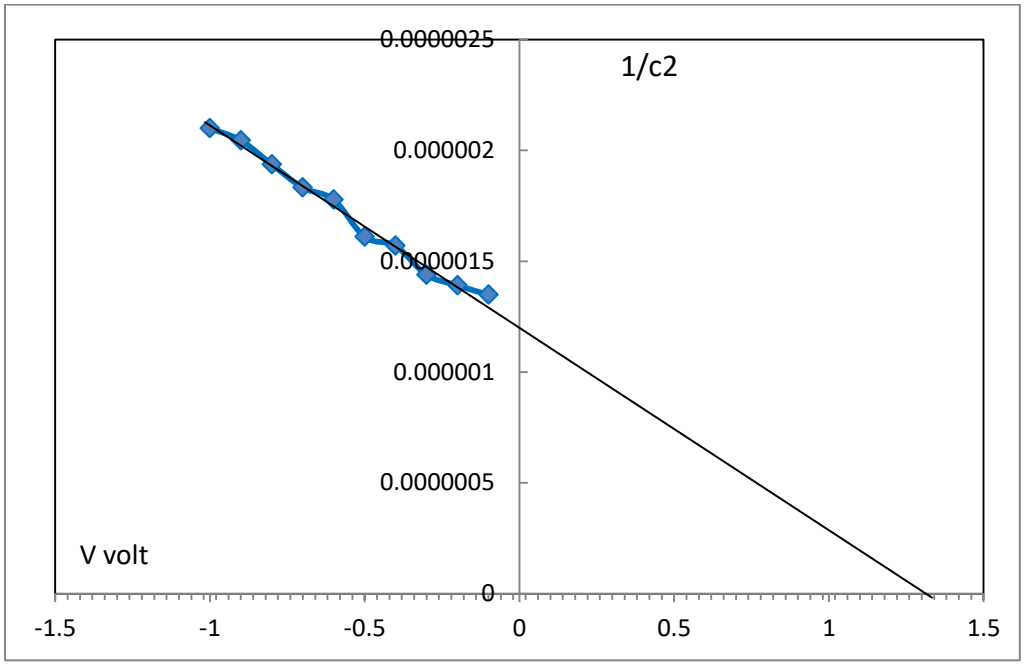

Fig. (4.20)d : Shows the relationship of the inverse square of the capacitance with the reverse bias voltage of CdS:Co:Mg thin film.

4.7 Photodector Results

4.7.1 current-voltage Characteristics under Drak and illumination

The measurement of current-voltage in the case of dark and illumination is one of the important parameters affecting the photoresponse properties of the detectors.

In Fig. (4.21) a,b,c and d shows the curves of changing the dark and light current values as a function of the reverse bias voltage for the prepared CdS/Si, CdS:Co/Si, CdS:Mg/Si and CdS:Co:Mg/Si. Where we notice when exposing the prepared reagents to white light with different intensities (15 and 30) mW/cm^2. The photocurrent increases with the increase of the

photovoltaic power and bias voltage and this was also found rouguly in [134,135]

This may be due to the increase in the generation of light carriers with the increase in the number of photons absorbed, and that the increase in the power of the incident light means an increase in the number of incident photons, which increases the number of photogenerated carriers within the depletion region and within the depth of carrier diffusion, which depends on the life period of the minority carriers on both sides of the depletion region, and thus increases the photocurrent increases the intensity of the incident light and this was also found rouguly in [93,135,136].

The increase in the photocurrent with the reverse bias voltage is due to the increase in the width of the depletion region with the increase in the bias voltage. We get the absorption of light within it or within the nearby region (the depth of carrier diffusion from it). Thus, the potential for the generated carriers to contribute to the increase in the photocurrent will increase and and this was also found rouguly in [129,136].

Increasing the reverse bias voltage applied to the prepared reagents leads to an increase in the value of the internal electric field within the depletion region, which increases the probability of electron-hole pair separation. Thus contributing to an increase in the photocurrent and a decrease in the probability of recombination processes and this result agree with rouguly agree with [137].

The case of the absence of the effect of the reverse voltage on the behavior of the photocurrent comes from the fact that the effect of the voltage is limited to changing the width of the depletion region. Where the

photocurrent depends in the case of reverse bias on the rate of generation of charge carriers and the depth of diffusion of carriers and this was also found rouguly in [137,138].

The results also showed that the photocurrent is improved by adding cobalt acetate and magnesium acetate to the cadmium sulfide compound, which may be attributed to better crystal growth, and this reduces crystalline defects and may lead to a decrease in lattice mismatch, which affects the mobility of photogenerated carriers. Thus, it increases the optical current flow through the hybrid p-n junction. In addition, the addition of cobalt acetate and magnesium acetate to the cadmium sulfide compound works to increase its transmittance to light and the occurrence of absorption within the depletion region, which in turn increases the photocurrent and this was also found rouguly in [138,139].

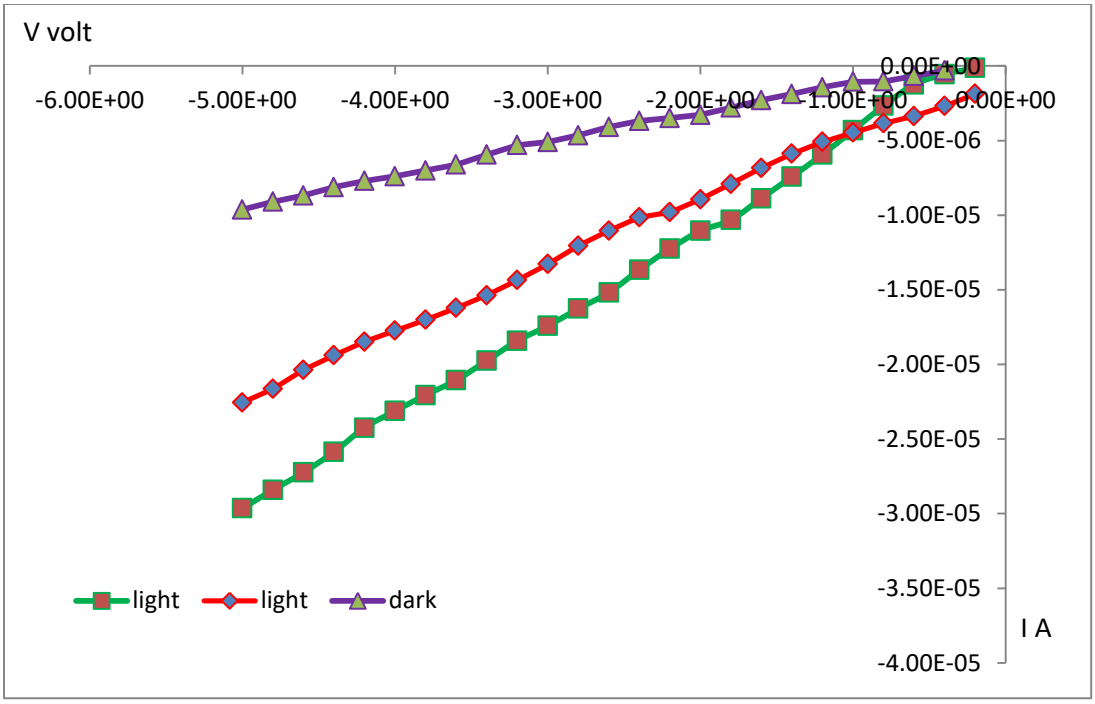

Fig. (4.21)a : Shows a current-voltage measurement of CdS/Si.

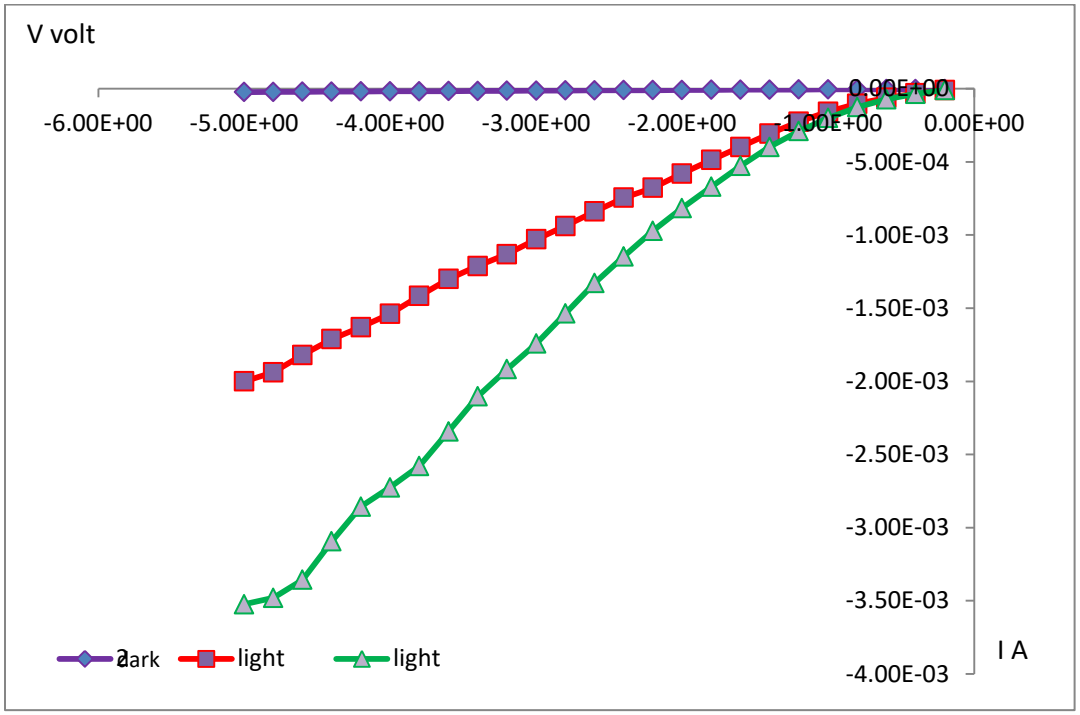

Fig. (4.21)b : Shows a current-voltage measurement of CdS:Co/Si.

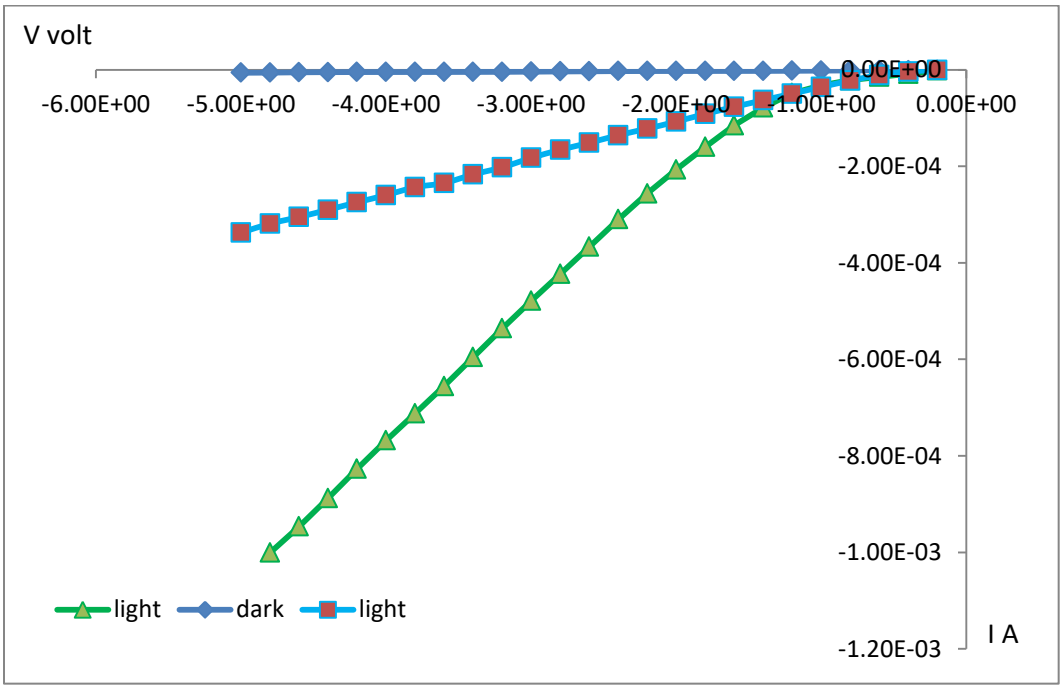

Fig. (4.21)c : Shows a current-voltage measurement of CdS:Mg/Si.

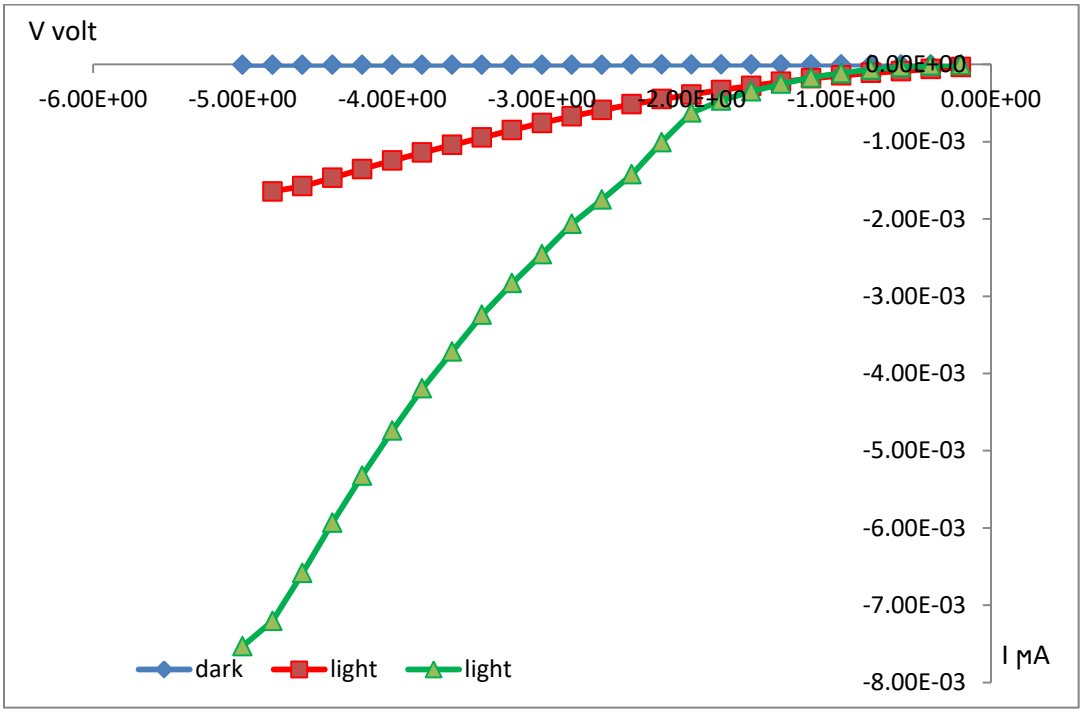

Fig. (4.21)d : Shows a current-voltage measurement of CdS:Mg:Co/Si.

4.8 Photo Detoctor

The photodector parameters such as spectral responsivity spectral, detectivits and specific respousivity.

4.8.1 Responsivity (R)

The spectral response is one of the important parameters through which it is possible to determine the spectral range in which the detector operates, as well as the spectral response is a function of the optical current.

The spectral response values were calculated for all the prepared detcotrs CdS/Si, CdS/CO, CdS:Mg/Si and CdS:Mg:Co/Si which were deposited on a p-type silicon substrate based on Eq. (2.46). In Fig. (4.22) a,b,c and d shows the change of the spectral response of all the prepared

reagents as a function of wavelength within the range of (350-1000) nm at a bias voltage of 3 volts.

The results showed that the prepared detector cds/si has two peaks of the spectral response. The first at a wavelength of 518 nm, which is caused by the energy gap of the prepared thin film cadmium sulfide. The second at a wavelength of 850 nm appeared due to the window phenomenon, which represents the value of the response of the silicon material and this result agree with rouguly agree with [139,140].

The results also showed that the prepared detectors CdS:Co/Si, CdS:Mg/Si and CdS:Co:Mg/Si have two peaks of the spectral response, but with the creep of the response peak towards the high wavelengths. This is due to the spread of cobalt acetate and magnesium acetate atoms with the cadmium sulfide compound, which leads to the formation of donor levels within the energy gap. So the Fermi level will creep towards the band Conduction, which makes the absorption of the material for long wavelengths higher and this result agree with rouguly agree with [140,141].

Table (4.19) shows the spectral response values for all prepared reagents. Where we notice through the results that the addition of cobalt acetate and magnesium acetate to the cadmium sulfide compound led to an increase in the spectral response values. This is attributed to the improvement of the structural properties of the prepared films, and thus a decrease in the resistance of the surface films and an increase in electrical conductivity, which leads to an increase in the optical current, and this in turn leads to an improvement in the spectral response Whereas, increasing

the spectral response values means detecting weak signals and this result agree with rouguly agree with [123,141].

We note that the spectral response of all the prepared reagents increases with the increase in the incident wavelength at a specific part of the visible region. This is due to the absorption of short wavelengths at the surface of the prepared films, which has a large absorption coefficient at those lengths. This means a small absorption depth at the surface. Where the surplus carriers recombine at the surface before reaching the p-n junction, and thus a slow rise in the spectral response and this was also found rouguly in [139,141].

As for the wavelengths between (750-900) nm, which represents the highest region of the spectral response obtained for the prepared detectors. Where these lengths are absorbed in the depletion region and at both ends, which is equal to the depth of diffusion of the minority carriers, where the depletion region has the ability to separate the carriers generated by the internal electric field in addition to the lack of operations Reunification in this region.

In addition to that, there is a decrease in the speed of recombination, and this is observed in terms of an increase in the life of the charge carriers, which leads to an increase in the length of the diffusion of the carriers, due to better crystal growth and this result agree with rouguly agree with [141].

Table (4.19) : Shows the spectral response values for all the prepared reagents.

sample	R1(A/W)	λnm	R2(A/W)	λnm
CdS/Si	0.035	518	0.041	850
CdS:Co/Si	0.389	550	0.535	800
CdS:Mg/Si	0.3	535	0.389	800
CdS:Co:Mg/Si	0.08	522	0.144	800

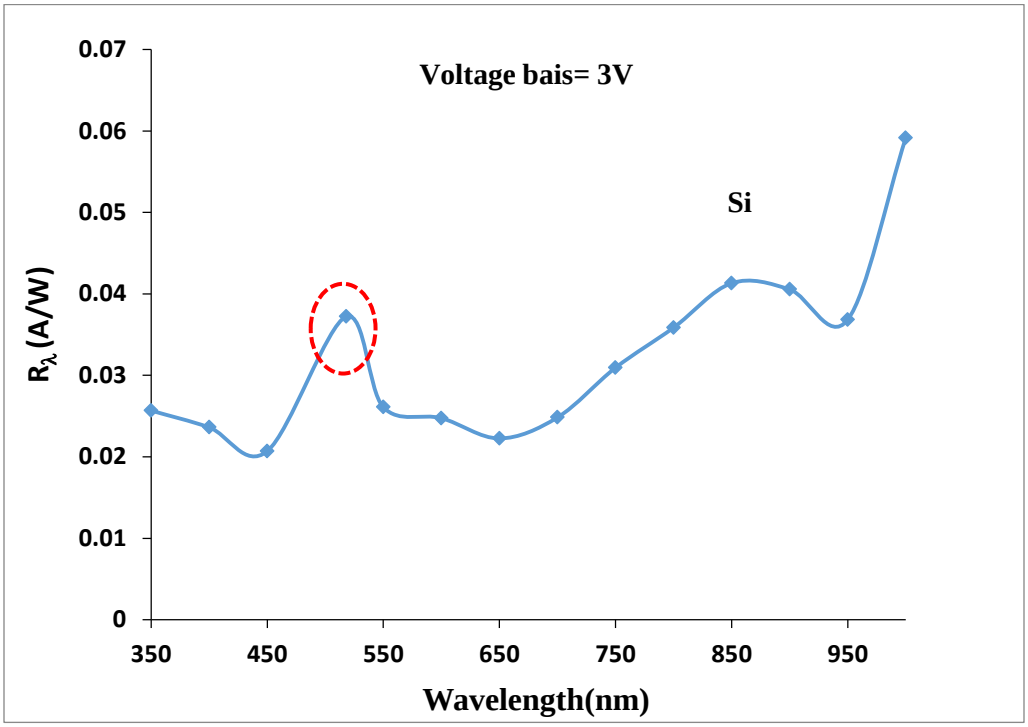

Fig. (4.22)a : Shows the spectral response as a function of the wavelength of the prepared detector CdS/Si.

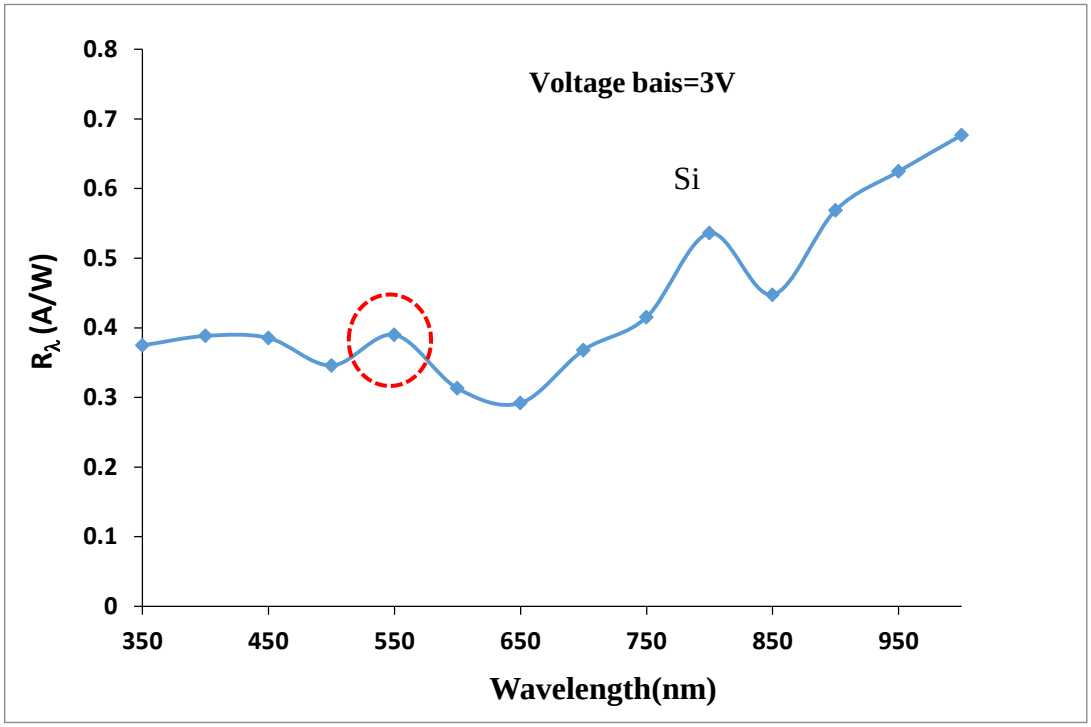

Fig. (4.22)b : Shows the spectral response as a function of the wavelength of the prepared detector CdS:Co/Si.

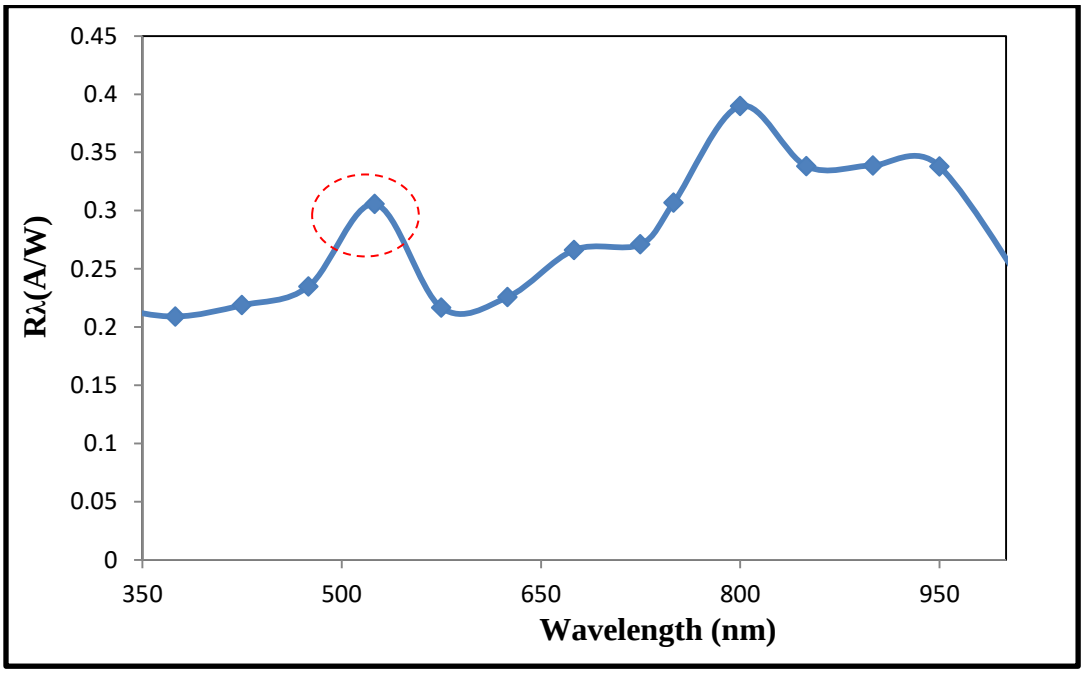

Fig. (4.22)c : Shows the spectral response as a function of the wavelength of the prepared detector CdS:Mg/Si.

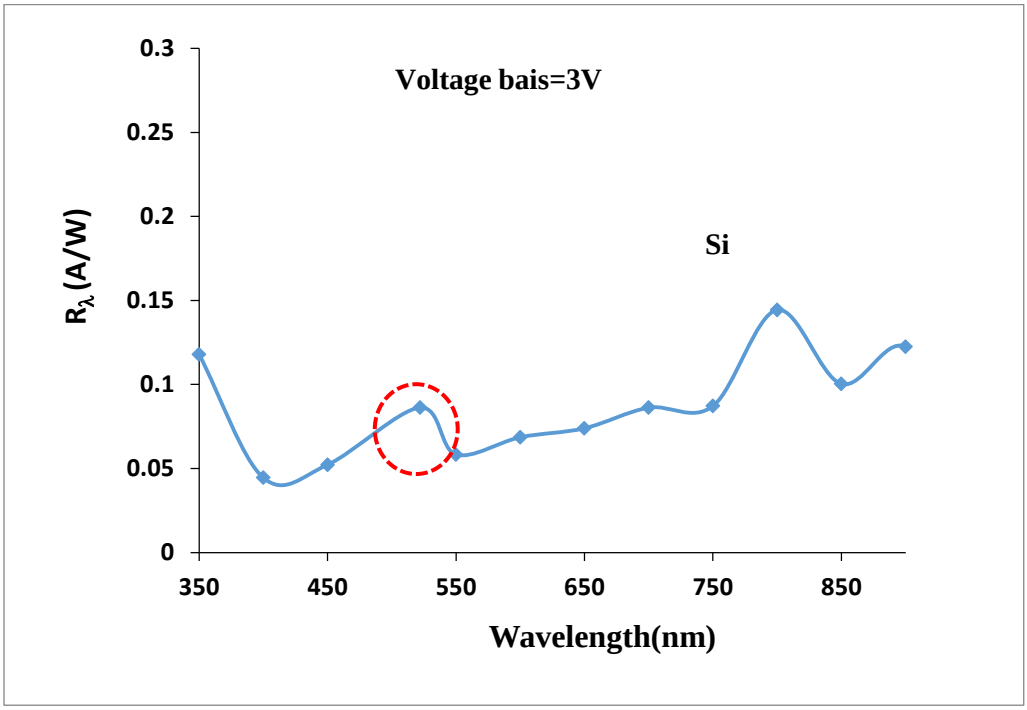

Fig. (4.22)d : Shows the spectral response as a function of the wavelength of the prepared detector CdS:Co:Mg/Si.

4.8.2 Specific Detectivity

The qualitative detection is considered one of the important parameters of the detectors that are necessary in determining their efficiency. The field of application, as it determines the lowest power falling on the detector that can be sensed by the detector. The value of the qualitative scouting is determined by the noise generated from the process of generation and recombination[96].

The qualitative detection of prepared reagents CdS/Si, CdS:Co/Si, CdS:Mg/Si and CdS:Co:Mg/Si was calculated based on Eq. (2.50). Fig.(4.23) a,b,c and d shows the change of the specific scouting curve as a function of wavelength within the range of (350-1000) nm.

Where the results showed that all the prepared reagents have two detection peaks at specific wavelengths, as shown in table (4.20).

We notice through the qualitative scouting results that the addition of cobalt acetate and magnesium acetate to the cadmium sulfide compound led to the displacement of the peak that determines the qualitative scouting value towards the higher wavelengths[148,149]. The addition of cobalt acetate and magnesium acetate led to an improvement in the spectral response and the specific detection. This may be attributed to the improvement of the structural and electrical characteristics, and thus reducing the recombination centers and reducing the noise current generated in the detector, and as a result, a clear increase in the specific detection values of the prepared detectors[132,141,142].

Table (4.20) : shows the qualitative detection values for all the prepared reagents.

sample	D1	λnm	D2	λnm
CdS/Si	5.1×10^{11}	518	5.907×10^{11}	850
CdS:Co/Si	5.572×10^{12}	550	7.661×10^{12}	800
CdS:Mg/Si	3.82×10^{12}	535	4.873×10^{12}	800
CdS:Co:Mg/Si	1.233×10^{12}	522	2.064×10^{12}	800

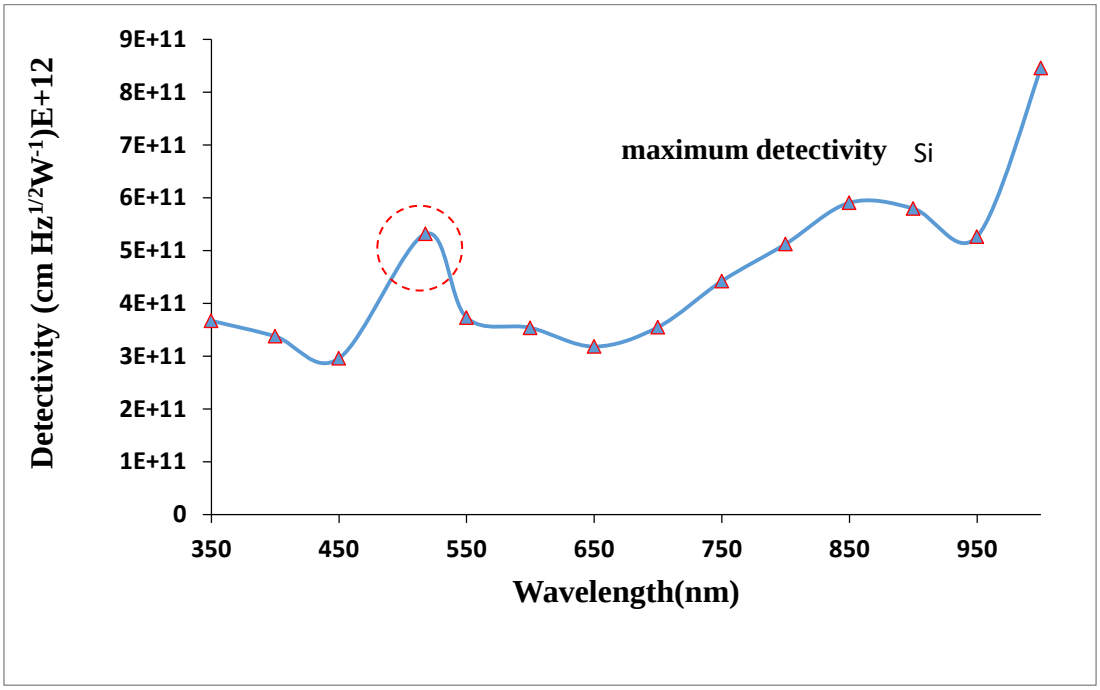

Fig. (4.23)a : Shows the qualitative detection as a function of the wavelength of the prepared detector CdS/Si.

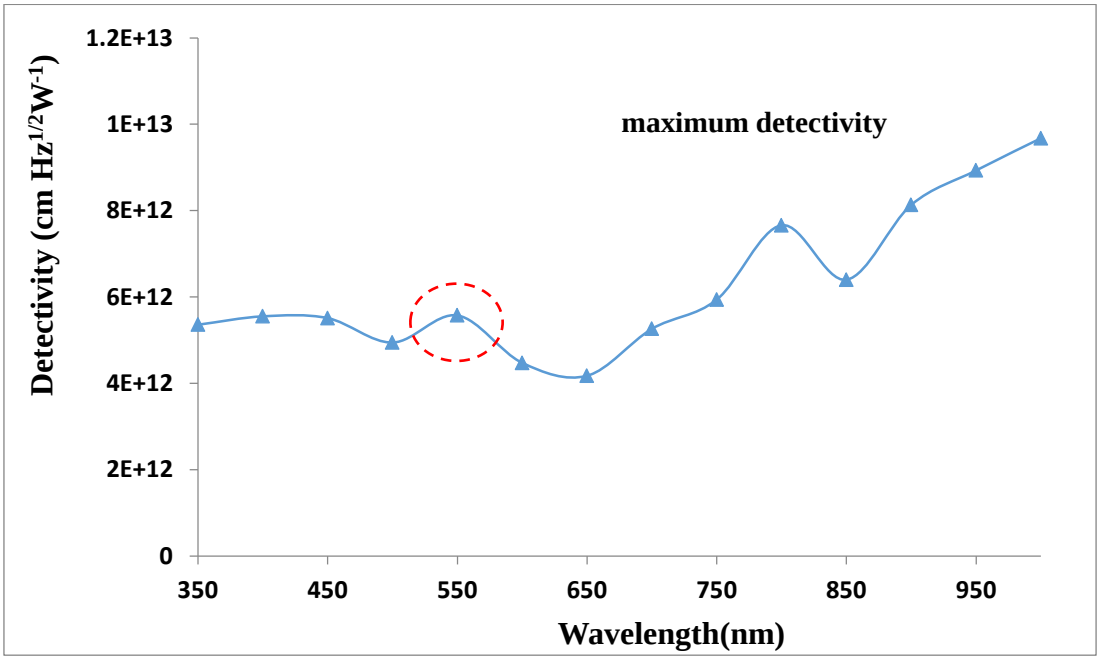

Fig.(4.23)a : Shows the qualitative detection as a function of the wavelength of the prepared detector CdS:Co/Si.

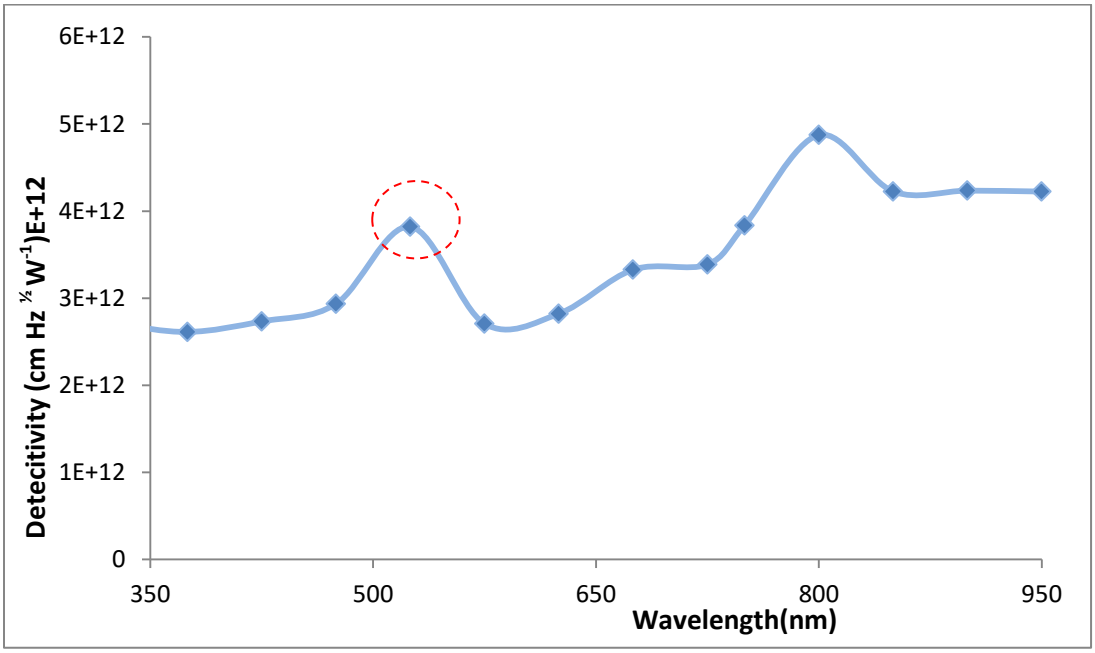

Fig.(4.23)c : Shows the qualitative detection as a function of the wavelength of the prepared detector CdS:Mg/Si.

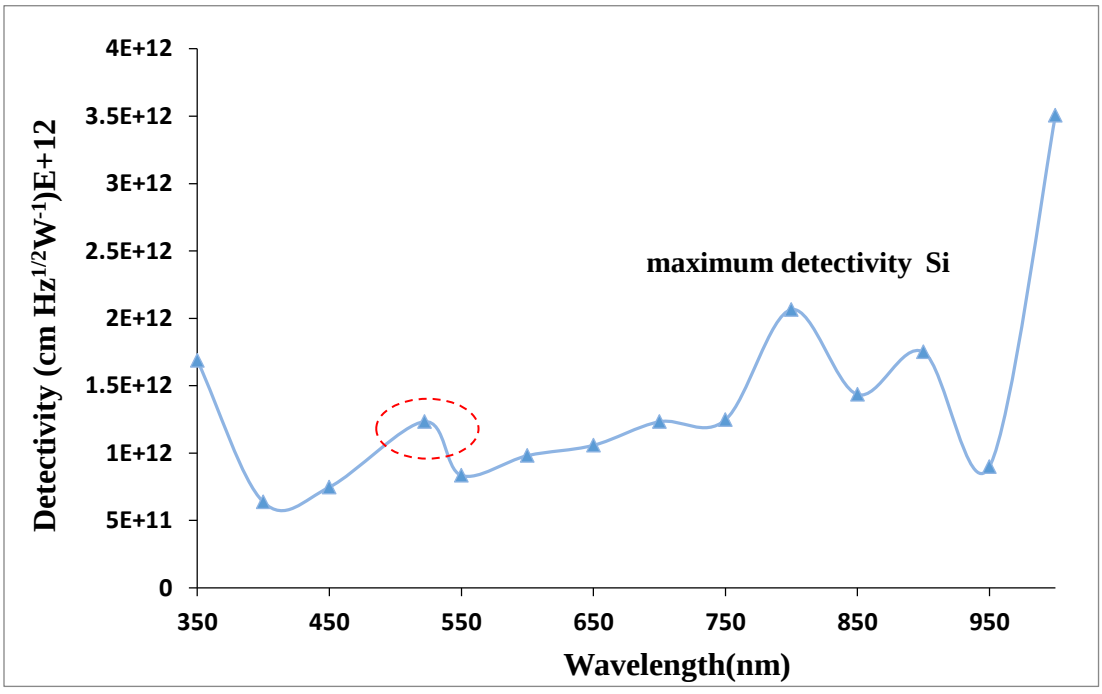

Fig. (4.23)d : Shows the qualitative detection as a function of the wavelength of the prepared detector CdS:Co:Mg/Si.

4.8.3 Efficiency

The measurement of efficiency is very important in detectors and systems that are characterized by the photoelectric effect and have a function of the spectral response[97].

The efficiencies for all the prepared reagents were calculated using Eq. (2.47). Fig. (4.24) a,b,c and d shows the change in the quantitative efficiency of the prepared detectors as a function of wavelength within the range of 350-1000 nm. The results showed that the prepared reagent cds/si has a lower efficiency value than the prepared reagents cds:co/si, cds:mg/si, and cds:co:mg/si.

This explains that the addition of cobalt acetate and magnesium acetate to the cadmium sulfide compound led to an improvement in the values of the prepared reagents. This is evident from the results of the spectral response, which in turn positively affects the improvement and increase of the quantitative efficiency of the prepared reagents and this was also found rouguly in [142,143].

We conclude from the results that the highest value of the quantitative efficiency of the prepared reagentCdS:Co/Si is at a wavelength of 550 nm, while all the prepared reagents gave the highest values of the quantitative efficiency at the specified wavelengths, which are 800 nm and 850 nm as shown in Table (4.21).

This is due to the increase in transmittance in this region and thus the increase generation of charge carriers in the depletion region and thus increase the spectral response, which reflects positively on increasing the quantum efficiency and this was also found rouguly in [135,143].

Table (4.21) : Shows the efficiency values for all the prepared reagents.

sample	η %	λnm	η %	λnm
CdS/Si	8.907	518	6.027	850
CdS:Co/Si	87.876	550	83.057	800
CdS:Mg/Si	72.197	535	60.431	800
CdS:Co:Mg/Si	20.488	522	21.383	800

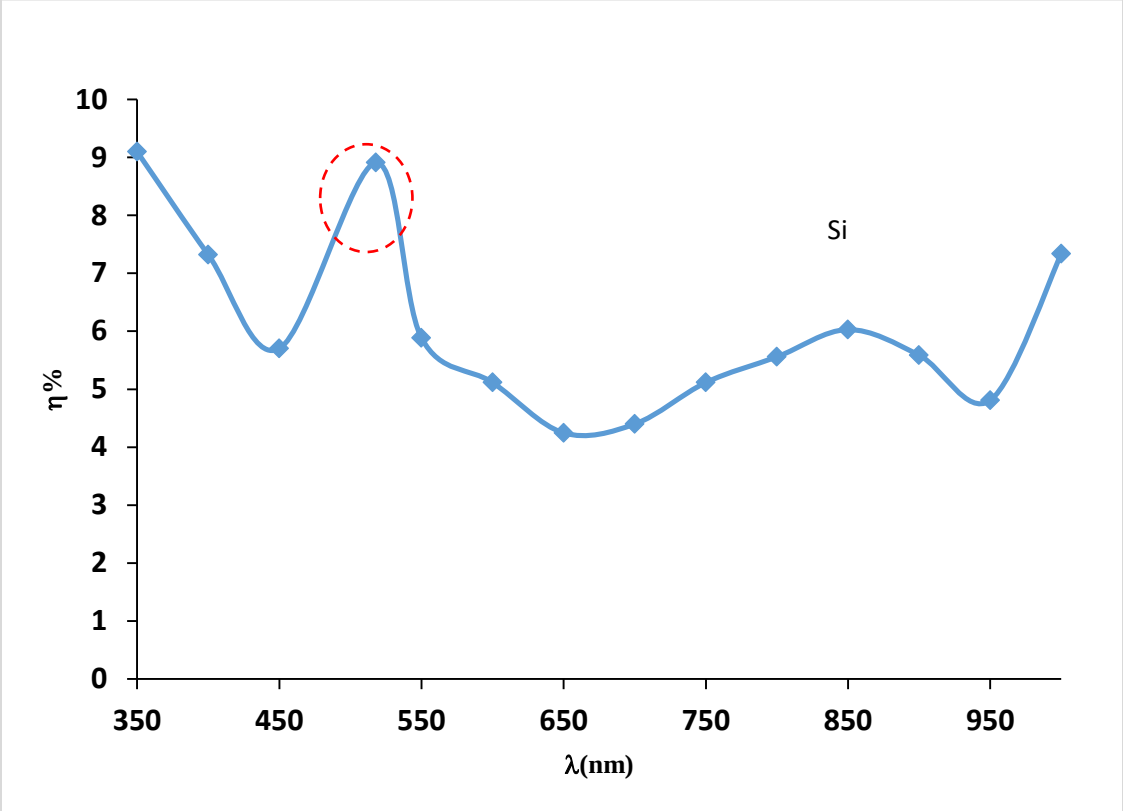

Fig. (4.24)a : Shows the efficiency as a function of the wavelength of the prepared detector CdS/Si.

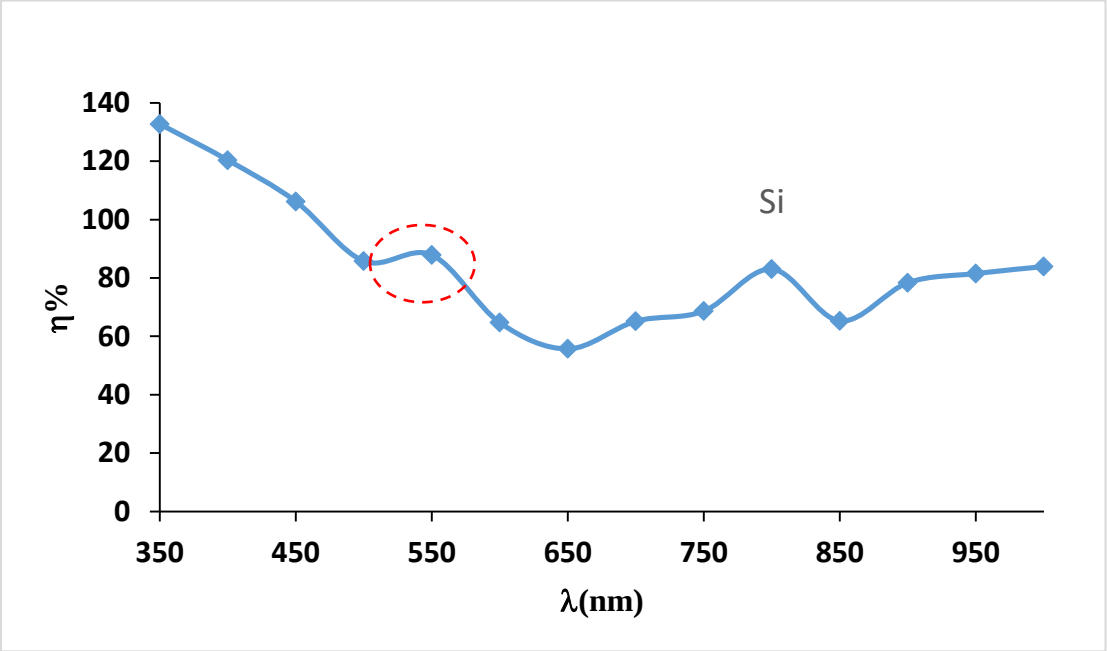

Fig. (4.24)b : Shows the efficiency as a function of the wavelength of the prepared detector CdS:Co/Si.

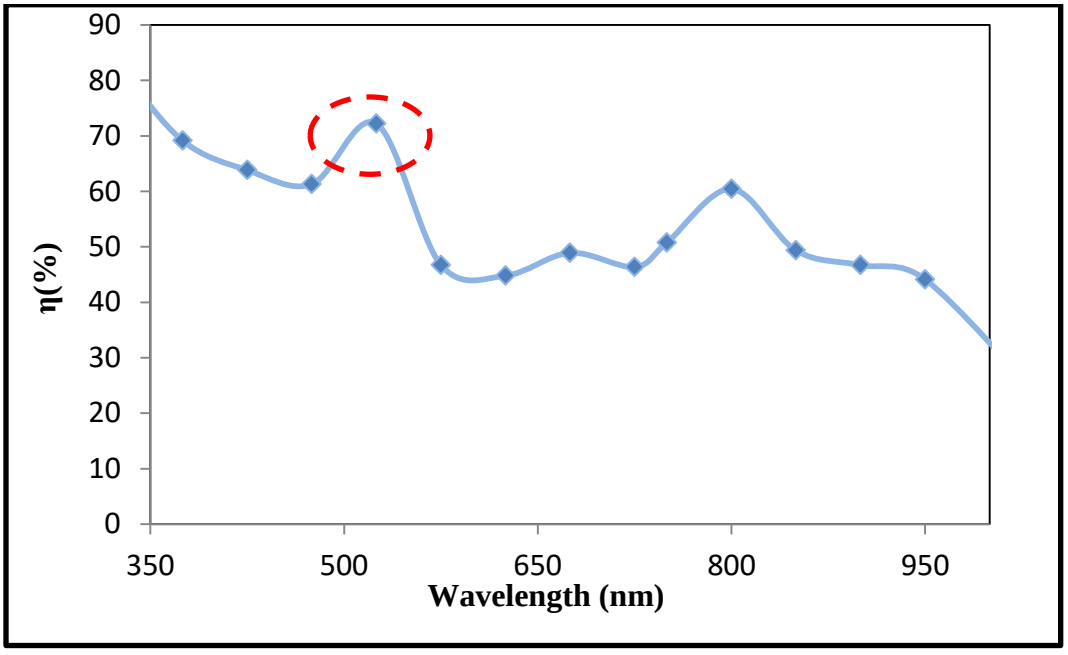

Fig. (4.24)c : Shows the efficiency as a function of the wavelength of the prepared detector CdS:Mg/Si.

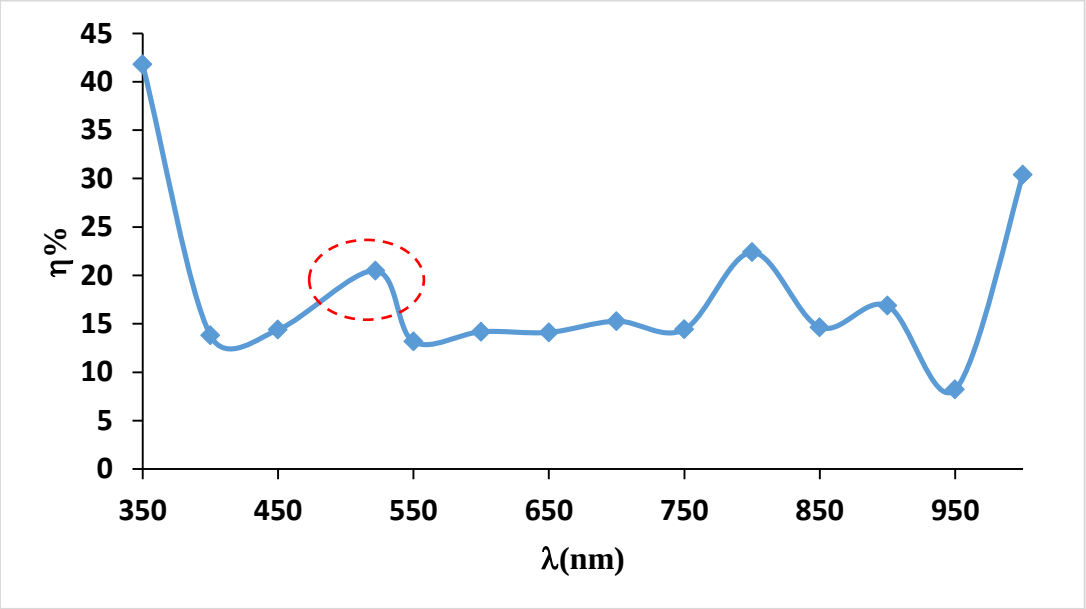

Fig. (4.24)d : Shows the efficiency as a function of the wavelength of the prepared detector CdS:Co:Mg/Si.

4.8.4 Life time

In Fig.(4.25) a,b,c and d shows an image of the voltage decay pulse of the open circuit coming out of the detector after exposure to light pulses from the stroposcope.

The life time of carriers was calculated using equation (t=1/f). Table (4.22) shows the values of the lifetime of the carriers for the prepared reagents.

We notice an increase in the life of the minority carriers of the reagents. This explains that the addition of cobalt acetate and magnesium acetate to the cadmium sulfide compound has an effect on determining the life time of the minority carriers. This can be attributed to the improvement of the structural properties of the prepared films through the improvement of the crystallization process and thus the decrease in the density of defects and

the sniping centers of the carriers, which represent effective centers for recombination. This leads to to increase the mobility of the carriers and increase the life of the carriers. This can be seen through the electro-optical results and to support what we have reached in explaining the increase in the internal construction effort with the addition of cobalt acetate and magnesium acetate to the cadmium sulfide compound. It can be explained that an increase in the lifetime of carriers means a decrease in the concentration of defects, and thus the probability of recombination processes is low and this was also found rouguly in [136,142,143].

Table (4.22) : Shows the values of the lifetime of carriers for the prepared reagents.

sample	Life time (1/HZ)
CdS	0.001886
CdS:Co	0.004548
CdS:Mg	0.002177
CdS:Co:Mg	0.002720

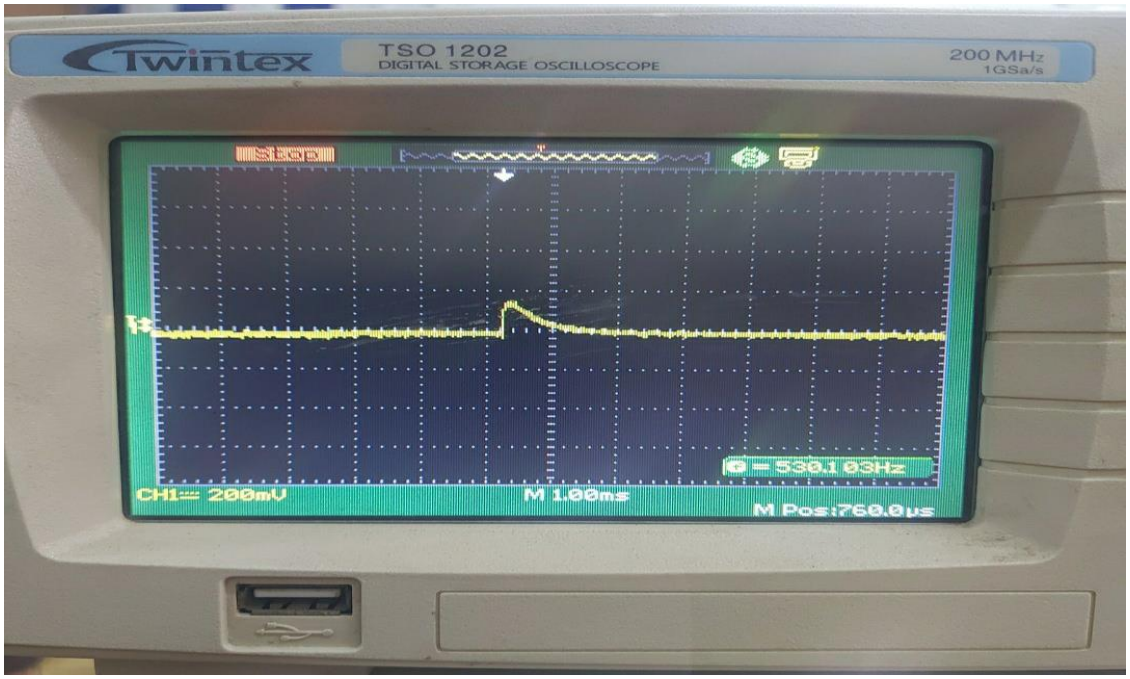

Fig. (4.25)a : Shows the measurement of the lifetime of the charge carriers of the record detector CdS/Si.

Fig. (4.25)b : Shows the measurement of the lifetime of the charge carriers of the record detector CdS:Co/Si.

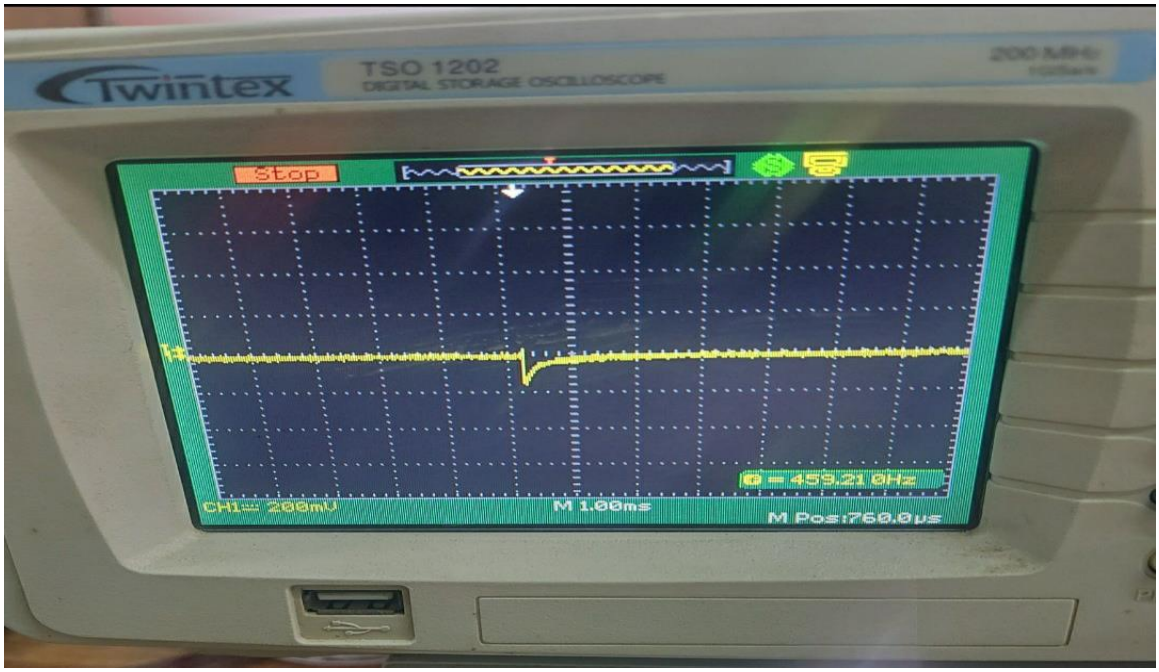

Fig. (4.25)c : Shows the measurement of the lifetime of the charge carriers of the record detector CdS:Mg/Si.

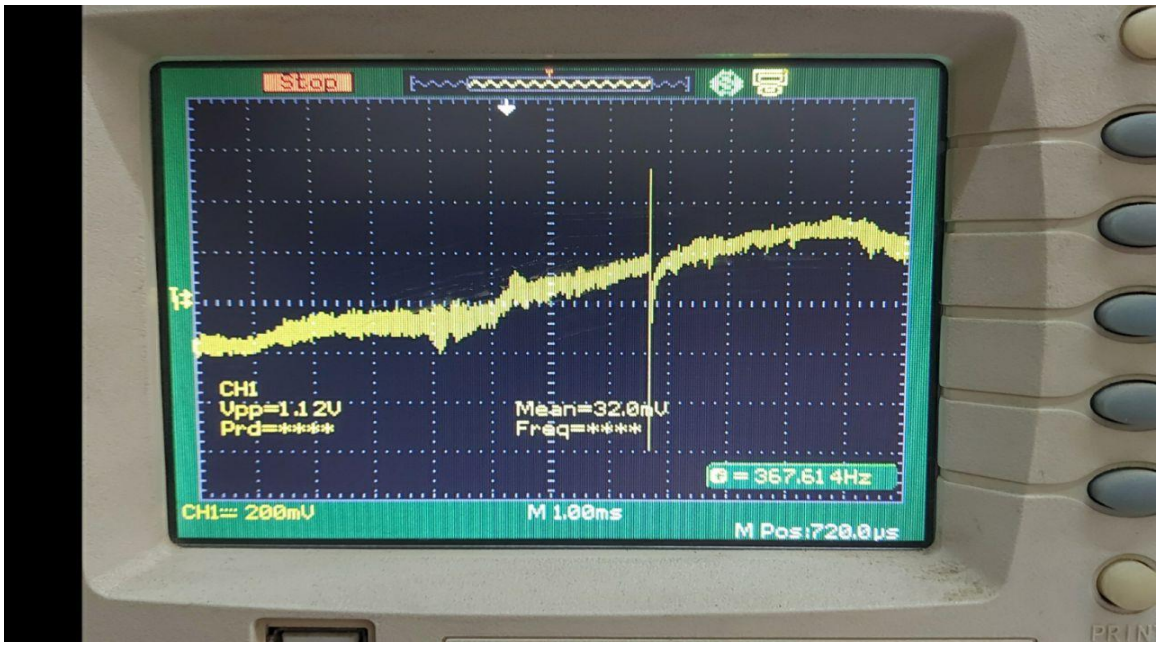

Fig. (4.25)d : Shows the measurement of the lifetime of the charge carriers of the record detector CdS:Co:Mg/Si.

4.9 Gas Senser

All prepared thin films were measured as gas sensors using two different gases, hydrogen sulfide gas(H_2S) and ethanol gas. The sensitivity, response time and return time were known and calculated.

4.9.1 Sensitivity, Response and Recovery Time

The sensitivity of the prepared thin films CdS,CdS:CO,CdS:Mg and CdS:Co:Mg . The sensitivity was studied and calculated by measuring the resistance in the absence of gas and then measuring the resistance in the presence of gas . Fig. (4.26 and 4.27) shows the change in the resistance of all prepared films with the gas reaction time at an operating temperature of 50ºC.

We notice through the figures that the amount of resistance changes with the time required to reach a stable state in the case of opening and closing the gas, noting that the time period specified for opening the gas is 5 seconds and this was also found rouguly in [74,100,144].

The results showed that the resistance values of the prepared films in the case of using hydrogen sulfide gas(H_2S) are less than the resistance values in the case of using ethanol gas(C_2H_5OH).

This is due to the prepared films being of the type n, where the electrons are the charge carriers as shown by the hall effect measurements. When an oxidizing gas such as ethanol is used, when the oxygen interacts with the surface, the electrons in the conduction band are displaced by the oxygen ions, and this works to reduce the concentration of the carriers, which leads to Increased sensor resistance. While when using a reducing gas

such as hydrogen sulfide, the electrons resulting from the chemical reaction return to the conduction band, and this leads to a decrease in the resistance of the senso and this was also found rouguly in [74,144,145].

The sensitivity values of the prepared films towards hydrogen sulfide gas and ethanol were calculated based on Eq. (2.54 and 2.55), respectively. The results showed that the highest value of sensitivity for the prepared cadmium sulfide film towards hydrogen sulfide gas.

We notice through the results that the addition of cobalt acetate and magnesium acetate to the cadmium sulfide compound led to a decrease in the sensitivity values.

The reason is that the sensitivity depends on the granular size and the granular boundaries of the prepared films. This explains that in the case of the prepared cadmium sulfide film, the granular size is small and the distance between the granular boundaries is large. This leads to the interaction between the absorbed oxygen and the gas occurring at the granular boundaries, so the reaction will increase and give high sensitivity .

When adding cobalt and magnesium to the cadmium sulfide compound, it led to an increase in the particle size values as indicated by X-ray diffraction, AFM, TEM and SEM measurements. This explains that an increase in the particle size leads to a decrease in the granular boundaries at which adsorption occurs between the gas and the adsorbed oxygen. So the adsorption will decrease and thus the sensitivity will decrease and this was also found rouguly in [97,100,145].

We can explain that the sensitivity is inversely proportional to the particle size, and this means that increasing the particle size leads to a

decrease in the surface area, which in turn works to decrease the adsorption and desorption process for gases. This reduces the sensitivity of the prepared membranes towards the used gases, which are hydrogen sulfide gas and ethanol gas and this was also found rouguly in [101102,145].

The response time was calculated for all prepared films in the case of opening the gas, as well as the recovery time was calculated in the case of closing the gas. Fig. (4.28) a and b shows the response time and recovery time for the prepared films as a function of sensitivity.

The results showed that the shortest response and recovery time of the prepared cadmium sulfide film towards hydrogen sulfide gas and this result agree with rouguly agree withrouguly agree with [102,146].

Table (4.23) shows the sensitivity values and the response and recovery time of the prepared films towards the used gases, hydrogen sulfide gas and ethanol gas.

We note that the addition of cobalt acetate and magnesium acetate to the cadmium sulfide compound led to an increase in the response and recovery time. This may be attributed to a decrease in the yield in the sensitivity values, because the response and recovery time are a measure in the sensor speed test and this was also found rouguly in [102,145,146].

Table (4.23): Shows the sensitivity values and response and recovery time for all prepared thin films.

sample	T_{on} s	R_{on} Ω	T_{off} s	R_{off} Ω	$T_{resp.}$ s	$T_{rec.}$ s	S%	gas
CdS	87	1.2	91	2.6	1	2	53	H_2S
CdS:Co	17	0.447	36	0.87	3	52	48.620	
CdS:Mg	22	0.918	28	1.137	2	12	17.815	
CdS:Co:Mg	61	2.951	67	2.993	1.5	7	1.423	
CdS	2	6.37	68	9.08	1.6	46	42.543	C_2H_5OH
CdS:Co	43	4.422	50	5.6	2.5	6	26.639	
CdS:Mg	151	13.16	177	15.53	2	3	18.009	
CdS:Co:Mg	24	74.4	35	75.3	2.3	4	1,209	

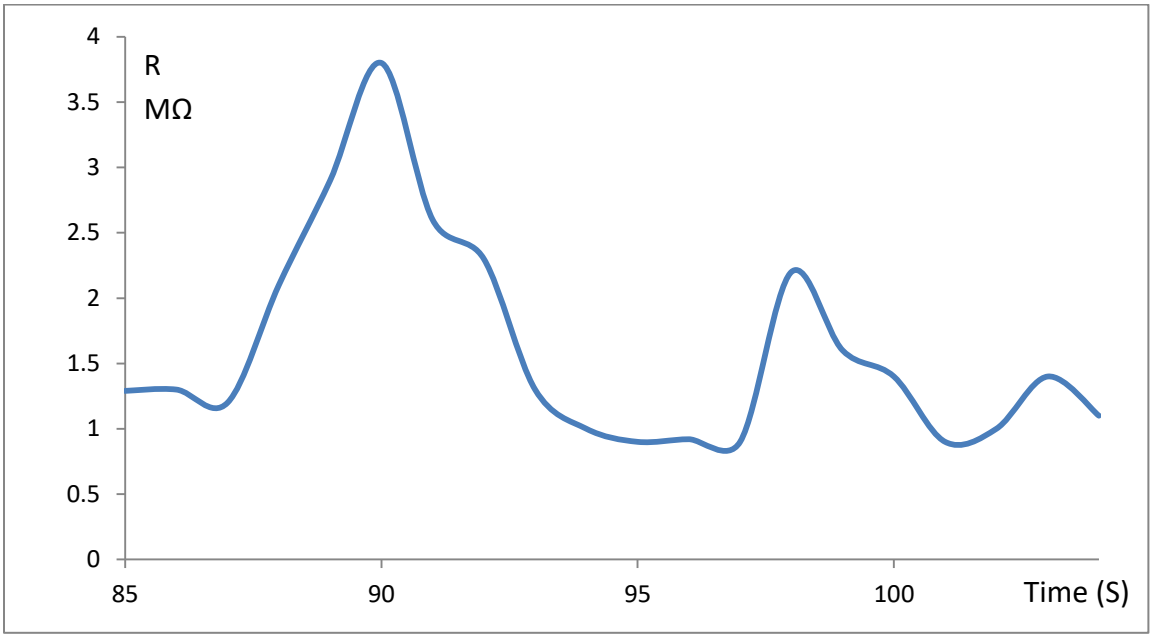

Fig. (4.26)a : Shows the change in resistance with the response time of hydrogen sulfide gas to the prepared CdS thin film.

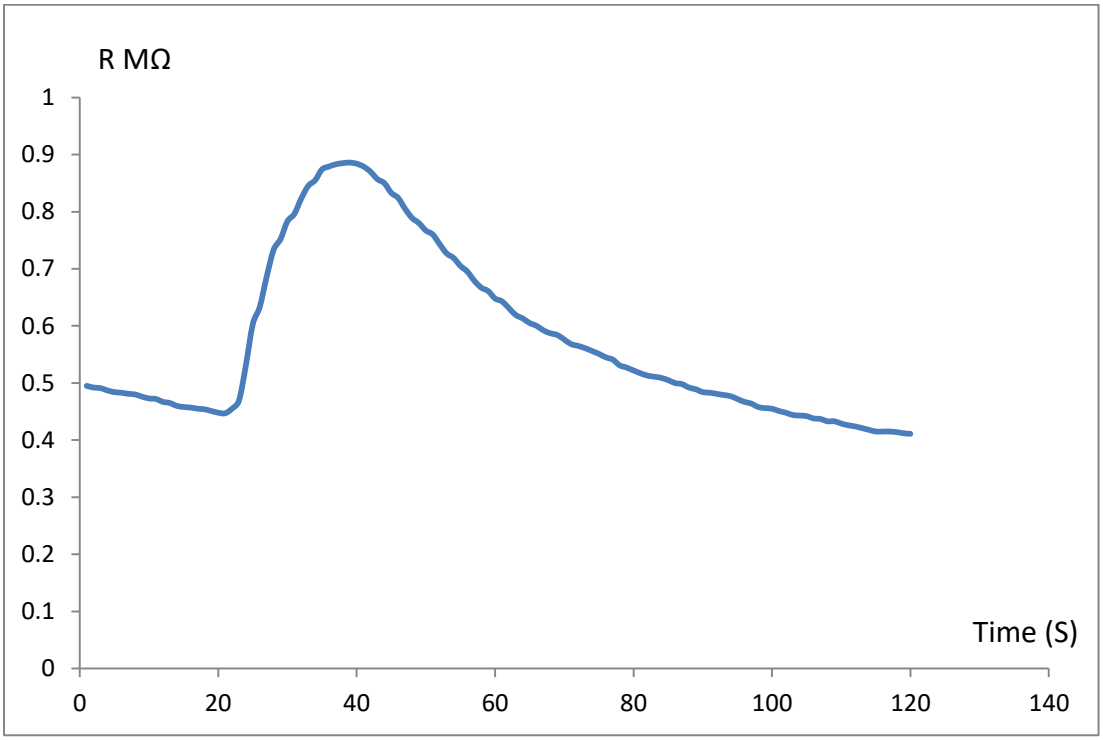

Fig. (4.26)b : Shows the change in resistance with the response time of hydrogen sulfide gas to the prepared CdS:Co thin film.

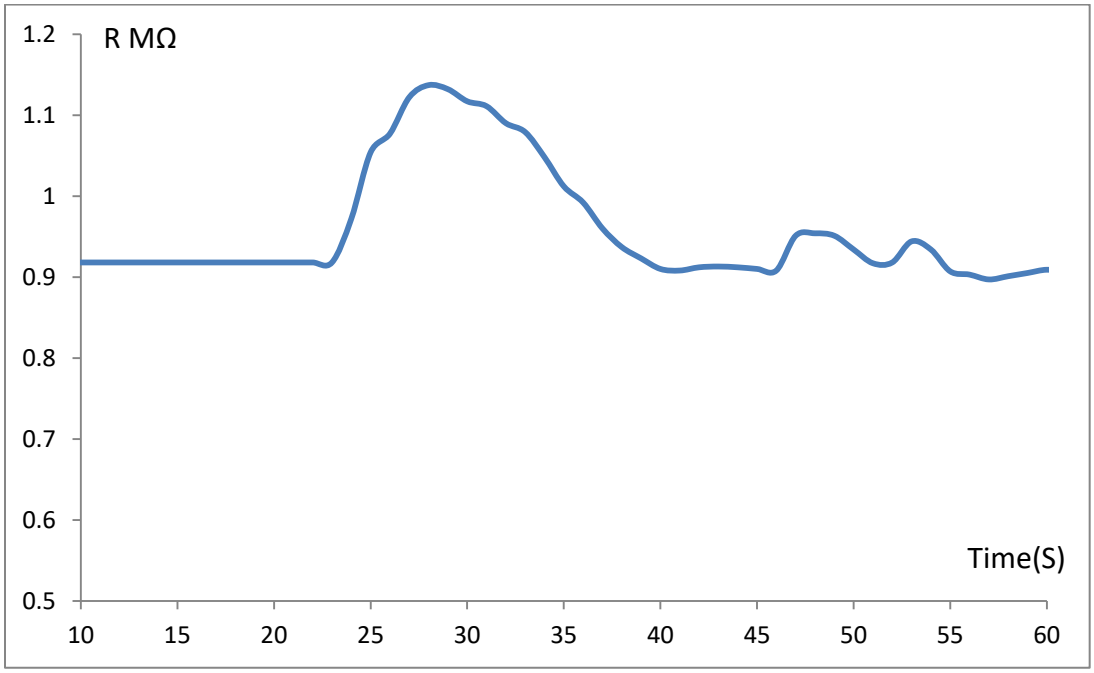

Fig. (4.26)c : Shows the change in resistance with the response time of hydrogen sulfide gas to the prepared CdS:Mg thin film.

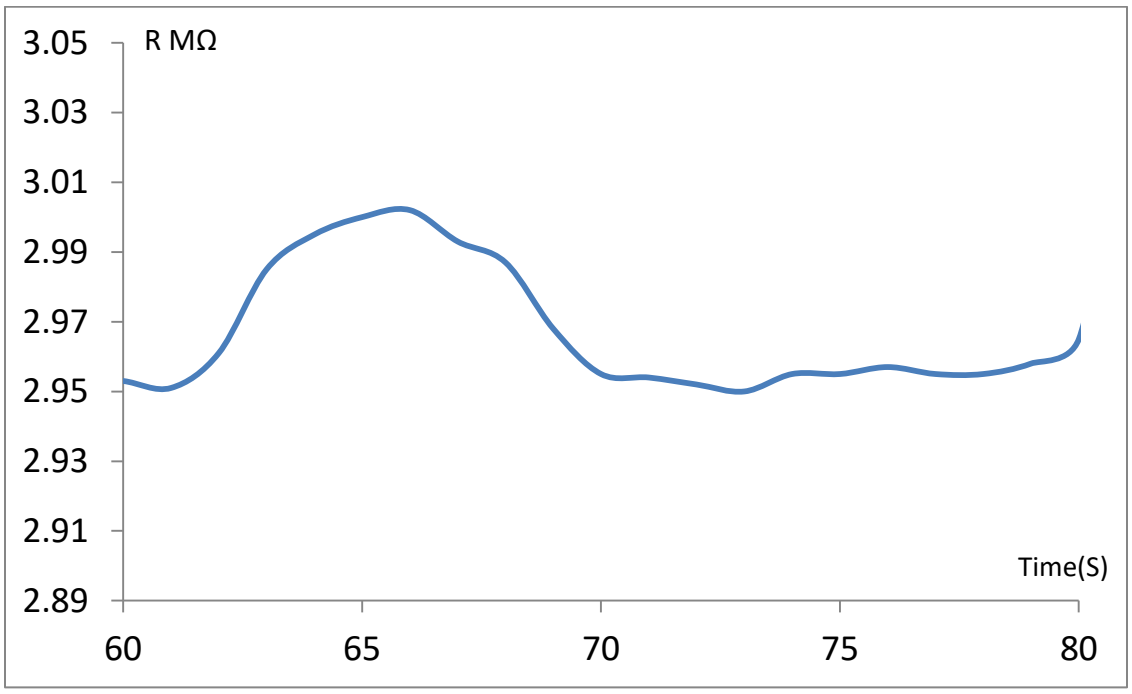

Fig. (4.26)d : Shows the change in resistance with the response time of hydrogen sulfide gas to the prepared CdS:Co:Mg thin film.

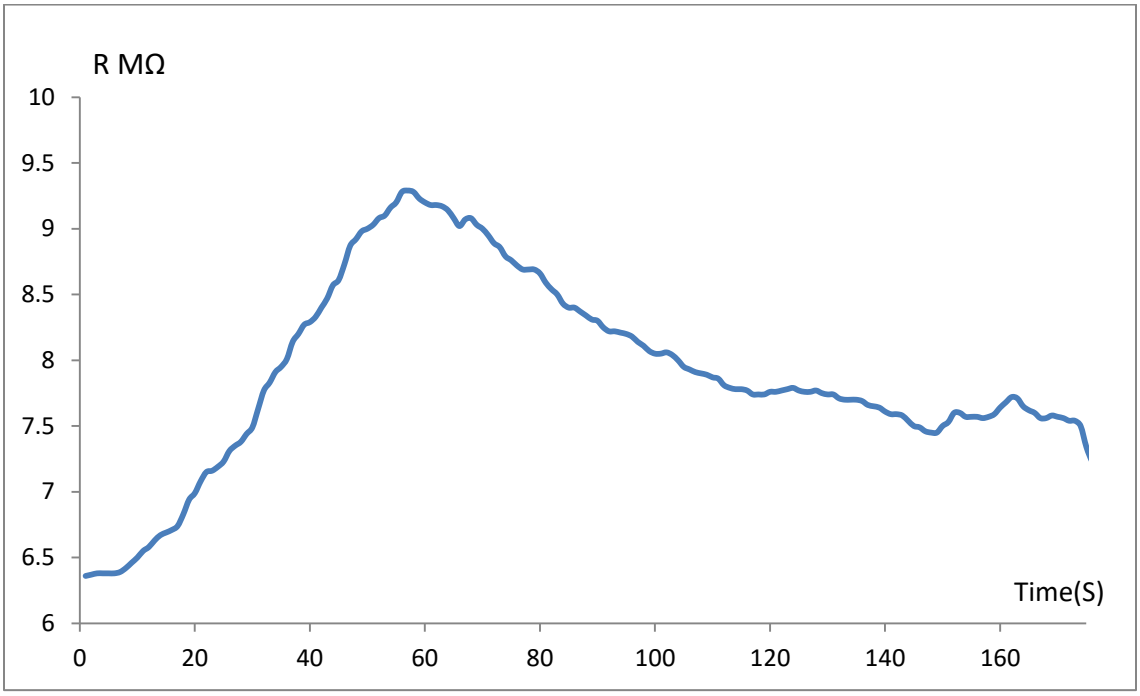

Fig. (4.27)a : Shows the change in resistance with the response time of eathnoal gas to the prepared CdS thin film.

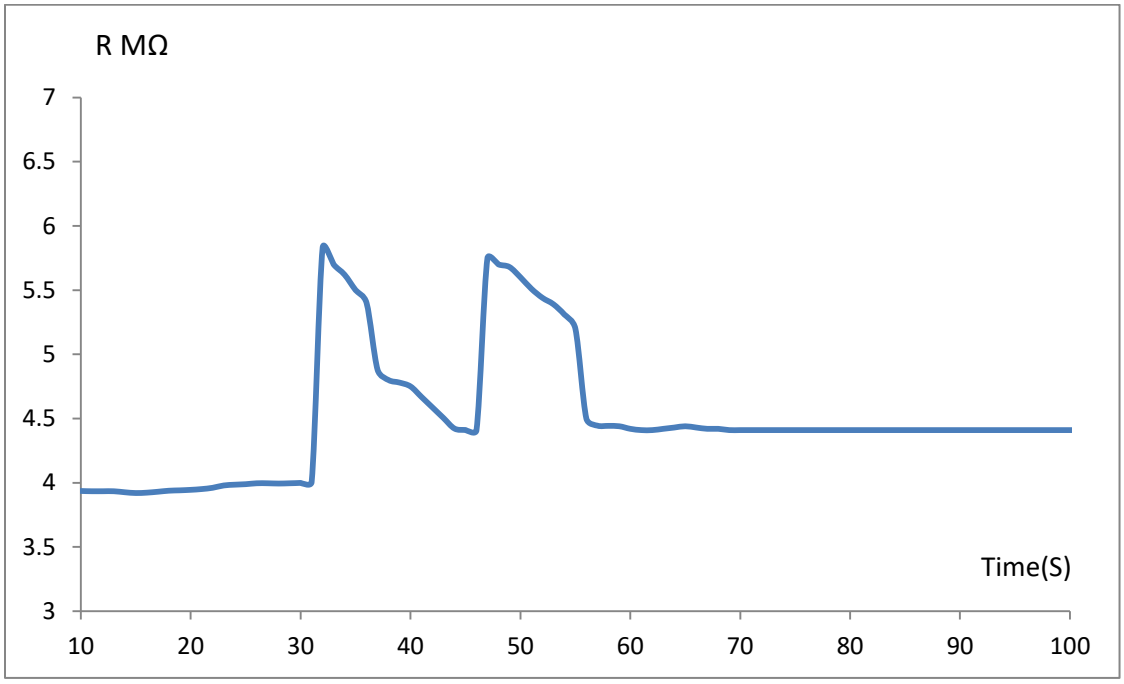

Fig. (4.27)b : Shows the change in resistance with the response time of eathnoal gas to the prepared CdS:Co thin film.

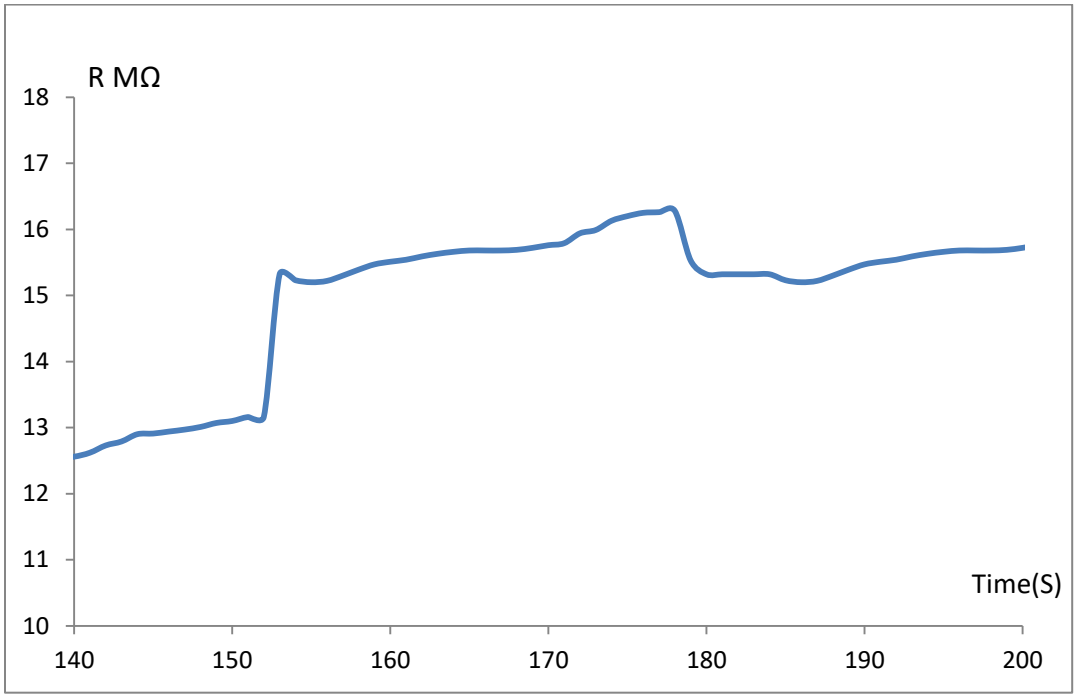

Fig. (4.27)c : Shows the change in resistance with the response time of eathnoal gas to the prepared CdS:Mg thin film.

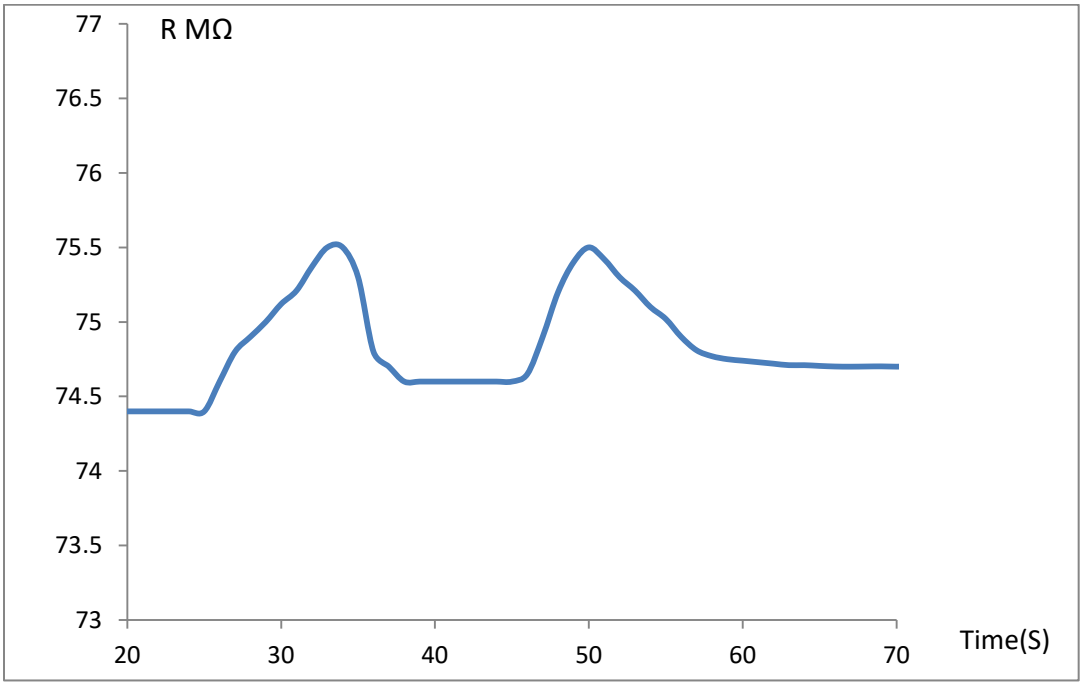

Fig. (4.27)d : Shows the change in resistance with the response time of eathnoal gas to the prepared CdS:Co:Mg thin film.

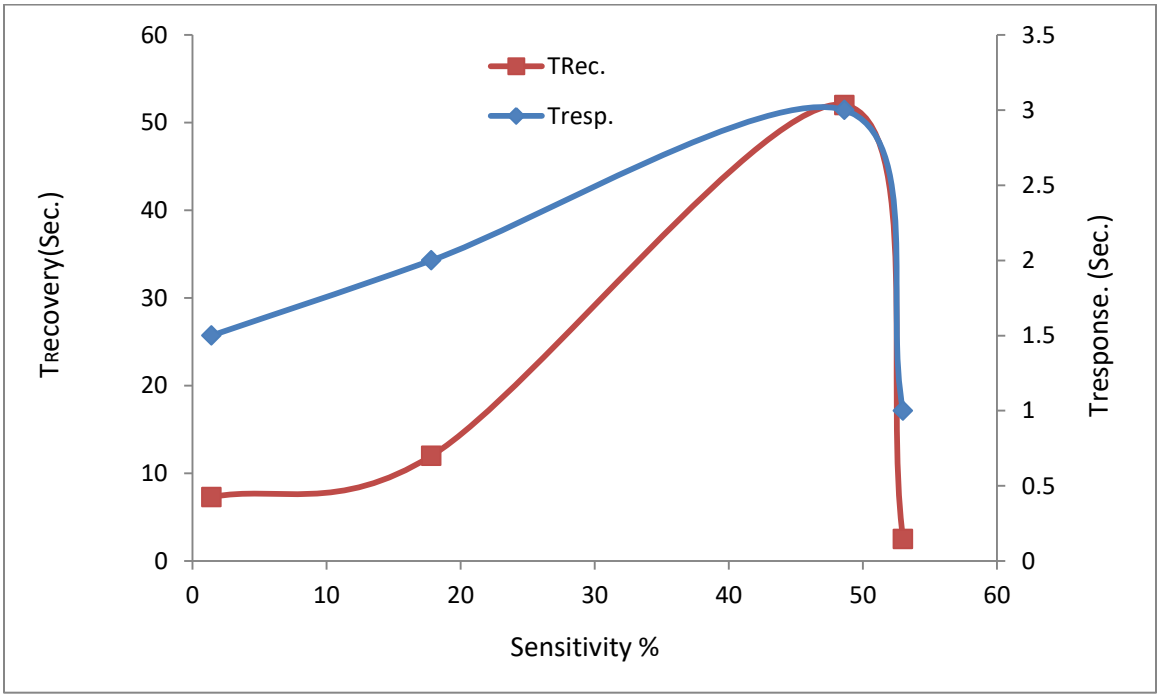

Fig. (4.28)a : Shows the change in the response and recovery time for all thin films by use H_2S gas .

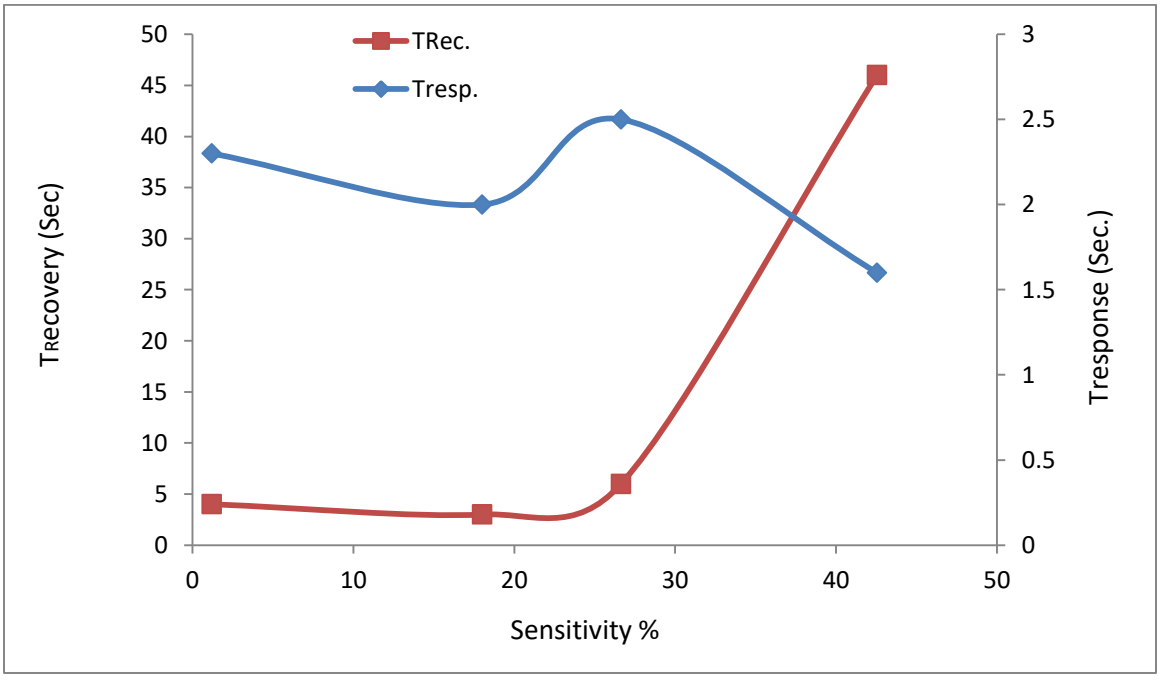

Fig. (4.28)b : Shows the change in the response and recovery time for all thin films by use eathanol gas .

4.10 Anti bectri Measurments

The activity of the soultion, CdS:Co, CdS:Mg and CdS:Co:Mg was tested against two types of bacteria, Gram-positive (staphylococcus) and Gram-negative (escherichia coil), using the bacteria culture method.

Fig. (4.29) shows pictures of the results of testing the activity of the prepared soultion against two types of gram-negative and gram-positive bacteria. The results showed through the images the presence of clear areas on the surface of the bacteria that were cultured and the prepared soultion, and this indicates the presence of the activity of the particles of the prepared membranes, a good area of inhibition to the bacteria that cause many diseases, and the diameter of each was measured and known as shown in table(4.24) and this was also found rouguly in [43,51,147,148]

The explanation of the activity of the prepared soultion in inhibiting bacteria may be attributed to the chemical composition of these prepared filmsAnd that the composition of each of the bacterial cell walls and its different level of susceptibility towards nanoparticles because it does not depend only on the chemical composition, but also depends on the selection of bacteria species. Perhaps the differential formation of cell roots between gram-negative and gram-positive bacteria plays an important role in the formation of the effective zone, where in gram-positive bacteria the cell wall consists of a deep layer of the membrane composed of many linear chains, while in gram-negative bacteria its wall consists of a very thin layer of the membrane Therefore, we show that the nanofilms have a sufficiently wide area for interactions that improve the activity of the prepared films in inhibiting bacterial growth. We conclude that the prepared membranes are

more effective in inhibiting gram-negative bacteri and this was also found rouguly in [39,40149,150].

Table(4.24): Shows the values of the diameters of the inhibited areas for all the .films prepared against bacteria

No.	sample	Diameters Escherichia coil	Diameters Staphylococcus
1	CdS	42mm	38mm
2	Cds:Co	42mm	40mm
3	Csd:Mg	40mm	40mm
4	Cds:Mg:Co	42mm	40mm

Fig.(4.29)a : Show the activity of the films against bacteria Escherichia coil.

Fig.(4.29)b : Show the activity of the films against bacteria Staphylococcus.

5.1 Conclusions

Successful depositions of mixed CdS,CdS:Co,CdS:Mg and CdS:CO:Mg thin films were done in this work by homemade spray pyrolysis technique. From an overall measurement and observations, one can conclude the following points:

1. Spray pyrolysis is a good technique in the preparation of thin films.
2. Through the results of X-ray diffraction measurements, we conclude that the cadmium sulfide urban compound has a cubic-type polycrystalline structure.
3. Through the results of the examination AFM, SEM and TEM and X-ray diffraction, we conclude that the addition of cobalt and magnesium to the cadmium sulfide compound led to an increase in the particle size, and this led to a decrease in the sensitivity values of hydrogen sulfide gases and ethanol.
4. Through the results of test AFM, it was shown that the addition of cobalt and magnesium to the cadmium sulfide compound led to an increase in the surface roughness values of the prepared films, and from this we conclude that it led to two decreases in the reflective optical properties values.
5. Through the results of the optical properties, we conclude that the prepared films have an absorption coefficient of the direct type.
6. The results of the optical properties calculation showed that the addition of cobalt and magnesium to the cadmium sulfide compound led to a decrease in the optical energy gap values. From this we conclude that the increase in the electrical conductivity is consistent

with the results of the Hall effect and the continuous electrical conductivity measurement.

7. Through the results of the Hall effect, we conclude that the addition of cobalt and magnesium does not affect the type of majority carriers, which are the electrons that have been known through the values of the Hall coefficient.
8. By measuring the potential capacitance, we conclude that the junction capacitance of all the prepared reagents is of the acute type.

5.2 Suggestions for Future Work

We suggest the following studies as a future work:

1. Improving the physical application of the gas sensor by adding other materials sach as Zno to the cadmium sulfide compound.
2. Adding a polymeric material, such as polyvinyl alcohol, to the cadmium sulfide compound and studying the mechanical, optical and electrical properties.
3. Study of the electrical properties including measuring the parameters of the prepared thin film solar cells.
4. Studying the effect of thikness thin films on the physical properties CdS,CdS:CO, CdS:Mg and CdS:CO:Mg
5. Preparation of cadmium sulfide nests using silicon sedimentation substrate and studying the sensitivity properties of different gases.
6. Study the effect of annealing at different temperatures on the structural, optical and electrical properties of all prepared cadmium sulfide films.

References

1. Callister Jr, W. D. (2007). *Materials science and engineering an introduction*.
2. Chopra, K. N., & Maini, A. K. (2010). *Thin films and their applications in military and civil sectors*: Defence Research and Development Organisation, Ministry of Defence.
3. Faris, R. A., Mahdi, Z. F., Jawad, H. A., & Altaify, D. O. (2009). The Optical Limiting Behaviour of Prepared Silver Nanoparticles Embedded in Polymer Film. Iraqi Journal of Laser, 10(23-29).
4. Fendler, J. H. (2008). *Nanoparticles and nanostructured films: preparation, characterization, and applications*: John Wiley & Sons.
5. Freund, L. B., & Suresh, S. (2004). *Thin film materials: stress, defect formation and surface evolution*: Cambridge university press.
6. Hashim, F. S., Habeeb, M. A., & Ghanim, I. R. (2013). Effect of zinc on structural and some optical properties of CdS thin films. *Chemistry and Materials Research, 3*(12), 67-74.
7. Lei, J.-F., Martin, L. C., & Will, H. A. (1997). Advances in thin film sensor technologies for engine applications (Vol. 78712): American Society of Mechanical Engineers.
8. Ramanujan, R. (2003). Nanostructured electronic and magnetic materials. Sadhana, 28, 81-96.
9. Fendler, J. H. (2008). *Nanoparticles and nanostructured films: preparation, characterization, and applications*: John Wiley & Sons.
10. Hashim, F. S., Habeeb, M. A., & Ghanim, I. R. (2013). Effect of zinc on structural and some optical properties of CdS thin films. *Chemistry and Materials Research, 3*(12), 67-74.(K. Chopra, 1969)
11. Chopra, K. (1969). Thin Film Phenomena MC Graw Hill Co. New York, USA.

12. Anand, T. J. S. (2004). Synthesis and microstructure of NixAl1-x (0.5 x 1) thin films. *HKU Theses Online (HKUTO)*.

13. Hullavarad, N., Hullavarad, S., & Karulkar, P. (2008). Cadmium sulphide (CdS) nanotechnology: synthesis and applications. *Journal of nanoscience and nanotechnology, 8*(7), 3272-3299.

14. Joseph, M., Tabata, H., & Kawai, T. (1999). Ferroelectric behavior of Li-doped ZnO thin films on Si (100) by pulsed laser deposition. *Applied physics letters, 74*(17), 2534-2536.

15. Knudson, M., Gupta, Y., & Kunz, A. (1999). *Picosecond Electronic Spectroscopy to Determine the Transformation Mechanism for the Pressure-Induced Phase Transition in Shocked CdS*. Retrieved from

16. Li, Y. (1991). Preparation and characterization of RF sputtered barium (2) silicon (2) titanium oxygen (8) thin films.

17. Qutub, N., & Sabir, S. (2013). Characterization of cadmium sulphide nanoparticles synthesized by chemical precipitation method. Advanced Science, Engineering and Medicine, 5(8), 852-857.

18. Singh, V., Sharma, P., & Chauhan, P. (2011). Synthesis of CdS nanoparticles with enhanced optical properties. Materials Characterization, 62(1), 43-52.

19. Hullavarad, N., Hullavarad, S., & Karulkar, P. (2008). Cadmium sulphide (CdS) nanotechnology: synthesis and applications. Journal of nanoscience and nanotechnology, 8(7), 3272-3299.

20. Merdan, M. G. Effect of Temperature on Electronic Structure of Silicon Using a Large Unit Cell within Intermediate Neglect of Differential Overlap (INDO).

21. AL–Gayem, N. (1999). Laser signals detection using CdS doped with copper. Collage of science, University of Babylon.

22. Olopade, M., Awobode, A., Awe, O., & Imalerio, T. (2013). Structural and optical characteristics of sol gel spin-coated nanocrystalline CdS thin film. International journal of research and reviews in applied sciences, 15(1), 120-124.

23. Al-Douri, Y., Waheb, J. H., Ameri, M., Khenata, R., Bouhemadou, A., & Reshak, A. (2013). Morphology, analysis and properties studies of CdS nanostructures under thiourea concentration effect for photovoltaic applications. *Int. J. Electrochem. Sci, 8*, 10688-10696.

24. Tang, C.-F., Ding, H., Jiao, R.-Q., Wu, X.-X., & Kong, L.-D. (2020). Possibility of magnesium supplementation for supportive treatment in patients with COVID-19. European journal of pharmacology, 886, 173546.

25. Andhare, D. D., Patade, S. R., Kounsalye, J. S., & Jadhav, K. (2020). Effect of Zn doping on structural, magnetic and optical properties of cobalt ferrite nanoparticles synthesized via. Co-precipitation method. Physica B: Condensed Matter, 583, 412051.

26. Abdel Maksoud, M., El-Ghandour, A., El-Sayyad, G. S., Fahim, R. A., El-Hanbaly, A. H., Bekhit, M., . . . Ashour, A. (2020). Unveiling the effect of Zn 2+ substitution in enrichment of structural, magnetic, and dielectric properties of cobalt ferrite. Journal of Inorganic and Organometallic Polymers and Materials, 30, 3709-3721.

27. Shakil, M., Inayat, U., Arshad, M., Nabi, G., Khalid, N., Tariq, N., . . . Iqbal, M. (2020). Influence of zinc and cadmium co-doping on optical and magnetic properties of cobalt ferrites. Ceramics International, 46(6), 7767-7773.

28. Favero, P., Souza-Parise, M. d., Fernandez, J., Miotto, R., & Ferraz, A. C. (2006). Surface properties of CdS nanoparticles. *Brazilian Journal of Physics, 36*, 1032-1034.

29. Trindade, T., O'Brien, P., & Pickett, N. L. (2001). Nanocrystalline semiconductors: synthesis, properties, and perspectives. *Chemistry of Materials, 13*(11), 3843-3858.

30. Castillo, S., Apolinar-Iribe, A., Berman-Mendoza, D., & Ramirez-Bon, R. (2011). Characterization of CdS thin films synthesized by chemical bath deposition using glycine as complexing agent. Chalcogenide letters, 8(10), 631-636.

31. Anderson, P. W. (1958). Absence of diffusion in certain random lattices. Physical review, 109(5), 1492.

32. Padiyan, D. P., Marikani, A., & Murali, K. (2003). Influence of thickness and substrate temperature on electrical and photoelectrical properties of vacuum-deposited CdSe thin films. Materials chemistry and physics, 78(1), 51-58.

33. Patidar, D., Rathore, K., Saxena, N., Sharma, K., & Sharma, T. (2008). Energy band gap and conductivity measurement of CdSe thin films. Chalcogenide letters, 5(2), 21-25.

34. Gibson, P., Özsan, M., Lincot, D., Cowache, P., & Summa, D. (2000). Modelling of the structure of CdS thin films. Thin Solid Films, 361, 34-40.

35. Alam, M., Chowdhury, M., Kamal, M., Ghose, S., Islam, M., Mustafa, M., . . . Ansary, M. (1999). The 226Ra, 232Th and 40K activities in beach sand minerals and beach soils of Cox's Bazar, Bangladesh. Journal of environmental radioactivity, 46(2), 243-250.

36. Pal, K., Maiti, U. N., Majumder, T. P., & Debnath, S. C. (2011). A facile strategy for the fabrication of uniform CdS nanowires with high yield and its controlled morphological growth with the assistance of PEG in hydrothermal route. Applied surface science, 258(1), 163-168.

37. Al-Hussam, A. M., & Jassim, S. A.-J. (2012). Synthesis, structure, and optical properties of CdS thin films nanoparticles prepared by chemical bath technique. *Journal of the Association of Arab Universities for Basic and Applied Sciences, 11*(1), 27-31.

38. Jing, Z., Tan, L., Li, F., Wang, J., Fu, Y., & Qian, L. (2013). Photocatalytic and antibacterial activities of CdS nanoparticles prepared by solvothermal method.

39. Li, L., Wang, L., Hu, T., Zhang, W., Zhang, X., & Chen, X. (2014). Preparation of highly photocatalytic active CdS/TiO2 nanocomposites by combining chemical bath deposition and microwave-assisted hydrothermal synthesis. *Journal of Solid State Chemistry, 218*, 81-89.

40. Kumar, A., Singh, S., & Kumar, D. (2014). Evaluation of antimicrobial potential of cadmium sulphide nanoparticles against bacterial pathogens. *Int. J. Pharm. Sci. Rev. Res, 24*(2), 202-207.

41. Rajeshkumar, S., Ponnanikajamideen, M., Malarkodi, C., Malini, M., & Annadurai, G. (2014). Microbe-mediated synthesis of antimicrobial semiconductor nanoparticles by marine bacteria. *Journal of Nanostructure in Chemistry*, *4*, 1-7.

42. Ayodhya, D., Venkatesham, M., Kumari, A. S., Reddy, G. B., Ramakrishna, D., & Veerabhadram, G. (2015). Synthesis, characterization, fluorescence, photocatalytic and antibacterial activity of CdS nanoparticles using Schiff base. *Journal of fluorescence*, *25*, 1481-1492.

43. Abd-Elkader, O. H., & Shaltout, A. A. (2015). Characterization and antibacterial capabilities of nanocrystalline CdS thin films prepared by chemical bath deposition. *Materials Science in Semiconductor Processing*, *35*, 132-138.

44. Jana, T., Maji, S., Pal, A., Maiti, R., Dolai, T., & Chatterjee, K. (2016). Photocatalytic and antibacterial activity of cadmium sulphide/zinc oxide nanocomposite with varied morphology. *Journal of colloid and interface science*, *480*, 9-16.

45. Nisha, K., Navaneethan, M., Harish, S., Archana, J., Ponnusamy, S., Muthamizhchelvan, C., . . . Hayakawa, Y. (2017). Influence of organic ligands on the formation and functional properties of CdS nanostructures. *Applied surface science, 418*, 346-351.

46. Narasimman, V., Nagarethinam, V., Usharani, K., & Balu, A. (2017). Optoelectronic, magnetic and antibacterial properties of Zr-doped CdS thin films. *Optik, 138*, 398-406.

47. Al Balushi, B. S., Al Marzouqi, F., Al Wahaibi, B., Kuvarega, A. T., Al Kindy, S. M., Kim, Y., & Selvaraj, R. (2018). Hydrothermal synthesis of CdS sub-microspheres for photocatalytic degradation of pharmaceuticals. *Applied surface science, 457*, 559-565.

48. Wang, X., Hu, Z., Chen, K., Dong, H., Li, S., Li, X., & Li, L. (2019). Efficient photocatalytic debromination of 2, 2′, 4, 4′-

tetrabromodiphenyl ether by Ag-loaded CdS particles under visible light. *Chemosphere, 220*, 723-730.

49. Ibraheem, F., Mahdy, M. A., Mahmoud, E. A., Ortega, J. E., Rogero, C., Mahdy, I. A., & El-Sayed, A. (2020). Tuning Paramagnetic effect of Co-Doped CdS diluted magnetic semiconductor quantum dots. *Journal of Alloys and Compounds, 834*, 155196.

50. Zhao, J., Yang, H., Li, Y., & Lu, K. (2020). Photocatalytic activity of CdS nanoparticles enhanced by the interaction between piezotronic effect and phase junction. *Journal of Alloys and Compounds, 815*, 152494.

51. Zgura, I., Preda, N., Enculescu, M., Diamandescu, L., Negrila, C., Bacalum, M., . . . Barbinta-Patrascu, M. E. (2020). Cytotoxicity, antioxidant, antibacterial, and photocatalytic activities of ZnO–CdS powders. *Materials, 13*(01), 182.

52. Khani, P., Sahraei, R., Sharifirad, Z., Ghavidel, E., Nourolahi, H., Jawhar, N. N., & Soheyli, E. (2021). Improved chemical deposition of cobalt-doped CdS nanostructured thin films via nucleation-doping strategy: Surface and optical properties. *Materials Science and Engineering: B, 272*, 115328.

53. Leng, Y. (2008). Introduction to Microscopic and Spectroscopic Methods. *Materials Characterization, Asia, Wiley*, 1.

54. Kumar, C. S., Singh, M. M., & Krishna, R. (2023). *Advanced Materials Characterization: Basic Principles, Novel Applications, and Future Directions*: CRC Press.

55. Corain, B., Schmid, G., & Toshima, N. (2011). *Metal nanoclusters in catalysis and materials science: the issue of size control*: Elsevier.

56. Murthy, K., & Virk, H. S. (2014). Luminescence phenomena: an introduction. *Defect and diffusion fórum, 347*, 1-34.

57. Ohring, M., Zarrabian, S., & Grogan, A. (1992). The materials science of thin films. *Appl. Opt, 31*(34), 7162.

58. Callister Jr, W. D. (2007). *Materials science and engineering an introduction*.

59. Waseda, Y., Matsubara, E., & Shinoda, K. (2011). *X-ray diffraction crystallography: introduction, examples and solved problems*: Springer Science & Business Media.

60. Cullity, B. D. (1956). *Elements of X-ray Diffraction*: Addison-Wesley Publishing.

61. Ashraf, M., Akhtar, S., Khan, A., Ali, Z., & Qayyum, A. (2011). Effect of annealing on structural and optoelectronic properties of nanostructured ZnSe thin films. *Journal of Alloys and Compounds, 509*(5), 2414-2419.

62. Mohammadigharehbagh, R., Pat, S., Özen, S., Yudar, H. H., & Korkmaz, Ş. (2018). Investigation of the optical properties of the indium-doped ZnO thin films deposited by a thermionic vacuum arc. *Optik, 157*, 667-674.

63. Mohammadigharehbagh, R., Pat, S., Özen, S., Yudar, H. H., & Korkmaz, Ş. (2018). Investigation of the optical properties of the indium-doped ZnO thin films deposited by a thermionic vacuum arc. *Optik, 157*, 667-674.

64. Abass, A., Collins, R., & Krier, A. (1993). The influence of oxygen on the electrical properties of monoclinic lead phthalocyanine. *Journal of Physics and Chemistry of Solids, 54*(3), 375-380.

65. Meyer, G., & Amer, N. M. (1990). Simultaneous measurement of lateral and normal forces with an optical-beam-deflection atomic force microscope. *Applied physics letters, 57*(20), 2089-2091.

66. Colchero, J., Marti, O., Mlynek, J., Humbert, A., Henry, C., & Chapon, C. (1991). Palladium clusters on mica: A study by scanning force microscopy. *Journal of Vacuum Science & Technology B: Microelectronics and Nanometer Structures Processing, Measurement, and Phenomena, 9*(2), 794-797.

67. Manne, S., Massie, J., Elings, V., Hansma, P., & Gewirth, A. (1991). Electrochemistry on a gold surface observed with the

atomic force microscope. *Journal of Vacuum Science & Technology B: Microelectronics and Nanometer Structures Processing, Measurement, and Phenomena, 9*(2), 950-954.

68. Blanchard, C. R. (1996). Atomic force microscopy. *The chemical educator, 1*, 1-8.

69. Mandal, S., Singha, R., Dhar, A., & Ray, S. (2008). Optical and structural characteristics of ZnO thin films grown by rf magnetron sputtering. *Materials Research Bulletin, 43*(2), 244-250.

70. Hasan, B. A., Al-Haddad, R., Nasir, E. M., & Kadhem, M. (2015). Nano Technology Enhanced Performance of a-(GeS2) 100-xGax/Ge, n, p-Si Hereterojunction. *relation (J. Millman, 1979), 2*, 2.

71. Ponz, E., Ladaga, J. L., & Bonetto, R. D. (2006). Measuring surface topography with scanning electron microscopy. I. EZEImage: a program to obtain 3D surface data. *Microscopy and Microanalysis, 12*(2), 170-177.

72. Mott, N. F., & Davis, E. A. (2012). *Electronic processes in non-crystalline materials*: Oxford university press.

73. Bakr, N. A., Kamil, A. A., & Alghalabi, I. A. Effect of Solution Molarity on Structural and Optical Properties of Zinc Oxide Thin Films Prepared by Chemical Spray Pyrolysis Technique.

74. Neaman, D. A. (1992). *Semiconductor physics and devices*: Irwin.

75. Macleod, H. A., & Macleod, H. A. (2010). *Thin-film optical filters*: CRC press.

76. Parkove, J. (1971). Optical process in semiconductors. In: Dover Publications, Inc., New York.

77. Sze, S. M. (2008). *Semiconductor devices: physics and technology*: John wiley & sons.

78. Kittel, C. (2005). *Introduction to solid state physics*: John Wiley & sons, inc.

79. Karunamoorthy, S., & Velluchamy, M. (2018). Design and synthesis of bandgap tailored porous Ag/NiO nanocomposite: an effective visible light active photocatalyst for degradation of organic pollutants. *Journal of Materials Science: Materials in Electronics, 29*, 20367-20382.

80. Saeed, N. M. (2009). Preparation and properties of Nanostructure Zinc Oxide Thin Films. Iraqi Journal of Physics, 7(8), 75-81.

81. Pires, J. M. A. C. (2003). Thin films for gas sensors .

82. Manasreh, O. (2005). *Semiconductor heterojunctions and nanostructures*

83. Siekkinen, A. R., McLellan, J. M., Chen, J., & Xia, Y. (2006). Rapid synthesis of small silver nanocubes by mediating polyol reduction with a trace amount of sodium sulfide or sodium hydrosulfide. *Chemical physics letters, 432*(4-6), 491-496.

84. Elangovan, E., & Ramamurthi, K. (2003). Optoelectronic properties of spray deposited SnO 2: F thin films for window materials in solar cells. *Journal of Optoelectronics and Advanced Materials, 5*(1), 45-54.

85. REMBEZA, S., REMBEZA, E., & SVISTOVA, T. (2004). Electrophysical properties of gas sensitive films SnO2 doped with palladium. *Sensors & Transducers Magazine, 40*, 145.

86. Bahadur, L., Hamdani, M., Koenig, J., & Chartier, P. (1986). Studies on semiconducting thin films prepared by the spray pyrolysis technique for photoelectrochemical solar cell applications: Preparation and properties of ZnO. *Solar Energy Materials, 14*(2), 107-120.

87. Bahadur, L., Hamdani, M., Koenig, J., & Chartier, P. (1986). Studies on semiconducting thin films prepared by the spray pyrolysis technique for photoelectrochemical solar cell applications: Preparation and properties of ZnO. *Solar Energy Materials, 14*(2), 107-120.

88. Piprek, J. (2013). *Semiconductor optoelectronic devices: introduction to physics and simulation*: Elsevier.

89. Poortmans, J., & Arkhipov, V. (2006). *Thin film solar cells: fabrication, characterization and applications* (Vol. 18): John Wiley & Sons.

90. Oman, D., Dugan, K., Killian, J., Ceekala, V., Ferekides, C., & Morel, D. (1999). Device performance characterization and junction mechanisms in CdTe/CdS solar cells. *Solar energy materials and solar cells, 58*(4), 361-373.

91. Aernouts, T. (2006). Organic bulk heterojunction solar cells: from single cell towards fully flexible photovoltaic module. *Katholieke Universiteit Leuven*.

92. Viswanathan, V. (2004). *Study of copper-free back contacts to thin film cadmium telluride solar cells*: University of south Florida.

93. Garde, A. (2010). LPG and NH^ sub 3^ Sensing Properties of SnO^ sub 2^ Thick Film Resistors Prepared by Screen Printing Technique. *Sensors & Transducers, 122*(11), 128.

94. Garde, A. (2010). LPG and NH^ sub 3^ Sensing Properties of SnO^ sub 2^ Thick Film Resistors Prepared by Screen Printing Technique. *Sensors & Transducers, 122*(11), 128.

95. Gnanasekar, K., & Rambabu, B. (2002). Nanostructure Semiconductor Oxide Powders and Thin Films for Gas Sensor. *Surface Science, 200*, 780.

96. Fong, W. G., Moye, H. A., Seiber, J. N., & Toth, J. P. (1999). *Pesticide residues in foods: methods, techniques, and regulations* (Vol. 214): John Wiley & Sons.

97. Kersen, Ç. (2003). *Gas sensing properties of nanocrystalline metal oxide powder produced by thermal deposition and mechanochemical processing.* dissertation of Ph. D., Helsinki University of Technology, department of …,

98. Ahlers, S., Müller, G., & Doll, T. (2005). A rate equation approach to the gas sensitivity of thin film metal oxide materials. *Sensors and Actuators B: Chemical*, *107*(2), 587-599.

99. Balaguru, R. J. B., & Jeyaprakash, B. (2004). Mimic of a gas sensor, metal oxide gas sensing mechanism, factors influencing the sensor performance and role of nanomaterials based gas sensors. *NPTEL–Electrical & Electronics Engineering–Semiconductor Nanodevices*, 1-30.

100. Madou, M. J., & Morrison, S. R. (2012). Chemical sensing with solid state devices: Elsevier.

101. Abdulazeez, M. O., & Trier, S. H. (2017). Effect of Doping and Temperature Operating on (NO2) Gas Sensing Properties for MgxZnO1-x/n-Si Heterojunction. *Al-Qadisiyah Journal of Pure Science*, *22*(2), 87-95.

102. Helan, V., Prince, J. J., Al-Dhabi, N. A., Arasu, M. V., Ayeshamariam, A., Madhumitha, G., . . . Jayachandran, M. (2016). Neem leaves mediated preparation of NiO nanoparticles and its magnetization, coercivity and antibacterial analysis. *Results in physics*, *6*, 712-718.

103. Ezhilarasi, A. A., Vijaya, J. J., Kaviyarasu, K., Maaza, M., Ayeshamariam, A., & Kennedy, L. J. (2016). Green synthesis of NiO nanoparticles using Moringa oleifera extract and their biomedical applications: Cytotoxicity effect of nanoparticles against HT-29 cancer cells. *Journal of Photochemistry and Photobiology B: Biology*, *164*, 352-360.

104. Ezhilarasi, A. A., Vijaya, J. J., Kaviyarasu, K., Kennedy, L. J., Ramalingam, R. J., & Al-Lohedan, H. A. (2018). Green synthesis of NiO nanoparticles using Aegle marmelos leaf extract for the evaluation of in-vitro cytotoxicity, antibacterial and photocatalytic properties. *Journal of Photochemistry and Photobiology B: Biology*, *180*, 39-50.

105. Kganyago, P., Mahlaule-Glory, L., Mathipa, M., Ntsendwana, B., Mketo, N., Mbita, Z., & Hintsho-Mbita, N. (2018). Synthesis of NiO nanoparticles via a green route using Monsonia

burkeana: the physical and biological properties. *Journal of Photochemistry and Photobiology B: Biology*, *182*, 18-26.

106. Sabouri, Z., Akbari, A., Hosseini, H. A., Hashemzadeh, A., & Darroudi, M. (2019). Eco-friendly biosynthesis of nickel oxide nanoparticles mediated by okra plant extract and

107. investigation of their photocatalytic, magnetic, cytotoxicity, and antibacterial properties. *Journal of Cluster Science*, *30*, 1425-1434.

108. Srihasam, S., Thyagarajan, K., Korivi, M., Lebaka, V. R., & Mallem, S. P. R. (2020). Phytogenic generation of NiO nanoparticles using Stevia leaf extract and evaluation of their in-vitro antioxidant and antimicrobial properties. *Biomolecules*, *10*(1), 89.

109. Kathirvel, D., Suriyanarayanan, N., Prabahar, S., & Srikanth, S. (2011). STRUCTURAL, ELECTRICAL AND OPTICAL PROPERTIES OF CdS THIN FILMS BY VACUUM EVAPORATION DEPOSITION. *Journal of Ovonic Research*, *7*(4).

110. Ullrich, B., Sakai, H., & Segawa, Y. (2001). Optoelectronic properties of thin film CdS formed by ultraviolet and infrared pulsed-laser deposition. *Thin Solid Films*, *385*(1-2), 220-224.

111. Martinez, J., Martinez, G., Torres-Delgado, G., Guzman, O., Angel, P. D., Zelaya-Angel, O., & Lozada-Morales, R. (1997). Cubic CdS thin films studied by spectroscopic ellipsometry. *Journal of Materials Science: Materials in Electronics*, *8*, 399-403.

112. Thambidurai, M., Murugan, N., Muthukumarasamy, N., Vasantha, S., Balasundaraprabhu, R., & Agilan, S. (2009). preparation and characterization of nanocrystalline CdS thin films. *Chalcogenide letters*, *6*(4).

113. Al Balushi, B. S., Al Marzouqi, F., Al Wahaibi, B., Kuvarega, A. T., Al Kindy, S. M., Kim, Y., & Selvaraj, R. (2018). Hydrothermal synthesis of CdS sub-microspheres for photocatalytic

degradation of pharmaceuticals. *Applied surface science, 457*, 559-565.

114. Wang, X., Hu, Z., Chen, K., Dong, H., Li, S., Li, X., & Li, L. (2019). Efficient photocatalytic debromination of 2, 2′, 4, 4′-tetrabromodiphenyl ether by Ag-loaded CdS particles under visible light. *Chemosphere, 220*, 723-730.

115. Mathew, J., & Anila, E. (2018). Hydrothermal assisted chemical bath deposition of (Cd: Zn) S thin film with high photosensitivity and low dark current. *Solar Energy, 172*, 165-170.

116. Hussain, T., Aslam, S., Mustafa, F., Ighodalo, K. O., & Ahmad, M. A. (2019). Study of the extrinsic properties of Copper doped Cadmium Sulfide Thin Film by Hydrothermal assisted CBD Method. *Materials Research Express, 6*(4), 045908.

117. Rengaraj, S., Venkataraj, S., Jee, S. H., Kim, Y., Tai, C.-w., Repo, E., . . . Sillanpaa, M. (2011). Cauliflower-like CdS microspheres composed of nanocrystals and their physicochemical properties. *Langmuir, 27*(1), 352-358.

118. Khanna, P., & Subbarao, V. (2004). Synthesis of fine CdS powder from direct in-situ reduction of sulphur and cadmium salts in aqueous N, N′-dimethylformamide. *Materials Letters, 58*(22-23), 2801-2804.

119. Chen, J., & Li, W. (2011). Hydrothermal synthesis of high densified CdS polycrystalline microspheres under high gravity. *Chemical engineering journal, 168*(2), 903-908.

120. Castillo, S., Apolinar-Iribe, A., Berman-Mendoza, D., & Ramirez-Bon, R. (2011). Characterization of CdS thin films synthesized by chemical bath deposition using glycine as complexing agent. *Chalcogenide letters, 8*(10), 631-636.

121. Yadav, A., & Masumdar, E. (2010). Preparation and characterization of indium doped CdS0. 2Se0. 8 thin films by spray pyrolysis. *Materials Research Bulletin, 45*(10), 1455-1459.

122. El Assali, K., Boustani, M., Khiara, A., Bekkay, T., Outzourhit, A., Ameziane, E., . . . Pouzet, J. (2000). Some structural and optical properties of CdS thin films prepared by RF sputtering. physica status solidi (a), 178(2), 701-708.

123. Akintunde, J. (2000). Effects of Deposition Parameters and Conditions on the Physical and Electro-Optical Properties of Buffer Solution Grown CdS Thin Films. physica status solidi (a), 179(2), 363-371.

124. Baban, C., Rusu, G., & Prepelita, P. (2005). On the optical properties of polycrystalline CdSe thin films. *Journal of Optoelectronics and Advanced Materials, 7*(2), 817-821.

125. Hambrock, J., Birkner, A., & Fischer, R. A. (2001). Synthesis of CdSe nanoparticles using various organometallic cadmium precursors. Journal of materials chemistry, 11(12), 3197-3201.

126. Metin, H., Ari, M., Erat, S., Durmuş, S., Bozoklu, M., & Braun, A. (2010). The effect of annealing temperature on the structural, optical, and electrical properties of CdS films. *Journal of Materials Research, 25*(1), 189-196.

127. Ichimura, M., Sato, N., Nakamura, A., Takeuchi, K., & Arai, E. (2002). Properties of photochemically deposited CdSe films. physica status solidi (a), 193(1), 132-138.

128. Murali, K., Elango, P., & Gopalakrishnan, P. (2006). Structural and optical properties of CdSe films brush plated on low temperature substrates. *Materials chemistry and physics*, *96*(1), 103-106.

129. Baban, C., Rusu, G., Nicolaescu, I., & Rusu, G. (2000). Optical properties of CdSe films deposited by the quasi-closed volume technique. Journal of Physics: Condensed Matter, 12(35), 7687.

130. Wemple, S., & DiDomenico Jr, M. (1971). Behavior of the electronic dielectric constant in covalent and ionic materials. *Physical Review B, 3*(4), 1338.

131. Zgair, I. A., Muhmood, A. A., & Alkhayatt, A. H. O. (2018). Influence of Ag dopant content on structural and optical energy gap of ZnS thin films deposited by spray pyrolysis technique. *Transylvanian Review*, *26*(29).

132. Blakemore, J. S. (1985). *Solid state physics*: Cambridge university press.

133. Hu, Y., Hu, B., Wu, B., Wei, Z., & Li, J. (2018). Hydrothermal preparation of ZnS: Mn quantum dots and the effects of reaction temperature on its structural and optical properties. Journal of Materials Science: Materials in Electronics, 29, 16715-16720.

134. Arif, M., Khan, Z. R., Gupta, V., & Singh, A. (2014). Effect of substrates temperature on structural and optical properties of thermally evaporated CdS nanocrystalline thin films.

135. Metin, H., Ari, M., Erat, S., Durmuş, S., Bozoklu, M., & Braun, A. (2010). The effect of annealing temperature on the structural, optical, and electrical properties of CdS films. *Journal of Materials Research*, *25*(1), 189-196.

136. Mahdi, M., Ramizy, A., Hassan, Z., Ng, S., Hassan, J., & Kasim, S. (2012). CdS nanocrystalline structured grown on porous silicon substrates via chemical bath deposition method. Chalcogenide letters, 9(1), 19-25.

137. Devi, L. S., Devi, K. N., Sharma, B. I., & Sarma, H. N. (2012). Structural and optical characterization of PVA capped cadmium sulphide nanoparticles by chemical coprecipitation method. *Chalcogenide letters*, *9*(2), 67-72.

138. Uosaki, K., & Kita, H. (1986). Theoretical aspects of semiconductor electrochemistry. *Modern Aspects of Electrochemistry: Volume 18*, 1-60.

139. Kalem, S., Yavuzcetin, O., & Altineller, C. (2000). Effect of light exposure and ultrasound on the formation of porous silicon. Journal of Porous Materials, 7, 381-383.

140. Möller, H. J. (1993). Semiconductors for solar cells. In *Semiconductors for solar cells* (pp. 343-343).

141. Padiyan, D. P., Marikani, A., & Murali, K. (2003). Influence of thickness and substrate temperature on electrical and photoelectrical properties of vacuum-deposited CdSe thin films. Materials chemistry and physics, 78(1), 51-58.

142. Kathirvel, D., Suriyanarayanan, N., Prabahar, S., & Srikanth, S. (2011). STRUCTURAL, ELECTRICAL AND OPTICAL PROPERTIES OF CdS THIN FILMS BY VACUUM EVAPORATION DEPOSITION. *Journal of Ovonic Research*, *7*(4).

143. Ullrich, B., Sakai, H., & Segawa, Y. (2001). Optoelectronic properties of thin film CdS formed by ultraviolet and infrared pulsed-laser deposition. *Thin Solid Films*, *385*(1-2), 220-224.

144. Gibson, P., Özsan, M., Lincot, D., Cowache, P., & Summa, D. (2000). Modelling of the structure of CdS thin films. Thin Solid Films, 361, 34-40.

145. Martinez, J., Martinez, G., Torres-Delgado, G., Guzman, O., Angel, P. D., Zelaya-Angel, O., & Lozada-Morales, R. (1997). Cubic CdS thin films studied by spectroscopic ellipsometry. *Journal of Materials Science: Materials in Electronics*, *8*, 399-403.

146. Baban, C., Rusu, G., & Prepelita, P. (2005). On the optical properties of polycrystalline CdSe thin films. Journal of Optoelectronics and Advanced Materials, 7(2), 817-821.

147. Padiyan, D. P., Marikani, A., & Murali, K. (2003). Influence of thickness and substrate temperature on electrical and photoelectrical properties of vacuum-deposited CdSe thin films. Materials chemistry and physics, 78(1), 51-58.

148. Thambidurai, M., Murugan, N., Muthukumarasamy, N., Vasantha, S., Balasundaraprabhu, R., & Agilan, S. (2009). preparation and characterization of nanocrystalline CdS thin films. Chalcogenide letters, 6(4).

149. Hambrock, J., Birkner, A., & Fischer, R. A. (2001). Synthesis of CdSe nanoparticles using various organometallic cadmium precursors. Journal of materials chemistry, 11(12), 3197-3201.

150. Iqbal, T., Ali, F., Khalid, N., Tahir, M. B., & Ijaz, M. (2019). Facile synthesis and antimicrobial activity of CdS-Ag2S nanocomposites. Bioorganic Chemistry, 90, 103064.